BEHAVIOR OF INTEGRAL ABUTMENT BRIDGES UNDER TEMPERATURE EFFECT AND SEISMIC EXCITATION

A THESIS

Submitted in partial fulfilment of the requirements for the award of the degree of

DOCTOR OF PHILOSOPHY

in

EARTHQUAKE ENGINEERING

by

PRADEEP KUMAR T V

M.G. CENTRAL LIBRARY
ACC No. G20643
Date 24/2/11
I.I.T. ROORKEE

DEPARTMENT OF EARTHQUAKE ENGINEERING
INDIAN INSTITUTE OF TECHNOLOGY ROORKEE
ROORKEE - 247 667 (INDIA)

DECEMBER, 2009

©INDIAN INSTITUTE OF TECHNOLOGY ROORKEE, ROORKEE, 2009
ALL RIGHTS RESERVED

INDIAN INSTITUTE OF TECHNOLOGY ROORKEE
ROORKEE

CANDIDATE'S DECLARATION

I hereby certify that the work which is being presented in the thesis entitled **BEHAVIOR OF INTEGRAL ABUTMENT BRIDGES UNDER TEMPERATURE EFFECT AND SEISMIC EXCITATION, in the partial fulfilment** of the requirements for the award of the Degree of Doctor of Philosophy and submitted in the Department of Earthquake Engineering, Indian Institute of Technology Roorkee, Roorkee, is an **authentic record of my own work carried out during a period from July** 2004 to December 2009 under the supervision of Dr. D.K Paul, Professor, Dr. Pankaj Agarwal, Assistant Professor, Department of Earthquake Engineering, Indian Institute of Technology Roorkee, Roorkee and Dr. Ram Kumar, Scientist, Central Road Research Institute, New Delhi. The matter presented in the thesis has not been submitted by me for the award of any degree of this or any other Institute.

(PRADEEP KUMAR T V)

This is to certify that the above statement made by the candidate is correct to the best of our knowledge. The candidate has incorporated all the examiner's comments and **resubmitted his thesis as per our satisfaction.**

(Ram Kumar)
Supervisor

(Pankaj Agarwal)
Supervisor

(D.K Paul)
Supervisor

Date: 29th December , 2009

The Ph.D. Viva-Voice Examination of **Mr. Pradeep Kumar T V**, Research Scholar, has been held on .....

Signature of Supervisors

Signature of External Examiner

ABSTRACT

Integral bridges being safe and aesthetically pleasing is gaining popularity in most of the countries including India, because of its low initial cost, reduced long-term maintenance expenses, faster construction and better seismic performance. The analysis of integral bridge is much more complicated as bridge deck, piers, abutments, embankments and moreover soil-pile interaction must be considered as a single system. Analysis of integral bridges without considering non-linear backfill and soil-pile interaction is impractical, as in most of the long span bridges soil respond beyond the elastic limit. The length of the integral bridges mainly depends on the pile capacity, soil type and abutment movement due to intensity of temperature and seismic load and other factors.

Most of the integral bridges are constructed in non-seismic regions, where the research has concentrated on secondary stresses, mainly due to temperature which govern the integral bridge design. The construction of integral bridges is increasing in India and other places, which are having high temperature variation and also high seismic zones. In integral bridges, the redundancy or static indeterminacy allows the formation of local mechanisms at selected locations for largely unknown seismic inputs. This concept in integral bridges is proved to be an excellent option for seismic prone areas. In regions of high seismicity, seismic displacement demand can be significantly more than the thermal movements. Thus, it is very much necessary to study the capacities of these integral bridges in resisting various levels of temperature and seismic loadings.

Most of the bridge agencies use steel H-piles for integral bridges, which have greater flexibility in comparison to concrete piles. In India, most of the integral abutment and deck extension bridges are constructed on bored-cast-in-situ concrete piles. These

bridges are located in the regions having high temperature variation and high seismic zones, where the length of bridge is restricted by lateral pile capacity due to temperature loading or seismic loading or a combination of both as mentioned in Indian codes.

In this study, the behavior of integral abutment bridges built on cast-in-situ piles are studied for temperature effects and seismic excitations to determine their maximum possible length under different environment conditions. To study the behavior of integral abutment bridge, a three dimensional non-linear finite element model has been developed considering material nonlinearity. Material nonlinearity is considered for soil-pile interaction by using Winkler soil model with non-linear soil springs, which were developed by using the guidelines given by API and Reese. The passive earth pressure behind the abutment wall is modeled by using the design curves given in Canadian Foundation Engineering Manual (CFM) for dense sand and Manuals for the Design of Bridge Foundations (NCHRP) for medium and loose sand respectively. Material nonlinearity for structural members is considered only for piers and piles, which were modeled as 2 noded beam elements. The finite element model developed is verified by comparing the results with the published literatures on temperature effects.

Three dimensional models of five span reinforced concrete integral abutment bridge of 130 m long and 12 m wide constructed on cast-in-situ piles is used to study the influence of abutment-backfill soil, soil surrounding the pile, predrilled hole, abutment and pier flexibility, pile type & pile longitudinal reinforcement on the length of the bridge. Non-linear static analysis is conducted in both temperature rise and temperature fall conditions until the formation of first plastic hinge in the pile to find the maximum yield displacement capacity of 1.0 m and 1.2 m diameter piles. Non-dimensional curves relating the temperature effect with length of integral abutment bridge are established.

Sensitive non linear dynamic analysis has been conducted by using five different response spectrum compatible time histories in both longitudinal and transverse directions to study the displacement demand and the force distribution in the integral abutment bridge. Non-linear dynamic analysis is too sophisticated, time consuming and also highly sensitive. However, non linear static procedure such as capacity spectrum method and displacement coefficient method are found to be of great interest and as a better alternative to achieve the displacement demand and the force distribution under considered earthquake intensity.

A simplified method to find the target displacement is proposed. In this method the capacity and design curves are retained without converting into capacity and design spectrums. The technique to find target displacement in the proposed simplified method is on the conceptual basis of capacity spectrum method which is very much similar to that of equal displacement approximation or displacement co-efficient method explained in ATC-40. The proposed method is validated by comparing it with capacity spectrum method and displacement co-efficient method. Target displacement and base shear obtained by non-linear pushover analysis is validated by comparing the results with nonlinear time history analysis. The best suitable pushover pattern is taken to limit the integral abutment bridge length. The target displacement obtained by pushover analysis for seismic loading is combined with temperature displacement to find the length of integral abutment bridges built on cast-in-situ concrete piles in high temperature variation and high seismic zone.

ACKNOWLEDGEMENT

Many a times **"THANK YOU"** is so less often said that we fail to let people know how grateful we are. There always have been many people who make a big difference to us and we hardly acknowledge their contribution. I take this opportunity to place on accord my gratitude to few of those who have helped me for my study.

I wish to express my deepest gratitude for first and foremost person, Dr. D.K. Paul, Professor, Department of Earthquake Engineering, for giving me the inspiring guidance and encouragement that enabled me to undertake the studies reported in the thesis, without whom this research work could not be completed. Author is very much grateful to Dr. Ramkumar and Dr. Pankaj Agarwal for their guidance and advice, throughout his doctoral studies.

The author is highly indebted to Prof. Mahesh Tandon, Managing Director, TCPL, New Delhi for providing the opportunity to understand the concept of the research area and Dr. Susan Faraji, Professor, University of Massachusetts, is greatly acknowledged for providing the materials which helped for successful completion of the research.

Author likes to acknowledge Dr. Ashwani Kumar, Professor and Head of the Department for extending all the departmental facility during the studies. Author is very thankful for all the faculty members for their constant support throughout the research. Author takes this opportunity to thank his life time teachers Shri. L Balu, Shri. K. Shankar Narayan and Dr. V. Devaraj, who are responsible for his today's success.

Author is thankful to Ministry of Human Resources and Development, Government of India, for providing the financial assistance throughout the course of research work. Author is thankful for all non-teaching staff for the help rendered during the course.

Author would never forget the time spent with the friends in the IIT Roorkee campus where author had fruitful discussion on various aspects and memorable time.

Finally, I don't have words to express my deep sense of gratitude for the valuable encouragement, help and moral support rendered by my beloved father Shri. T.V. Venkatachaliaha and mother Smt. Varalakshmmama Venkatachaliaha through out my educational and personal life. I would like to thank my wife Ms. Deepthi, my sister Ms. Kavya Rani, brother Mr. Prathap Kumar T V and my Best Friends and other relatives for extending their support at every stage, to see this day.

(Pradeep Kumar T V)

CONTENTS

LIST OF FIGURES

LIST OF TABLES

CHAPTER-1

INTRODUCTION

Integral bridges being safe and aesthetically pleasing is gaining popularity in most of the countries including India, because of its low initial cost, reduced long-term maintenance expenses, faster construction and better seismic performance . These are single or multiple span bridges in which bearings and expansion joints are eliminated or minimized to maximum extent which are weakest link in the chain of durability and maintenance of bridges. They are designed based on the experience of the designers, in the absence of specific Codal guidelines (Mistry, 2005). The main reason for adopting integral bridges in most of the US and European states is to eliminate the expansion joints which are prone to leakage and which allows the ingress of deicing salts into the bridge deck and substructure. In integral bridges, the redundancy or static indeterminacy allows the formation of local mechanisms at selected locations for largely unknown seismic inputs. This concept in integral bridge is proved to be an excellent option for seismic prone areas.

Integral bridges are suitable for small and medium lengths. The length of the integral bridges mainly depends on the pile capacity, soil type and abutment movement due to temperature, seismic load etc. (Greimann *et al.* 1984). The analysis of integral bridge is complicated as bridge deck, piers, abutments, embankments and soil-pile interaction must be considered as a single system. The important feature in these bridges is the ability of the foundation piles to carry vertical load even when the piles are subjected to temperature and seismic induced lateral displacements. The vertical load carrying capacity of piles may be reduced due to lateral displacements.

1.1 FAILURES OF CONVENTIONAL BRIDGES

Bearings and expansion joints are weakest link in the chain in respect of durability and maintenance of the conventional bridge. Joints are expensive to buy, install, maintain and repair. Repair costs of joints can be as high as replacement costs. Even waterproof joints will leak over a time, leading to corrosion, causing damage to girder ends, bearings and supporting reinforced concrete substructures. Snow deposit and relentless pounding of heavy traffic causes damage of hardware in joints which is hazardous to motorists and a liability to owners (Wasserman and Walker, 1996). The lateral and vertical loads of superstructure transferred to the substructures through fixed and movable bearings allow longitudinal movement between superstructure and the substructure. The failure of most of the bridges in Bhuj earthquake in 2001 in India were due to the failure of bearings, non availably of seating width and failure of expansion joints. The dynamic displacement can cause significant damage to these types of bearings (Milutinovic *et al.* 1982), as shown in Fig. 1.1a. The anchor bolts connecting the bearings to the substructure or the bearings itself fail suddenly during earthquakes, resulting in the falling of the narrow seated super structure, as shown in Fig. 1.1b. Failure of the bearings can cause redistribution of internal forces, leading to failure of substructures. For the small differential movements during earthquake, expansion joints may be either pushed against each other, causing a compression type of failure Fig. 1.1c, or pulled apart, causing a tensile failure, as shown in Fig. 1.1d. In a study conducted by Federal Highway Administration for bridge maintenance requirements world wide, it was determined that joints and bearings were the major source of bridge maintenance problem. In search of solution for joint and bearing maintenance problems, engineers became aware that the bridges constructed without joints were outperforming jointed bridges by remaining in service for longer periods. Also engineers concluded that eliminating bearings and expansion joints will reduce both initial

and maintenance cost. This development in the field of bridge engineering has given rise to a new bridge technology which is structurally efficient and aesthetically superior known as integral bridge.

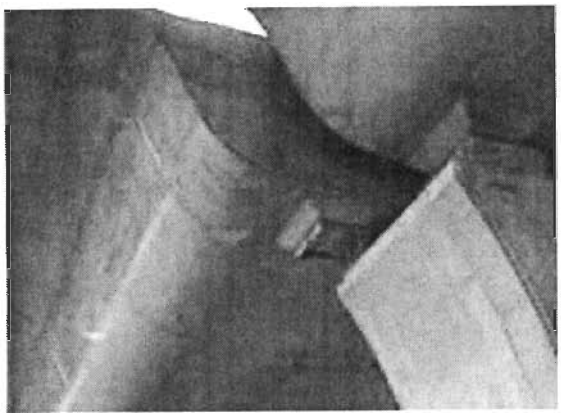

(a) Unseating of superstructure

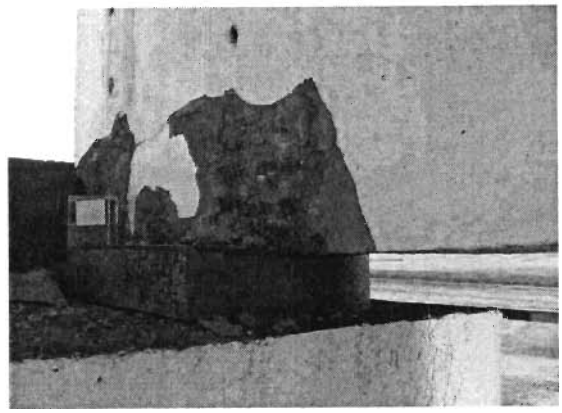

(b) Failure of anchor bolts

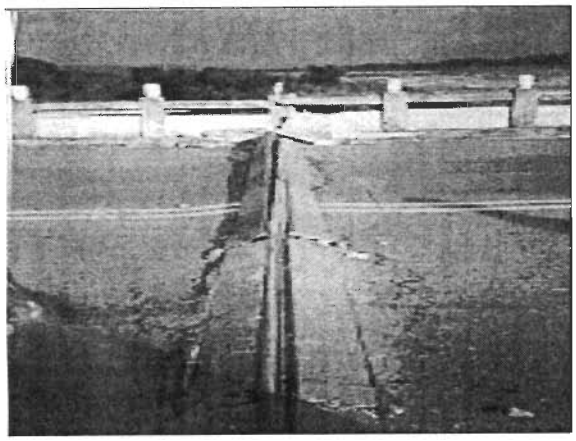

c) Compressive failure of expansion joints

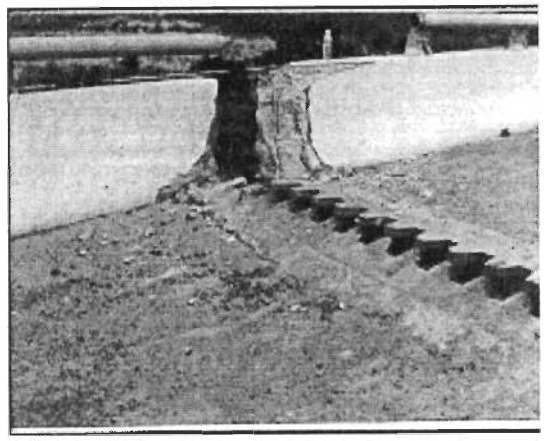

(d) Tensile failure of expansion joints

Fig. 1.1: Failure of bearings and expansion joints

1.2 INTEGRAL BRIDGES

Integral bridges are simple or multiple span bridges in which bearings and expansion joints are eliminated and the deck is continuous across the length of the bridge and connected monolithically with the abutment and piers which are supported on soil-foundation system. The use of integral pier has been demonstrated as economical and aesthetically pleasing (Bekir and Chung, 1999 and Jayaram *et al.* 2001). Integral bridges can be classified mainly into three types, Full Integral Bridge, Semi-Integral Bridge and Deck Extension Bridge (Rodolfo and Petro, 2005)

1) In full integral bridge/ integral abutment bridge the beams or girders are cast into a concrete end diaphragm which is connected to a concrete pile cap generally supported by a single row of piles as shown in Fig. 1.2.

2) Semi-integral bridges are having continuous superstructure supported by abutments which are structurally separated as shown in Fig. 1.3. The key advantage of these bridges is that the superstructure behavior is independent of the foundation type. A small gap is provided between the integral backwall and the substructure to allow it to move freely in the longitudinal direction. The concept of semi-integral bridges is being adopted at places where rigid abutments or long span integral bridges are necessary (Burke, 1994).

3) In deck extension integral bridges, the deck slab is extended from the end piers and taken over the traditional backwall into adjoining approach pavement as shown in Fig. 1.4. In India, the integral bridges which have a continuous superstructure with integral piers are built with the expansion joints near abutment face (Tandon, 2000 and 2005) as shown in Fig. 1.5. The main beams or slab is not cast into a concrete end diaphragm and is preferred because the abutment backfill design is not a serious issue and they can be adopted for the flyovers in urban areas.

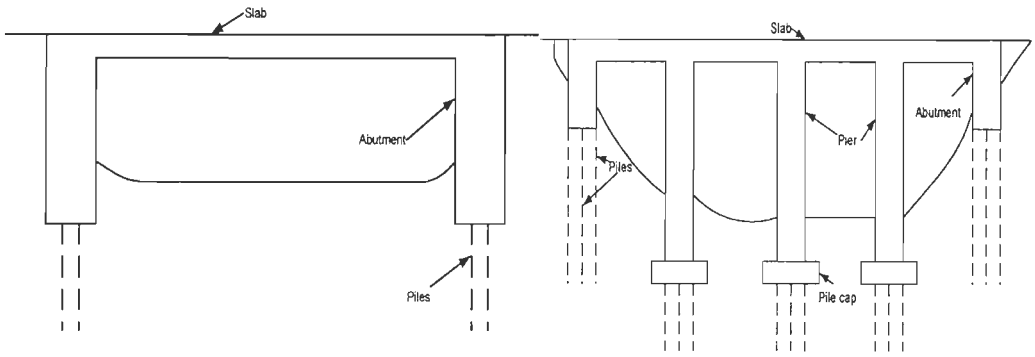

Fig. 1.2: Integral abutment bridge or full integral bridge

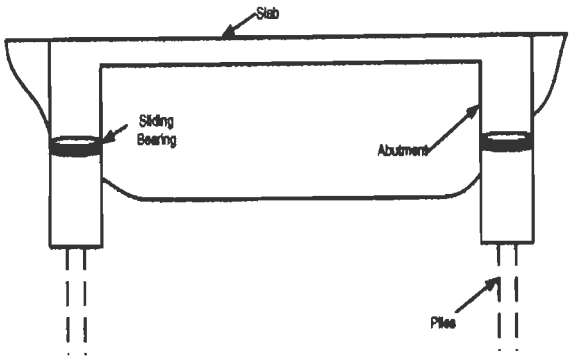

Fig. 1.3: Semi-integral bridge

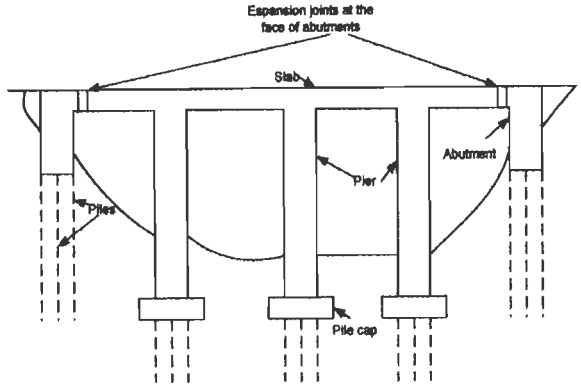

Fig. 1.4: Deck extension integral bridge

Fig. 1.5: Deck extension integral flyover built in New Delhi, piers integral with superstructure and expansion joint near abutment backwall

Several integral bridges have been built in high temperature and high seismic zones in India upto a length of 150m (Pandey and Tandon 2005). The integral connections between deck slab and piers enhance the seismic performance and also provide graceful and elegant appearance to the structures, as shown in Fig 1.6. Most of the integral bridges are built on cast-in-situ piles with different superstructure configuration such as cast-in-situ girders with reinforced (RC) slabs, cast-in-situ voided slabs, precast RC girders with composite RC deck, steel girders with concrete composite deck etc as shown in Figs. 1.6 and 1.7. Integral abutment bridge with 70^{o} skew is constructed successfully for Delhi Metro Rail Corporation Ltd. (DMRC), India, shown in Fig. 1.8. Many integral flyovers are

constructed in the heart of urban cities like Delhi as shown in Figs 1.9 and 1.10. Similar flyovers at the intersection of outer ring road are under construction. One of the proposed constructions of grade separation at Mukarba Chowk GT Karnal Road – New Delhi, is shown in Fig 1.11.

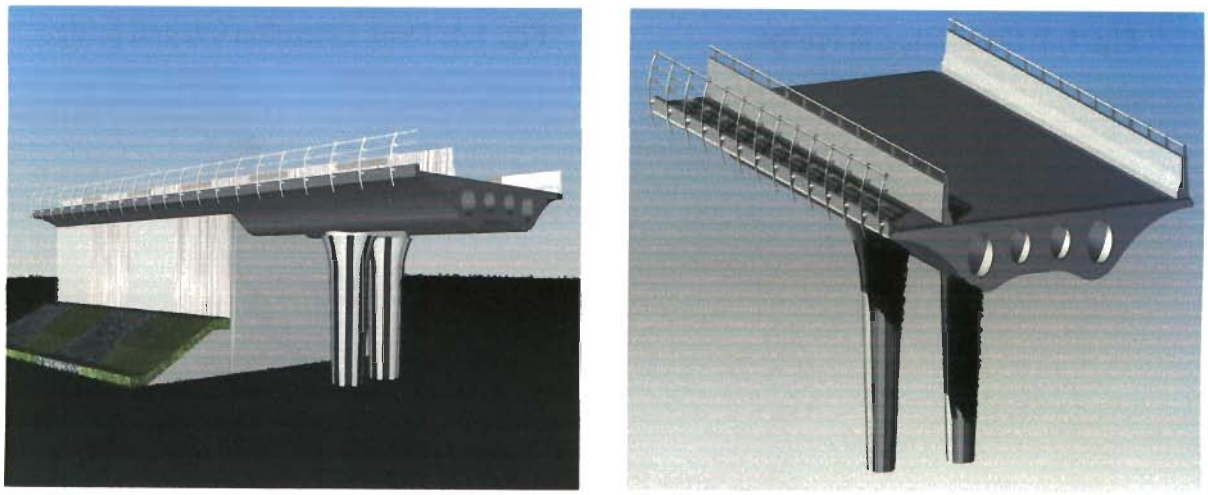

Fig. 1.6: Cast-in-situ piers integral with voided deck slab - used in Kalkaiji Flyover (Courtesy-Tandon Consultants Pvt. Ltd.)

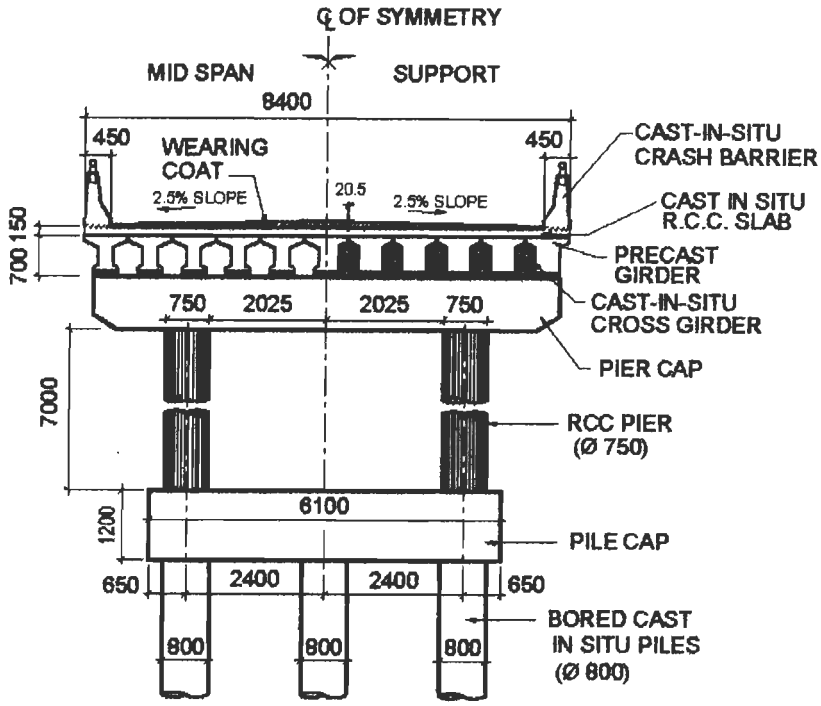

Fig. 1.7: Cross-section of cast-in-situ piles, piers and precast girders used in integral bridge (Courtesy-Tandon Consultants Pvt. Ltd)

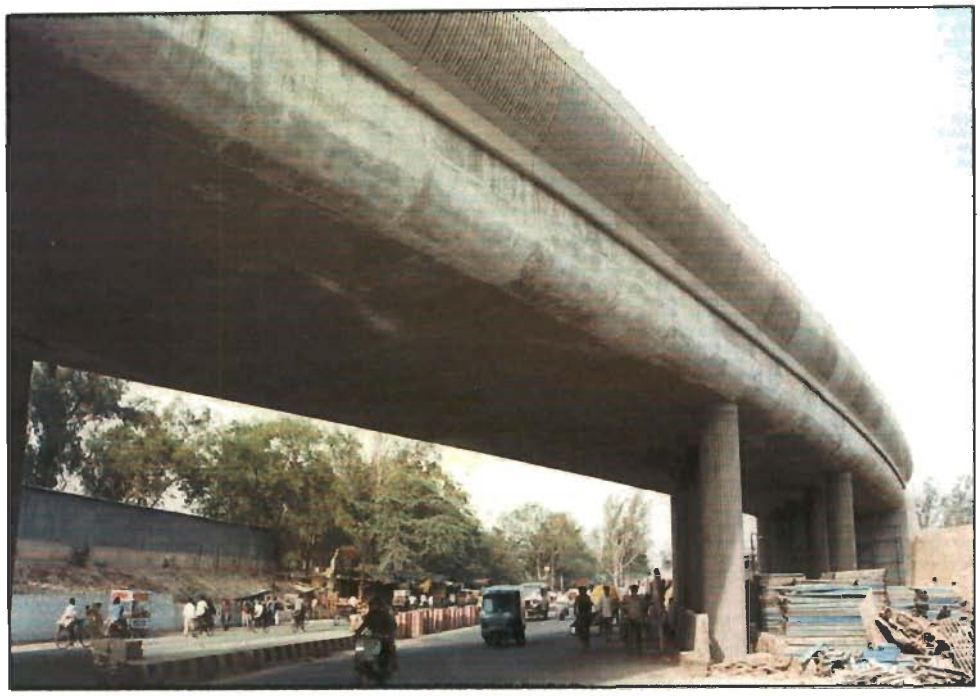

Fig. 1.8: Integral abutment bridge flyover for Delhi Metro with 70^{o} skew

Fig. 1.9: Integral concept used in Khegon Marg intersection flyover, New Delhi, India

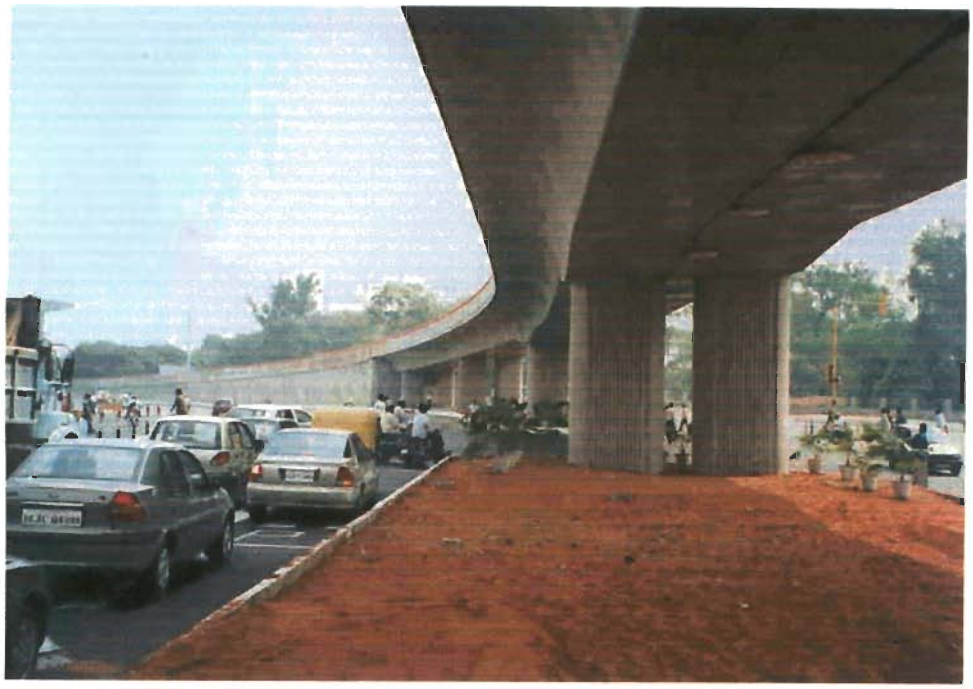

Fig. 1.10: Integral flyover with RC voided slab in Kalkaiji flyover, New Delhi, India

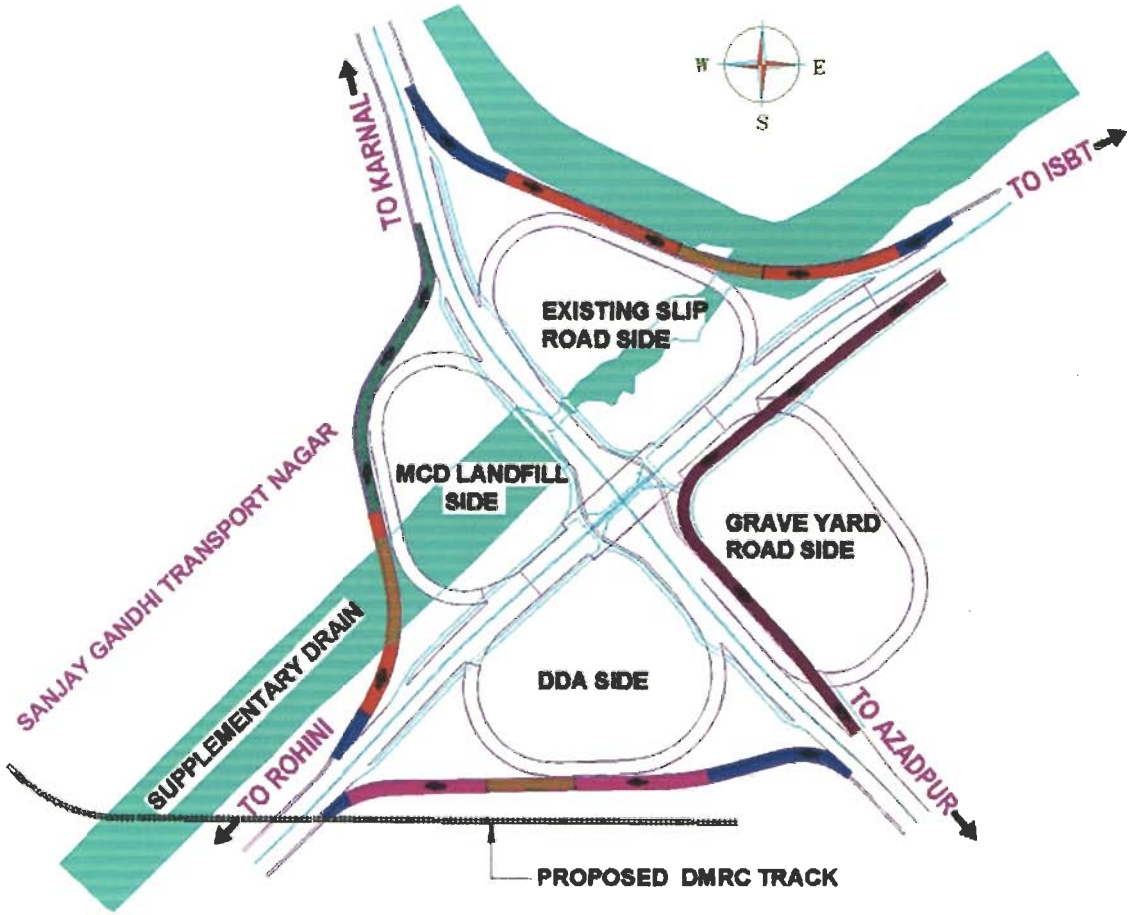

Fig. 1.11: Construction of grade separation at Mukarba Chowk GT Karnal Road New Delhi, outer ring road junction-Integral bridge loops (Courtesy-Tandon Consultant Pvt. Ltd.)

Tennessee and Sweden suggested that the integral abutment bridge of length upto 100 m can be achieved without incurring problems (Prithchard, 1994). Tennessee is having an experience of more than 50 years in building jointless bridges and it has a current inventory of over 2,400 integral abutment bridges, up to 120 m long with steel girders, and 240 m using concrete. According to Scottish executive development department, BA 42/96 (1996) all the bridges need to be continuous over intermediate supports and bridges with overall lengths not exceeding 60 m and skewness not exceeding 30° are to be integral with their abutments.

The design of integral bridges by most of the designers is based on judgment and empirical rules rather than on scientific and engineering understanding of material and structural response. The reasons for not attempting more designs of integral bridges from last 50 years may be absence of rational design methods and guidelines or the absence of any performance evaluation of such structures (Hussain and Bagnariol, 1996). Presently the concept of integral bridges are gaining popularity in all the countries including India, because of reduction in capital cost, greater flexibility in span configuration, and considerably reduced maintenance, improved construction tolerance, increased structural redundancy and enhanced seismic resistance. For the better design process, performance evaluation of integral bridges is very essential.

1.3 STATEMENT OF THE PROBLEM

The performance of integral bridges is not well known. Moreover, rational design methods are required to increase the design and construction of integral bridges. Due to the elimination of bearings and expansion joints, all the lateral forces due to temperature, shrinkage, creep and seismic effects will be transferred to the substructures and then to the soil. Analysis of integral bridges without considering non-linear backfill and soil-pile interaction is impractical. As in most of the long span bridges, soil responds beyond the

elastic limit. The length of integral bridges is determined by the soil response and the capacity of substructures. Most of the integral bridges are constructed in non-seismic regions, where the research has concentrated on secondary stresses, mainly temperature which has affected the integral bridge construction. The construction of integral bridges is increasing in India, California and other places, which are highly seismic zones. Thus, it is very much necessary to study the capacities of these integral bridges in resisting various levels of seismic loading. As in regions of high seismicity, seismic displacement demand can be significantly more than the thermal movements.

Most of the bridge agencies use steel H-piles for integral bridges, which have greater flexibility in comparison to concrete piles. In India, most of the integral abutment and deck extension bridges are constructed on bored-cast-in-situ concrete piles. These bridges are located in the regions having high temperature variation and high seismic zones, where the length of bridge is restricted by lateral pile capacity due to temperature loading or seismic loading or a combination of both as mentioned in Indian codes. The absence of specific IRC codes or guidelines on the design and detailing issues has dampened the construction of integral bridges in India (Bhowmick, 2005). It is necessary to study the performance of these bridges to provide the guidelines for designers.

Non-linear static and non-linear dynamic analyses are required to study the performance of integral bridges under temperature and seismic loadings. Nonlinear dynamic analysis is too sophisticated and time consuming. However, non linear static procedure such as capacity spectrum method and displacement coefficient method are found to be of great interest and as a better alternative to achieve good results for nonlinear seismic analysis. The main objective of this study is to provide better understanding on the behavior of integral abutment bridges and to evaluate its response towards temperature and seismic loadings and also to limit its length based on the yield capacity of cast-in-situ piles.

1.4 OBJECTIVES AND SCOPE OF PRESENT RESEARCH

i. Critical review of literature on modeling of soil-pile and abutment backfill interaction and the behavior of integral abutment bridges under lateral loadings.

ii. To select a best suitable existing non-linear model for soil-pile and abutment-backfill interaction that represents the actual behavior of integral abutment bridge and to develop a program for the models using MATLAB and use them as input in the finite element program.

iii. To develop a complete three dimensional, nonlinear finite element model of integral abutment bridges including soil-structure interaction and to validate the model by comparing the results with published results.

iv. To conduct parametric study by nonlinear static analysis on three dimensional finite element model and study its behavior under temperature loading. Further to assess the maximum length of integral abutment bridge under different soil conditions and structural configurations.

v. To perform nonlinear time history analysis and pushover analysis to obtain the displacement demand and the force distribution in the integral abutment bridges and to propose a simplified empirical method of analysis to find out target displacement under the considered earthquake intensity. Also, to compare the results of the nonlinear time history and pushover analysis to validate the results and use the best suitable pushover pattern to limit the integral bridge length.

vi. To develop the recommendations for the maximum length of integral abutment bridge on cast-in-situ piles under different soil conditions by representing the static and dynamic displacement in the form of temperature loading.

1.5 OUTLINE OF THE THESIS

The thesis is spread across seven Chapters and References

The **Chapter 1** gives an overview of the integral bridges along with the problem stated and the objective of the research study.

Chapter 2 consists of literature review concerning the performance of integral bridges under temperature and seismic loading conditions. It also consists of a brief review of the published literature on the analytical modelling, experimental and field studies of integral bridges.

Chapter 3 briefly discusses about the analytical models available for non-linear soil pile response for both sand and clay soil. It also summarizes the available design curves and recommended relationships by interpreting the design curves given in different manuals for the estimation of lateral earth pressure behind abutment walls. The available design curves have been compared with the recommended relationships of the test results to choose the best suitable relationship for modelling.

Chapter 4 describes the three dimensional finite-element models of integral bridges for nonlinear static and dynamic study. The models includes soil interaction with the abutment and piles. The finite element model is verified by comparing the results with published literatures for temperature effect.

Chapter 5 presents the effects of longitudinal temperature variation on integral bridges. Parametric studies are performed to investigate the significance of interactions among the abutment-backfill and soil surrounding the pile. The maximum lengths of integral bridges are arrived using 1.0 and 1.2 m dia bored cast in-situ concrete piles under different

structural configuration and soil conditions by conducting non-linear static analysis, based on the maximum yield capacity of the piles.

Chapter 6 presents the non-linear time history analysis by considering five different response spectrum compatible time histories and its comparison with non linear pushover analysis to obtain the displacement demand and the force distribution under considered earthquake intensity. A new simplified method to determine target displacement is recommended. Seismic load is combined with temperature to find out maximum length of integral abutment bridge.

Chapter 7 summarizes the study and presents the recommendations drawn from the research. Finally , suggestions for future research work are presented.

CHAPTER-2

INTEGRAL BRIDGES - A REVIEW

2.1 INTRODUCTION

Integral bridges are also known as integral abutment bridges, rigid-frame bridges, portal bridges, jointless bridges, semi-integral bridges and deck-extension integral bridges. The Ohio, South Dakota and Oregon started the use of continuous bridge construction in the 1930's and California started the use of jointless bridges in 1950's (Wasserman and Walker, 1996). Along with the development of continuous bridge concept, integral abutment was introduced to achieve jointless bridge. In 1960's, bridge maintenance research stated that joints and bearings are major sources of bridge maintenance problems, it was observed that bridge constructed without joints were performing well when compared to conventional bridge with joints. Minimum damage like cracking in abutments was observed in the jointless bridges, which were not detrimental to serviceability. In 1960's, Tennessee and five other states adopted continuous bridges with integral abutments as standard construction. In 1970's and 1980's New York state department of transportation (Yannotti *et al.* 2005) started the construction of integral abutment bridges on the experimental basis. In a survey conducted by Federal Highway Administration (FHWA), there were about 7000 integral abutment bridges and 1100 deck extension integral bridges in 1995 but in 2004 it was having approximately 13000 integral abutment and 3900 deck extension integral bridges in 50 states (Rodolfo and Petro, 2005). In India, more than 50 integral bridges have been constructed since last 5 years, but this number may exceed more than twice in another 3 years. On all the interchanges and overpasses, nearly 45 bridges in the upcoming Bangalore-Mysore corridor in India are designed as

integral bridges (Bhowmick, 2005). Most of these bridges are on cast-in-situ concrete piles.

2.2 LOADS INFLUENCING THE BEHAVIOUR OF INTEGRAL BRIDGES

Primary loads on integral bridges are dead and live load. The primary concern in the design of integral bridges is the high stresses caused due to seismic forces and secondary loads like shrinkage, creep and thermal gradients. In secondary loads, thermal-induced movement of an integral bridge causes larger stresses in integral bridge components (Lawver *et al.* 2000) and therefore they should be given careful consideration. They are subjected to passive pressure effects when abutment backfill is compressed during superstructure elongation. The stresses developed as a result of thermal movement are functions of bridge geometry, soil properties and pile design. Due to the soil-structure interaction it is difficult to predict the stress levels accurately. The effects of creep and shrinkage have been ignored by many designers (Rodolfo and Petro, 2005). Their effects are considered to be small when compared to the effects of thermal movement. The most of the integral bridges are constructed in non-seismic regions where the research has been concentrated on the secondary stresses mainly due to temperature, which have affected the integral bridge construction (Patty *et al.* 2001). The concept of integral bridges have started gaining popularity in most part of the India, California and other place· ·hich are highly seismic zones, because of its better seismic performance (Tandon, 2005). Hence, it is very much necessary to study the capacities of these integral bridges in resisting various levels of seismic loading.

2.2.1 Temperature Loading

Integral bridges are designed for the same temperature ranges as other bridges. The effective temperature is the temperature that governs the overall longitudinal movement of

the bridge superstructure. High stresses can develop in the components of an integral bridge when the structure undergoes the thermal length changes of its bridge deck. Article 3.12.2 in the AASHTO LRFD (2004) Bridge Design Specifications recommends two procedures for calculating effective bridge temperature. Second procedure (procedure 'B') is recommended for determining the temperature of integral bridges (Oesterle and Volz, 2005). This specification presents maps of the United States that show temperature isobars of minimum and maximum, bridge temperatures for steel-girder and concrete-girder bridges. Clause 218 of Indian Road Congress (IRC: 6-2000) gives the isotherms of shade air temperature to calculate effective bridge temperature for Indian conditions. The total movement of the superstructure due to temperature Δeffect shall be determined as (Roeder, 2003)

$$\Delta = \varepsilon_t L \qquad \ldots (2.1)$$

$$\varepsilon_t = \alpha \Delta T_{ave} \qquad \ldots (2.2)$$

where, ε_t is the temperature strain; ΔT_{ave} is the average change in temperature; L is the total length of the bridge (m) and α is the coefficient of thermal expansion (mm/mm/^{0}C). The coefficient of thermal expansion α depends on nature of cement, aggregate, cement content, concrete age, the relative humidity and the sizes of sections. Girton *et al.* (1991) recommended the coefficient of the thermal expansion from 4.5×10^{-6} in/in/°F (8.1 $\times 10^{-6}$ m/m/°C) to 5.0×10^{-6} in/in/°F (9.0 $\times 10^{-6}$ m/m/°C) for bridges. From the experiments Oesterle *et al.,* (1999) recommended the value of α = 4.9×10^{-6} in/in/°F (8.82 $\times 10^{-6}$ m/m/°C). Article 5.4.2 of the AASHTO and Clause 5.4.7 of BS 5400 recommends different specification for α. Indian code IS: 456-2000 gives the value of α for concrete with different aggregates as shown in Table 2.1. Measured deck coefficients for different decks by different researchers are shown in Table 2.2. Since thermal movements of

integral bridges are a key parameter of their behavior, it is important to make an accurate estimate of the coefficient of thermal expansion.

Table 2.1: Thermal coefficient with different aggregates (IS: 456 -2000)

Type of aggregate	Quartzite	Sandstone	Granite	Basalt	Limestone
Coefficient of thermal expansion for concrete /^{0}C (10^{-6})	12.0 to 13.0	9.0 to12.0	7.0 to 9.5	8.0 to 9.5	6.0 to 9.0

Table 2.2: Measured thermal coefficient

Ref	Location	Deck	α/$^\circ$C (10^{-6})
Girton,1989	Iowa(Boone)	Concrete-limestone aggregate	8.1
Girton,1989	Iowa(Maple)	Concrete-gravel aggregate	9.0
Darley, 1995	UK	Concrete on rock	11.3
Darley, 1995	UK	Concrete on stiff clay	13.7

2.2.2 Seismic Loading

Integral bridges are termed as seismically safe structures because of their better performance in past earthquakes (Mistry, 2005). The continuity between the superstructure and substructure increases the redundancy which can allow the formation of local mechanisms at selected locations in which design detailing can be provided for large inelastic ductile deformations. Seismic bridge design places these inelastic mechanisms, or plastic hinges, in the columns where damage can be inspected and repaired without bridge closure. Concrete substructures have high axial load carrying capacity and with proper transverse reinforcement, large flexural capacities and ductile deformations can be achieved making it an ideal material for bridge columns to provide the required plastic hinge deformation during seismic loading. To ensure that the inelastic mechanism occurs

in the desired location of the column, adjacent members must be designed to ensure elastic response.

The seismic loading is uncertain and hence seismic displacement demand can be significantly more than the thermal movements in regions of high seismicity (Patty *et al.* 2001). Predicting the distribution of seismic forces on different elements of the bridge is a difficult task, because the seismic respons of integral bridges are greatly affected by soil-structure interaction. Dynamic forces exerted by the backfill soils on the abutments and soil-pile interaction will have great effect on seismic forces and its distribution. Monolithic abutments were found to be the best by Caltrans Seismic Design Manual (2004) because of their additional capacity to absorb or dissipate the seismic energy in both longitudinal and transverse directions. Many studies have shown that abutment response significantly influences the response of short and medium length bridges (Chen and Penzien, 1975). The integral bridge design also depends on the connection of the superstructure to the piers and the abutment for the transfer of horizontal forces. The connections should be properly designed to transform such forces without damage to the piles or the soil behind the abutment. Sritharan *et al.* (2005) made an experimental study on integral bridge pier system consisting of concrete column and steel girders to test the seismic response on the integral bridge pier system and suggested a design approach for column to cap connection using simplified strut-tie-model. Torsional behavior and moment capacity of the bent cap was investigated for seismic loading by Patty *et al.* (2002) and found that the concept of capacity design used for reinforced concrete bridges in seismic regions can also be applied to a steel plate girder superstructure bridge integrally connected to a single column concrete substructure with a concrete bent cap.

2.3 PERFORMANCE OF INTEGRAL BRIDGES

In the survey conducted by Greimann *et al.* (1984), twenty nine out of fifty two agencies indicated the use of integral abutment bridges. Survey revealed that the construction details for an integral bridge vary widely from state to state. The length of integral bridge was established on the basis of experience and engineering judgment. Pile head was considered either hinge, fixed or partially restrained to the bottom of the abutment and the use of pile caps was varied. The length was limited to 265 ft (80.79m) for bridges with integral abutments as conservative side using HP steel piles. Few states showed the detailing of predrilled hole filled with loose sand at the top of the pile to reduce the pile stresses. The analytical work conducted by Greimann *et al.* (1987) recommended the pile construction in a predrilled hole to reduce the pile stresses significantly for lateral loadings. They recommended further research on the effect of horizontal displacement on the passive pressure behind the abutment and also construction of integral bridges using ductile concrete and timber piles.

The FHWA Technical Advisory Committee recommended the length limits for integral abutment bridges to 91.4 m for steel, 152.4 m for poured-in-place concrete and 182.9 m for prestressed concrete (Wolde-Tinsae *et al.* 1987). These tentative FHWA length recommendations have indeed been exceeded by some highway agencies like Tennessee and Missouri. Bridge engineers for the State of Tennessee permit the construction of the longest, PC-girder, integral-abutment bridges of 800 ft (243.9m).

Most of the integral bridges were found on Steel HP piles, but cast-in-place, prestressed, pipe and concrete-filled steel-sheet piles have also been used. The design and performance of integral-abutment and semi-integral-abutment bridges in Ontario, Canada was reported

by Hussain and Bagnariol (1999, 2000) and the report showed that both bridges exhibit good performance and only minimal signs of distress were observed.

A survey performed by Kunin and Alampalli (1999) for the New York State Department of Transportation discussed the various aspects including bridge lengths, skew-angle limits, design assumptions, design procedures, and analytical procedures. State of Arizona, based on their experience with expensive repairs of the approach slabs, did not recommend the use of integral-abutment bridges. Very small problems like minor cracking in the deck near the piers, concrete cracking and spalling in bearing areas, drainage problems for the abutment backfill, and settlement of the bridge-approach slabs were reported by other design agencies. The majority of the bridge-design agencies followed the AASHTO specifications for calculating concrete-shrinkage strains and selecting the coefficient of thermal expansion and contraction of steel and concrete elements. The survey showed that passive-soil pressure was considered in the design of integral-abutment bridges. Twelve out of thirty design agencies used pre-bored holes for the abutment piles to reduce temperature stresses. Few design agencies neglected the effect of earth pressure on the abutments during longitudinal expansion of the bridge. The States of Alaska and North Dakota considered specific soil pressure regardless of the actual design conditions. Survey also revealed most of the integral bridges were found on steel HP piles, but cast-in-place, prestressed, pipe and concrete-filled steel-sheet piles are also used. Kunin and Alampalli (2000) found that design practice and assumptions concerning limits of thermal movements, soil pressure and pile design vary considerably among the design agencies and they are based on past experience of designers. He suggested the investigation by testing and analysis to ensure efficient and reliable design.

2.4 ANALYTICAL STUDY OF INTEGRAL BRIDGES

A girder extension model was developed by Girton *et al.* (1989) to predict the longitudinal bridge displacements caused due to change in bridge temperatures. Abutment rotations and passive soil pressures behind the abutment were neglected. The strains in the steel H-pile were predicted in weak axis using a fixed-head model. The pile is idealized as an equivalent cantilever with a length determined by the surrounding soil conditions and pile properties. Both the girder extension model and the fixed-head model are concluded to be conservative for design purposes. A longitudinal frame model was also developed to account for abutment rotations. The longitudinal displacement and weak axis pile strains predicted by frame model was better than the simpler models.

A comparative analytical study was taken by Thippeswamy *et al.* (1995) on five in-service integral abutment bridges. The analysis was performed using two-dimensional frame models considering different loading conditions such as gravity, soil pressure, creep, shrinkage and temperature. The effect of orientation of abutment steel H-piles in strong or weak axis were studied. They concluded from the analysis that temperature loading produces significant stresses in the bridge. Concrete creep and shrinkage reduces the bending stresses due to temperature rise; soil pressure induces negligible stress in the bridge.

Siros (1995) developed a non-linear three-dimensional model of a composite steel girder integral abutment bridge to predict the forces in the bridge that are induced by temperature, creep and shrinkage. The uniform temperature was applied along the length of the bridge superstructure and temperature gradient across the depth of concrete deck. The different boundary conditions were considered at the bottom of the abutment. Horizontal stiffness of back soil was based on lower bound or upper bound. He compared

the stresses obtained for 3D model with linear two dimensional analytical model and found very small difference in the results obtained by two different analytical models.

Faraji *et al.* (1997, 2001) performed a three-dimensional finite-element analysis on a three-span, non-skewed, steel girder, integral-abutment with H-piles considering non-linear soil response by varying the levels of soil compaction in the cohesion-less soils behind the abutment wall and adjacent to the piles for temperature loading using GT-STRUDL program. Two geometric conditions were considered for the horizontal alignment between the girders and the deck. One model considered the vertical eccentricity between the center of gravity of the girders and the mid-thickness of the bridge deck and other model without the eccentricity effect. The soil backfill behind the abutments and the soil along the length of the piles were modeled as uncoupled non-linear springs. The results showed that the vertical eccentricity between the center of gravity of the girders and the mid-thickness of the bridge deck must be considered to properly predict bridge behavior. The study was conducted by varying the soil conditions behind the abutment wall and next to HP piles. The results concluded that the full passive pressure was reached behind the abutment backfill and the distribution of the soil pressures over the depth of an abutment was nonlinear. They suggested to study the effect of predrilled holes with loose granular fill and varying backfill for thermal, gravity and seismic loads to streamline the design process for integral abutment bridge.

A nonlinear, finite-element analysis that involved the interaction between an abutment and the soil backfill was conducted by Oesterle *et al.* (1999 and 2005). They concluded that for large abutment thermal movement the Rankine passive-soil-pressure model provides an adequate estimation of the soil pressures behind the abutment and the design curves given by Clough and Duncan gives upper-bound value. They noted that high soil pressure occurs near the base of an abutment and the base pressure decreases with an increase in the

abutment rotation. Decrease in the compaction of the soil backfill from 90 to 80 percent results in reduction of passive-soil-pressure force by a factor of about 2.5. Also, decrease in the slope of the in-situ soil backfill from 45 to 30 deg resulted in decrease of resultant passive-soil-pressure force by 2.

Dicleli (2000, 2001) developed the computer program capable of analysing an integral bridge accounting for the earth pressure coefficient for the backfill soil as a function of abutment's lateral displacement and also taking into consideration the non-linear force-deformation relationship of the members. Dicleli and Suhail (2003 and 2004) studied the maximum length limits for integral bridges based on the ability of steel H-piles supporting the abutments to sustain thermal induced cyclic lateral displacements and the flexural capacity of the abutment. The nonlinear behavior of the piles and soil–bridge interaction effects are implemented in nonlinear structural models of two typical integral bridges. Static pushover analysis of these bridges are conducted using 2D model to study the effect of various geometric, structural and geotechnical parameters on the performance of integral bridges subjected to uniform temperature variations. Pushover analyses results were used to develop the guidelines and to determine the maximum length of integral bridges. In sandy soil, they recommended the maximum length of concrete integral bridges to 190 m in cold climates and 240 m in moderate climates where as steel integral bridges are limited to 100 m in cold climates and 160 m in moderate climates. In clayey soil, they recommended the maximum length of concrete integral bridges to 210 m in cold climates and 260 m in moderate climates and steel integral bridges are limited to 120 m in cold climates and 180 m in moderate climates.

Arockiasamy *et al.* (2004) carried a parametric study to know the response of laterally loaded piles supporting the abutment of the integral abutment bridge under various conditions. Eleven conditions were considered in the study taking the effect of predrilled

hole filled with sand having different degrees of compaction, predrilled hole with different depths, piles without a predrilled hole, different types of soil, pile orientation and variation in the elevation of the water table. The moment-induced secondary pile forces are determined by considering passive earth pressure, horizontal force and moment induced in the pile from horizontal translation by using LPILE and FB-Pier programs. He found that the piles with predrilled holes are more flexible and experience slightly lower stresses when compared with those without predrilled holes and bending moment are found to be higher for the piles in stiff clay and dense sand.

2.5 EXPERIMENTAL AND FIELD STUDIES ON INTEGRAL BRIDGES

The full scale field test program was conducted on steel H-shaped friction piles by Greimann *et al.* (1987) to study the effect of longitudinal expansion and contraction of bridge superstructure on vertical load carrying capacity of pile. Piles were subjected to three different load cases such as vertical load, horizontal load and combined horizontal and vertical loads. The results were compared with the analytical model by assuming the nonlinear soil springs as uncoupled springs, described by Ramberg-Osgood equations. The analytical results compared well for the test cases.

Kamel *et al.* (1996) studied the lateral-load versus lateral-displacement relationship for both prestressed concrete piles and steel H-shaped piles. The lateral displacements was found to be larger in steel piles than that of prestressed concrete piles before the allowable-moment strength was developed for a cross section of the pile. Laboratory tests revealed that piles placed in pre-bored holes for integral-abutment piles had a significant effect on the lateral displacements of both types of piles. The lateral displacements of a pile head were dependent on the lateral stiffness of the soil against the upper 10 ft (3.05m) of the pile length. The lateral stiffness of the soil below this depth had a negligible effect on the

lateral displacement at the pile head. This behavior was observed for both the prestressed concrete and steel piles.

Based on experimental and analytical data BA 42/96 (1996) provides different equations to calculate earth pressure on different types of integral abutments. For bank pad abutment which acts as an end support must have adequate weight and the end span should have adequate flexibility, to avoid uplift from live load or from differential settlement. The end screen abutment acts only as a retaining wall for embankment earth pressure and transfers longitudinal loads. The vertical loads on the deck are supported by separate supports, which are usually located within two meters of the end screen in order to limit the vertical movement of the end screen. The typical height of an end screen or bank pad abutment is up to 3 meters. The earth pressure coefficient K for bank pad, end screen and embedded abutments is given by

$$K^* = K_o + (d/0.025H)^{0.4} K_p \qquad \ldots (2.3)$$

The framed abutment supports the vertical loads from the bridge and acts as a retaining wall for embankment earth pressure. The magnitude of passive pressure acting on the wall is significant. The pressure coefficient K for these abutments shown in Fig. 2.1 is given by

$$K^* = (d/0.05H)^{0.4} K_p, \qquad K \le 0.6 \qquad \ldots (2.4)$$

For portal frames having the hinge at the base of its leg, the earth pressure coefficient is

$$K^* = K_o + (d/0.03H)^{0.6} K_p \qquad \ldots (2.5)$$

where, K_p is the passive pressure coefficient for backfill material with friction angle ϕ and wall friction $\delta = \phi/2$ and K_o is the coefficient of earth pressure at rest. The Guidance note also stipulates that K^* should be greater than the earth pressure at rest K_o.

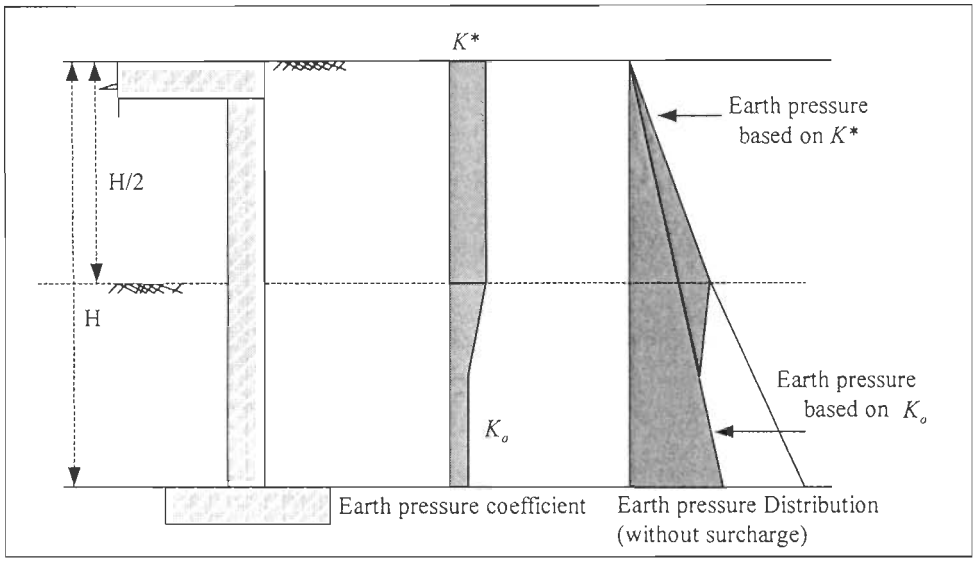

Fig. 2.1: Earth pressure distribution on framed abutments (BA 42/96 -1996)

The influence of daily and seasonal displacements, effect of superstructure type, bridge length, settlement and resulting backfill pressures were studied by England *et al.* (2000) on integral abutment walls. He investigated the abutments backfilled with granular material with a pinned base to understand the temperature induced cyclic soil-structure interaction. The tests were carried out to simulate the movement of 60, 120 and 160m span bridges over a 50°C temperature range. The following recommendations were drawn from the experimental results

(i) England et al. recommended the earth pressure to calculate using

$$K^* = K_o + (d/0.03H)^{0.6} K_p \quad \ldots (2.6)$$

(ii) Settlement of abutments for bridges upto 60m long and with strip footings is not considered to be significant.

(iii) Seasonal and daily temperature cycles were considered to play an important role in defining the interaction problem and recommended both to be considered in calculations.

The recommendations proposed by England *et al.* (2000) are based on limited experimental data. Therefore, while practical design it should be taken care.

The ability of the piles and the abutments to withstand cyclic loads was investigated by Arsoy *et al.* (1999, 2000 and 2002) by conducting large-scale cyclic load tests. Three pile types and three semi-integral abutments were tested in the laboratory. Numerical analyses were conducted to investigate the interactions among the abutment, the approach fill, the foundation soil, and the piles. The revised hinge detail shown in Fig. 2.2 performed well compare to other hinge details. Steel H-piles are recommended when compared to pipe piles and concrete piles. Numerical analyses indicate that the interactions between the approach fill and the foundation soils create favorable conditions for stresses in piles supporting integral bridges by softening the foundation soil.

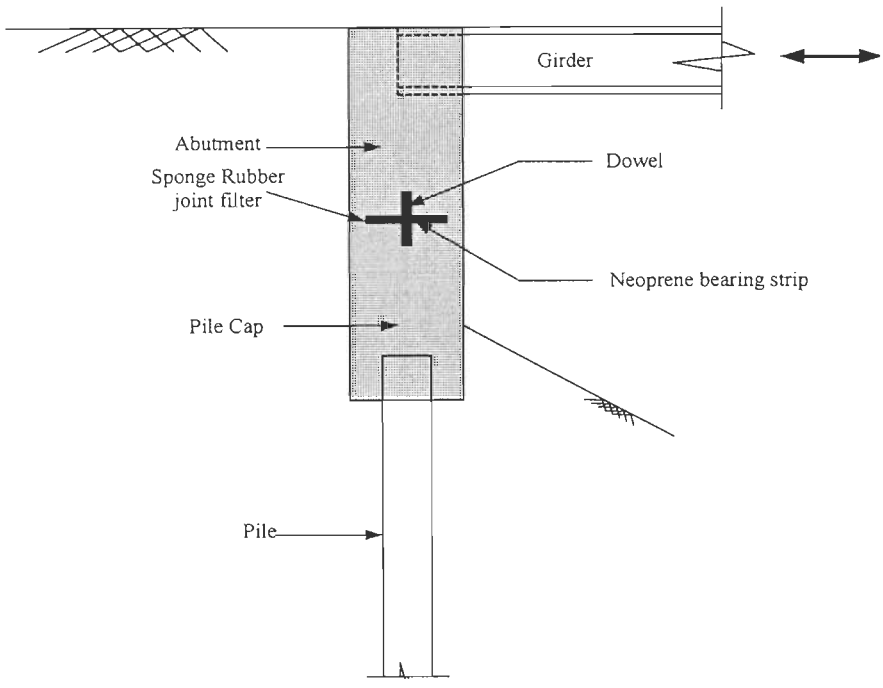

Fig. 2.2: Hinge details in the abutments (Arsoy *et al.* 2002)

Darley and Alderman (1995) measured the thermally-induced cyclic movements of two portal-frame bridges consisting of reinforced concrete abutments and solid reinforced concrete decks as shown in Fig. 2.3. The aim was to test whether the thermal expansion of

a bridge can be accommodated by deck to a certain extent. They determined that most of the bridge expansion was accommodated by movements of the abutments.

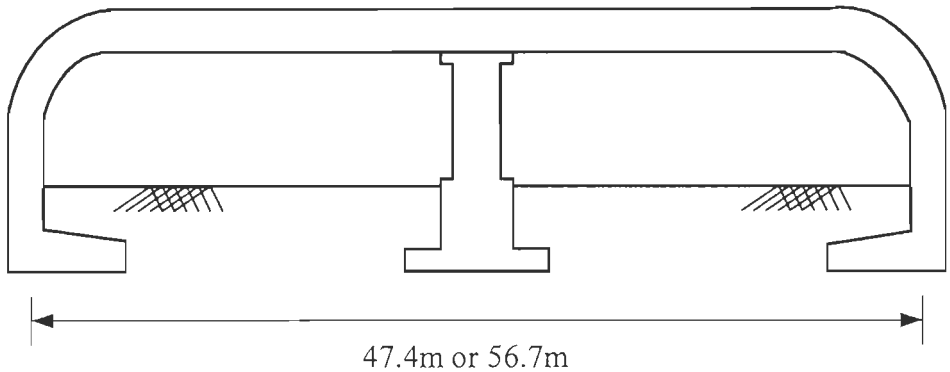

Fig. 2.3: Portal frame bridge (Darley and Alderman,1995)

The Long-term monitoring of PC-girder integral-abutment bridge was performed by Lawver *et al.* (2000) in Minnesota. The abutments were shallow and supported by a row of six steel piles of 24 m long and oriented in weak-axis bending. The investigation was started in 1996 with 180 instruments installed in and around the bridge. Double-curvature bending was observed in the abutment piles. Tensile strains were recorded in a reinforcing bar in the approach slab near the connection of the slab to the deck of the bridge during winter, when the superstructure is pulled away from the abutment backfill. The axial strains caused by the weight of the bridge superstructure were also measured in specific piles. As the temperature of the bridge deck increased, the axial strains increased in an interior pile and decreased in an exterior pile for the abutment. The maximum, compressive strains in an abutment pile that were induced by combined, axial forces and bending moments were larger than the yield strain of the steel for the pile. This maximum strain was measured in the flange tips of the pile near the pile cap and on the approach-slab side of the monitored exterior pile.

The abutment and piles of Scotch road integral abutment bridge built over I-95 interchange in Trenton consisting of composite concrete slab, reinforced concrete

substructure and integral abutments supported on steel piles was instrumented during and studied by Yasser and Hassiotis (2004 and 2005), Hassiotics et al. (2005) and Roman *et al.* (1998) . The displacement induced by temperature changes were measured in the field and used as an input to the three-dimensional non-linear finite element model developed using ABAQUS software. The soil behind the abutment and under the approach slab was well-compacted. The piles were first installed into pre-augured holes, followed by concreting up to 7.6 m (or 60%) of the pile length. The size of the pre-augured holes is 0.76 m in diameter. Corrugated steel sleeve was inserted and extended to the top of the pile. The gap between the pile and the sleeve was filled with sand to facilitate the movement of the piles subjected to lateral loads transferred from the superstructure. The analytical results were compared with experimental data. It was found that the influence of the lateral loads imposed by the superstructure on the piles is confined within a small volume of soil around the piles.

The ten-span bridge of 302 m long and 13 degree skew with an individual spans varying from 26.4 to 35 m having four PSC girders of 1.8m depth and spaced at 3.15m was monitored and studied for abutment-pile-soil system by Forsch *et al.* (2005). AASHTO temperature gradients were used to design the bridge and resulted anticipated movement was found to be1.6 to 2.3 inch (0.0406 to 0.058m) in each direction. Computer program COM624P was used to model the spring coefficients for various soil layers. H piles were used and oriented in strong axis to avoid the possibility of local flange buckling. The bridge was instrumented with a combination of strain, tilt, crack and temperature meters. The piles connected to abutment were found to bend in double curvature. Lateral displacements in the soil corresponded directly with temperature changes. This study is still under process.

Mitoulis et al., (2006) has proposed an alternative solution for a stub-type abutments with flexible H-steel piles or called as "movable" abutment for integral bridges. The proposed methodology was using the full height abutment whose thickness was based on service requirements and which was supported by foundation of micropiles. Appropriate measures against ratcheting effect were considered. It was finally concluede that the proposed configuration of the abutment is possible to be implemented also in long integral bridges as the required flexibility is possible to be adjusted through the micropiles foundation and the thickness of the abutment's web.

2.6 SEISMIC PERFROMANCE OF INTEGRAL BRIDGES

The contribution of abutment participation in two-span concrete integral bridge using actual earthquakes was studied by Goel and Chopra (1997). The bridge was 265-feet (80.79m) long with two unequal spans of 111 and 146 feet (33.84m to 44.51m), having continuous reinforced concrete multicell box-girder deck supported on integral abutments at the two ends and with reinforced concrete two-column bent at intermediate support. It was observed from the records that period and damping increases with increase in abutment flexibility and the deformation demand on the columns in the central bent of the bridge increases significantly with period elongation.

Dicleli (2000 and 2001) proposed a 3-D model shown in Fig. 2.4 for a realistic representation of the behavior of an integral bridge and load distribution among its various members when it is subjected to seismic loads in the transverse or longitudinal direction. The abutments and piles were idealized as 3-D beam elements and they were connected by using rigid bars. The pile elements are divided into a number of equal segments. The lateral stiffness of the soil is calculated at each node level along the pile member using the coefficient of subgrade reaction for the foundation soil and represented by spring elements at each node. The seismically induced soil force behind the integral bridge abutments was

proposed to be calculated using the modified Mononobe–Okabe method. The defined analytical model was used to conduct a response spectrum analysis or a single mode spectral analysis to obtain the seismic response of the structure using an appropriate site response spectrum.

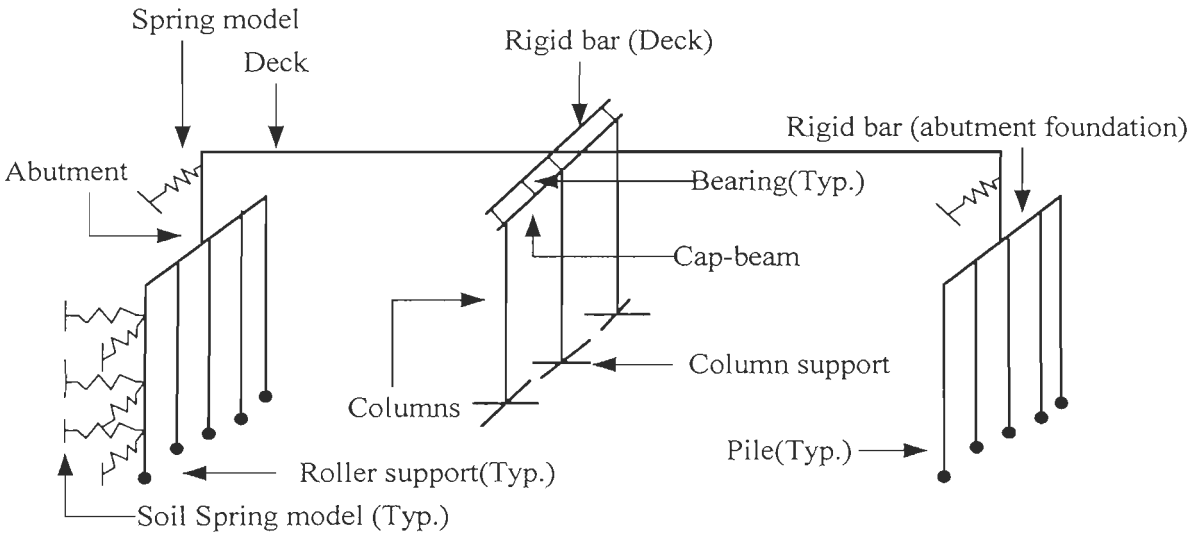

Fig. 2.4: Analytical model of 3D integral bridge for seismic analysis

Dehne and Hassiotis (2000) evaluated the seismic response of the actual integral abutment bridge considering soil-structure interaction and three-dimensional effects of ground excitation by using finite element package SAP 2000. The bridge considered for study was located on scotch road over I-95 interchange in Trenton, New Jersey. The length of the bridge was 90.9m with two equal spans having 10 steel plate girders at 3.466m apart and 260mm thick concrete deck supported by 3 m high and 0.9 m thick abutments on both the sides. HP 14x102 steel piles oriented in weak axis were used. The bridge has a skew angle of about 15 degree. The combination of dense backfill and loose sand around the piles was proved to be best for seismic design of integral bridges.

Patty *et al.* (2001 and 2002) conducted an experimental study on the behavior of an integral bridge consisting of steel superstructure with a concrete substructure using a

concrete bent cap. The objective of this research was to establish a behavior profile of the bent cap connection in order to design the bent cap to remain essentially elastic during seismic loading conditions. The effect of torsional behavior and capacity design parameters were studied on the bent cap. The parameters investigated were 1) bent cap reinforcement (post-tensioned versus conventionally reinforced) and 2) girder web configuration inside the bent cap (with or without bearing stiffeners). All tests were conducted at 40% scale model and subjected to a quasi-static, fully reversed cyclic loading protocol. He recommended a post-tensioned bent cap and steel girders with a single pair of full height bearing stiffeners for the integral bridge systems.

Tuladhar *et al.* (2005) studied the seismic behavior of piles by conducting a full scaled lateral loading tests on a single concrete piles embedded into the ground. One dimensional monotonic loading and a cyclic loading was applied on different concrete pile specimens. The piles were hollow prestressed concrete piles of 0.3m diameter and 0.6m thickness. Strain gages were attached to the steel bars at top 12m. The aim was to study the effect of non-linearity of soil and soil-pile interaction. From the experimental results it was observed that the plastic hinge in the pile was formed at the top 2D depth from ground level for monotonic loading condition and at 4D depth from ground level for cyclic loading conditions. The lowering of plastic hinge in reverse cyclic loading is due to the decrease in the soil resistance caused by repeated cyclic loadings.

2.6.1 Non-Linear Static or Pushover Analysis

The Non linear static procedure (NSP) or pushover analysis described in Eurocode-8, FEMA-273/356, and ATC-40 documents, are widely used for inelastic seismic design of structures. Simplified nonlinear procedures are used for practical applications and they

have been found to be most rationalised methods. The different simplified nonlinear procedures used to implement the pushover analysis are

(i) Capacity Spectrum Method (CSM) (ATC-40, 1996)

(ii) Displacement Coefficient Method (DCM) (FEMA-273, 1997)

(iii) The secant method and

(iv) Modal Pushover Analysis (MPA) (Chopra et al. (2001).

The different methods used for evaluating the NSP may lead to similar results in most of the analysis but they differ in respect to simplicity, transparency and clarity of theoretical background. Non linear static procedure (NSP) is a powerful tool for evaluating the inelastic seismic behavior of structures. Bridge researchers and engineers are currently investigating concepts and procedures to develop simplified procedures for performance-based seismic evaluation of bridges (Dutta, 1999; Shinozuka, 2000).

Fenves and Ellery (1998) studied the three-dimensional nonlinear model of the multiple-frame highway bridge failed in 1994 Northridge earthquake using DRAIN-3DX computer program. The objective was to ascertain the cause of failure by comparing the capacities and demands of various components in the bridge, and to examine the earthquake modelling and analysis recommendation for highway bridges. Nonlinear static pushover analysis was conducted in modal pattern to determine the capacity of the piers, superstructure and intermediate hinges to understand the failure criteria. To validate the nonlinear static procedure, especially displacement coefficient method and capacity spectrum method for bridges, AlAyed (2002) analysed the three span bridge using nonlinear time-history and pushover analysis. The spine model of bridge using frame elements with lumped mass was used to evaluate the force and displacement. The displacements, base shears and rotation of plastic hinges from pushover analysis were compared with nonlinear modal time history analysis to get the response similar or close

to the actual seismic response. Jeremic *et al.* 2004 studied the influence of soil foundation structure interaction on seismic response of viaduct and found that SFS interaction can have both beneficial and detrimental effects on structural behavior and is dependent on the characteristics of the earthquake motion.

Paraskeva *et al.* (2006) studied the seismic behavior of bridge by modal pushover analysis procedure taking the higher mode effects into consideration. In their study the pushover analysis are carried out separately for each significant mode and the contribution from individual modes to calculate response quantities (displacement, base shear etc) are combined using an appropriate combination rules like SRSS and CQC. The results have been compared with the results of load pattern resulting from statistical combination of modal loads and nonlinear time history analysis. The modal pushover results were found to be closer to nonlinear time history analysis.

2.7 CONCLUDING REMARKS

A comprehensive literature review has been under taken and based on the study following conclusions are drawn

i. Lawver *et al.* (2000) and Thippeswamy *et al.* (1995) suggested that thermal-induced movement of an integral bridge caused greater stresses in integral bridge components and hence they should be considered carefully.

ii. Greimann *et al.* (1987) recommended the pile construction in a predrilled hole to reduce the pile stress significantly for lateral loadings. According to Kunin and Alampalli (2000), twelve of the thirty agencies that design integral bridges use pre-bored holes for the abutment piles to reduce temperature stresses. From the comparison of two survey report from Greimann *et al.* (1984) and Kunin and Alampalli (1999) it was found that the number of design agencies using the piles

placed in a pre-drilled has significantly increased. Laboratory tests conducted by Arsoy (2000) revealed that piles placed in pre-bored holes for integral-abutment piles had a significant effect on lateral displacements. Long-term monitoring of PC-girder integral bridge pile by Lawver *et al.* (2000) found the double-curvature bending in the abutment piles.

iii. From the experimental results by Tuladhar *et al.* (2005) on full scale model it was observed that the plastic hinge in the pile was formed at the top 2D depth from ground level for monotonic loading condition and at a 4D depth from ground level for cyclic loading conditions. The lowering of plastic hinge in reverse cyclic loading is due to a decrease in the soil resistance caused by repeated cyclic loadings.

iv. The survey report by Kunin and Alampalli (2000) showed that few design agencies neglected the effect of earth pressure on the abutments during longitudinal expansion of the bridge. The States of Alaska and North Dakota assume a specific soil pressure regardless of the actual design conditions. Siros (1995) suggested the horizontal stiffness of back soil based on lower bound or upper bound for the analysis. Design curves by Clough and Duncan are recommended by Faraji *et al.* (2001) for the modeling of non-linear properties of backfill soil.

v. Static pushover analysis conducted on 2D integral abutment bridges model with various structural and geotechnical parameters for uniform temperature variations by Dicleli and Albhaisi (2003) recommended the maximum length of concrete integral bridges to be 190 m in cold climates and 240 m in moderate climates and steel integral bridges are limited to 100 m in cold climates and 160 m in moderate climates. In clay soil, they recommended the maximum length of concrete integral bridges to be 210 m in cold climates and 260 m in moderate climates and steel

integral bridges are limited to 120 m in cold climates and 180 m in moderate climates. The FHWA technical advisory recommended the following length limits for integral abutment bridges to 91.4 m for steel, 152.4 m for poured-in-place concrete and 182.9 m for prestressed concrete.

vi. The study made from Faraji *et al.* (1997 and 2001) suggested to account the vertical eccentricity between the center of gravity of the girders and the mid-thickness of the bridge deck to properly predict bridge behavior.

vii. Greimann *et al.* (1987) recommended further research on the effect of horizontal displacement on the passive pressure behind the abutment and also construction of integral bridges using ductile concrete and timber piles.

viii. The study accounting the effect of predrilled holes with loose granular fill and varying backfill for thermal, gravity and seismic loads is recommended by Faraji *et al.* (2001) to streamline the design process for integral abutment bridge.

ix. The investigation is in process by bridge researchers to develop concepts and simplified procedures for performance-based seismic evaluation of bridges. Very few research papers related to nonlinear pushover analysis of bridges are available and as far as our knowledge goes, no technical papers are found based on the performance-based seismic analysis of integral abutment bridges.

CHAPTER-3

SOIL-STRUCTURE INTERACTION IN INTEGRAL BRIDGES

3.1 INTRODUCTION

In integral bridges thermal and seismic deck movements are accommodated by soil-structure interaction between abutment-backfill soil and the supporting piles with surrounding strata. Piles in integral bridges should be designed for both vertical and lateral loads coming from substructures and also for bending induced by superstructure moment (Mistry, 2005). These piles should be designed to be flexible to accommodate lateral movements without failure. The deflected shape of the loaded pile is dependent upon the soil-response and in turn, the soil response is a function of pile deflection. Deck and substructure loading get affected by the stiffness of soil behind the abutment wall and next to piles that acts as both load and supporting system to the piles. The bridge deck, piers, abutments, embankments and soil-pile interaction must be considered as a single system in integral bridges. Accounting of soil-pile interaction and abutment-backfill interaction are important in finding the response of integral bridges for temperature and seismic loading. This chapter reviews the non-linear soil models used in the analysis of integral bridges.

3.2 LATERAL SOIL-PILE INTERACTION

3.2.1 Analytical Model for Laterally Loaded Piles

The capacity of piles to accommodate lateral displacement is a significant factor in determining the maximum possible length of integral bridges. The lateral resistance of the soil near the surface is significant to pile design (Kamel *et al.* 1996). Winkler developed a model "beam on elastic foundation" to simulate the soil-structure interaction. In Winkler model equivalent reaction of soil at each depth is represented as linear vertical and lateral

springs along the length of the pile. Model assumes that there is no interaction between the different soil springs as the pile is displaced. The governing equation of Winkler model is given as

$$EI\frac{d^4y}{dz^4}+P_z\frac{d^2y}{dz^2}+k_h(z)y=0 \qquad \ldots (3.1)$$

where, EI is the flexural rigidity of the pile; P_z is the axial force and k_h is the coefficient of horizontal reaction, $k_h(z)y=p(z)$, $p(z)$ is the soil spring pressure having a unit of force/length; y is the lateral deflection of the pile; z is the depth below the ground surface. The solution for Eq. 3.1 can be obtained either by closed form or using approximate solution methods. The vertical and lateral loads are considered as uncoupled in closed form solution. The governing differential Eq. 3.1 can be represented as

$$EI\frac{d^4y}{dz^4}+k_h(z)y=0 \qquad \ldots (3.1a)$$

The general solution to the above fourth order differential equation is

$$y=(C_1\cos Rz+C_2\sin Rz)e^{Rz}+(C_3\cos Rz+C_4\sin Rz)e^{-Rz} \qquad \ldots (3.2)$$

where, $R=\sqrt[4]{\frac{k_h}{4EI}}$, $1/R$ is called interaction distance or characteristics length of the pile. C_1, C_2, C_3 *and* C_4 are the constants depending on boundary conditions. Closed form solutions are time consuming hence the approximate methods like finite difference techniques given by Reese *et al.* (1970) or finite element method can be applied to Eq. 3.1 to obtain the solution. In finite difference method, the pile will be divided into a number of small elements as shown in Fig. 3.1 and soil response over each pile element is lumped into discrete soil springs. The finite difference expressions for the first two terms in Eq. 3.1 are given as

$$EI\frac{d^4y}{dz^4}=\left(\frac{d^2M}{dz^2}\right)_i=\frac{1}{h^4}[y_{i-2}EI_{i-1}-2y_{i-1}(EI_{i-1}+EI_i)+y_i(EI_{i-1}+4EI_i+EI_{i+1})-2y_{i+1}(EI_i-EI_{i+1})+y_{i+2}EI_{i+1}] \quad \ldots (3.3)$$

$$P_z\left(\frac{d^2y}{dz^2}\right)_i=\frac{P_z(y_{i-1}-2y_m+y_{i+1})}{h^2} \quad \ldots (3.4)$$

where, h is the height of the ith element and M is the moment in the pile. Substituting Eqs 3.3 and 3.4 in Eq. 3.1 and applying boundary conditions leads to a set of linear equations which can be solved to get displacements and moments at each node.

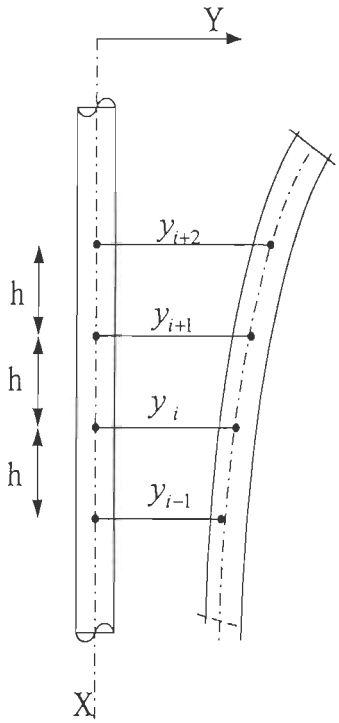

Fig. 3.1: Deflection of pile for small strips or elements

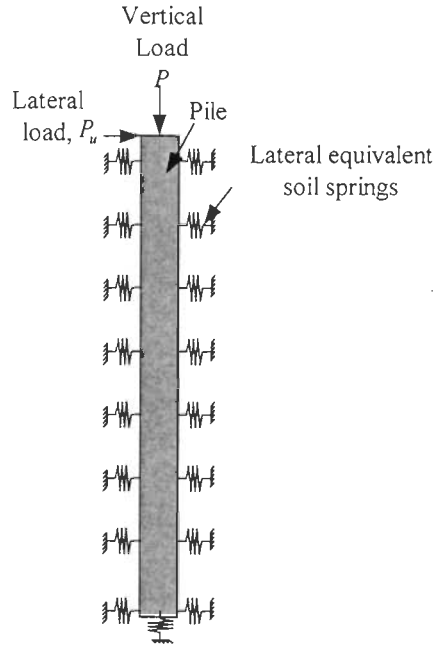

Fig. 3.2: Laterally loaded pile with full sets of *p-y* curves

Theoretical approaches consider soil and pile as elastic, but the lateral soil resistance is non-linear and hysteretic in nature. The soil characteristics in the soil-pile interaction can be described by three types of resistance-displacement curves (API-RP2A-2000) such as (i) *p-y* curves, which describe the relationship between the lateral soil pressure (horizontal force per unit length of pile) and the corresponding lateral pile displacement; (ii) *t-z* curves, which describe the relationship between skin friction (vertical force per unit length of pile) and the relative vertical displacement between the pile and the soil; and (iii) q-z

curves, which describe the relationship between the bearing stress (vertical force on effective pile tip area) at the pile tip and the pile tip settlement. All three types of curves assume the soil behavior to be nonlinear. Again, the Winkler model assumes that these springs are uncoupled, the stiffness of one spring does not affect another stiffness.

Analytical solution for the soil-pile system accounting for non-linear soil behavior can be incorporated by replacing the soil response $k(z)y = p(z)$ with a displacement dependent value $p(u,z)$ (John and Faraji, 1998) in Eq. 3.1. The non-linear soil reactions $p(u,z)$ are called *p-y* curves. where p is the lateral soil resistance per unit length and y is lateral deflection. Soil properties, pile geometry and nature of loading influences the shape of *p-y* curves. The computation of lateral force-displacement response of a pile involves the construction of full sets of *p-y* curves along the pile to model the force-deformation response of the soil, as shown in Fig. 3.2. Analytical solution for the soil-pile system accounting for non-linear soil behavior is quite complicated and they need advanced computer programs for analysis. The non-linear pile and non-linear soil spring behavior can be solved numerically using nonlinear finite element method. Griton *et al.* (1989) have used the modified Ramberg-Osgood model and Faraji *et al.* (2001), Dicleli and Suhail (2003) and Arockiasamy *et al.* (2004) have used curves given in API-RP2A-2000 derived by Reese to approximate the lateral curves (*p-y* curves) for use in the finite element solution of integral bridges.

3.2.2 Soil-Pile Interaction Behavior in Sand

The pressure distribution of laterally restrained pile in cohesionless soil given by Broms is shown in Fig. 3.3. Several methods are available for determining the ultimate lateral resistance to piles in cohesionless soils. Broms (1964) suggested the following expression for calculating the ultimate lateral resistance p_u in cohesionless soils

$$p_u = 3K_p \gamma z D \quad \ldots (3.5)$$

$$K_p = \frac{1+\sin\phi}{1-\sin\phi} \quad \ldots (3.6)$$

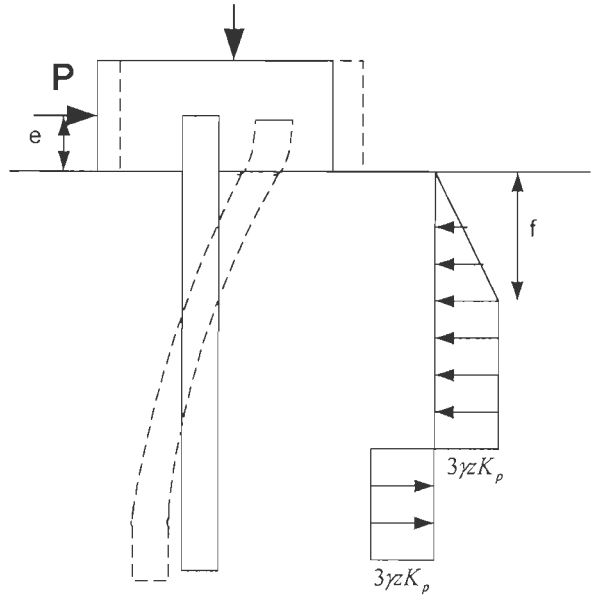

Fig. 3.3: Ultimate pressure distribution of laterally loaded piles in cohesionless soil
(a) Pile deflection (b) Soil resistance (Broms, 1964)

where, 'f' is the distance from ground surface to second plastic hinge. K_p is the co-efficient of passive earth pressure as calculated by the Rankine earth pressure theory; γ is the effective soil weight in kN/m^3; D is the diameter of the pile in m; z is the depth from the ground surface in m and ϕ is the angle of internal friction, deg.

Reese *et al.* (1974) suggested two types of soil behavior that are generally considered in estimating ultimate lateral load p_u for laterally loaded piles. The first type of behavior occurs near the surface, where the pile may push up a soil wedge by lateral movement. In second type of behavior the soil attempts to flow around the pile at some depth below the ground surface which is known as plane-strain failure. Ultimate lateral resistance with depth, taking into account of wedge type failure near the ground surface and is given by

$$p_u = \gamma z \left[D(K_p - K_a) + z(K_p - K_o)\sqrt{K_p}\tan\alpha + zK_0\sqrt{K_p}\left(\frac{1}{\cos\alpha}+1\right)\tan\phi \ \sin\beta \right] \quad \ldots (3.7a)$$

p_u at considerable depth below the ground surface taking plane-strain failure is given by

$$p_u = \gamma z D\left(K_p^3 + K_o K_p^2 \tan\phi - K_a\right) \quad \text{.. (3.7b)}$$

$$K_a = \frac{1-\sin\phi}{1+\sin\phi} \text{ or } K_a = \tan^2\left(45 - \frac{\phi}{2}\right) \quad \text{... (3.8)}$$

$$\beta = 45 + \frac{\phi}{2} \quad \text{... (3.9)}$$

where, K_a is the active earth pressure coefficient; $K_o \approx 0.4$, coefficient of earth pressure at rest; $\alpha_w = \phi / 2$, angle defining the shape of the wedge.

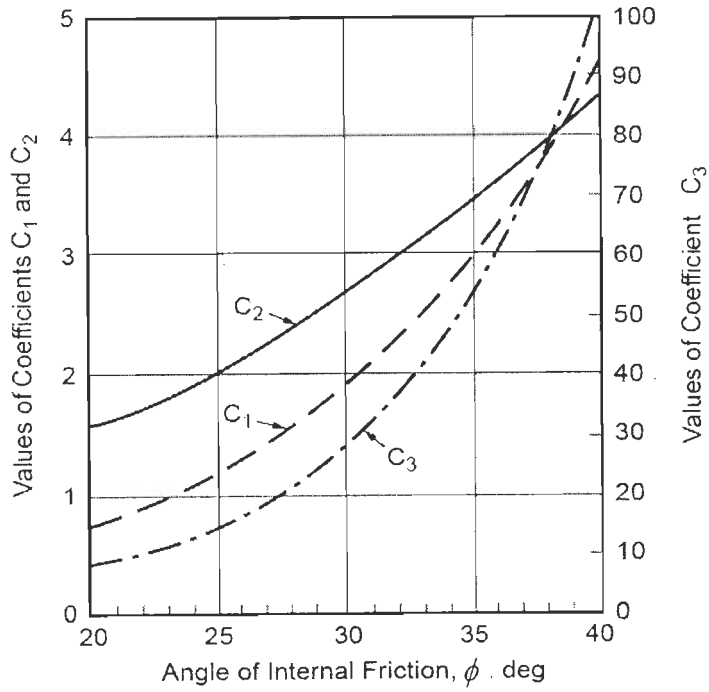

Fig. 3.4: Coefficients as function of ϕ (API-2000)

Matlock *et al.* (1980) simplified the equation given by Reese by grouping the terms to form factors that vary with ϕ. The ultimate lateral resistance p_u is expressed near ground surface as

$$p_u = \left(C_1 z + C_2 D\right)\gamma z \quad \text{... (3.10a)}$$

and below ground surface as

$$p_u = C_3 D \gamma z \quad \text{... (3.10b)}$$

The parameters C_1, C_2 *and* C_3 are functions of ϕ and are shown in Fig. 3.4

Reese *et al.* (1970) & Matlock *et al.* (1970) have conducted many experimental studies and have developed *p-y* curves for single pile in clay and sand. Based on the experimental studies empirical equations were formed to predict *p-y* curves. American Petroleum Institute design recommendation follows the hyperbolic tangent curves recommended by Reese. The curves were revised in API-RP2A-1993 by O'Neill *et al.* (1983). API uses the ultimate lateral resistance expression given by Matlock which was simplified equation of Reese. The lateral soil resistance-deflection relationship for sand recommended in API-RP2A-2000 is given by

$$p = Ap_u \tanh\left[\frac{kz}{Ap_u} y\right] \quad \ldots \quad (3.11)$$

where, A is a factor to account for cyclic or static loading conditions, 0.9 for cyclic loading;

$$A = \left(3.0 - 0.8\frac{z}{D}\right) \geq 0.9 \text{ for static loading.} \quad \ldots (3.12)$$

where, p_u is the ultimate bearing capacity at depth z in kN/m^2; k is the initial modulus of subgrade reaction in kN/m^3; y is the lateral deflection in m and z is the depth in m. The plot between p and y shown in Fig. 3.5 will gives lateral soil-resistance (p-y) curve which is non-linear.

The comparative study between the design curves and the 14 full scale static pile tests conducted by John and Faraji (1998) showed that the extended hyperbolic model of O'Neill followed by API-RP2A-1993 as the preferred method for modeling lateral soil response for accuracy and ease of use. The full-scale *p-y* test data would be useful to evaluate the response of integral bridges. In the absence of full-scale data, API procedure can be used for the development of *p-y* curves in sand.

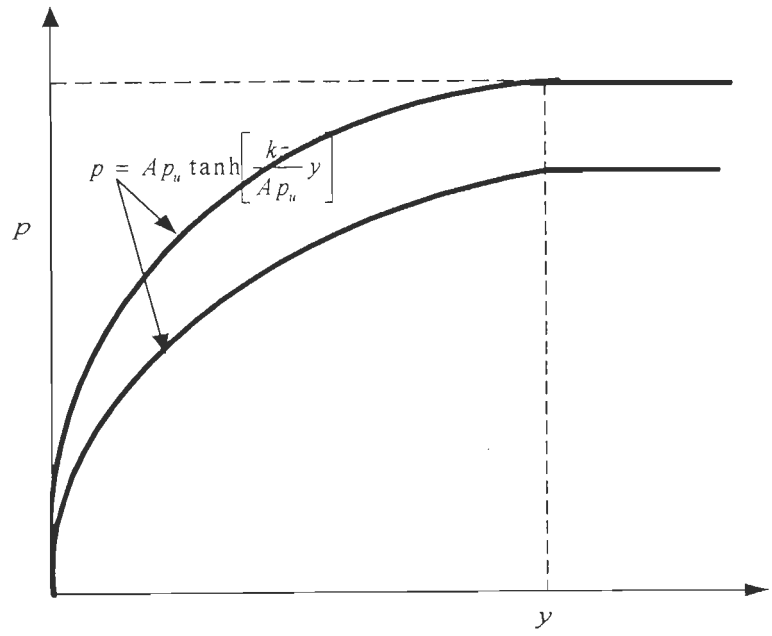

Fig. 3.5: $p - y$ curves for static and cyclic loading in sand (API-2000)

3.2.3 Soil-Pile Interaction Behavior in Clay

Broms and Reese have given different mechanism for the distribution of lateral earth pressure of a pile that is restrained at its top, shown in Fig. 3.6. According to Reese *et al.* (2001) the variation of ultimate lateral resistance in stiff clay, taking account of the wedge type failure near the ground surface is given by

$$p_u = 2c_a D + \gamma Dz + 2.83c_a z \quad \ldots (3.13a)$$

p_u at considerable depth below the ground surface taking plane-strain failure is given by

$$p_u = 11c_u D \quad \ldots (3.13b)$$

The ultimate soil resistance per unit length of pile for soft clay given by Matlock *et al.* (1970) is as follows

$$p_u = (3c_u + \gamma z + J\frac{c_u z}{D})D \quad \ldots (3.14a)$$

$$p_u = 9c_u D \quad \ldots (3.14b)$$

where, c_a is the average drained shear strength and c_u is the undrained shear strength of the clay. The strain corresponding to c_u is termed as characteristic strain ε_{50}. In absence of

test data, the value of c_u and ε_{50} for different types of clay can be assumed as shown in Table 3.1. *p-y* curves for stiff and soft clay are shown in Figs. 3.7 to 3.9.

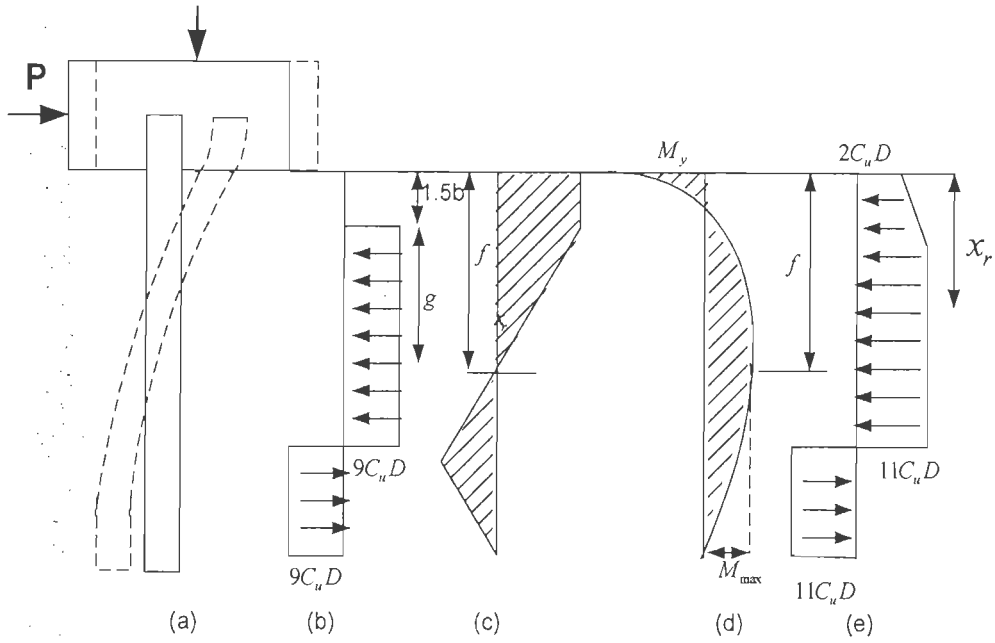

Fig. 3.6: Ultimate pressure distribution of laterally loaded piles in cohesive soil
(a) Pile deflection; (b) soil resistance (Broms, 1964); (c) Shear force;
(d) Moment diagram and (e) soil pressure (Reese *et al.* 1970)

where, f is the distance from ground surface to second plastic hinge in m; x_r is depth below soil surface to bottom of reduced resistance zone or critical depth in m and M_{max} is the maximum bending moment in kN-m.

Table 3.1: Representative values of ε_{50} and c_u for normal and over consolidated clays

Normally Consolidated		Over Consolidated	
c_u in 'kPa'	ε_{50}	c_u in 'kPa'	ε_{50}
<48	0.020	50-100	0.007
48-96	0.010	100-200	0.005
96-192	0.005	200-400	0.004

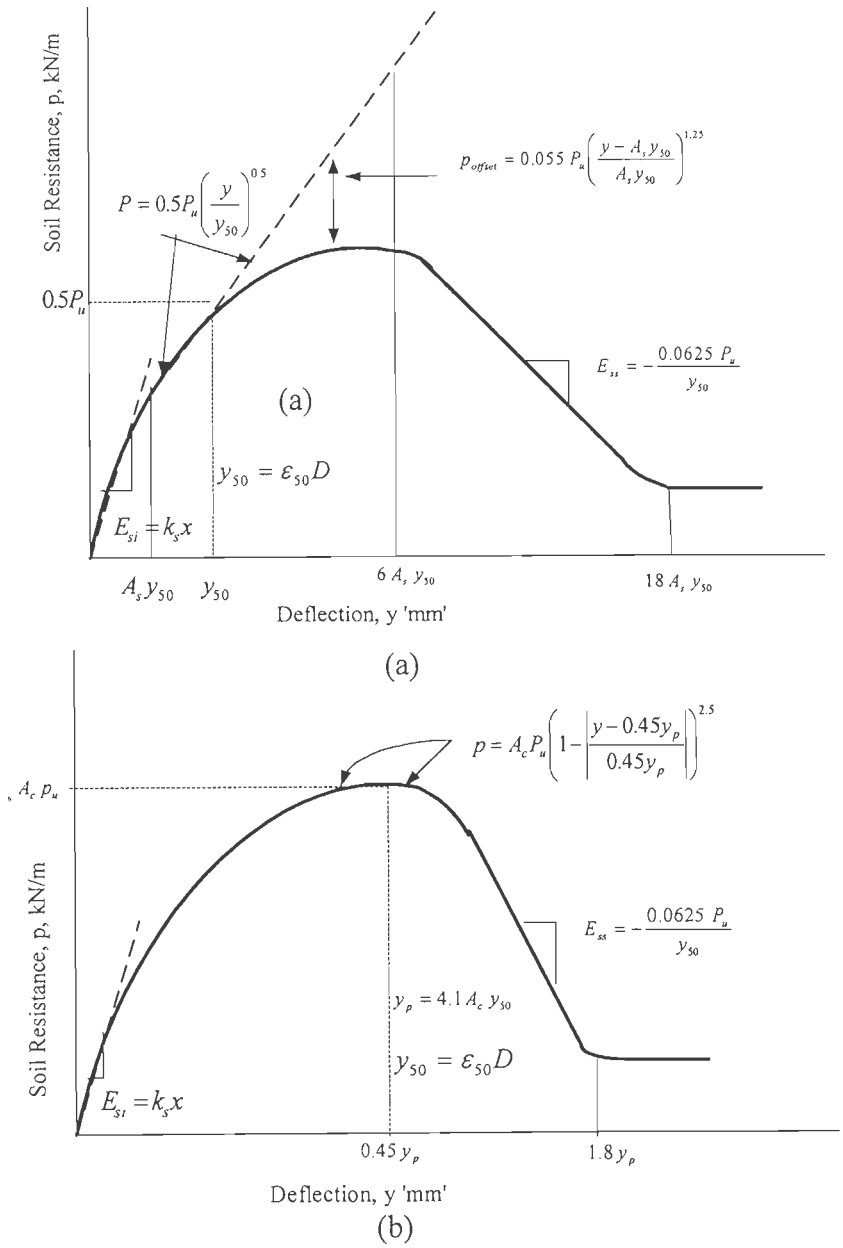

Fig. 3.7: Characteristic shape of *p-y* curve for stiff clay below water table (a) Static Loading (b) Cyclic Loading (Reese *et al.* 1979)

In Fig 3.7, y_{50} is the deflection at one-half the ultimate soil resistance given by

$$y_{50} = \varepsilon_{50} D \qquad \ldots (3.15)$$

$$y_p = 4.1 A_c y_{50} \qquad \ldots (3.16)$$

A_s *and* A_c are the constants for static and cyclic loading conditions.

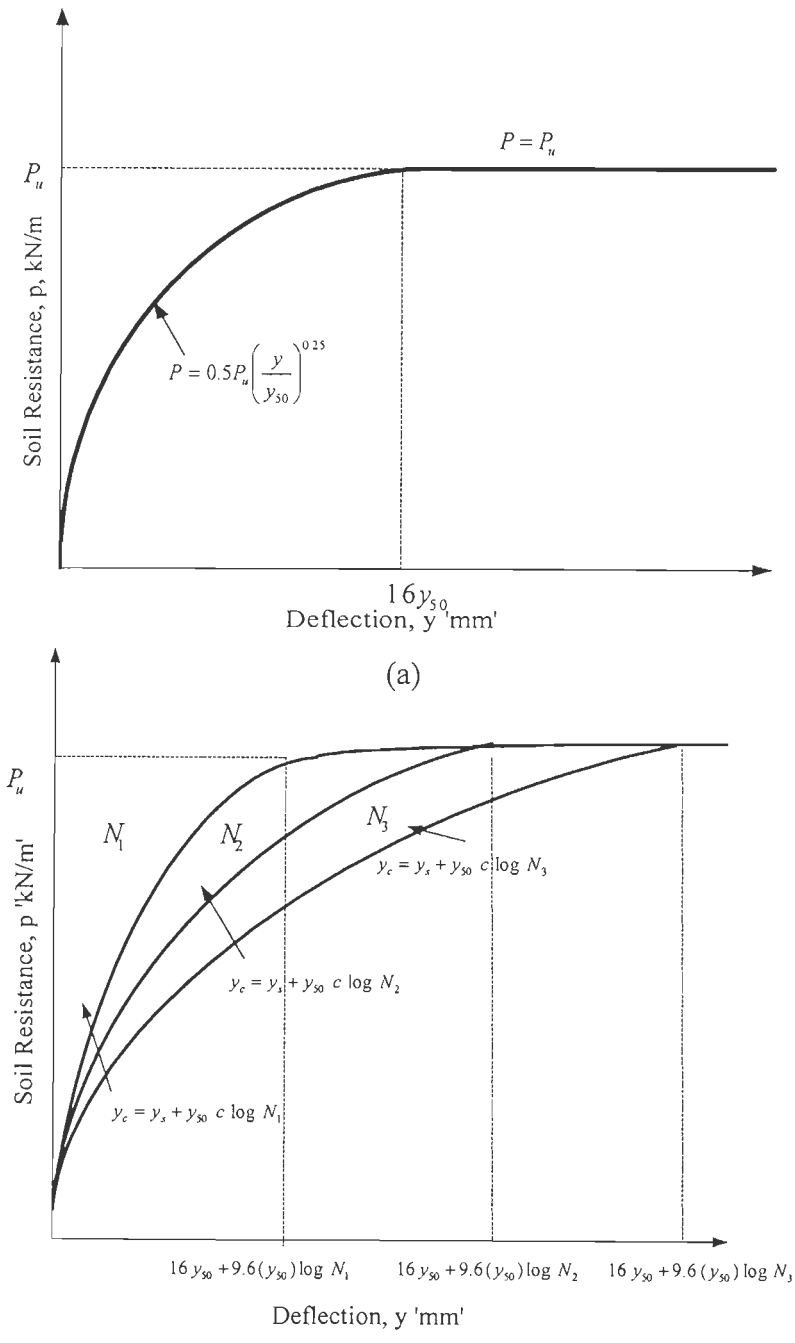

Fig. 3.8: Characteristic shape of *p-y* curve for stiff clay above water table
(a) Static Loading (b) Cyclic Loading [Reese *et al.* 2000]

In Fig 3.8, N is the number of cycles of load application; y_s is the deflection under short-term static load and y_c is the deflection under N- cycles of load

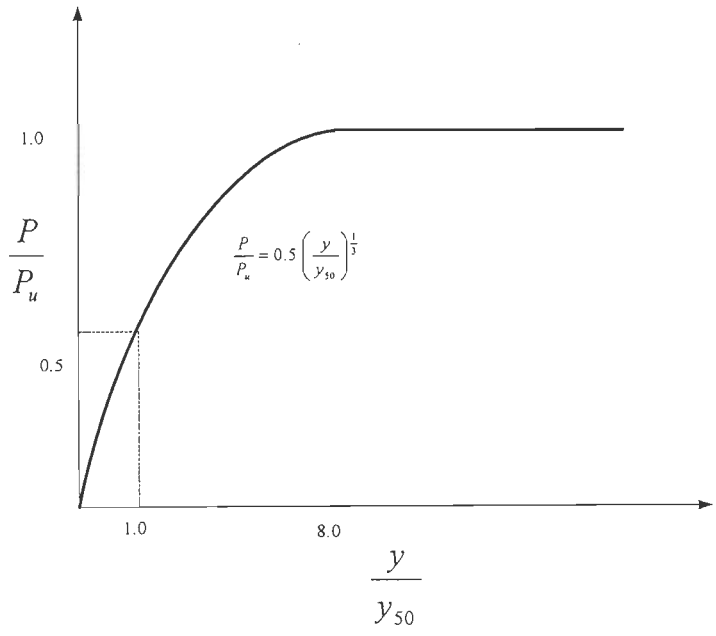

(a)

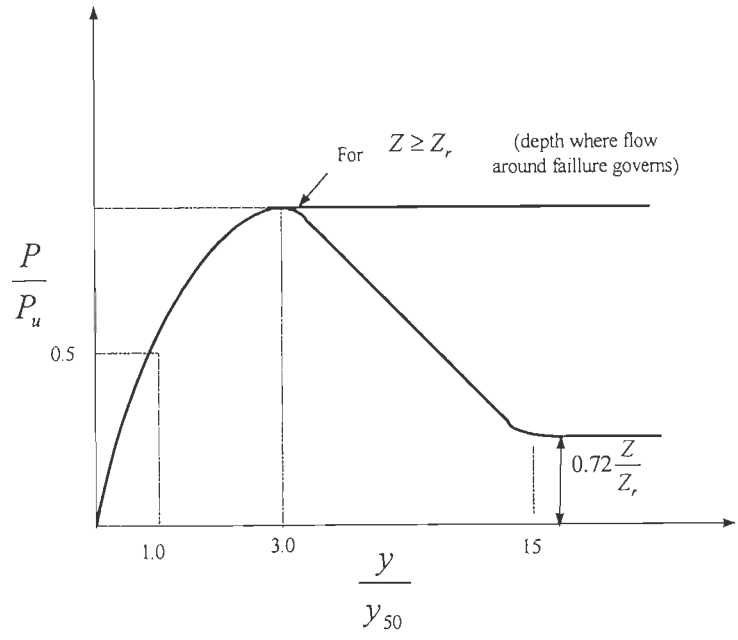

(b)

Fig. 3.9: Characteristic shape of *p-y* curve for soft clay below water table (a) Static Loading (b) Cyclic Loading (Matlock, 1970)

In Fig 3.9, Z is the depth from ground surface in *p-y* curve and Z_r is the depth were transition occurs, which is given by

$$Z_r = \frac{6c_u D}{(\gamma D + Jc_u)} \quad \ldots (3.17)$$

J is a dimensionless empirical constant with values 0.5 for soft clay and 0.25 for medium clay.

The MATLAB program is been developed for the extraction of p-y curves for sand, stiff and soft clay. The output of this program is used in SAP for non-linear soil modeling.

M.G. CENTRAL LIBRARY
G 20643
ACC No.....
Date.....
I.I.T. ROORKEE

3.3 LATERAL EFFECTS OF PILE GROUP

The pile group capacity will not be equal to the sum of the capacity of individual piles. According to O'Neill *et al.* (1983) all the models proposed for pile group effect are approximate because none of the models account for installation effect. The behavior of a pile group is not well defined. Elastic half space theory was used for pile group effects by Poulos (1971) to soften the elastic stiffness. Since the soil cannot be generally characterized as linear, homogeneous and elastic material the elastic half space model was not widely accepted. The dynamic stiffness of pile and pile groups were studied by using beam on dynamic Winkler foundation simplified model by Kaynia and Kausel (1991) and Boominathan *et al.* (2001 and 2005). Full scale test conducted by Brown *et al.* (1987) found that the most logical approach to account the pile group effect is the use of interaction factor for the modification of *p-y* curves which was proposed by Focht. The *p*-multiplier obtained from various experiments conducted by different researchers listed by Polam *et al.* (1998) is shown in Table 3.2.

Table 3.2: *p*-Multipliers for 3x3 pile groups at 3D center-to-center (Polam *et al.* 1998)

Pile Test, Soil Description, Reference	*p*-multiplier on single *p-y* curves		
	Front Row	Middle Row	Back Row
Free-Head, Medium Dense Sand, $D_r = 50\%$, Brown *et al.* (1988)	0.80	0.40	0.30
Fixed-Head, Medium Dense Sand, $D_r = 55\%$, Mc Vay, Centrifuge (1995)	0.80	0.45	0.30
Fixed-Head, Medium Dense Sand, $D_r = 50\%$, Mc Vay, Centrifuge (1995)	0.65	0.45	0.35
Fixed-Head, Medium Dense Sand, $D_r = 50\%$, Rollins *et al.* (1997)	0.60	0.38	0.43

The Caltrans bridge design manual follows the *p*-multipliers given by Brown for center to center pile spacing of 3 pile diameters. The lateral pile group effect can be neglected for center to center pile spacing of 6 pile diameters. For the piles having center to center spacing between 3 and 6 pile diameters, p multiplier can be obtained by linear interpolation between 0.5 and 1.0. The experiment conducted by McVay *et al.* (1995) for pile centre-to-centre spacing of 5 pile diameter, *p*-multiplier of 1.0 for lead row, 0.85 for second row and 0.7 for third row is recommended.

The response of a pile group during an earthquake is different from its response to a static lateral loading. The seismic waves pass through the soil layer and cause the soil layer to move laterally along with the pile. This movement induces additional bending moments and stresses in piles. In cyclic earthquake conditions, the leading row piles will become rear row when loading changes its direction. To account for the practical design of earthquake loading, the p-multiplier of 0.5 is recommended by Polam *et al.* (1998) to represent the average adjustment factor to develop an average condition to fit overall group effect. ATC-32(1996) recommend to neglect the group effect for earthquake loading due to uncertainty in group effects for piles placed at three diameter center-to-center spacing.

3.4 AXIAL CAPACITY OF PILES

Axial load-displacement characteristics are generally assumed to be effectively uncoupled with lateral load-deflection behaviour because the soil resistance associated with axial loading will come from relatively deep elevations, where as lateral loading is associated with shallower soil-structure interaction. The axial carrying capacity 'Q_a'of the piles is provided by a combination of soil-pile frictional and end bearing resistance of the pile tip, which is given as

$$Q_A = Q_f + Q_p = fA_s + qA_p \quad \ldots (3.18)$$

$$\begin{cases} f = \alpha_c c_a \\ q = 9c_u \end{cases} \qquad for\ clay \quad \ldots (3.19)$$

$$\begin{cases} f = k p_o \tan\beta_{sp} \\ q = pN_q + 0.5D\gamma N_r \end{cases} \qquad for\ sand \quad \ldots (3.20)$$

where, Q_f is the skin friction resistance in kN; Q_p is the total end bearing capacity of the pile in kN; f is the unit skin friction capacity in kN /m^2; A_s is the side surface area of pile in m^2; q is the unit end bearing capacity in kN /m^2; A_p is the gross end area of pile in m^2; α_c is the dimensionless factor; k is the coefficient of earth pressure and varies from 1 to 2 for bored piles; p_o is the effective overburden pressure at the respective nodal point in kN /m^2 ; β_{sp} is the friction angle between soil and pile; p is effective overburden pressure at pile tip in kN /m^2, N_r *and* N_q are the bearing capacity factors depending upon the angle of internal friction. The *t-z* curves are used to describe the relationship between skin friction (force per unit length of the pile) and the relative vertical displacement between the pile and the soil. The analytical relationship to find the skin-friction capacity in both sand and clay is given by

$$\frac{t}{t_{\max}} = 2\sqrt{\frac{z}{z_c}} - \frac{z}{z_c} \quad \ldots (3.21)$$

z_c is the relative displacement required; z_c= 0.01 m for sand and z_c= 0.005 m for clay; $t_{\max}$ is the maximum shear stress in kN/m^2; t is the shear stress at nodal point in kN/m^2 and z is the local pile deflection in m. In the absence of more experimental data, API-RP2A-2000 recommends following values shown in Table 3.3 to develop *t-z* curves, the shape of the t-z curve is shown in Fig. 3.10

Table 3.3: Axial pile load transfer-displacement values (t-z) (API-RP2A-2000)

				Clay			
z/D	0.0016	0.0031	0.0057	0.0080	0.0100	0.0200	∞
t/t_{max}	0.30	0.50	0.75	0.90	1.00	0.70 to 0.90	0.70 to 0.90
				Sand			
z/D	0.00	0.0254	∞				
t/t_{max}	0.00	1.00	1.00				

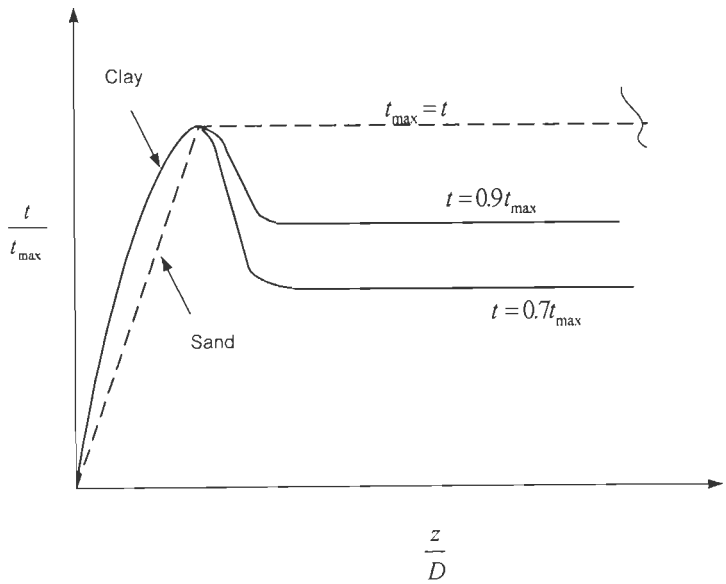

Fig. 3.10: Axial pile load transfer-displacement curves (t-z curves) (API-RP2A-2000)

The relationship between the bearing stress at the pile tip and the pile tip settlement is described by q-z curves. The large pile tip movements are required to mobilize the full end bearing resistance. The total pile tip force is q times the effective pile tip area. The analytical form of pile tip-settlement (q-z) curves in both sand and clay is given by (Wolde-Tinsae *et al.* 1987)

$$\frac{q}{q_{max}} = \left(\frac{z}{z_{cb}}\right)^{\frac{1}{3}}. \qquad \ldots (3.22)$$

where, q_{max} is the maximum bearing stress in kN/m^2; z is the axial tip deflection, m and z_{cb} is the maximum displacement required to develop q_{max}. In the absence of more definite criteria the API-RP2A-2000 recommends following values shown in Table 3.4. It is

assumed that a pile tip displacement of 10% is required for full mobilization in both sand and clay and the shape of the q-z curve is shown in Fig. 3.11

Table 3.4: Pile-tip-load-displacement values (API-RP2A-2000)

$\frac{z}{D}$	0.002	0.013	0.042	0.073	1.0
$\frac{q}{q_{max}}$	0.25	0.50	0.75	0.90	1.0

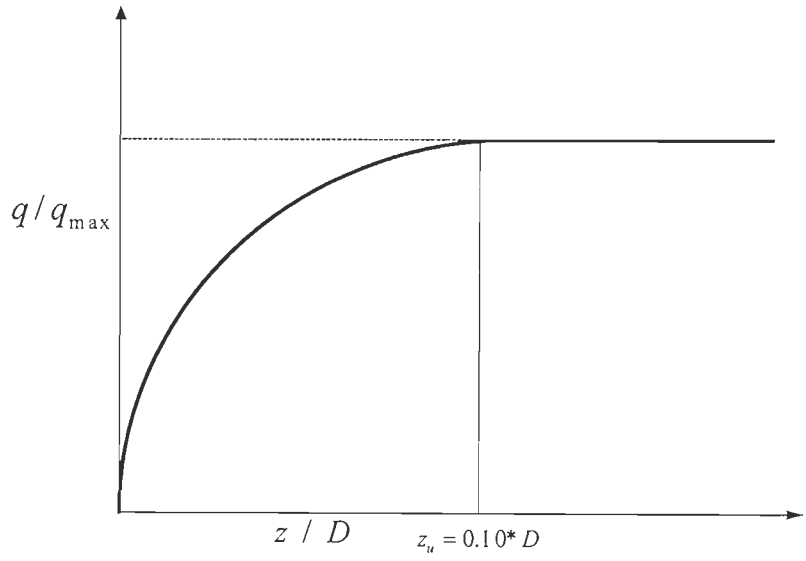

Fig. 3.11: Pile tip-load displacement curves (q-z curves) (API-RP2A-2000)

3.5 EQUIVALENT CANTILEVER METHOD

The lateral displacement of the pile in integral bridges are generally confined to the upper portion of a pile as per the study conducted by Greimann *et al.* (1987), the soil-pile system are generalised to an equivalent cantilever column as shown in Fig. 3.12. The equivalent cantilever length of a pile "L_C"is a function of both pile and surrounding soil properties. Equivalent cantilever length is given by

$$L_C = l_e + l_u \quad \ldots (3.23)$$

l_e is the equivalent embedded length of the pile and l_u is the pile length above undisturbed soil strata. For a pile embedded in soil, the lateral displacement and bending moment will

be very small below a certain depth "l_c" called critical depth. Critical depth for a soil with constant horizontal subgrade reaction throughout the pile length is given by

$$l_c = 4R_c \text{ or } 4R_s \quad \ldots (3.24)$$

$$R_c = \sqrt[4]{\frac{EI}{k_h}} \text{ for cohesive soil} \quad \ldots (3.25a)$$

$$R_s = \sqrt[5]{\frac{EI}{k_h}} \text{ for cohesionless soil} \quad \ldots (3.25b)$$

where, R_c or R_s is relative stiffness factor.

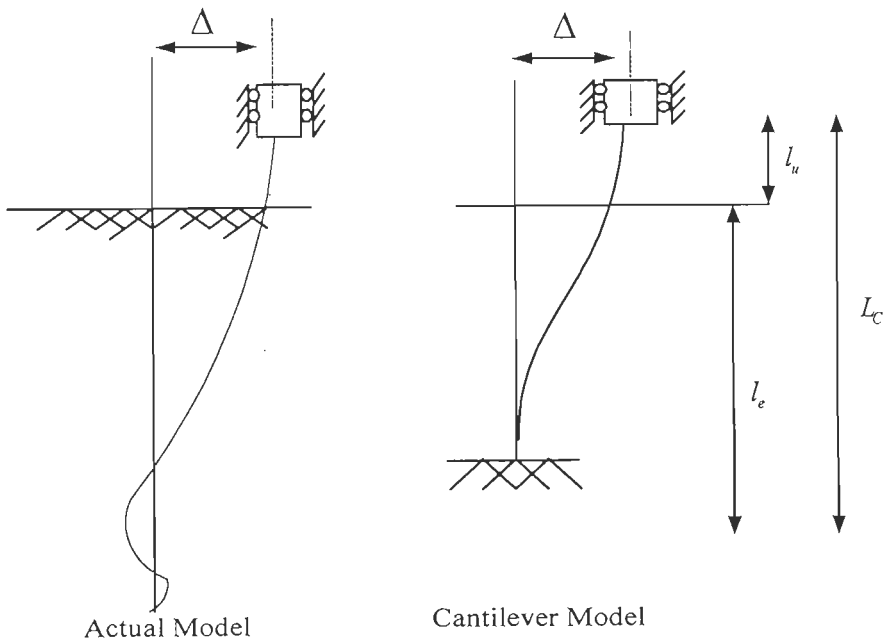

Fig. 3.12: Idealised equivalent cantilever pile length for fixed head

For a layer of soil profile, $k_h = k_e$ where k_e is equivalent horizontal stiffness for a layered soil. Iterative procedure is proposed by Greimann to evaluate the equivalent horizontal stiffness k_e, the procedure is as follows

i. To assume an initial value of equivalent horizontal stiffness "k_e" for layered soil.

ii. Calculate the active length l_o of the pile in bending, which is assumed to be equal to half of the critical length, $l_o = 2\sqrt[4]{\frac{EI}{k_e}}$ ... (3.26)

iii. Calculate the second moment I_k, for linearly varying soil stiffness as shown Fig 3.13 (a)

$$I_k = k_{h1}\left[\frac{d^3}{36} + \frac{d}{2}\left(\frac{a+2d}{3}\right)^2\right] + k_{h2}\left[\frac{d^3}{36} + \frac{d}{2}\left(\frac{a+d}{3}\right)^2\right] \quad \ldots (3.27)$$

iv. For uniform soil stiffness, as shown Fig 3.13 (b)

$$I_k = k_h\left[\frac{d^3}{12} + dc^2\right] \quad \ldots (3.28)$$

where, $k_h(z)$ represents the variation of the stiffness k_h with soil depth

v. Calculate the new equivalent horizontal subgrade reaction

$$k_e = \frac{3I_k}{l_o^3} \quad \ldots (3.29)$$

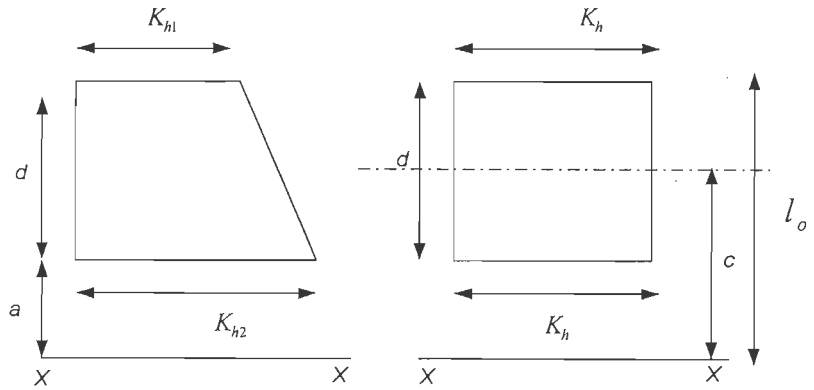

(a) (b)

Fig. 3.13: Second moment about reference X-X

Figure 3.14 gives the equivalent cantilever lengths to calculate the displacement, force and moment at the top of the pile. Greimann *et al.* (1987) by the experimental analysis has concluded that the equivalent cantilever column model gives sufficient accurate results for design purpose and the displacement and moment at the top pile can be obtained as

$$\Delta_p = \frac{P_h L_{CS}^3}{12EI} \quad \text{for fixed head pile} \quad \ldots (3.30)$$

$$\Delta_p = \frac{P_h L_{CS}^3}{3EI} \quad \text{for free head pile} \quad \ldots (3.31)$$

$$M_p = \frac{6EI\Delta_p}{L_{CM}^2} \text{ for fixed head pile} \quad \ldots (3.32)$$

$$M_p = \frac{3EI\Delta_p}{L_{CM}^2} \text{ for free head pile} \quad \ldots (3.33)$$

where, L_{CS} is the equivalent cantilever length based on the horizontal stiffness of the pile; L_{CM} is the equivalent cantilever length based on the maximum moment in the pile; I is the moment of inertia of the pile cross section, E is the modulus of elasticity of pile and Δ_p is the deflection at the top of the pile.

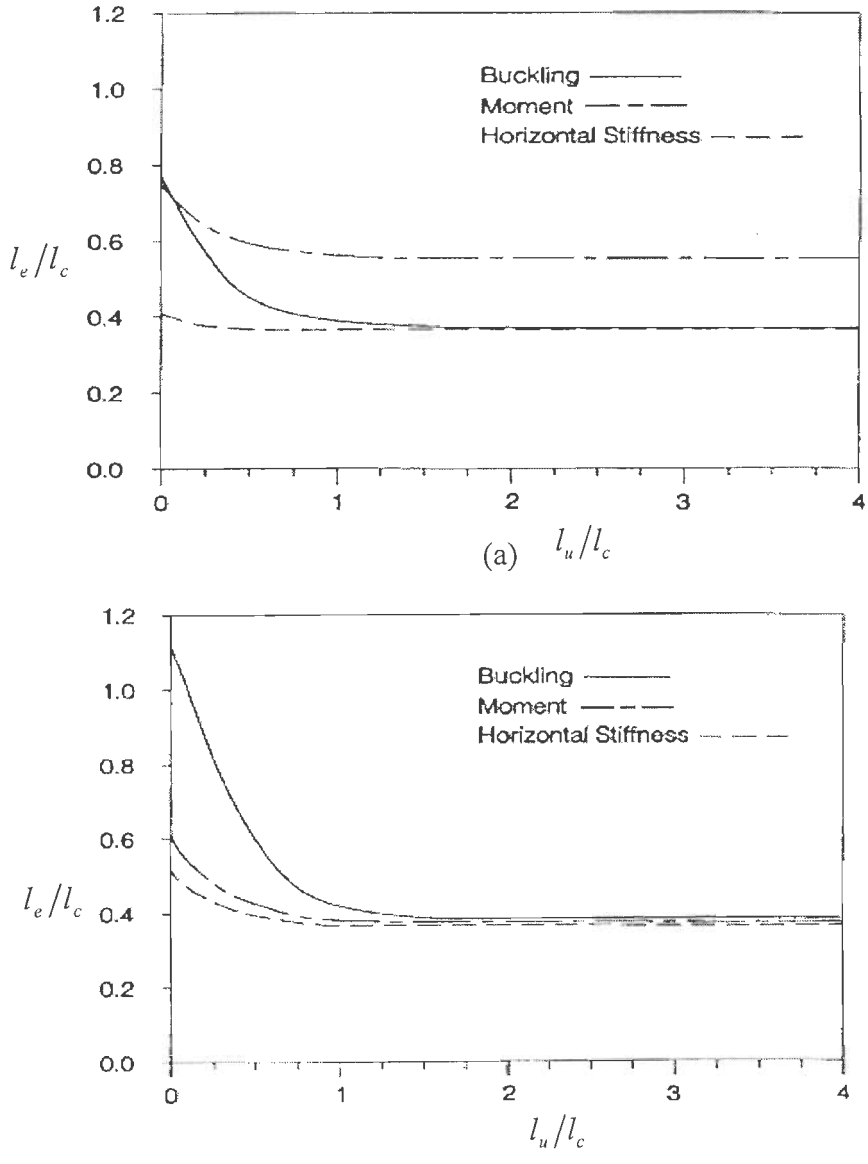

Fig. 3.14: Equivalent cantilever length for (a) Pinned head pile and (b) Fixed head pile (Greimann *et al.* 1987)

3.6 ABUTMENT-BACKFILL INTERACTION

Abutments in integral bridges are usually designed to with stand self weight, horizontal and vertical loads from bridge superstructure, vertical and lateral soil pressures and live load surcharge on the abutment backfill materials (Mistry, 2005). As temperature changes daily and seasonally, the length of integral bridges increases and decreases, pushing the abutment against the approach fill and pulling it away, understanding this is important for effective design and satisfactory performance of integral bridges. To evaluate the influence of soil stiffness on bridge response, soil spring properties representing abutment backfill is modeled as non-linear force-deflection curves. Number of approaches or models is available to evaluate earth pressure on abutments and some of them have been compared to use the best suitable model for integral abutment bridge.

In bridges, the cohesionless soil is widely used as backfill material for abutments and the use of cohesive soil is generally avoided. Active earth pressure develops when the abutment moves away from the soil and passive earth pressure develops as abutment moves toward the soil, thereby producing compressive lateral strain in the soil (Terzaghi *et al.* 1966). Maximum passive earth pressure acts on the abutment, when the strength of soil is fully mobilized. Rankine have developed the simplest procedure to calculate minimum active and maximum passive earth pressure. He considered the state of stress in a soil mass when a state of plastic equilibrium has been reached by either relaxing the horizontal soil stresses or increasing the horizontal soil stresses. For a smooth/frictionless vertical retaining wall resting against a horizontal stratum of cohesionless soil, the active and passive earth pressure are given by

$$P_a = K_a \gamma z \quad \ldots (3.34a)$$

$$P_p = K_p \gamma z \quad \ldots (3.34b)$$

where, $K_a = \frac{(1-\sin\phi)}{(1+\sin\phi)}$, K_a is the coefficient of active earth pressure, ... (3.35a)

$K_p = \frac{(1+\sin\phi)}{(1-\sin\phi)}$, K_p is the coefficient of passive earth pressure, ... (3.35b)

γ is the unit weight of soil; z is the depth below the ground surface and ϕ is the friction angle. Practically there are no perfect smooth retaining wall surfaces. Since back of retaining wall is more or less rough, the friction exists between the wall and the soil. The roughness on the back of a wall commonly reduces the active pressure and increases the passive earth pressure. Rankine analysis is a lower bound method and it underestimates the passive pressure. The boundary conditions for the Rankine's theory are rarely satisfied. Coulomb's was the first to study the problem of lateral earth pressure and his wedge theory can be adapted to any boundary condition and it gives more accurate values of earth pressure compare to Rankine's method. While calculating the passive earth pressure, the soil is assumed as isotropic, homogeneous and that the deformation of the soil occurs only parallel to a vertical section at right angles to contact face. Figures 3.15 (a) and (b) represent the vertical sections of wall through a plane face *ab*, which is in contact with a mass of soil with a plane surface.

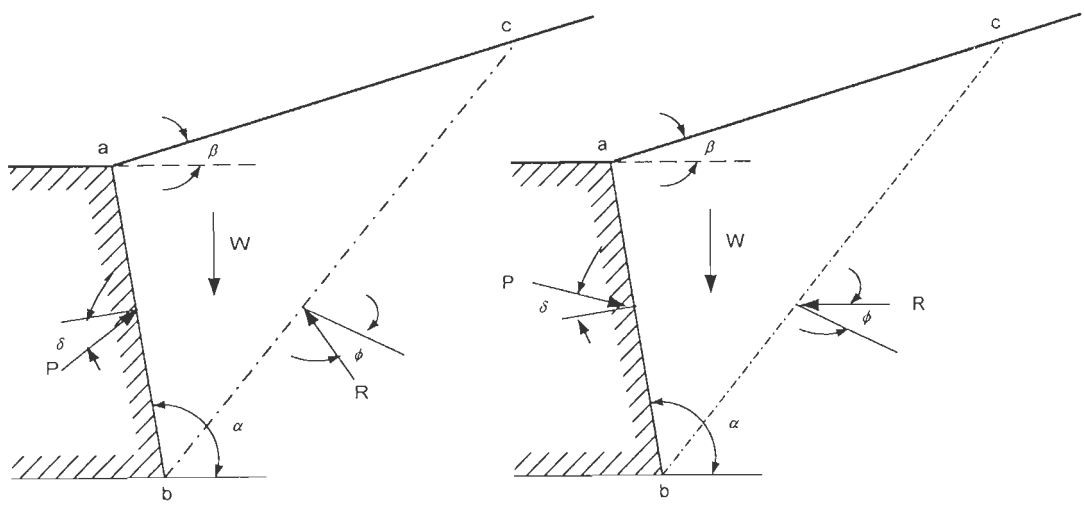

Fig. 3.15: Coulomb's failure wedge theory for active and passive earth pressure

The total active and passive earth pressure/thrust is given by

$$p_a = \frac{1}{2}\gamma H^2 K_a \quad \text{... (3.36a)}$$

$$p_p = \frac{1}{2}\gamma H^2 K_p \quad \text{... (3.36b)}$$

where, $$K_a = \left[\frac{\sin(\alpha-\phi)/\sin\alpha}{\sqrt{\sin(\alpha+\delta)}+\sqrt{\frac{\sin(\phi+\delta)\sin(\phi-\beta)}{\sin(\alpha-\beta)}}}\right]^2 \quad \text{... (3.37a)}$$

$$K_p = \left[\frac{\sin(\alpha+\phi)/\sin\alpha}{\sqrt{\sin(\alpha-\delta)}-\sqrt{\frac{\sin(\phi+\delta)\sin(\phi+\beta)}{\sin(\alpha-\beta)}}}\right]^2 \quad \text{... (3.37b)}$$

According to IS: 1893 (1984), the pressure coefficient from earthquake behind the retaining wall can be estimated by using the Mononobe-Okabe model which is given as

$$K_a = \frac{\sin^2(\alpha-\phi-\theta')}{\cos\theta'\sin^2\alpha\sin(\alpha+\delta-\theta')\left[1+\sqrt{\frac{\sin(\phi+\delta)\sin(\phi-\theta'-\beta)}{\sin(\alpha+\theta'-\delta)\sin(\alpha-\beta)}}\right]} \quad \text{... (3.38a)}$$

$$K_p = \frac{\sin^2(\alpha-\phi+\theta')}{\cos\theta'\sin^2\alpha\sin(\alpha+\phi+\theta')\left[1-\sqrt{\frac{\sin(\phi+\delta)\sin(\phi-\theta'+\beta)}{\sin(\alpha+\theta'+\delta)\sin(\alpha-\beta)}}\right]} \quad \text{... (3.39a)}$$

$$\theta' = \tan^{-1}\left[\frac{A_h}{1\pm A_v}\right] \quad \text{... (3.40)}$$

where, A_h and A_v are the horizontal and vertical seismic coefficients and $\delta = \phi/2$, is a wall friction angle.

In a survey conducted by Federal High-Way Administration (FHWA-05), 59% of the states accounted for passive earth pressures while designing the integral abutment bridges (Rodolfo and Petro, 2005). Many bridge engineers prefer to use Rankine or Coulomb

passive pressure calculations because of their simplicity. Oesterle (1999) reported that Rankine passive pressure is in good agreement with experimental result and in few cases the actual passive pressure can exceed the design values. According to the survey made by the Kunin and Alampalli, (1999) almost all the agencies considering the soil pressure in design followed uniform triangular Rankine load distribution. In the final report of integral bridge submitted by bridge engineering division, Edmund Hambly Ltd (Chakrabarti 1993), the relationship for earth pressure coefficient K was established by interpreting the test results and passive pressure distribution was considered as parabolic in shape, than triangular. The equation given in the report, to calculate earth pressure coefficient K is given by

$$K = (d/0.05H)^{0.4} K_p \gamma_m \qquad \ldots (3.41)$$

$$K = K_p \text{ at } (d/H) = 0.05.$$

where, γ_m is a material partial safety factor; $0.5 \le \gamma_m \le 2.0$; d is the maximum thermal movement at the top of the abutment, m and H is the height of soil behind abutment or height of the abutment. The BA 42/96 recommends different equations to calculate earth pressure on different types of integral abutments

$$K = (d/0.05H)^{0.4} K_p, \; K \le 0.6 \qquad \text{For framed abutment} \qquad \ldots (3.42)$$

$$K = K_o + (d/0.03H)^{0.6} K_p \qquad \text{For portal frames} \qquad \ldots (3.43)$$

$$K = K_o + (d/0.025H)^{0.4} K_p \qquad \text{For embedded abutment} \qquad \ldots (3.44)$$

Many of the design manuals use the design curves recommended by Colugh and Duncan, which were based on the numerical study using finite element method. Design handbooks and manuals like NAVFAC DM-7" (U.S Dept. of Navy), Canadian Foundation Engineering Manual (CFM 1992) and Manuals for the Design of Bridge Foundations (NCHRP 1991) give passive earth pressure curves for vertical wall subjected to lateral

movement. The curves given in "NAVFAC DM-7" and Canadian Foundation Engineering Manual are almost the same. The comparison of the curves given in these manuals is shown in Fig. 3.16.

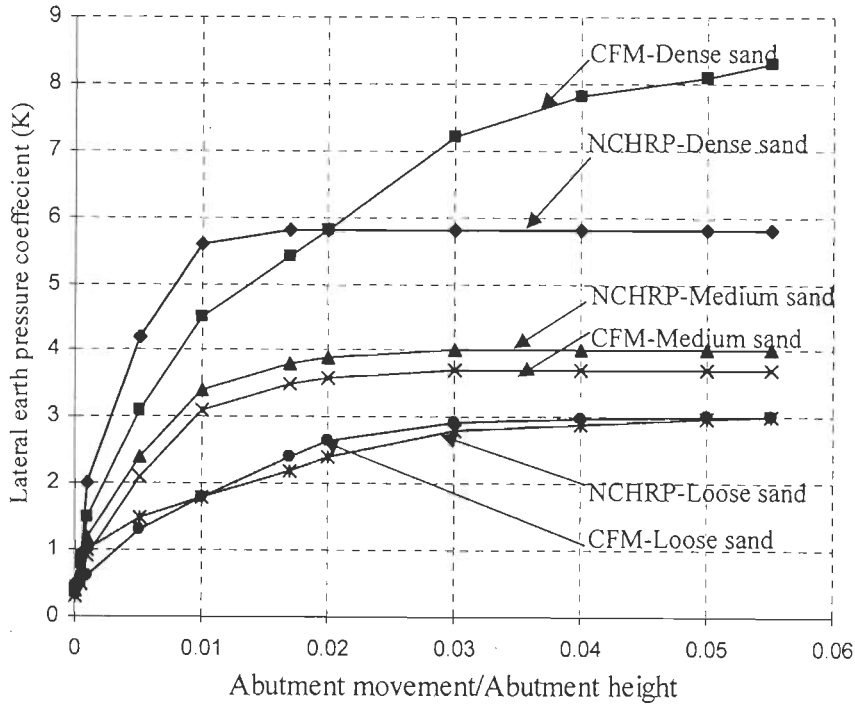

Fig. 3.16: Comparison of design curves given in different manuals

John and Faraji (1998) has compared the design curves given in NAVFAC DM-7, Canadian Foundation Engineering Manual and NCHRP (1991) with eleven experimental results conducted by different researchers for translation and base rotation of the abutment wall and concluded that NCHRP design manual underestimates peak passive resistance for dense cohesionless soils and also overestimates the initial soil stiffness. The design curves given in Canadian Foundation Engineering Manual are recommended for dense soil. For loose or medium soil, the curves given in NCHRP and CFM manuals follow the same path.

The equation to calculate the coefficient of passive earth pressure which suits the NCHRP design curves (Bonczar *et al.* 2005) is given by

$$K = 0.43 + 5.7[1 - e^{-190(d/H)}] \quad \ldots (3.45)$$

England *et al.* (2000) based on the limited experimental data, recommended the equation to calculate earth pressure on integral abutments, which is shown in Eq. 3.46, it was based on the lateral earth pressure distribution assumed in BA/42 with modification in the initial limits

$$K = K_o + (d/0.03H)^{0.6} K_p \quad \ldots (3.46)$$

The plot of the different equations used to calculate the coefficient of passive earth pressure against the integral abutment movement is shown in Fig. 3.17.

The design curves for medium and dense soil given in CFM and NCHRP 1991 are compared with the equations used by different researchers for integral abutment modeling, the results are shown in Fig 3.18 and Fig 3.19.

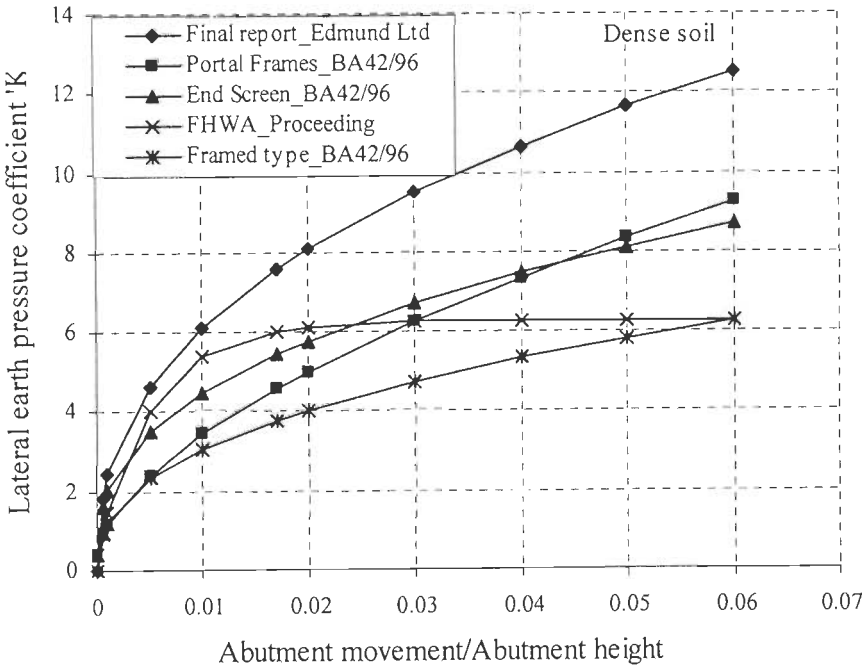

Fig. 3.17: Comparison of equations given by different manuals and researchers to find lateral earth pressure in dense sand

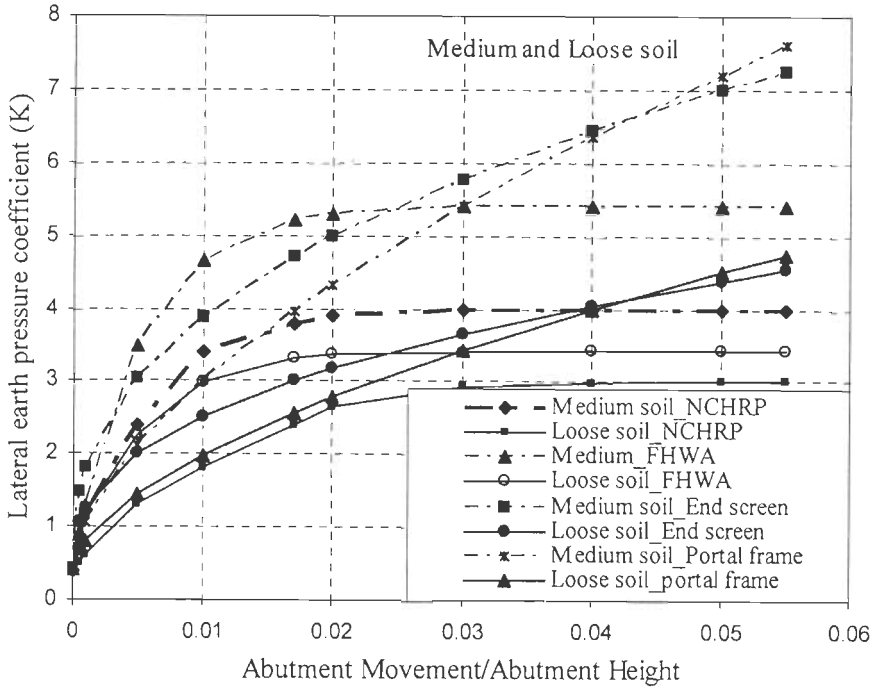

Fig. 3.18: Comparison of design curves and proposed equations of lateral earth pressure in medium and loose sand

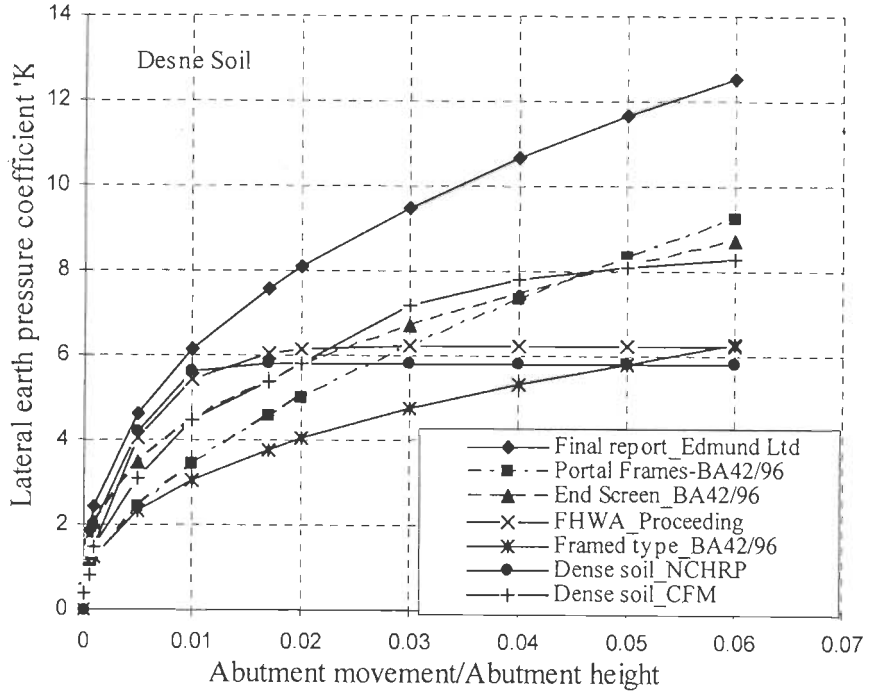

Fig. 3.19: Comparison of design curves and proposed equations of lateral earth pressure in dense sand

From Fig. 3.18, for medium and loose soil the equation used by Bonczar follows the curves given in NCHRP and CFM. For dense soil, from Fig. 3.19 it is seen that the equation given by BA 42/96 for portal frame and end screen embankment are very close to the curves given in Canadian Foundation Engineering Manual. The following equations are used to model dense soil behind integral abutment

$$K = K_o + (d/0.03H)^{0.6} K_p \quad \text{or} \quad K = K_o + (d/0.025H)^{0.4} K_p \qquad \ldots (3.47)$$

For Loose and Medium soil

$$K = 0.43 + 5.7[1 - e^{-190(d/H)}] \qquad \ldots (3.48)$$

Using the coefficient of earth pressure K, obtained from above equations, the passive earth pressure p_p is given by

$$p_p = K\gamma z \qquad \ldots (3.49)$$

The force F in the spring is obtained by multiplying calculated backfill pressure with the area tributary to each spring element.

$$F = K\gamma zhs \qquad \ldots (3.50)$$

where, γ is the effective soil weight of the backfill, kN/m^3 ; z is the distance from the top of the abutment, m; h is the vertical spacing between two springs or nodes, m and s is the horizontal spacing between two springs or girder spacing, m.

The non-linear force-displacement relationship for the spring is obtained from above equations, for dense soil, substituting Eq. 3.47 to Eq. 3.50,

$$F = (K_o + (d/0.03H)^{0.6} K_p)\gamma zhs$$

or $$F = (K_o + (d/0.025H)^{0.4} K_p)\gamma zhs \qquad \ldots (3.51)$$

For medium and loose soil, substituting Eq. 3.48 to Eq. 3.50

$$F = \{K_o + K_p[1 - e^{-190(d/H)}]\}\gamma zhs \qquad \ldots (3.52)$$

3.7 CONCLUDING REMARKS

Modeling the soil-pile interaction as a Winkler beam-column with nonlinear soil springs has been found to be adequate if the soil near the ground surface is properly modeled. The non-linear curves used in API (2000) given by Reese and Matlock are found to be suitable for the modelling lateral soil stiffness in integral bridges. The comparative study between the available design curves and proposed equations by experimental analysis has helped to conclude that the design curves for abutment backfill pressure given in Canadian Foundation Engineering Manual are suitable for modelling the dense soil, and for loose and medium soils the design curves given in both CFM and NCHRP manuals are found to be suitable. Based on the study, the non-linear force-displacement relationships as given by Eqs. (3.51) and (3.52) are recommended to capture in backfill behavior.

CHAPTER-4

MODELLING OF INTEGRAL ABUTMENT BRIDGES AND ANALYSIS

4.1 INTRODUCTION

The three dimensional structural model of the Integral Abutment Bridge is developed which includes the modelling of the bridge deck, piers, abutments, piles, soil-pile interaction and abutment backfill interaction. Analysis of the bridge model is concentrated mainly on temperature and seismic loadings using the finite element program (SAP). The details of the structural system of integral bridges with respect to the modelling are discussed.

4.1.1 Numerical Example of an Integral Abutment Bridge

A typical five span continuous concrete bridge with integral abutments is taken for the study. Bridge is 130 m long and 12 m wide with three lanes as shown in Fig. 4.1. Superstructure consists of concrete deck of 200 mm thick and five cast-in-situ reinforced concrete girders equally spaced at 2.5 m center to center as shown in Fig. 4.2 and cross beams places at 5.0 m center to center. Piers are of circular in shape having 1.5m dia resting on the pile foundation consisting of two rows of piles with 4 piles in each row of 1.0 m dia spaced at 3.0m center to center and thickness of pile cap is 1.5m as shown in Fig. 4.3. The abutment width is 1.0/1.2 m and rest on a row of 5 piles of 1.0/1.2 m each. The depth of the pile is taken as 25.0m. Pile and abutment junctions are locally thickened to accommodate the piles.

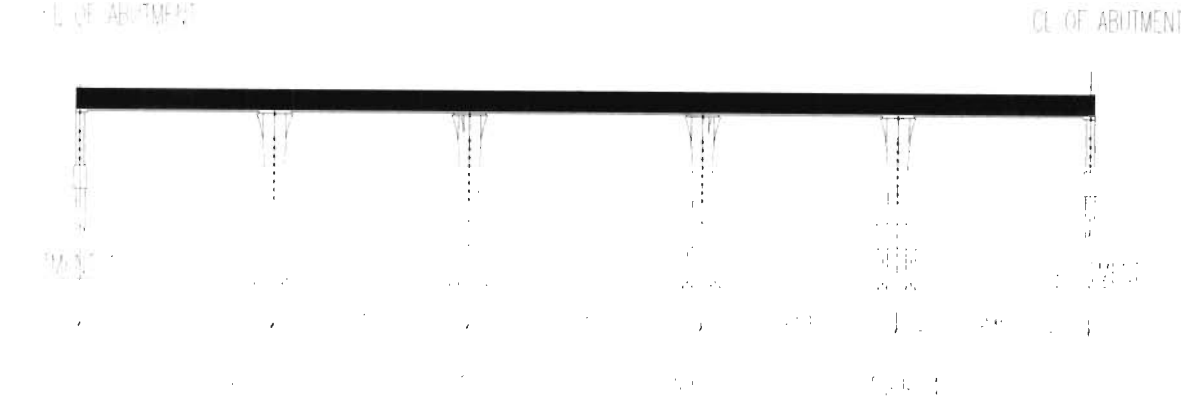

Fig. 4.1: Typical integral abutment bridge of 5 span

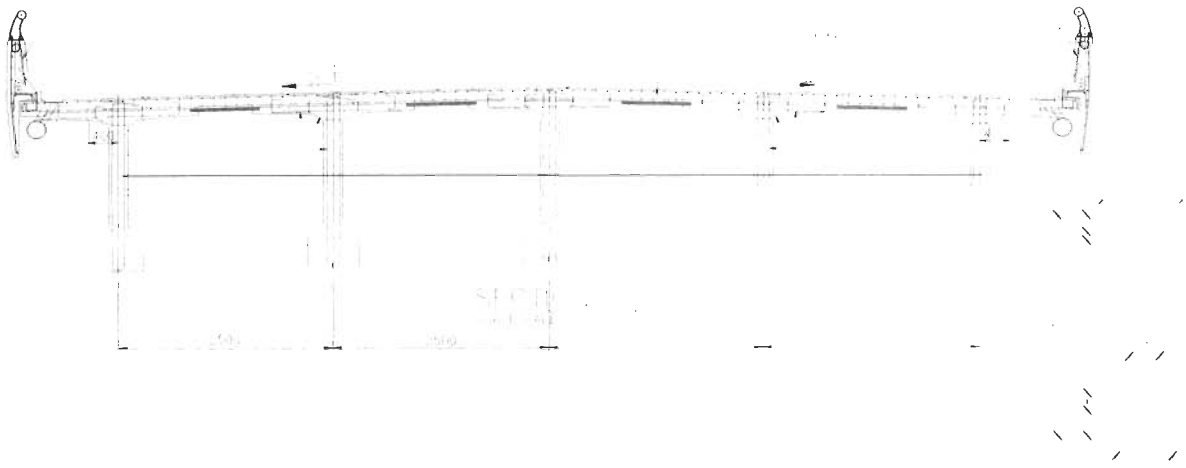

Fig. 4.2: Typical cross-section of concrete deck and cast-in-situ reinforced concrete girders

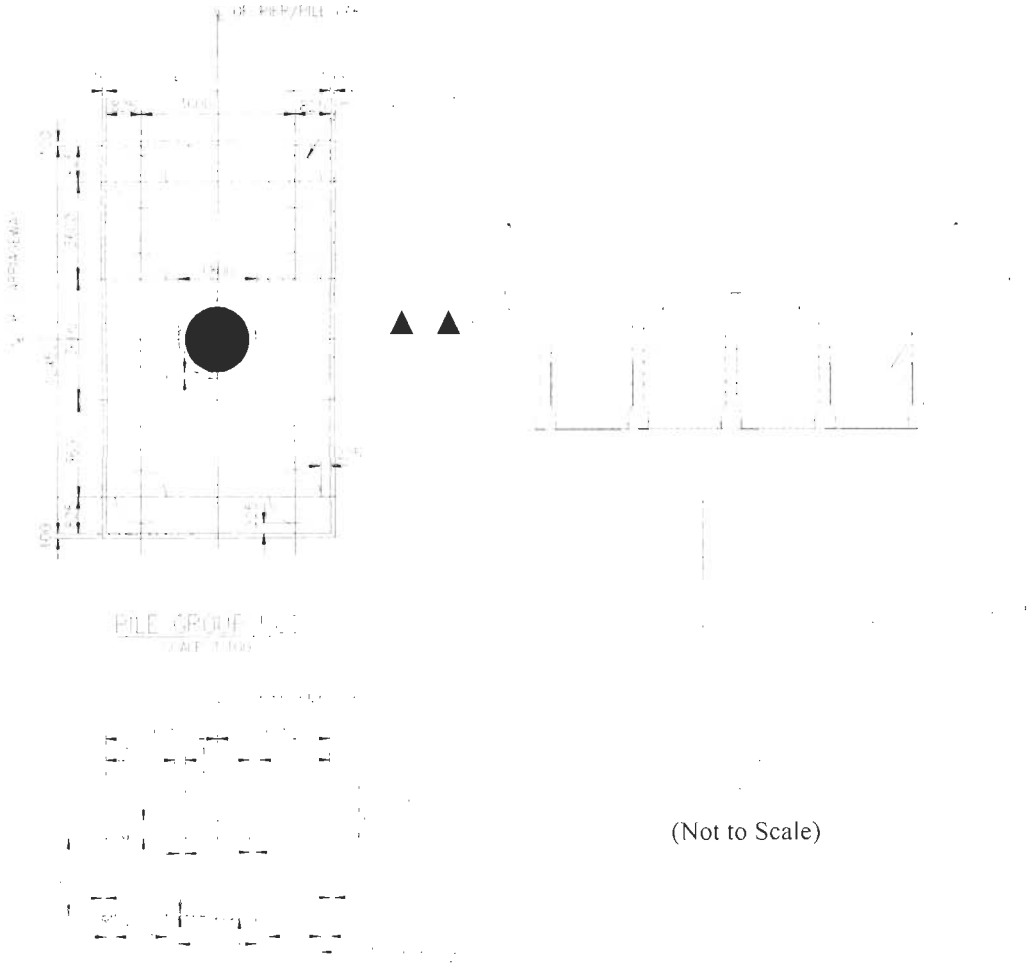

Fig. 4.3: Cross-section of pier and pile cap

4.2 MATERIAL MODELS

4.2.1 Concrete and Reinforcement Steel

Modulus of elasticity of concrete is given by $E_c = 5000\sqrt{f_{ck}}$, where f_{ck} is the characteristic cube compressive strength of concrete, N/mm^2. Figure 4.4 (a) shows idealized stress-strain curve for unconfined concrete in uniaxial compression. The maximum flexural strain at the outer most compression fiber of the concrete is limited to 0.0035 (IS 456:2000). The grade of steel denotes the specified characteristic yield stress. The stress-strain relation of reinforced steel used in the substructure modelling is shown in Fig 4.4 (b). Modulus of elasticity of steel is taken as 2.1E5 N/mm^2.

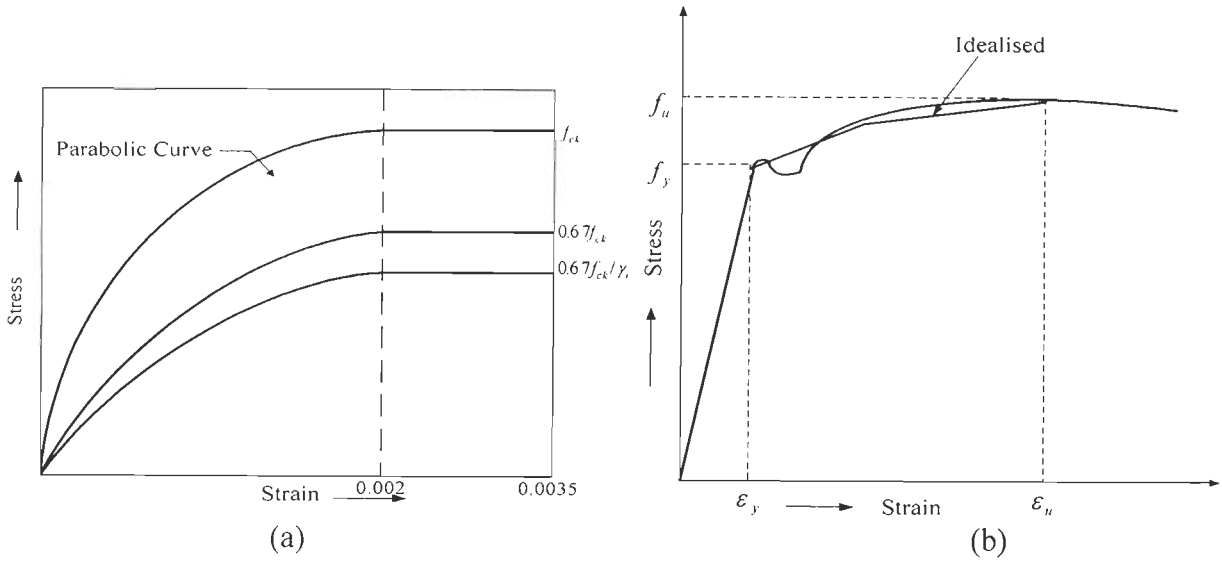

Fig. 4.4: Stress-strain curve for concrete and reinforced steel (IS 456: 2000)

4.2.2 Confinement Effect of Concrete

Confined concrete model proposed by Mander *et al.* (1988) shown in Fig. 4.5 is used for material modelling of the piers and piles. Piers and piles are provided with circular or spiral reinforcement to satisfy the confinement effect. The compressive stress-strain response used for the core and cover concrete is as follows,

$$\varepsilon_{cc} = \varepsilon_{co}\left[1 + 5\left(\frac{f_{cc}^{'}}{f_{co}^{'}} - 1\right)\right] \quad \ldots (4.1)$$

$$E_{c} = \frac{f_{cc}^{'}}{\varepsilon_{cc}} \quad \ldots (4.2)$$

$$E_{\sec} = \frac{f_{co}^{'}}{\varepsilon_{co}} \quad \ldots (4.3)$$

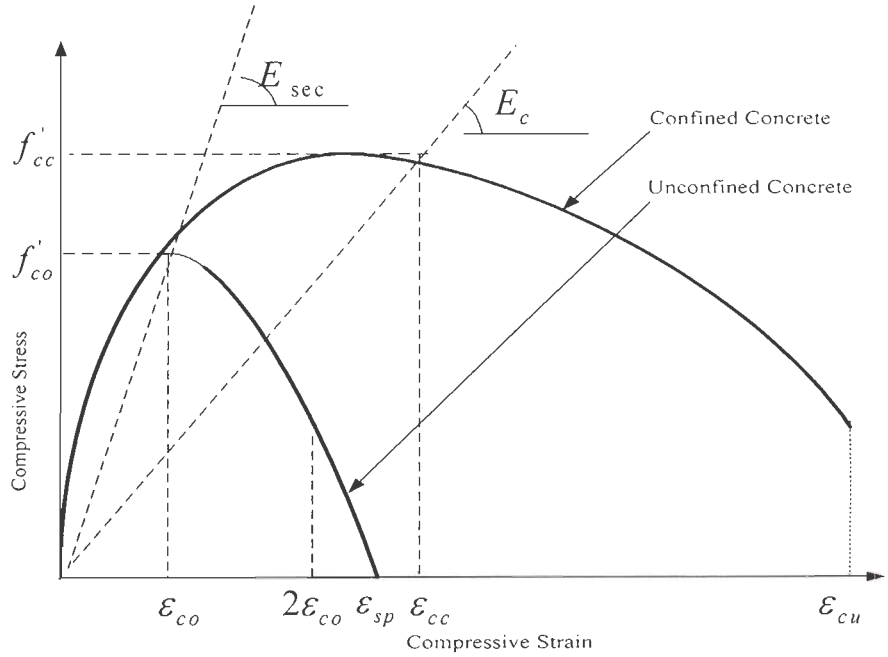

Fig. 4.5: Stress-strain curve (Mander *et al.* 1988)

The confined concrete compressive stress for circular sections is given by

$$f_{cc}^{'} = f_{co}^{'}\left[2.254\sqrt{1 + \frac{7.94 f_{1}^{'}}{f_{co}^{'}}} - \frac{2f^{'}}{2f_{co}^{'}} - 1.254\right] \quad \ldots (4.4)$$

$$f_{1}^{'} = \frac{1}{2} K_{e} \rho_{s} f_{yh} \quad \ldots (4.5)$$

$$K_{e} = \begin{cases} (1 - S/2d_{s})^{2}/(1 - \rho_{cc}) & \textit{for circular hoops} \\ (1 - S/2d_{s})/(1 - \rho_{cc}) & \textit{for circular spirals} \end{cases} \quad \ldots (4.6)$$

$$\rho_{s} = \frac{4A_{sp}}{d_{s}S} \quad \ldots (4.7)$$

where, $f_{cc}^{'}$ and ε_{cc} are compressive strength of confined concrete and corresponding longitudinal strain, ε_{cc} increases linearly with $f_{cc}^{'}$; $f_{co}^{'}$ and ε_{co} are compressive strength of unconfined concrete and corresponding strain. $f_{1}^{'}$ is the effective lateral confining

pressure; f_{yh} is the yield stress of the transverse reinforcement; S is the clear vertical spacing of stirrups, d_s is the diameter of the bar, ρ_{cc} is the longitudinal steel ratio and K_e is confinement effectiveness coefficient (0.95 for circular section and 0.75 for rectangular column section). f_y is the yield stress of steel. Properties of the structural members are shown in Table 4.1

Table 4.1: Properties of structural members

Members	Concrete	f_{ck} (Mpa)	Steel	f_{ck} (Mpa)
Girders	M 45	45	Fe 500	500
Deck & Abutment	M 45	45	Fe 500	500
Piers	M 45	45	Fe 500	500
Piles	M 35	35	Fe 500	500

The Mander's material model for concrete considered for the moment curvature is as follows. For concrete the yield strain is taken as 0.002 and crushing strain as 0.0035 and spalling strain as 0.005. After the crushing strain is reached, the model assumes straight line strength degradation to the post crushing strength at the completion of spalling. The steel used is the High Yield Strength Deformed (HYSD) bars, the yield point is obtained at 0.2% proof strain The bilinear steel material model is used, in which a linear relation up to yield (0.002 as per Indian code), then a secondary linear relationship i.e hardening is based on the percentage of the primary slope. The ultimate strain is taken as 0.06. The yield moment in moment curvature relationship is corresponding to the first yield of steel.

4.3 FINITE ELEMENT MODELLING

4.3.1 Superstructure

The superstructure is modeled using four nodded shell element and two nodded frame elements. Both shell and beam elements are having six degrees of freedom and interaction of in-plane and out-of-plane forces takes place throughout the shell element. Behavior of frame element is fully three-dimensional and they can be oriented arbitrarily.

The eccentricity of the deck and girder elements were modeled explicitly, with rigid links connecting the girders and deck slab to ensure strain compatibility and shear transfer between the deck slab and the girder elements. Superstructure is connected to diaphragm with rigid link elements as shown in Fig. 4.6. Superstructure is expected to remain in elastic state under seismic forces but the bending in reinforced concrete superstructure can enhance already existing cracking from gravity load, live load and secondary forces like temperature, shrinkage and creep. Hence effective or cracked stiffness properties are used for superstructure. Effective cracked stiffness EI_e is given by (Priestley *et al.* 1996)

$$EI_e = \begin{cases} 0.5EI_g - 0.75EI_g & \text{Reinforced Concrete} \\ 1.0EI_g & \text{Prestressed Concrete} \end{cases} \quad \ldots (4.8)$$

where, EI_g is the gross-section stiffness. In reinforced concrete, the lower and upper limit of effective stiffness represents lightly and heavily reinforced sections respectively.

4.3.2 Substructure

Substructure is mainly containing the piers and abutments. Piers are modeled by using non-linear three dimensional frame elements. The monolithic connection between superstructure and substructure creates additional location for energy dissipation under seismic condition. Significant inelastic action is expected at top and bottom of the pier, during which the strain is transferred into adjacent members and gives additional flexibility (Priestley *et al.* 1996). This additional flexibility is modeled with additional beam elements as shown in Fig. 4.7.

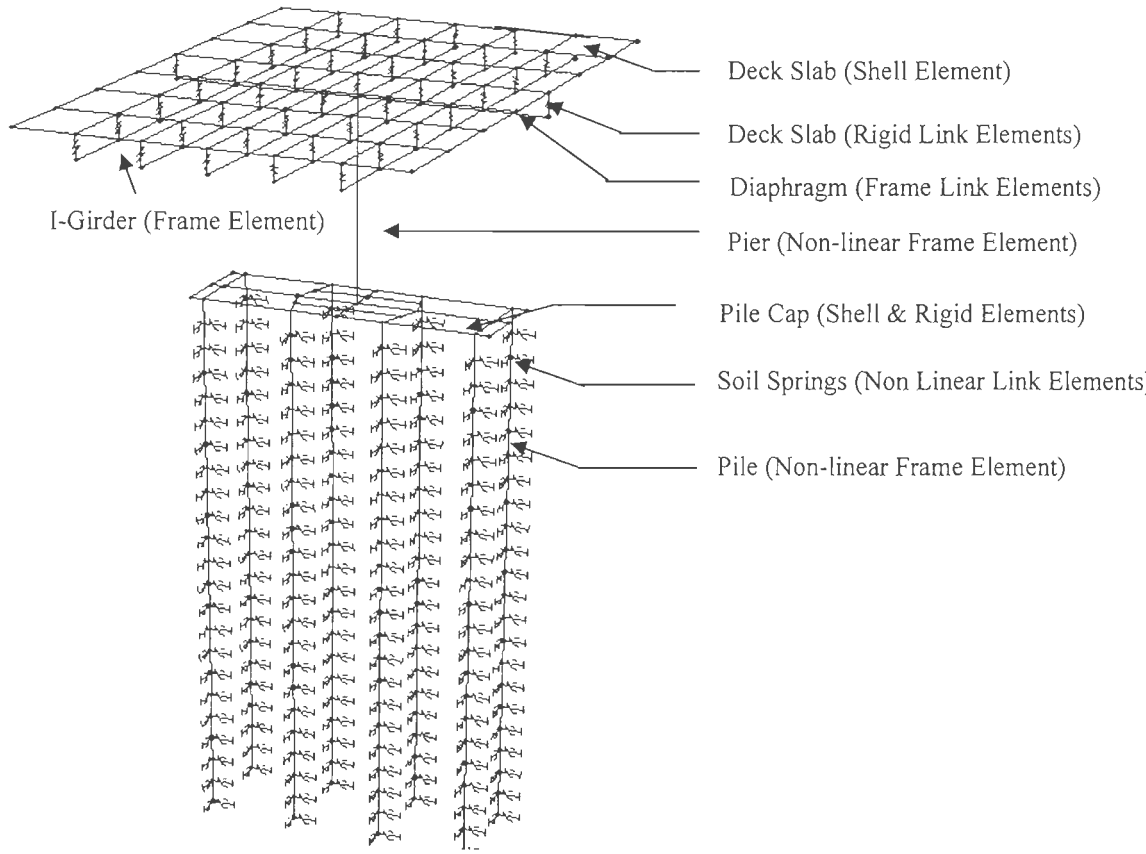

Fig. 4.6: Finite element model of integral bridge representing lateral-soil-pile, pier and superstructure modelling

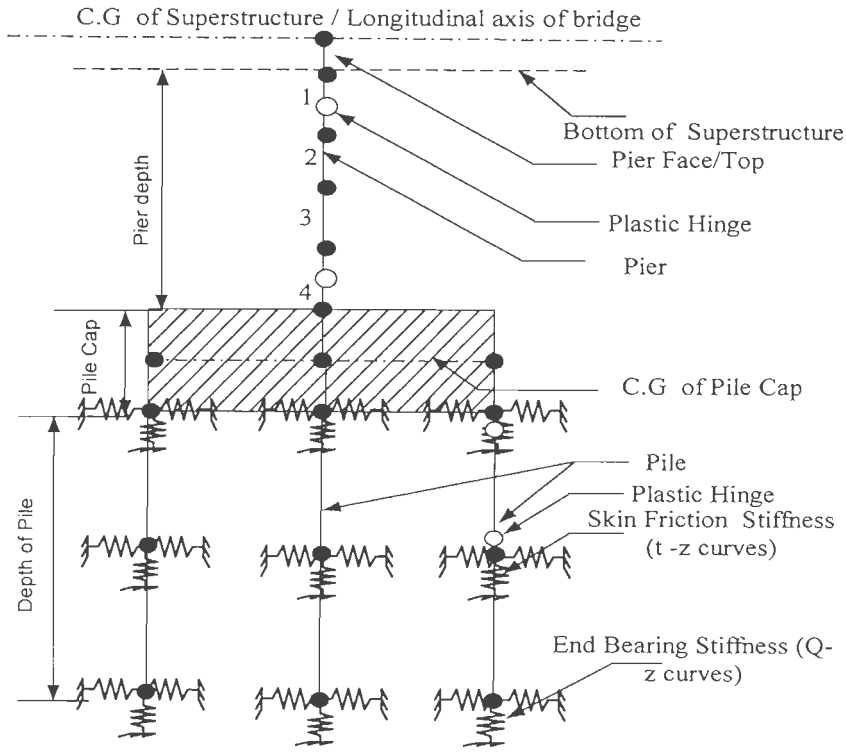

Fig. 4.7: Modelling of single-pier-bent along with soil-pile interaction

Four frame elements are used to model single-pier-bent between superstructure soffit and the top of footing. The plastic hinge length L_p proposed by Priestly *et al.* (1996) is given by

$$L_p = 0.08f + 0.022d_l f_y \geq 0.044 f_y d_l \quad \ldots (4.9)$$

where, d_l is the diameter of longitudinal reinforcement. According to Priestly, in absence of specific data plastic hinge length can be approximately taken as $0.5D$.

The plastic hinge length used for piles (Soong *et al.* 2005) is given by

$$L_p = 0.04f + 0.022d_l f_y \geq 0.044 f_y d_l \quad \ldots (4.10)$$

Non-linear characteristics of frame elements are taken based on moment-curvature of the frame section taking axial load and confinement effects into consideration. For the ductile elements like piers and piles the effective flexural stiffness is obtained from the initial slope of the $M-\phi$ curve between the origin and the point designating the first reinforced bar yield. According to Priestly *et al.* (1996) effective stiffness is given as

$$EI_{eff} = \frac{M_y}{\phi_y} \quad \text{(or)} \quad \ldots (4.11)$$

$$EI_{eff} = 0.7EI_g \text{ (According to Caltrans and FEMA 273)} \quad \ldots (4.12)$$

where M_y and ϕ_y are yield moment and rotation. The moment-curvature curves for 1.0 and 1.2 m pile having longitudinal reinforcement (P) of 1.0%, 1.5% and 2.0% and 1.0 % transverse reinforcement using Mander's confined concrete model for the core and unconfined concrete mode for cover is shown in Fig. 4.8.

4.3.3 Fatigue Damage Model for Piles

Piles in the integral bridges will be subjected to lateral loads due cyclic temperature and seismic loads which induce the large curvature demand in the pile. The undesirable failure modes due to this cyclic lateral loads in the piles should be avoided. It can be

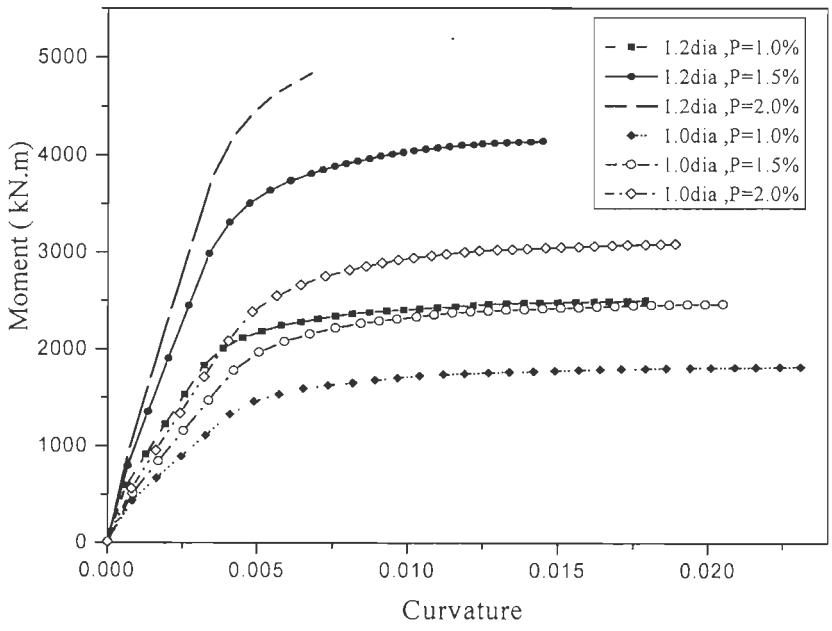

Fig. 4.8: Moment curvature curves for the piles of different dia

done by controlling the curvature ductility demand in the potential plastic hinge region of the pile. The field test have confirmed that small strain cycles due to daily temperature variations ranges from 20 to 40% of that of large strain cycles which are caused yearly once (Dicleli and Suhail, 2003). The amplitude of positive and negative strain cycles corresponding to the summer and winter may not be equal. But they can be assumed as same to simplify the analysis. There are many models available to quantify damage caused due to low cycle fatigue, in which most of them are based on Miner's rule (Perera *et al.* 2000), which is given as

$$D_{ni} = \sum \frac{n_i}{N_f} \qquad \ldots (4.13)$$

where, n_i is the number of cycles for the current amplitude and N_f is the number of cycles to failure at the same amplitude. According to Perera *et al.* (2000) four levels of damage index have been identified for the concrete columns. They are as follows, $0 \le D_n \le 0.33$ insignificant, $0.33 \le D_n \le 0.45$ minor, $0.45 \ge D_n \le 0.55$ moderate and $D_n \ge 0.55$ heavy. The experimental studies by Mander *et al.* (1994) and Koh and Stephen (1991) have given the equations to calculate N_f based on the strain amplitude,

$$\varepsilon_t = 0.08(2N_f)^{-\frac{1}{3}} \quad \text{according to Mander } et\ al. \qquad \ldots (4.14a)$$

$$\varepsilon_p = 0.08(2N_f)^{-\frac{1}{2}} \quad \text{according to Koh and Stephen} \qquad \ldots (4.14b)$$

where ε_t is total strain and ε_p is plastic strain as shown in Fig. 4.9.

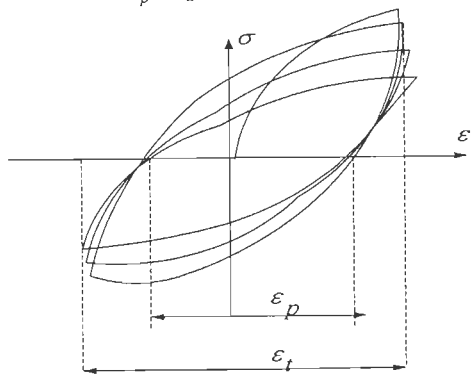

Fig. 4.9: Total and plastic strain amplitude (Perera *et al.*

It is possible to transform the low cycle fatigue behavior of individual reinforcing bars into familiar fatigue life expression for concrete columns and piles (Dutta and Mander, 2001). The relationship between the total plastic strain range ε_p with the dimensionless plastic curvature of section is given by

$$\varepsilon_p = \phi_p \frac{d}{2} \qquad \ldots (4.15)$$

where, d is the distance between outer layers of steel in rectangular section or pitch circle diameter of the longitudinal bars in a circular section as shown in Fig. 4.10

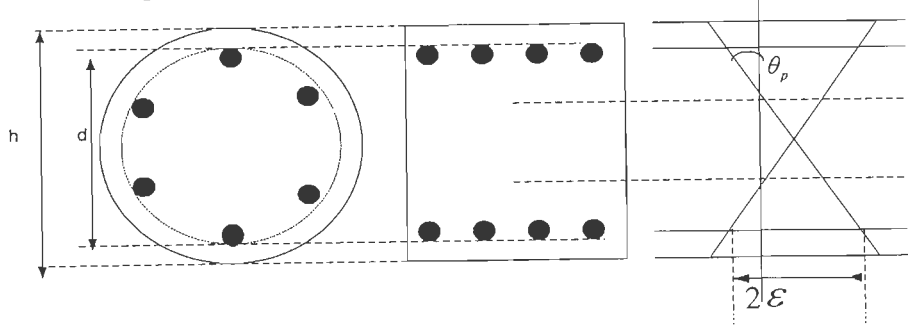

Fig. 4.10: Cross section of pile and relation strain and plastic curvature (Dutta and Mander, 2001)

$$\phi_p d = 0.16(2N_f)^{-\frac{i}{2}} \qquad \text{(from Eqs 4.14b - 4.15)} \qquad \ldots (4.16)$$

The length of the integral abutment bridge is restricted based on the yield displacement capacity of piles. Assuming the piles of 1.0 m and 1.2 m diameter to undergo one cycle of large displacement per year and the design life of bridge is100 years than the piles will

be subjected to 100 ($n_i = 100$) large cycles, the damage index based on the yield strain of the pile is shown in Table 4.2. The damage index for both 1.0m and 1.2m dia piles is found to be within 0.03 for 100 years bridge life, which shows insignificant damage as per the damage levels given by Perera *et al.* (2000).

Table 4.2: Yield curvature and damage index for piles

Pile Dia 'm'	Reinforcement '%'	ϕ_y	d 'm'	N_f	D_n
1.0	1.0	3.79E-03	0.9	4401	0.023
1.0	1.5	4.20E-03	0.9	3583	0.028
1.0	2.0	4.23E-03	0.9	3533	0.028
1.2	1.0	3.05E-03	1.1	4561	0.022
1.2	1.5	3.39E-03	1.1	3682	0.027
1.2	2.0	3.48E-03	1.1	3494	0.029

4.3.4 Abutment-Backfill with Pile Foundation

Abutments are modeled by using shell elements and soil behind the abutment is modeled by using non-linear spring elements as shown in Fig. 4.11.The centroid of deck and centroid of girder are rigidly connected to abutment walls using rigid link elements. The non-liner spring properties of the backfill soil are calculated using (BA 42/96 & Bonczar *et al.* 2005),

$$F = K_0 + (d/0.03H)^{0.6} K_p \gamma z h s \text{ or } F = K_0 + (d/0.025H)^{0.4} K_p \gamma z h s \quad \ldots (4.17)$$

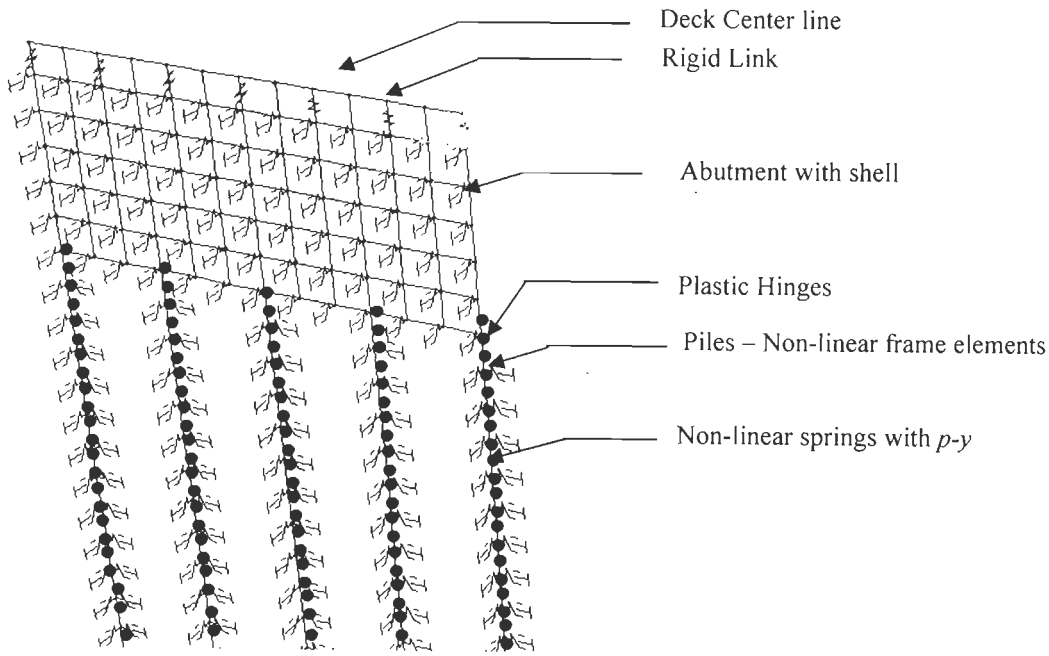

Fig. 4.11 Finite element modelling of abutment and backfill soil

$$F = \{K_0 + K_p[1 - e^{-190(d/H)}]\}\gamma zhs \qquad ...(4.18)$$

The properties of backfill soil used in the analysis are shown in Table 4.3. Figures 4.12 and 4.13 represent non-linear backfill soil behaviour behind the right and left abutment for soft and hard soil respectively. Curves are generated for 6.0 m height abutment taking the horizontal and vertical distance between the nodes as 1.0m.

Table 4.3: Backfill soil properties used in analysis

Abutment Backfill	ϕ in Degree	γ	K_p
Loose Sand	30.00	12	3.00
Medium Sand	37.00	16	4.00
Dense Sand	45.00	20	5.80

The modelling of the pile beneath the abutments follows the same procedure given in Section 4.3.2. Since the abutment is resting on single row of end bearing piles the '*P*' multiplier of 0.5 is applied only for transfer stiffness of the springs. Piles are modeled to take the moments from the abutment wall. The piles under the piers the '*P*' multiplier of 0.5 is applied in both the directions.

Foundation consists of pile cap and piles. Piles are modeled using frame elements and soil-pile interaction is modeled by using non-linear spring elements with *p-y* curves (Hutchinson *et al.* 2002). Axial and lateral soil resistances are assumed to be uncoupled. The lateral soil behavior is assumed to be independent in the two orthogonal lateral directions and the soil at a particular depth is taken independent of the soil behavior at another depth. The properties of sand and clay used for *p-y* curve generation are given in Tables 4.4-4.5. Hyperbolic tangent method is used to generate *p-y* curves in sand (discussed in Section 3.2.2). *p-y* curves generated for loose sand, medium sand and dense sand are shown in Figs. 4.14 to 4.16. The methods proposed by Reese and Matlock

(discussed in Section 3.2.3) are used to develop *p-y* curves for soft clay and stiff clay, which are shown in Figs 4.17 and 4.18 respectively. The size of pile was considered as per Standard Specifications and Code of Practice for Road Bridges- Foundation and Substructure (IRC 78-2000) and as per IS 2911:1979.

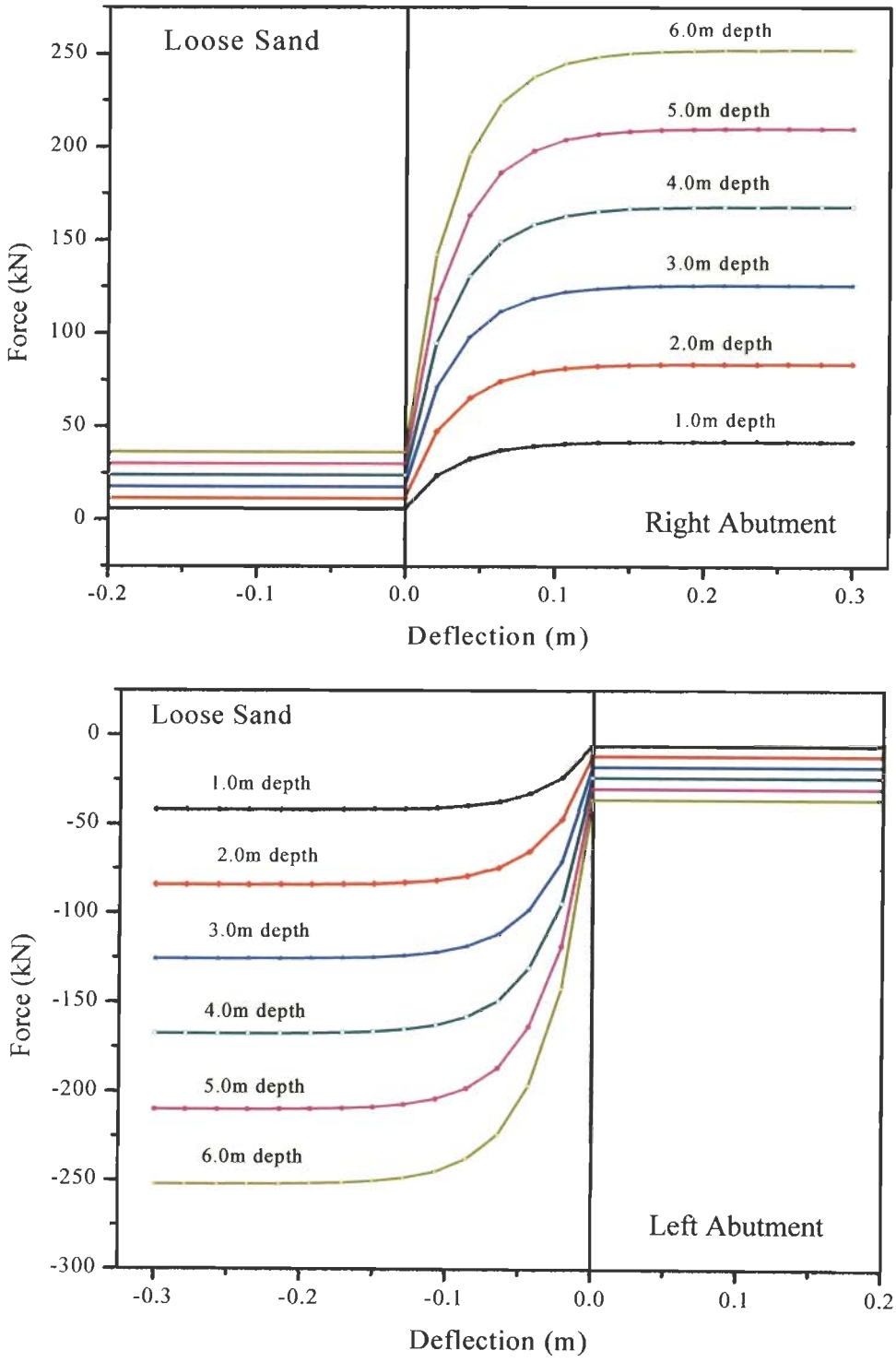

Fig. 4.12: Force deflection curve for right and left abutment backfill-loose sand

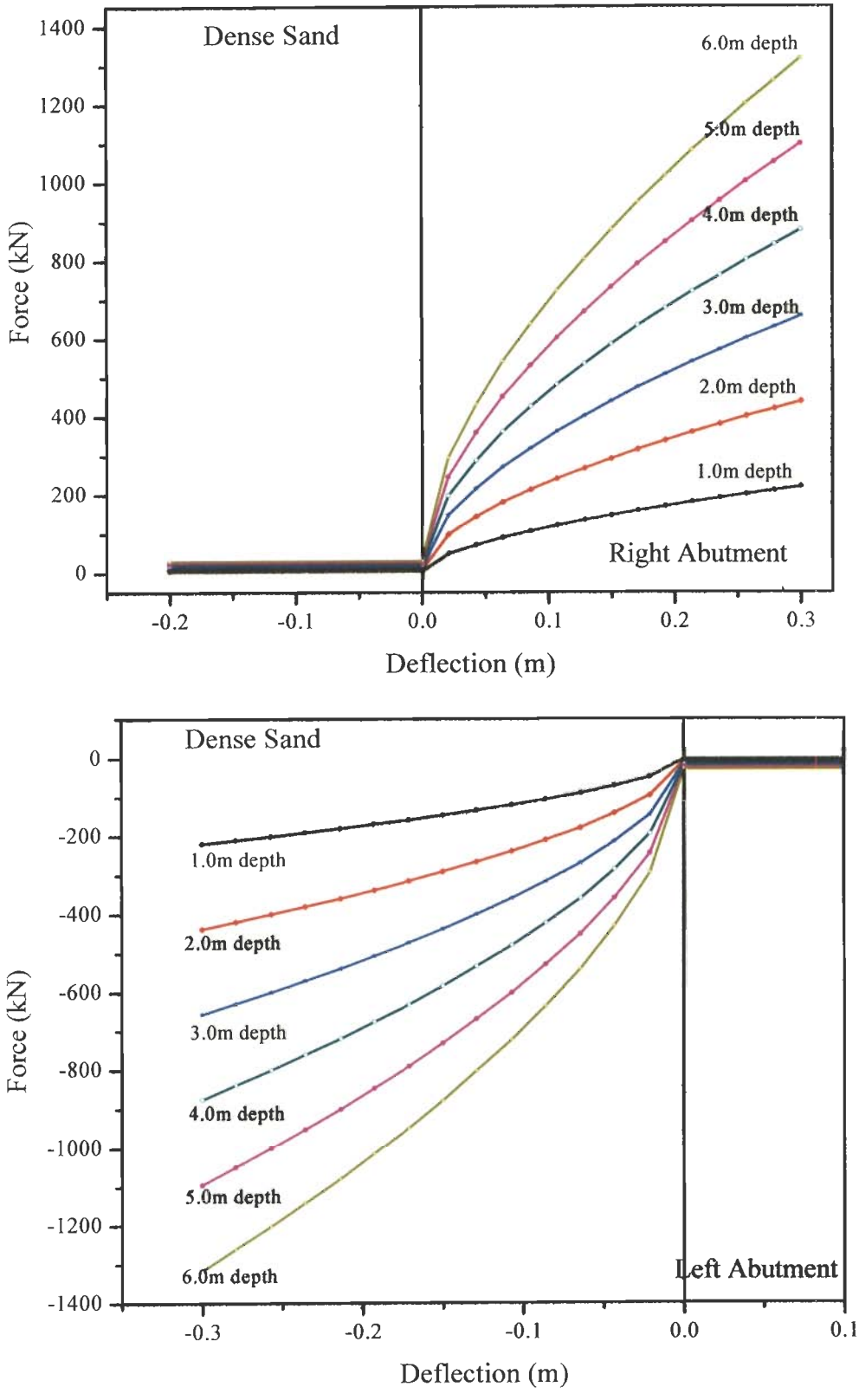

Fig. 4.13: Force deflection curve for right and left abutment backfill-dense sand

Table 4.4: Properties of sand used in the analysis

Sand type	ϕ	γ	k	p_0	N_q	N_γ
Loose Sand (LS)	25.00	12	12000	65	18	22
Medium Sand(MS)	30.00	16	35000	90	39	70
Dense Sand(DS)	40.00	20	60000	120	64	109

Table 4.5: Properties of clay used in the analysis

Clay type	c_u	γ	ε_{50}	J
Soft Clay (SC)	40.00	12	0.02	0.5
Stiff Clay(PC)	135.00	20	0.005	0.3

In table 4.4, N_q is the bearing capacity factor depending on the angle of internal friction; N_r is the bearing capacity factor depending on the angle of internal friction, p_o is the effective over burden pressure, k is the initial modulus of subgrade reaction, for abutment piles the subgrade modulus accounts for the effect of weight of the backfill and embankment. J is the dimensionless factor and c_u is the undrained shear strength of the clay.

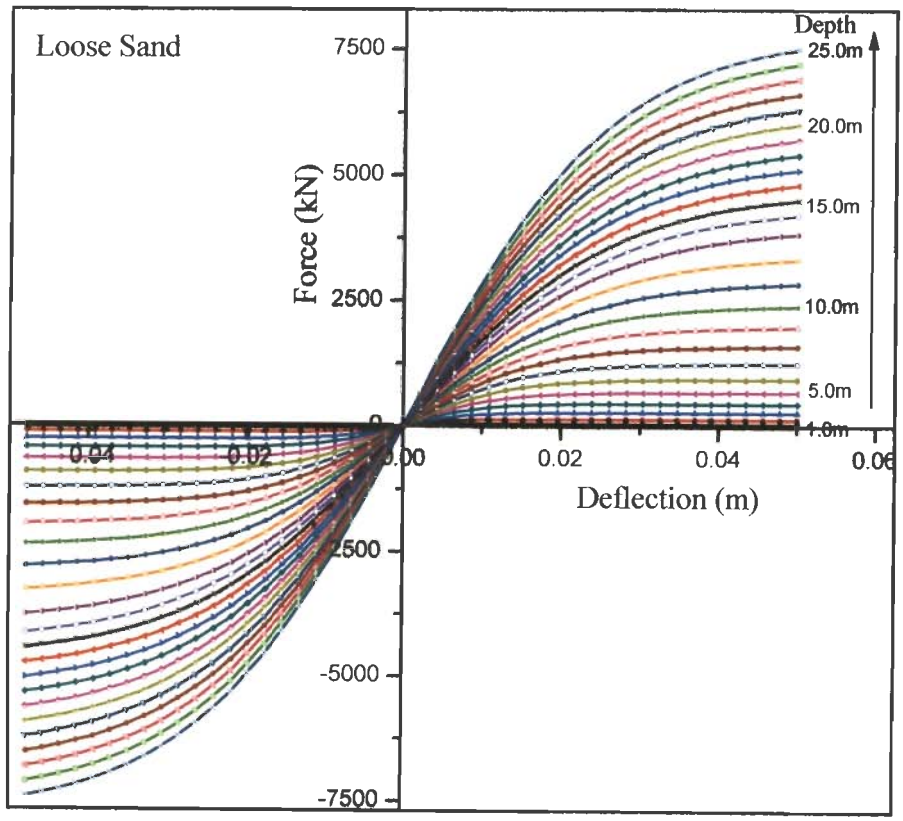

Fig. 4.14: Force-deflection curves at different depths in loose sand for 1.0 m dia pile

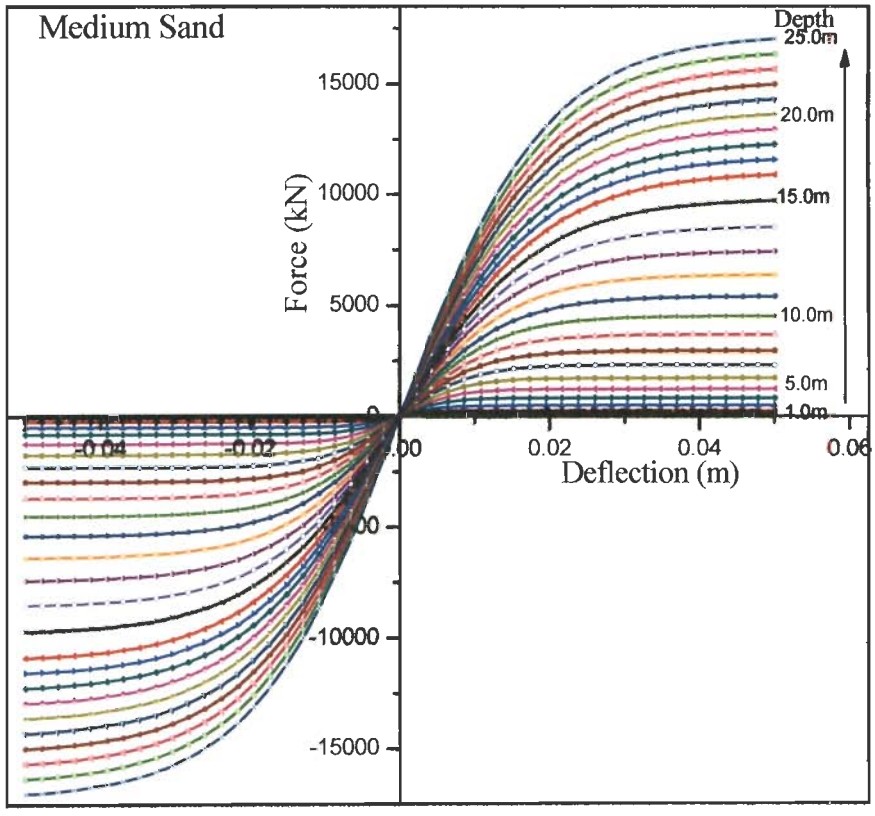

Fig. 4.15: Force-deflection curves at different depths in medium sand for 1.0 m dia pile

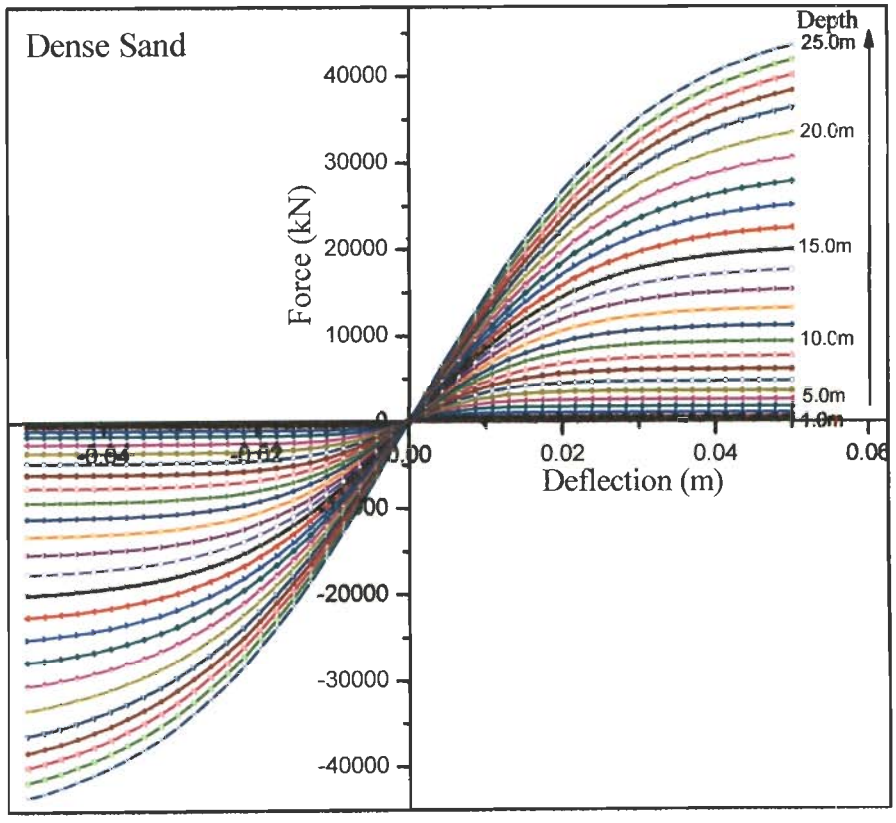

Fig. 4.16: Force-deflection curves at different depths in dense sand for 1.0 m dia pile

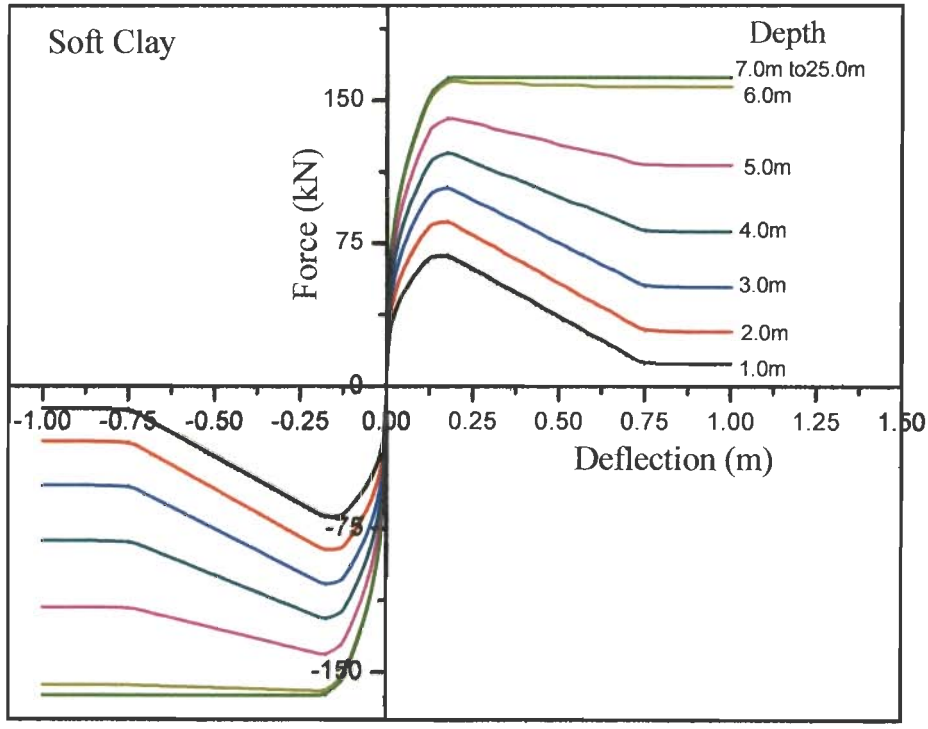

Fig. 4.17: Force-deflection curves at different depths in soft clay for 1.0 m dia pile

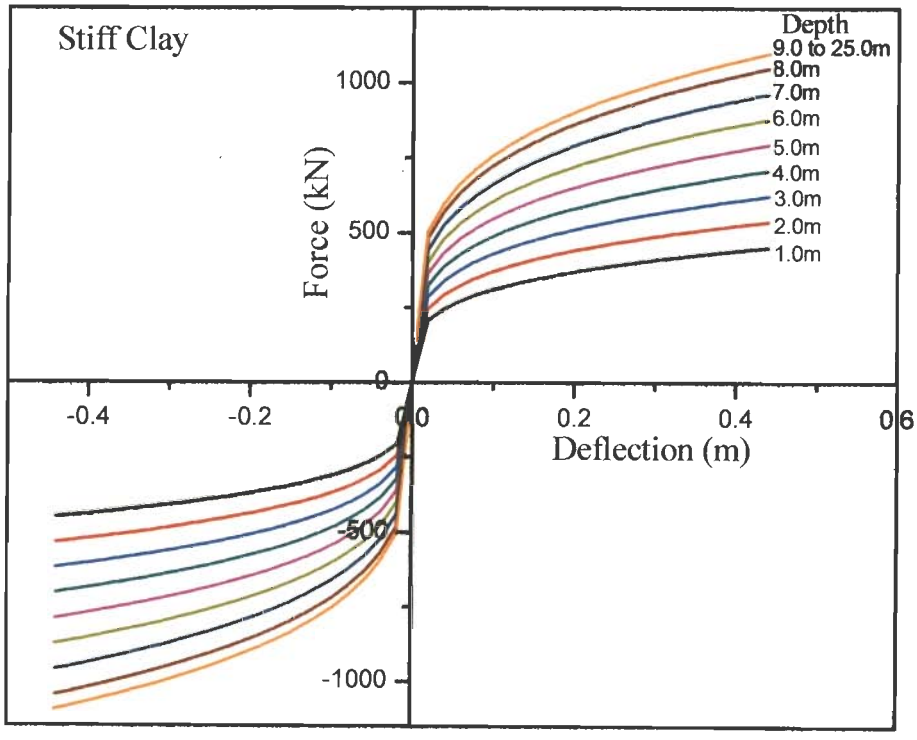

Fig. 4.18: Force-deflection curves at different depths in stiff clay for 1.0 m dia pile

The *t-z* curves and Q-*z* curves representing the soil-pile frictional and end bearing resistance, which contributes for axial capacity of the pile are shown in Figs. 4.19 and 4.20 for sand and clayey soils respectively. They are developed based on the API-RP2A-1993 recommendations as explained in Section 3.4. The complete three dimensional finite element model of integral abutment bridge is shown in Fig. 4.21.

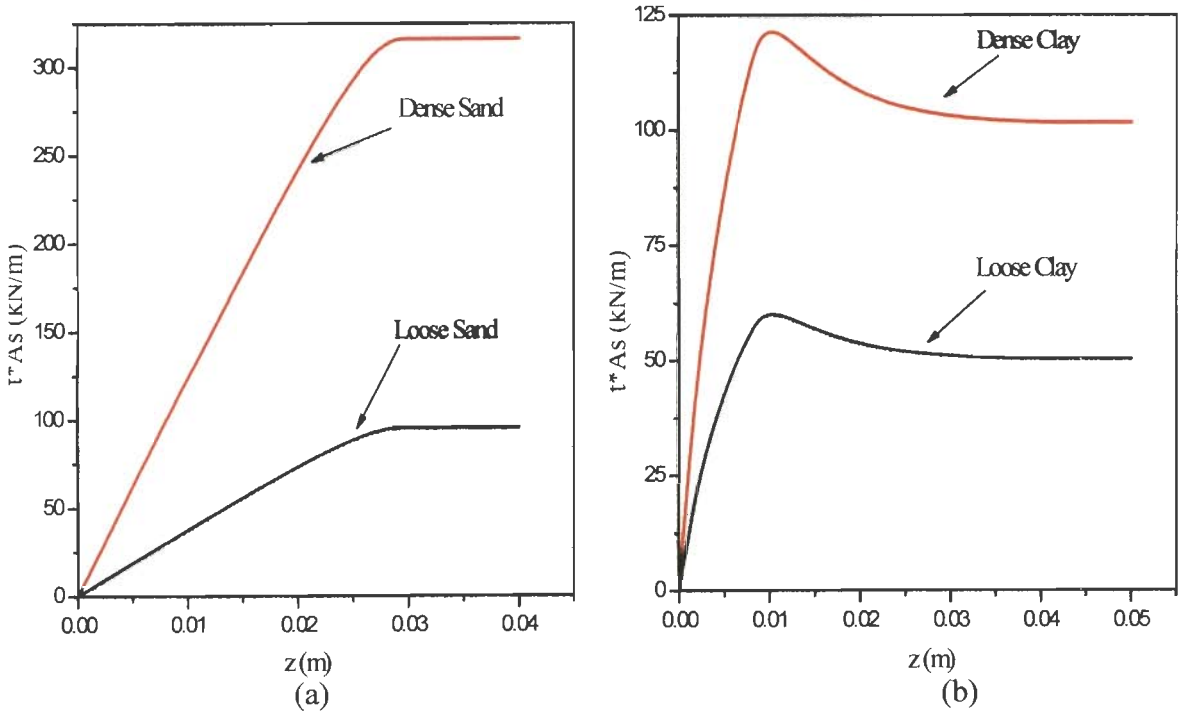

(a) (b)

Fig. 4.19: *t-z* Curves for 1.0 m dia pile (a) Sand and (b) Clay

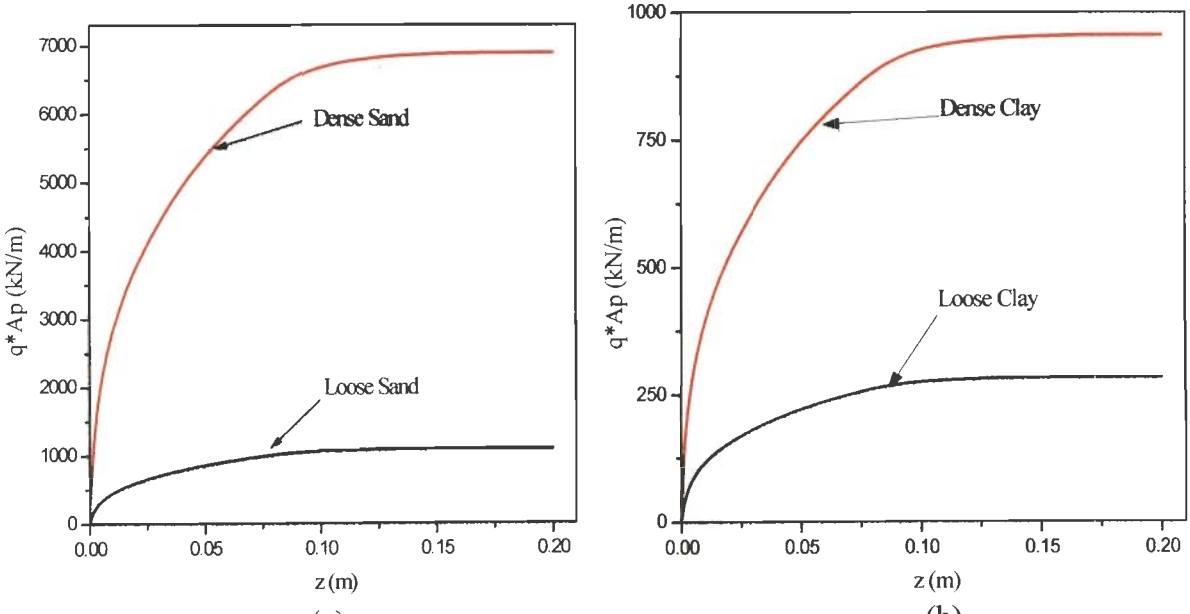

(a) (b)

Fig. 4.20: *q-z* Curves for 1.0 m dia pile (a) Sand and (b) Clay

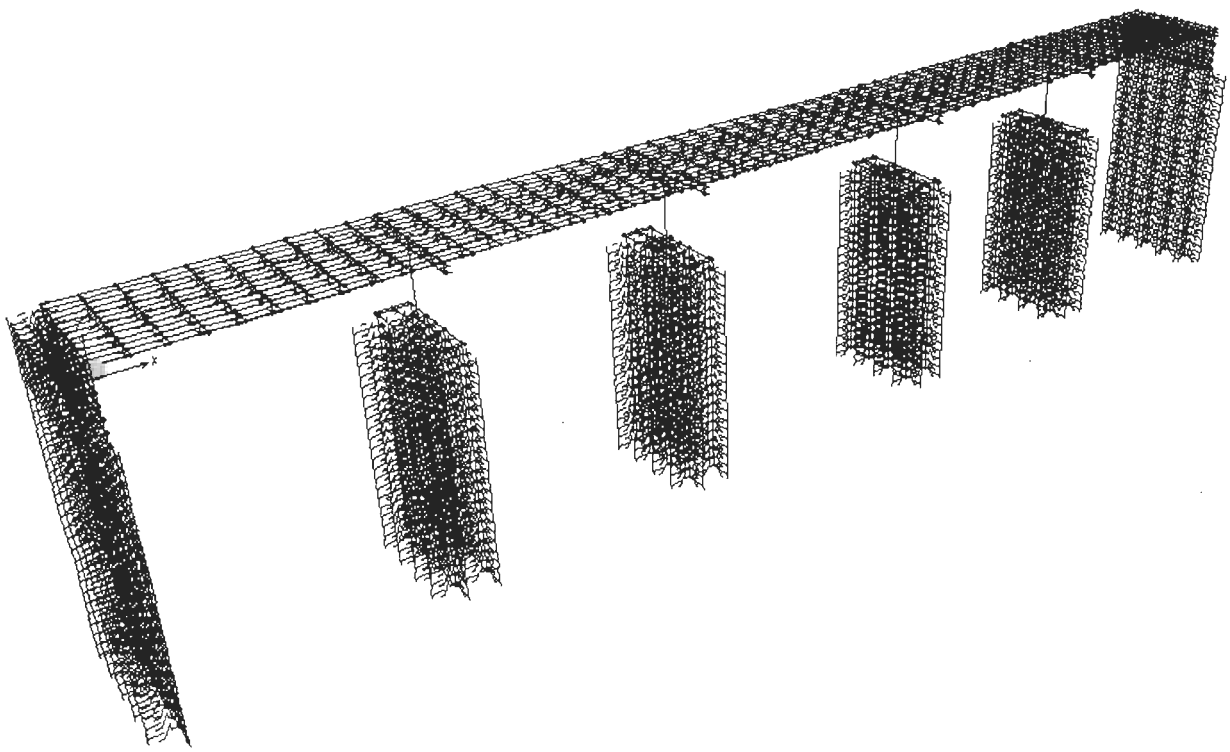

Fig. 4.21: Three-dimensional finite element model of integral abutment bridge

4.4 NONLINEAR SOLUTION TECHNIQUES

The static displacement of the linear structural system can be computed by solving the set of linear simultaneous stiffness equations

$$\underline{K}\,\underline{\delta} = \underline{p} \qquad \ldots (4.19)$$

where, $\underline{\delta}$ is the vector of joint displacements ; $\underline{p}$ is the vector of applied joint loads and $\underline{K}$ is the global stiffness matrix of the structure. The global stiffness matrix of the structure $\underline{K}$ can be constructed from stiffness matrices of the individual members of the structure by the general assembly procedure. The terms in $\underline{K}$ are constant for linear structural system. For a nonlinear structural system, the stiffness changes as the structure deforms, this complicates the analysis to some extent. In nonlinear analysis, the stiffness matrix $\underline{K}$ depends on the joint displacements $\underline{\delta}$.

$$K(\delta)\,\underline{\delta} = \underline{p} \qquad \ldots (4.20)$$

Numerical solution techniques are usually used for solving such nonlinear simultaneous equations for the displacement vector $\underline{\delta}$.

4.4.1 Incremental Load Technique

The conditions of equilibrium for a given structure are satisfied by solving the structural stiffness equations for the unknown generalized (global) displacements and a known applied loading. The most suitable approach to analysis is by applying the total load in a series of small finite-sized increments. For each load increment the resulting increment of displacement is determined from the incremental stiffness equations where the stiffness parameters are evaluated to reflect the instantaneous state of the total displacement, total stress and material characteristics that exist just prior to the application of the load increment. The total displacement after the load increment is evaluated by adding the computed displacement increment to the total displacement that exists prior to the application of the load increment. This type of solution is a piecewise linear solution, a physical representation of which is illustrated in Fig. 4.22. This figure shows three load-displacement curves for a single degree-of-freedom system. Curve **A** represents the linear behavior which would result by solving the governing stiffness equation for the total load applied in one increment; curve B is the piecewise linear solution which would result by applying the total load in several increments and curve C represents the exact nonlinear behavior. It is clear that as the size of the load increment approaches zero (or the number of load increments approaches infinity), the piecewise linear curve approaches the true curve. Since load increments of infinitesimal order are impossible to achieve, a reasonable number of moderately sized load increments is applied.

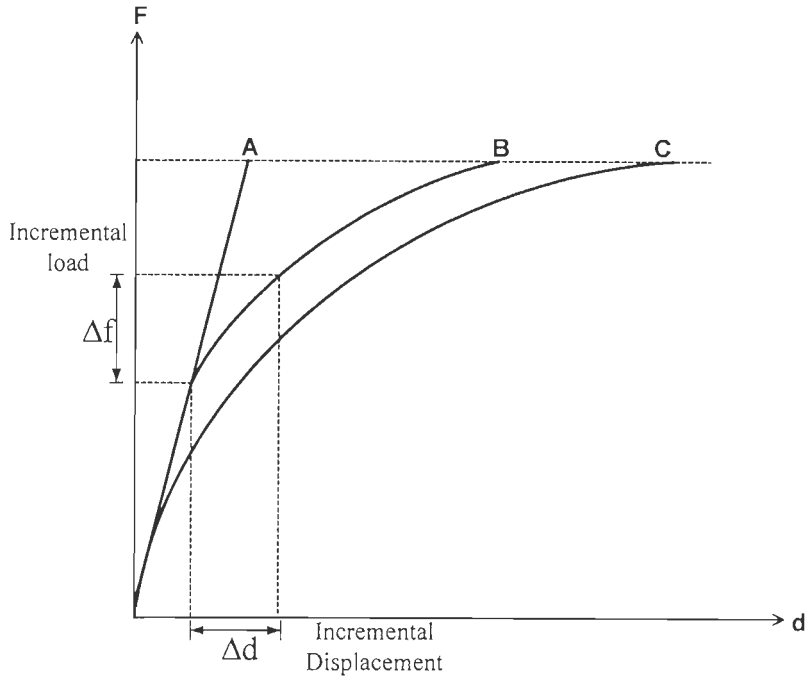

Fig. 4.22 Piecewise linear solution for a single degree freedom system

4.4.2 Push-Over Analysis

Nonlinear static analysis also called as pushover analysis is used to determine displacement capacity of structures and also to estimate available plastic rotational capacities to ensure satisfactory seismic performance. Seismic demands in pushover analyses are estimated by establishing the capacity curve for a structure by monotonically increasing the displacement at a control node until a prescribed displacement is reached or the structure collapses. Control node is a node which is used to monitor the displacement of the structure and it should satisfy two conditions,

i) it should have a maximum displacement &

ii) its deflection should reflect the behavior of the structure.

In longitudinal direction, integral abutment bridge moves as a rigid body, the nodes at the top of the carriage way will have same maximum displacement with a small difference due to axial deformation of superstructure. In case of longitudinal pushover analysis any node may be selected as a control node. In case of transverse direction of integral abutment bridges, since the bridge is restrained at both the ends, the center of

mass can be considered as a control node, if the bridge is symmetric. In case of non-symmetric, maximum displacement point may be considered as a control node.

The distribution of lateral inertia forces varies continuously during earthquake response. Loading pattern is the most important factor affecting the capacity curve, which in turn affects the target displacement. Different load patterns such as Uniform pattern, Modal pattern and Spectral pattern are recommended by FEMA-273 and ATC-40 to represent the load distribution produced by earthquake.

i. Uniform pattern is one which is widely used and it is based on lateral forces that are proportional to the total mass assigned to each node. In buildings, the uniform load pattern is applied based on the lateral forces that are proportional to the total mass at each floor level. In bridges it can be directly taken as

$$F_i = m_i a_g \qquad \ldots (4.21)$$

ii. In Modal pattern, monolithically incremental displacement is applied in the mode shape of the structure and can be represented as

$$F_i = \left(\frac{m_i * \phi_i}{\sum_{i=1}^{N} m_i * \phi_i} \right) V \qquad \ldots (4.22)$$

where, F_i is the lateral force at node $i\,(i = 1,2,.....n)$, n is the number of nodes, a_g is the ground acceleration, m_i is the mass assigned to i^{th} node, ϕ_i is the amplitude of the fundamental mode at i^{th} node, and V is the base shear. This pattern may be used in the fundamental mode having maximum total mass participation. The value of V is optional since the distribution of forces is important while the values are increased incrementally until reaching the prescribed target displacement or collapse.

iii. Spectral pattern is used when the higher mode effects are deemed to be important (Jangid and Datta 1993). This load pattern is based on modal forces combined using Square Root of Sum of the Squares (SRSS) or Complete Quadratic Combination (CQC) method, it can be represented as

$$F_i = \left(\frac{m_i * \delta_i}{\sum_{i=1}^{N} m_i * \delta_i} \right) V \qquad \ldots (4.23)$$

where, δ_i is the displacement of node i resulted from response spectrum analysis.

The ATC-40 and FEMA-273 and 356 have developed the acceptance criteria for pushover analysis using two different methods such as Capacity Spectrum Method (CSM) and Displacement Coefficient Method (DCM) to find out the performance point or target displacement of the structure.

4.4.2.1 Capacity Spectrum Method (CSM)

The procedure for the CSM has been developed by ATC-40 (1996). In CSM, the design curve shown in Fig. 4.23 (a) is reduced by using spectral reduction factors to intersect the capacity curve shown in Fig. 4.23(b) to find the performance point. The performance point indicates the seismic capacity of structure which will be equal to seismic demand imposed in structure by ground motion. In push-over analysis, the performance point or target displacement is based on the assumptions that the fundamental mode or uniform mode of vibration is the predominant response of the structure and mode shapes remain unchanged until collapse occurs. The performance point must satisfy two relationships

- The point must lie on the capacity spectrum or capacity curve in order to represent a structure at given displacement.

- The point must lie on the spectral demand curve, reduced from the elastic 5percent-damped design spectrum

The structure to satisfy the above two relationships the spectral acceleration of structure and spectral acceleration of the response spectra should be same and the performance point requires a trial and error method to satisfy the above condition. ATC-40 (1996) proposed three procedures 'a', 'b' and 'c' to determine the performance point. Procedure 'a' and 'b' are analytical and 'c' is graphical procedure. Step-by-step procedure for 'a', 'b' and 'c' are explained in ATC-40 (1996). ATC simulates three categories of structural behavior A, B and C to consider the damping modification. 'A' represents reasonably full hysteresis loops, 'B' represents moderate reduction in hysteresis area and 'C' represents poor hysteric behavior.

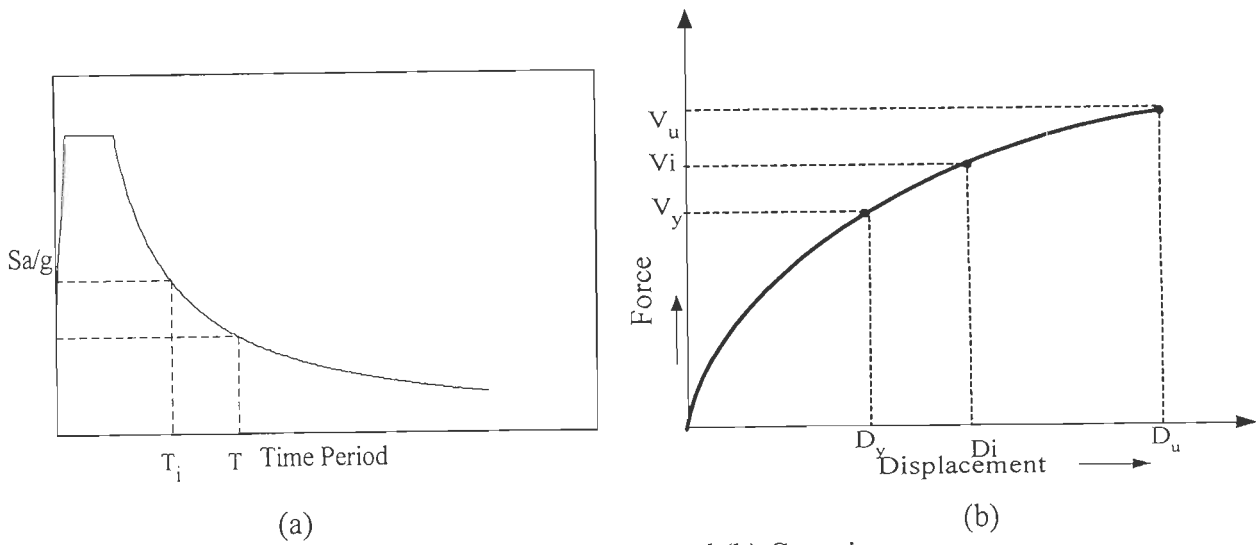

Fig. 4.23: (a) Design curve and (b) Capacity curve

4.4.2.2 Displacement Co-efficient Method (DCM)

The DCM uses pushover analysis and a modified version of the equal displacement approximation to estimate target displacement and it is simple compared to capacity spectrum method. According to DCM, the target displacement δ_t is calculated by

$$\delta_t = C_0 C_1 C_2 C_3 S_a \frac{T_e^2}{4\pi^2} \quad \ldots (4.24)$$

where, T_e = Effective fundamental time period of the building

$$T_e = T_i \sqrt{\frac{K_i}{K_e}} \quad \ldots (4.25)$$

C_0 = The first mode participation factor

$$C_0 = PF_j \, \phi_{CN,J} = \frac{\sum w_i \phi_{ij} / g}{\sum w_i \phi_{ij}^{\ 2} / g} \phi_{CN,j} \quad \ldots (4.26)$$

where, w_i is the tributary weight at the location i varying from 1 to n, n is the total number of discrete weights, $\phi_{i,j}$ is the amplitude of mode j at node i and $\phi_{CN,j}$ is the amplitude of mode j at the control node. The value of C_0 can be taken from Table 4.6

Table 4.6: Values for modification factor C_0 (FEMA 273)

Number of stories	1	2	3	5	10+
Modification factor	1.0	1.2	1.3	1.4	1.5

C_1 is the modification factor to relate expected maximum inelastic displacements to displacements calculated for linear elastic response.

$$C_1 = 1.0 \; for \; T_e \geq T_0$$

$$C_1 = [1.0 + (R-1)T_0/T_e]/R \quad for \; T_e < T_0 \quad \ldots (4.27)$$

$$R = \frac{S_a}{V_y/W} \frac{1}{C_0} \leq \frac{S_a}{V_y/W} \quad \ldots (4.28)$$

where, T_0 is the characteristic period of the response spectrum, define as the period associated with transition from the constant acceleration segment to the constant velocity segment of the spectrum and R is the strength ratio.

C_2 is the modification factor to represent the effect of stiffness degradation and strength degradation on maximum displacement response, shown in Table 4.7

Table 4.7: Values for modification factor C_2 (FEMA 273)

Performance Level	$T = 0.1$ Second		$T \geq T_0$ Second	
	Frame Type 1	Frame Type 2	Frame Type 1	Frame Type 2
Immediate Occupancy	1.0	1.0	1.0	1.0
Life Safety	1.3	1.0	1.1	1.0
Collapse Prevention	1.5	1.0	1.2	1.0

Type 1: Structures in which more than 30% of the story shear at any level is resisted by components or elements whose strength and stiffness may deteriorate during the design earthquake.

Type 2: All frames not assigned to frame type 1

C_3 is the modification factor to take dynamic $P-\Delta$ effect into consideration. For building with positive yield stiffness, C_3 is taken as 1.0. For building with negative post-yield stiffness, C_3 is given by

$$C_3 = 1.0 + \frac{|\alpha|(R-1)^{3/2}}{T_e} \quad \ldots (4.29)$$

α is the ratio of post-yield stiffness to effective elastic stiffness

4.4.3 Newton –Raphson Iterative Procedure

This approach is characteristic of the tangent stiffness method where, in a given load increment, the Newton-Raphson iteration method is applied so that the element nodal displacements are successively corrected until joint equilibrium is satisfied. These displacement corrections are computed using element tangent stiffness matrices, which are successively computed to reflect the most current state of total displacement, total stress, and material properties. Let $\underline{p}_o$ and $\underline{\delta}_o$ be the initial loads and displacements for which structure is subjected to $\underline{\delta}_o$. $\underline{p}_o$ may or may not be null vectors depending on the case. For the ith cycle of the iteration process,

$$\underline{p}_i = \underline{p} - \underline{p}_{e,i-1} \quad \ldots (4.30)$$

where, $\underline{p}$ is the total load applied and $\underline{p}_{e,i-1}$ is the load equilibrated after previous step.

Increment to the displacements is computed using the relation,

$$\underline{K}_T^i \, \underline{\Delta\delta} = \underline{p}_i \qquad \ldots (4.31)$$

Total displacement after ith cycle of the iteration is computed from,

$$\underline{\delta}_i = \underline{\delta}_o + \sum_{j=i}^{i} \underline{\Delta\delta}_j \qquad \ldots (4.32)$$

Finally, $\underline{p}_{e,i}$ is calculated as the load necessary to maintain displacements $\underline{\delta}_i$ with newly formed stiffness matrix $\underline{K}_T^{i+1}$ as shown in Fig. 4.24. The procedure is repeated until the increments of displacements or unbalanced forces become zero, i.e., $\underline{\Delta\delta}_i$ or $\underline{p}_i$ becomes null or sufficiently close to null according to some pre-selected convergence criterion.

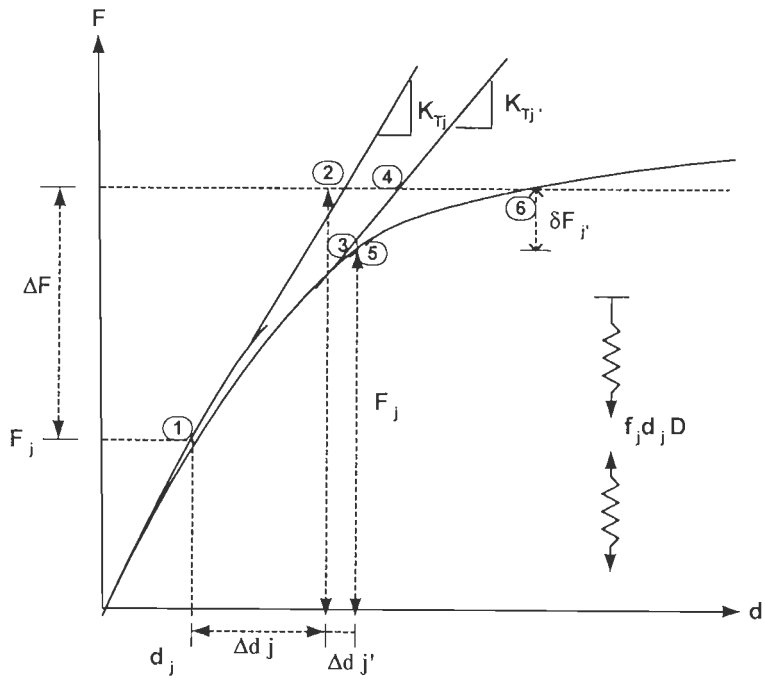

Fig. 4.24 Characteristics of Newton-Raphson iteration in a simple SDOF system

4.4.4 Convergence Criteria

A convergence criterion is required for determining when the current solution is close enough to the true or equilibrating solution to terminate the iteration. The convergence criterion and tolerance must be carefully chosen, so as to provide accurate and economic solutions. The convergence criterion usually employed in the non-linear analysis of structure based on displacements, residual forces or energy. In the nonlinear analysis, the results may also diverge. Therefore, a divergence tolerance limit is also specified. If the displacement computed at any step exceeds the tolerance value then the results are diverging and the iterative process is terminated. Divergence can be caused by a numerical instability because of the stiffness changing too rapidly within the load increment. In the event of such behavior, a smaller load increment may produce more stable behavior. The convergence criteria which are generally used in the analysis are as follows:

- Norm of displacement changes

  The norm $\|\Delta\delta\| = \left(\Delta\delta^T \Delta\delta\right)^{\frac{1}{2}}$ is computed and compared with percentage of norm of the actual displacement.

- Norm of residual forces

  The norm $\|\Delta R\| = \left(\Delta R^T \Delta R\right)^{\frac{1}{2}}$ is specified not to execute a percentage of the norm of the applied forces $\|F\|$ where $\|F\| = \left(P^T P\right)^{\frac{1}{2}}$.

- Residual force absolute magnitude

  The absolute value of the largest term in $\|\Delta R\|$ is found and checked to see if it exceeds a fraction of the norms of the applied forces.

4.5 ANALYTICAL VERIFICATION OF FINITE ELEMENT MODEL

Three dimensional finite element model have been developed to solve the nonlinear soil-integral bridge interaction problem. An example has been analyzed to establish its reliability or accuracy of the soil modelling by comparing the results of the bridge analysed by Faraji and John (2001). Bridge F-4-20 in Fitchburg, Massachusetts is used for the analysis by Faraji. Bridge F-4-20 is a continuous steel stringer bridge with integral abutments. The each outer spans measure 13.72m and middle span is 18.29m. Superstructure consists of 0.216 m thick slab acting in composite with girders and beams. Seven lines of W36X135 girders are spaced at 2.74 m center to center. Abutments walls are 0.762 m thick, 2.44 m high and supported by seven lines of HP 12X 74 piles fixed into the walls. The piles are spaced at 2.74m center to center. NCHRP design curves were used for abutment-backfill modelling and API RP2A design curves were used for modelling of soil around the piles. The bridge was analysed by using GT-STRUDL finite element model by Faraji. The same bridge is analysised by using finite element package SAP with little modifications in the modeling. Each pile is modeled with 9 (nearly 1.0m each) long beam elements along with uncoupled nonlinear soil springs. A uniform thermal load of $44.4^{o}C$ was applied to the composite deck. Coefficient of thermal expansion of $1.2x10^{-5}/^{o}C$ is used which is used by Faraji. Model is analysed by varying the soil properties behind wall from dense sand (D) and loose sand(L) and adjacent to the piles from dense sand(D) to loose sand (L).

Figures 4.25 and 4.26 show the comparison between the plot of the lateral deflection and moment of the abutment wall and connecting HP piles as a function of depth for different soil conditions obtained by STRUDL and SAP-2000 models. The difference in the results by STRUDL and SAP-2000 are very small and negligible.

LL- **Loose** sand backfill and **Loose** sand surround the pile

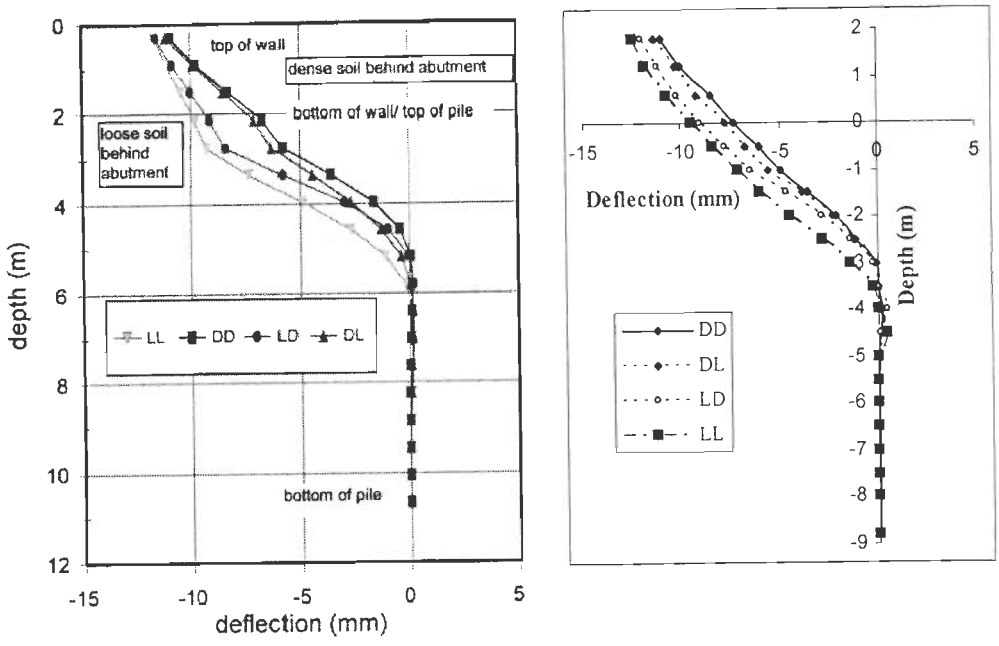

(a) STRUDL (b) SAP-2000

Fig. 4.25: Lateral deflection of the abutment wall and connecting HP

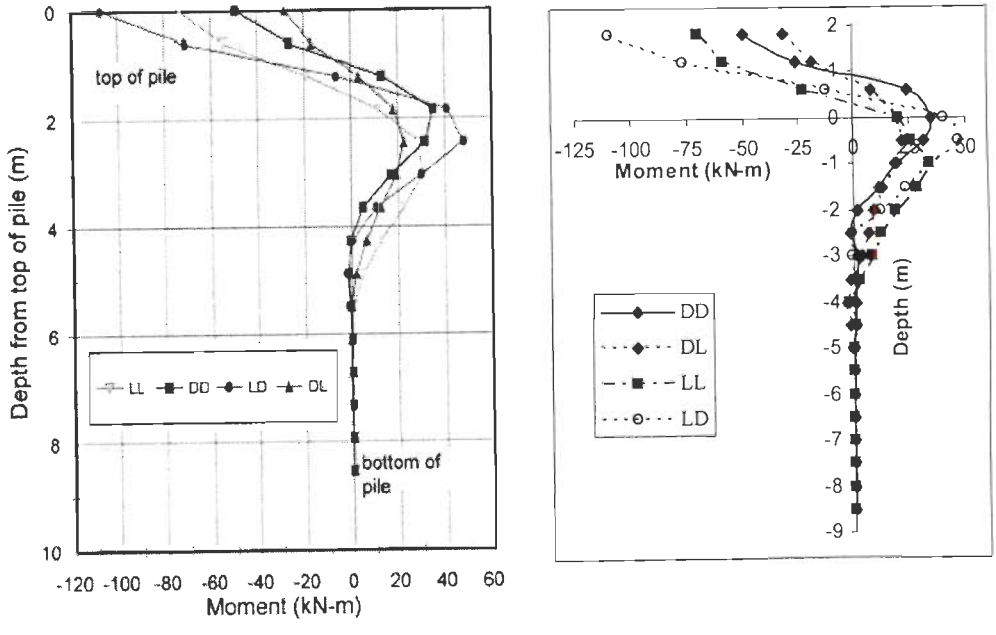

(a) STRUDL (b) SAP-2000

Fig. 4.26: Moment in HP piles under abutment

4.6 CONCLUDING REMARKS

The modeling and analysis of integral bridges considering soil and structural nonlinear properties are explained briefly in this Chapter. The finite element modeling technique is adopted for the modeling. Frame, shell and spring elements are used to model superstructure, substructure and foundation. The material nonlinearly in the concrete members is taken care by moment curvature relationship using stress-strain curve from Mander's model. The fatigue damage of piles due to cyclic temperature loading is verified by the damage model proposed by Mander et al. (1994). The vertical eccentricity between the center of gravity of the girders and the mid-thickness of the deck is taken care in the modeling. The lateral stiffness of the backfill and the soil surrounding the pile are modeled by using nonlinear lateral springs. The lateral springs along the pile length which represents the soil stiffness is obtained by using the program written in MATLAB. The nonlinear solution techniques, especially Newton-Raphson iteration method is explained in brief which is used for the analysis of structure. The nonlinear static analysis also called as pushover analysis is used for seismic study.

The five span integral abutment bridge is taken as numerical example and its structural details are introduced. The complete finite element model of the bridge considering vertical eccentricity between the center of gravity of the girders and the mid-thickness of the deck, abutment backfill interaction and soil-pile interaction is explained in detail. The model of integral abutment bridge having linear structural property and nonlinear soil property has been developed by using computer program SAP V 10.1.3. The results are validated with the published literature from Faraji which are comparable.

CHAPTER-5

NON-LINEAR STATIC ANALYSIS FOR TEMPERATURE EFFECTS

5.1 INTRODUCTION

The temperature of a structure is a function of climatic temperature, specific heat of material, mass, surface volume ratio, heat conductivity, wind conditions, shade etc. Field studies and analytical methods are useful in the evaluation of thermal effects on bridges. The temperature effect on bridges is mainly classified into two types. First type is uniform change in temperature that occurs over the entire superstructure. This temperature causes an overall change in the length for an unrestrained structure. If the structure is restrained, a uniform temperature change will produce internal stresses in the structure. The second type is the vertical temperature gradient that occurs through the depth of a bridge superstructure when it is heated unevenly. The length of integral bridges is greatly affected by uniform temperature variation.

Creep and shrinkage are the time-dependent long term effects and they increase the magnitude of the contraction of the bridge superstructure. Creep is a non-elastic deformation of concrete occurring over a period of time. Creep affects the deformations of all concrete bridges, but it's effect on the stresses depends on the type of construction. The effect of creep is neglected in the present study of reinforced concrete integral abutment bridge. Concrete shrinks slightly as it ages and this can affect stresses and deformations in bridges. The effect of shrinkage will be same as that of temperature fall. Most of the designers neglect the shrinkage effect considering that overall shortening of a concrete bridge is much smaller than the range of thermal movement and it will be nullified by cyclic thermal movements.

The combination of shrinkage with temperature fall may govern the design of integral abutment bridges when compared to temperature rise. The maximum length of integral

abutment bridges subjected to temperature and shrinkage effects depends upon the displacement capacity of piles which depends upon the type of soil and structural configuration of bridge. The movement of the superstructure due to temperature is given by

$$\Delta_t = \varepsilon_t L/2 \quad \text{... (5.1)}$$

$$\varepsilon_t = \alpha \Delta T \quad \text{... (5.2)}$$

$$\Delta T = T_{\max} - T_{ref} \text{ and } \Delta T = T_{\min} - T_{ref} \quad \text{... (5.3a)}$$

$$T_{ref} = \Delta T_{ave} \pm 10^0 C \quad \text{as per Indian Standards (IRC:6-2000)} \quad \text{... (5.3b)}$$

$$\Delta T_{ave} = (T_{\max} + T_{\min})/2 \quad \text{... (5.3c)}$$

where, ε_t is the temperature strain; L is the total length of the bridge (m); ΔT_{ave} is the uniform temperature difference (^{0}C), T_{ref} is the reference construction temperature (^{0}C), ΔT is bridge temperature difference (^{0}C) and α is the coefficient of thermal expansion (mm/mm/^{0}C). The codes specify different values for coefficient of thermal expansion 'α', which depends on nature of cement, the aggregate, the cement content, the relative humidity and the sizes of sections. α is taken as 11.7E-5 (M-40 Concrete) for the analysis.

Since concrete creep and shrinkage increase the magnitude of the contraction of the bridge superstructure, the total maximum contraction of the bridge superstructure can be represented by

$$\Delta_{Tf} = \varepsilon_{Tf} L/2 \quad \text{... (5.4)}$$

$$\varepsilon_{Tf} = \varepsilon_{tf} + \varepsilon_s + \varepsilon_c \quad \text{... (5.4a)}$$

The maximum expansion due to temperature rise is represented by

$$\Delta_{Tr} = \varepsilon_{Tr} L/2 \quad \text{... (5.5)}$$

where, ε_{Tf} is the total contraction strain; $\varepsilon_s = 2x10^{-4}$, is the shrinkage strain; ε_c is the creep strain and ε_{tf} is the strain due to temperature fall and ε_{Tf} is the strain due to temperature rise . Both creep and shrinkage can be converted into equivalent temperature load and can be added with temperature fall for the estimation of integral abutment bridge.

5.2 ESTIMATION OF LENGTH OF INTEGRAL ABUTMENT BRIDGE

The secondary effects play important role in the design of integral bridges. In the secondary effects the effective temperature is the most important which governs the design of integral bridges. In this Chapter, the performance of reinforced concrete integral abutment bridge explained in Section-4.1 is studied for temperature loading. The bridge is chosen based on the current construction practices in India and the structural members of the bridge are designed as per Indian codes. Dead load is taken into account by considering the density of the members, superimposed load which consist of 65mm wearing coat and parapet load of 2t/m on end girders are considered as external load on the bridge. A parametric study is conducted to investigate the effect of foundation soil and structural properties on the maximum length of integral abutment bridges. The foundation consisting of 1.0m and 1.2 m dia cast-in-situ pile having 1.0%, 1.5% and 2.0% longitudinal reinforcement is considered for the study. The height of the abutment is varied from 3m to 5m and flexibility of piers are considered by varying pier height from 5m to 9m. The soil conditions behind the abutment backfill wall are varied as dense sand backfill (DSB), medium sand backfill (MSB) and loose sand backfill (LSB) and the soil surrounding pile are varied as dense sand backfill (DS), medium sand (MS), loose sand (LS), stiff clay (STC) and soft clay (SOC). The effect of piles in the predrilled hole filled with loose sand is also taken into account. Parametric study includes nearly 150 models and 300 pushover analysis cases of 3D model of an integral abutment bridge (explained in Sec-4.1) to find the maximum limits of bridge length that can be constructed using bored cast-in-situ concrete piles of 1.0m and 1.2m dia under different soil conditions.

Non-linear pushover analysis is carried out for both the temperature rise and the temperature fall condition until the first plastic hinge in the pile is formed, while restricting the pile deflection to yield displacement the flexural cracking in structural elements such as piles, abutments, piers and superstructure are maintained within the

specified limits as per the international codes and also the maximum spacing of reinforcements bars are restricted to 300 mm. The influence of abutment-backfill soil, soil surrounding the pile, predrilled hole, abutment and pier flexibility, pile type and pile longitudinal reinforcement on the length of integral abutment bridge is studied.

5.2.1 Effect of Backfill Soil and Soil Surrounding the Pile

Figures 5.1 and 5.2 show the lateral deflection and the bending moment of the abutment wall and connecting concrete pile as a function of pile depth for different compaction levels of backfill soil. The maximum deck displacement is limited to 0.008 times the abutment height for integral abutment bridges with 4.0m high abutments built on concrete piles of 1.0m dia with 1.0% longitudinal reinforcement with dense backfill and dense sand surrounding the pile. By varying the backfill soil from dense to loose for both the temperature rise and fall load conditions, the maximum variation in yield displacement and bending moment of the pile is found to be within 10%. The point of maximum bending moment or hinge formation in the pile for temperature rise and fall case are found to be nearly at the depth of 3D below the ground level as shown in Figs. 5.1(b) and 5.2 (b). Stiffness of abutment backfill soil is observed to have very small effect on the yield displacement of 1.0m and 1.2m diameter cast-in-situ pile in both the temperature rise and fall case.

Figures 5.3 and 5.4 show the lateral deflection and the bending moment of the abutment wall and connecting concrete pile as a function of pile depth for dense sand and medium sand backfill and the stiff and soft clay surrounding the pile. Variation upto 15% has been observed in both the displacement and bending moment of the pile by changing the backfill soil from dense to medium sand and keeping the clay soil surrounding the pile unchanged. In the piles placed in soft clay, plastic hinges were observed at two places one at the top of the pile and another at 7D below the ground level, whereas in case of piles in

stiff clay formation of plastic hinge is observed at a depth of 3D from the ground level, shown in Figs 5.5(b) and 5.6(b).

The stiffness of the subgrade soil surrounding the pile is observed to have a remarkable effect on the abutment top displacement. Figures 5.3 to 5.6 show the lateral deflection and the bending moment of the abutment wall and connecting concrete pile as a function of pile depth for different compaction levels of soil surrounding the pile. As the stiffness of the soil surrounding the pile increases the displacement capacity of the pile decreases. The maximum deck displacement for the bridge having dense backfill and varying soil such as loose, medium and dense sand surrounding the pile is limited to 0.013, 0.010 and 0.009 times the abutment height for temperature rise and 0.012, 0.0095 and 0.0081 times the abutment height for temperature fall loading condition. Increase in the soil stiffness from 12000 kN/m^3 to 60000 kN/m^3 results in the reduction of pile yield displacement capacity from 0.022 m to 0.013 m, nearly 50% reduction is observed. The point of maximum bending moment in the piles placed in dense sand is found at a depth of 2D from the ground surface and for piles placed in loose sand it is found at a depth 4D from the ground surface, shown in Figs. 5.5(b) and 5.6 (b).

5.2.2 Effect of Pre-drilled Hole

Horizontal displacement and variation of moment along the pile depth, for a pile with predrilled hole of 2.0m & 4.0m depth filled with loose sand under temperature fall loading is shown in Fig. 5.7. The loose sand in the predrilled hole increases the yield displacement capacity of the pile. From the results tabulated in Table-5.1, in case of temperature rise, the magnitude of horizontal displacement at the top of the pile for dense subgrade soil increase to 18mm and 24mm from 14mm in case of predrilled hole of 2 m and 4 m filled with loose sand respectively. This variation in the pile yield displacement can result in 28 to 71 % increase in the bridge length without allowing the piles to undergo the hinge formation. The magnitude of pile top yield displacement in the medium subgrade increases

to 19mm and 25mm from 18mm by having a predrilled hole of 2 and 4 m filled with loose sand. This results in 5 to 38 % increase in bridge length. Nearly same variation is absorbed in temperature fall condition. Predrilled hole filled with loose sand allows the pile to be more flexible and results in the increase of overall bridge length. For piles in the stiff clay, predrilled hole of 2 m and 4 m filled with loose sand resulted in 30 to 80% increase in the pile yield displacement. The stiffness of soft clay is lesser than the stiffness of loose sand, hence predrilled hole for piles in soft clay are not preferred.

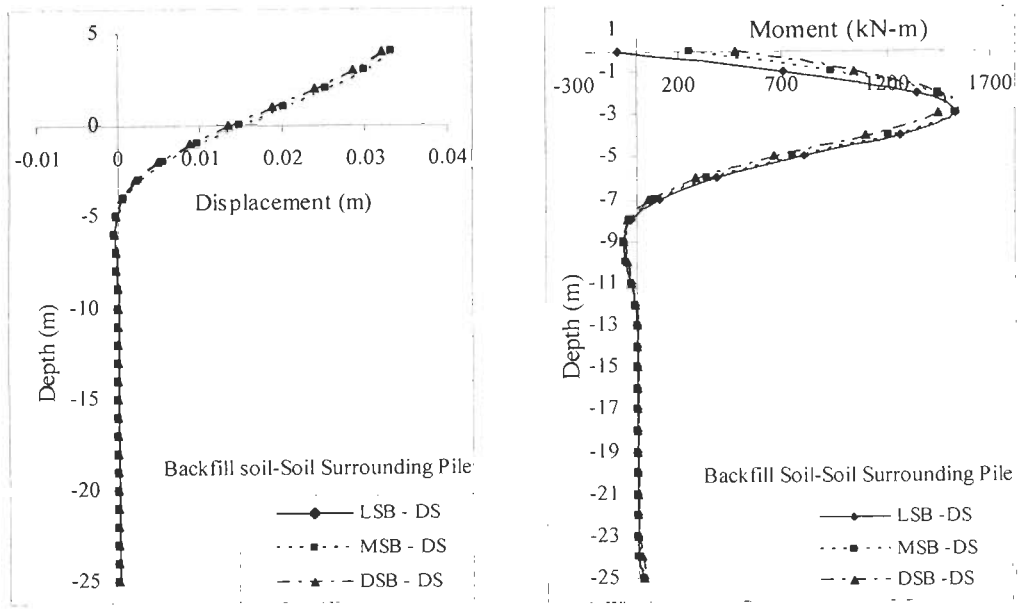

(a) (b)

Fig. 5.1: Variation of displacement and moment along the pile height with varying backfill soil subjected to temperature rise loading

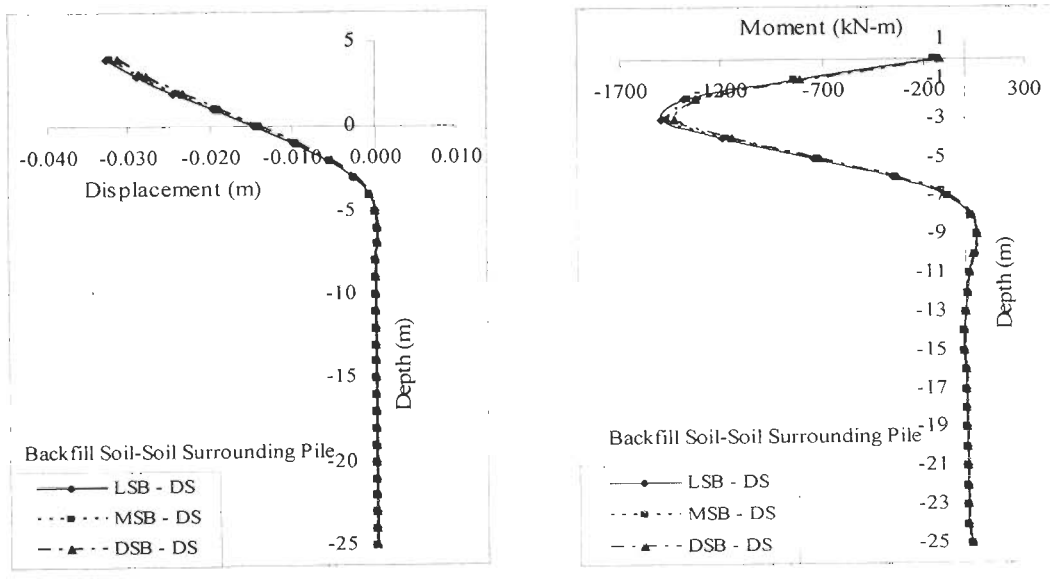

(a) (b)

Fig. 5.2: Variation of displacement and moment along the pile height with varying backfill soil condition subjected to temperature fall loading

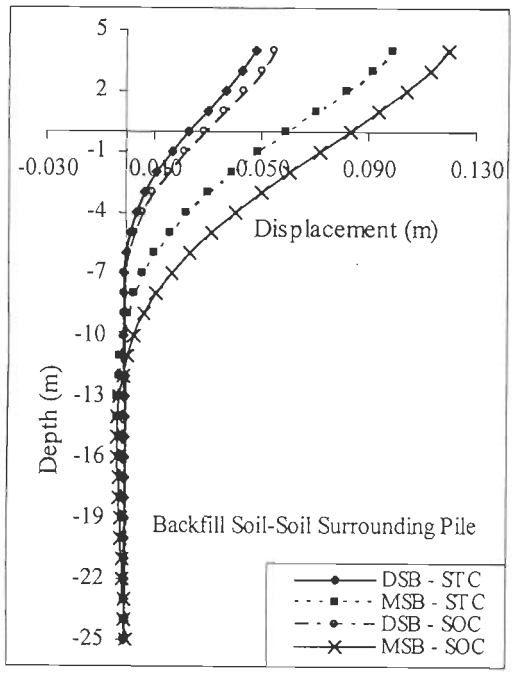

(a)

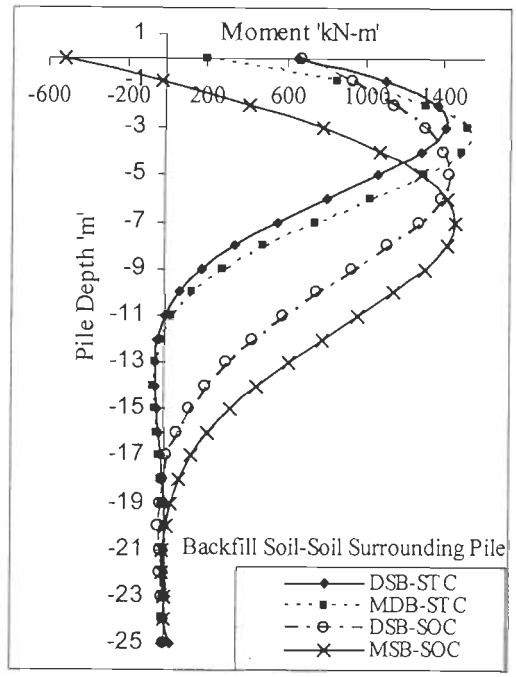

(b)

Fig. 5.3: Variation of displacement and moment along the pile height with varying backfill soil and soil around pile subjected to temperature rise loading

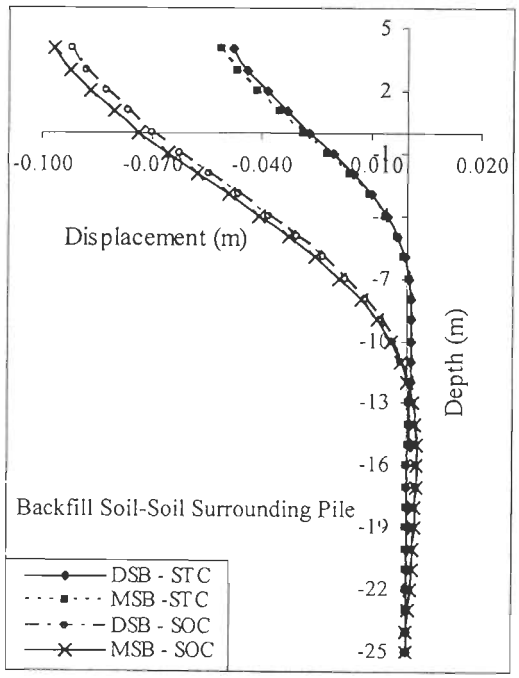

(a)

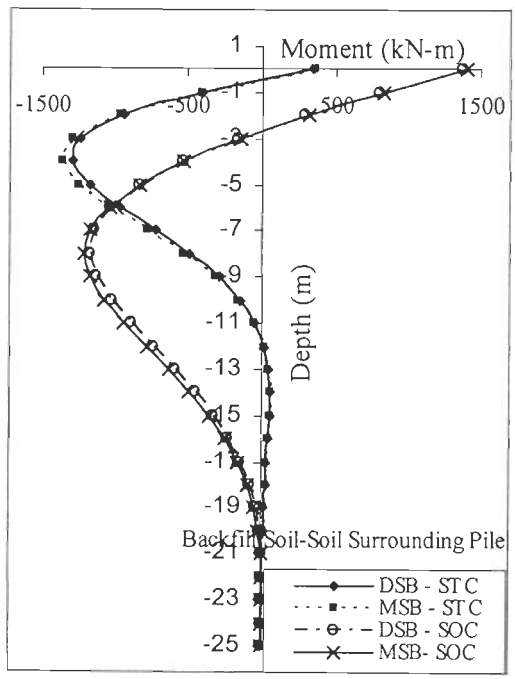

(b)

Fig. 5.4: Variation of displacement and moment along the pile height with varying backfill soil and soil around pile subjected to temperature fall loading

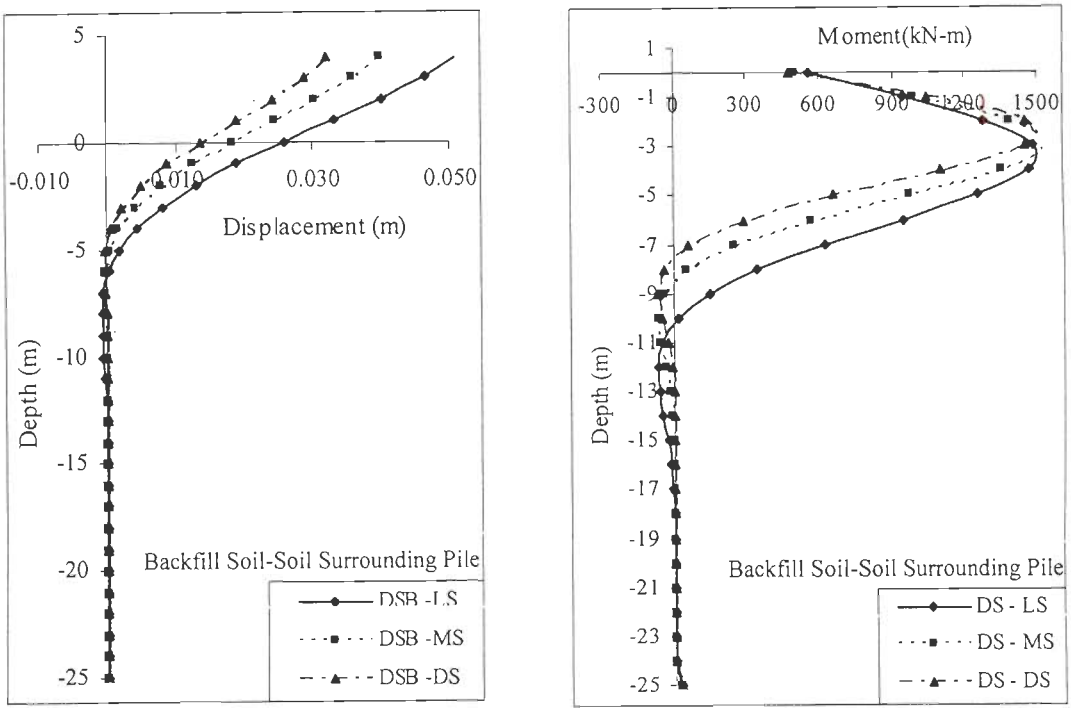

(a) (b)

Fig. 5.5: Variation of displacement and moment along the pile height with varying soil around pile subjected to temperature rise loading

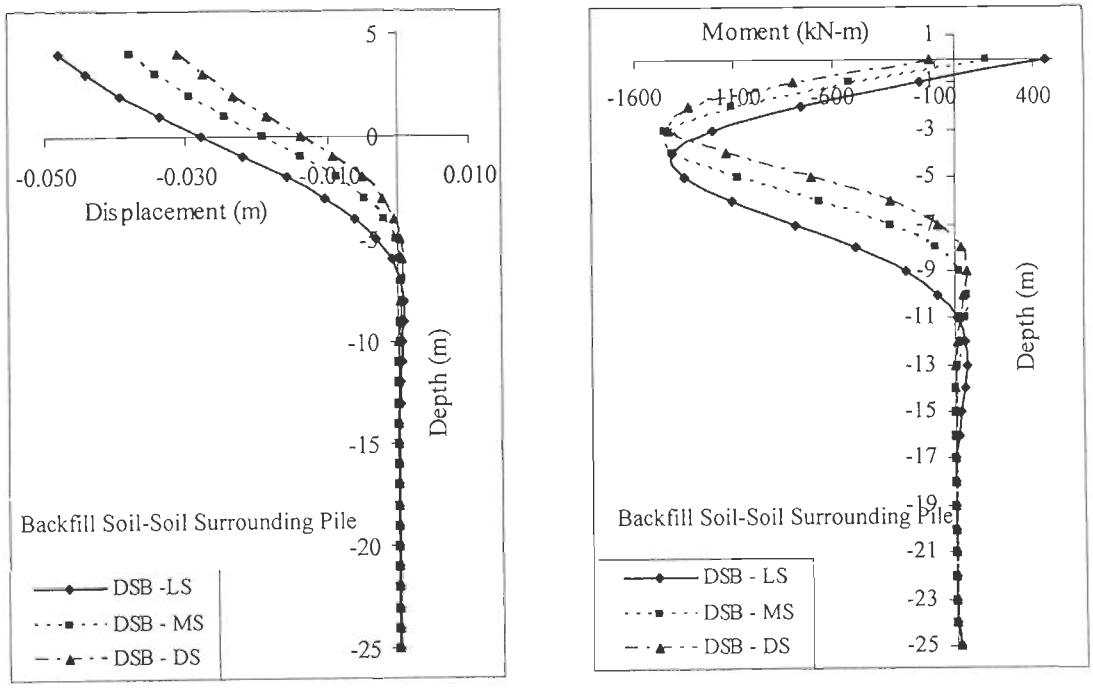

(a) (b)

Fig. 5.6: Variation of displacement and moment along the pile height with varying soil around pile subjected to temperature fall loading

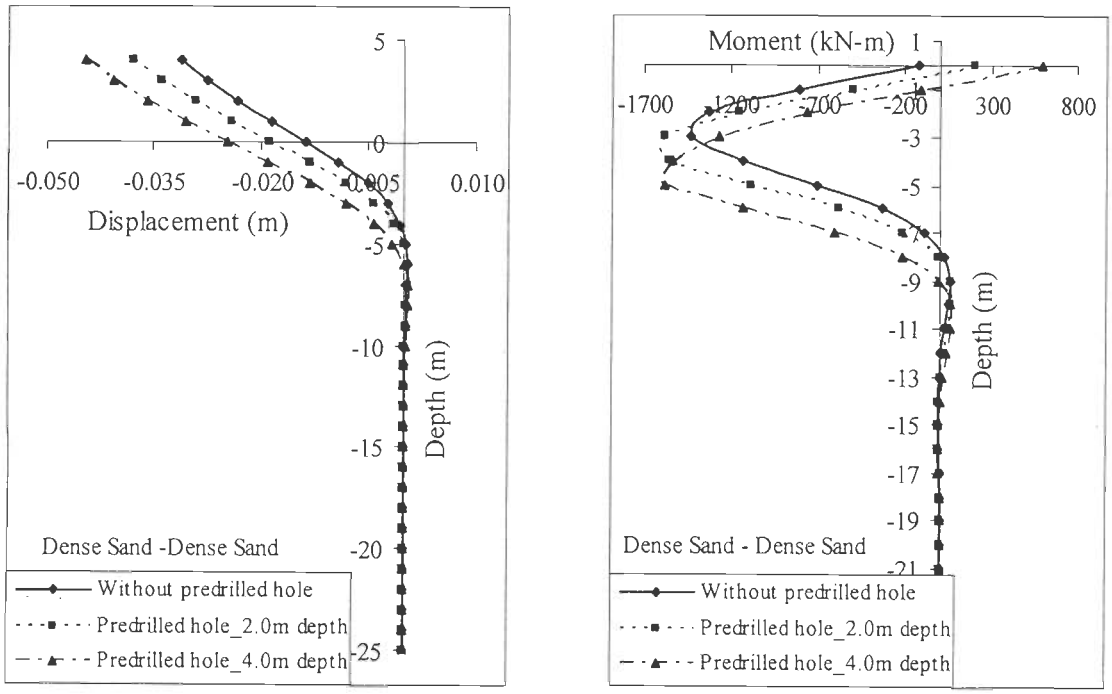

(a) (b)

Fig. 5.7: Variation of displacement and moment along the pile height with varying height of predrilled holes under temperature fall loading

Table 5.1: Displacement variation at abutment and pile top with predrilled hole

Location	Predrilled Hole with Loose Sand	Displacement in 'm' (temperature rise)			Displacement in 'm' (temperature fall)		
		DSB-LS	DSB-MS	DSB-DS	DSB-LS	DSB-MS	DSB-DS
Abutment top	0*	0.051	0.040	0.032	0.048	0.038	0.031
	2	0.051	0.041	0.040	0.049	0.039	0.038
	4	0.051	0.051	0.049	0.048	0.046	0.045
Pile top	0*	0.026	0.018	0.014	0.028	0.019	0.014
	2	0.026	0.019	0.018	0.028	0.020	0.019
	4	0.026	0.025	0.024	0.028	0.026	0.025

DSB - LS = Dense Sand Backfill & Loose Sand Subgrade soil surrounding pile

0* = without predrilled hole

5.2.3 Effect of Abutment and Pier Flexibility

Increase in the abutment height is found to have a positive response on the bridge displacement capacity. Figures 5.8 and 5.9 show the lateral deflection and the bending

moment of the abutment wall and connecting concrete pile as a function of pile depth for different abutment height under temperature rise and fall loading. Increase in the abutment height results in the increase in the deck displacement but the yield displacement capacity of the pile remains almost same for temperature fall case. In case of temperature rise with increase in the height of abutment from 3m to 5m, the yield displacement capacity of the pile is reduced from 16mm to 10mm and from 30 mm to13 mm for soil conditions DSB –DS and DSB –LS respectively, shown in Figs. 5.8(ia) and 5.9(ia). The passive pressure developed behind the abutment reduces the bottom displacement of the abutment compared to top displacement. Figures 5.8(ib) and 5.9(ib) show that point of maximum yield moment or plastic hinge location for temperature rise condition in the pile. The plastic hinge in the pile shifts from a depth 3D from the ground surface to the top of the pile by varying the height of abutment from 3m to 5m in both DSB-DS and DSB-LS soil condition.

Figure 5.10 shows the lateral deflection and the bending moment of the abutment wall and connecting concrete pile as a function of pile depth for varying pier flexibility under temperature rise loading. The change in the flexibility of intermediate pier is found to have negligible effect on the yield displacement and bending moment of the pile and abutment for both temperature rise and fall loading.

For the dense sand backfill and stiff clayey soil surrounding the pile, abutment top displacement reduces from 0.016H to 0.008H by increasing the height of abutment from 3 m to 5m for temperature rise loading and the displacement capacity of the pile is reduced from 33mm to 12mm as shown in Fig. 5.11 (ia). In case of temperature fall, increase in the abutment height from 3m to 5m, the abutment top displacement reduced from 0.015H to 0.011H and negligible reduction in the yield displacement capacity of pile is observed as shown in Fig. 5.11 (iia). From Figs. 5.11(ib) and (iib) in both

temperature fall and rise conditions it is observed that the point of maximum yield moment in pile shifts from a depth 3D from the ground surface to the top of the pile with increase in abutment height from 3m to 5m. Temperature rise loading condition is found to be critical when compared to temperature fall for determining the displacement capacity of piles in integral abutment bridges with greater abutment heights.

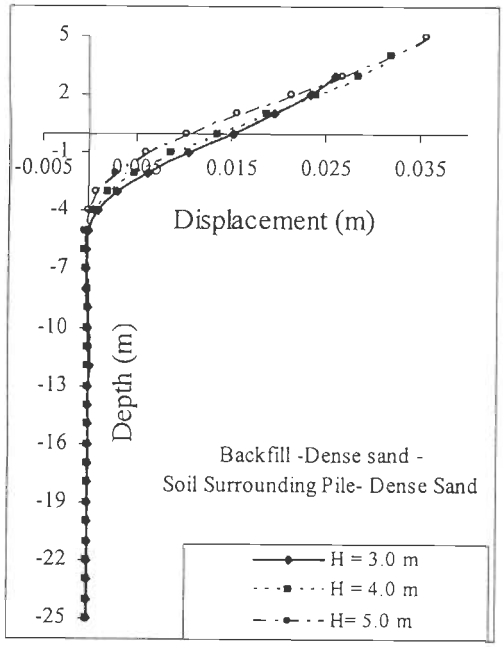

(i a)

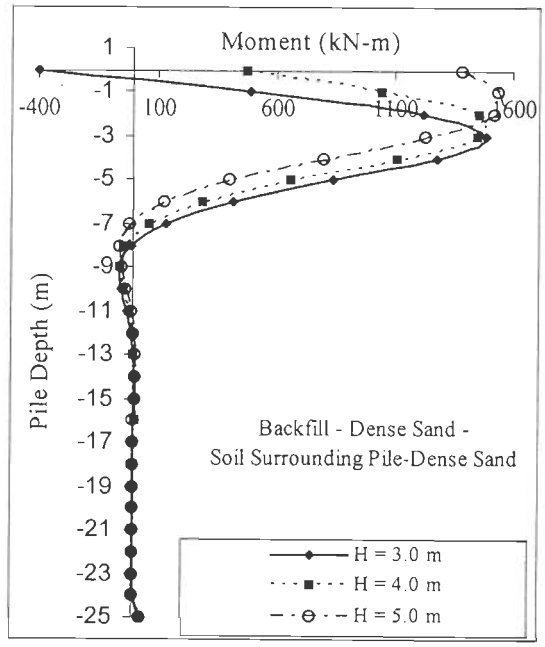

(i b)

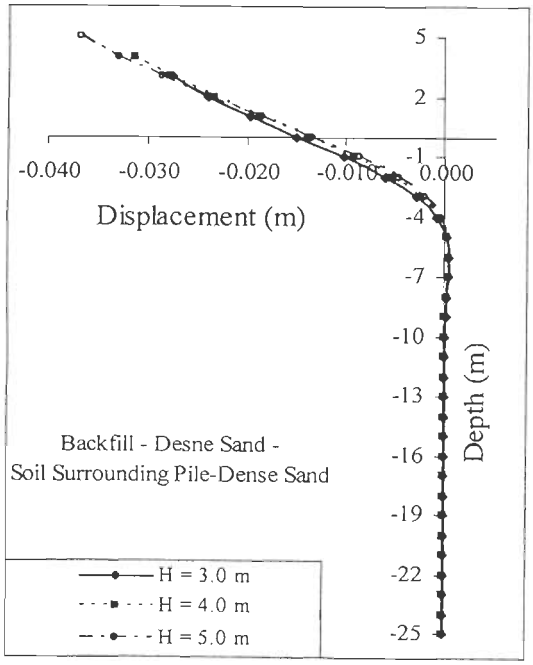

(ii a)

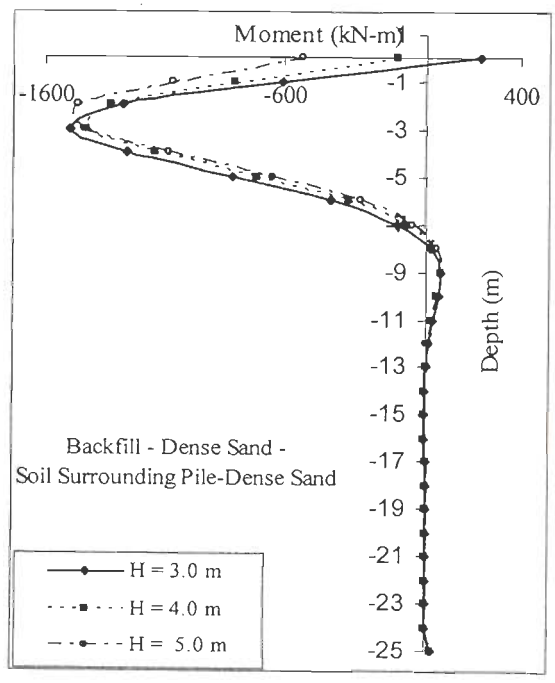

(ii b)

Fig. 5.8: Variation of displacement and moment along the pile height for varying abutment height under temperature (i) rise and (ii) fall loading

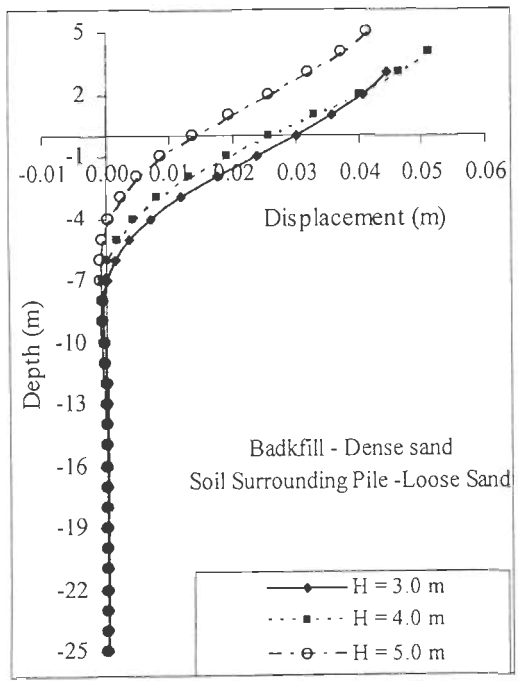

(i a)

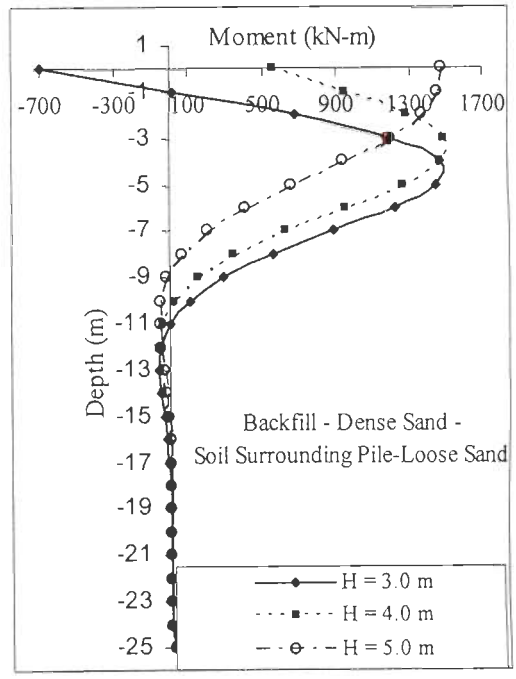

(i b)

Fig. 5.9: Variation of displacement and moment along the pile height for varying abutment height under temperature rise case for DSB-LS condition

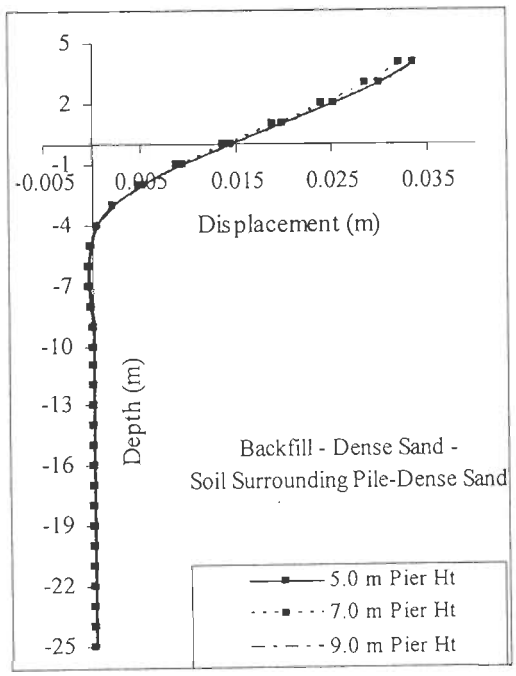

(i a)

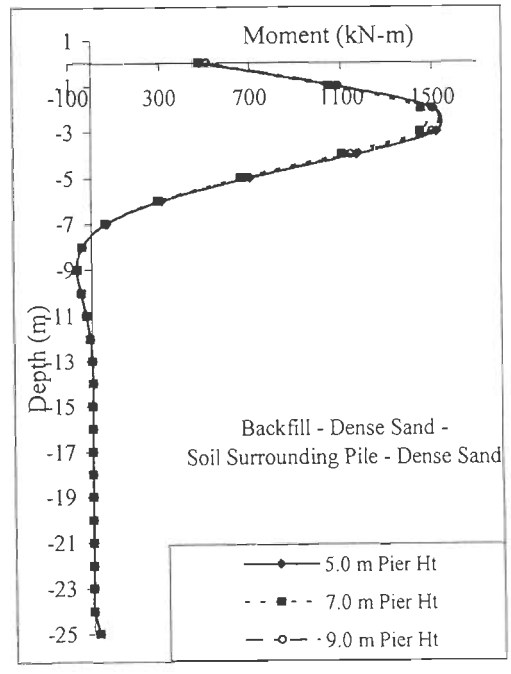

(i b)

Fig. 5.10: Variation of displacement and moment along the pile height for varying abutment height under temperature rise case for DSB-DS condition

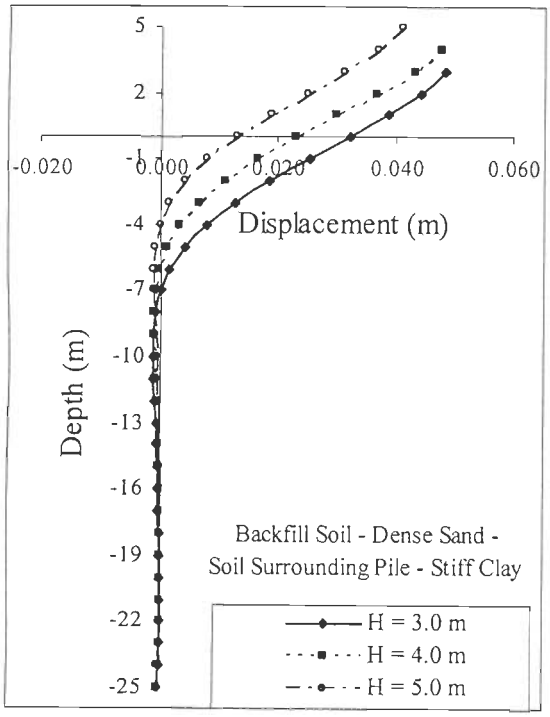

(i a)

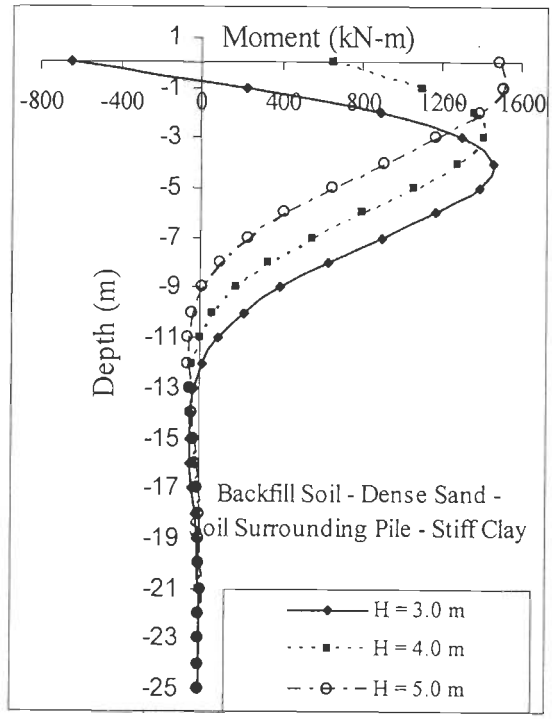

(i b)

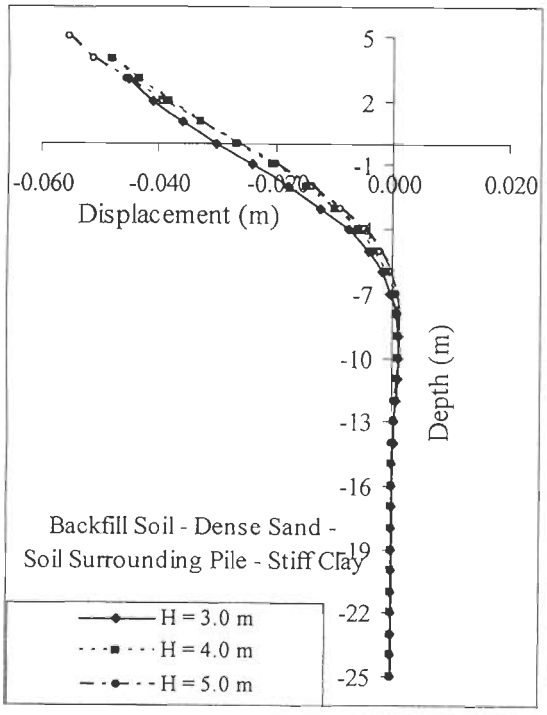

(ii a)

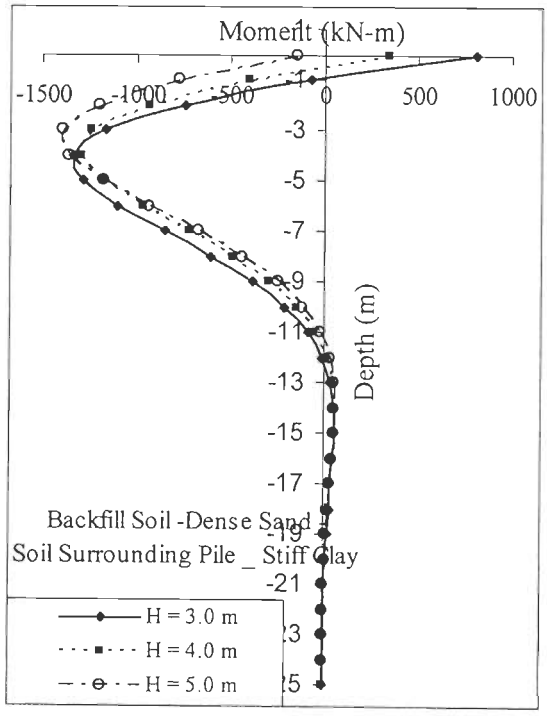

(ii b)

Fig. 5.11: Variation of displacement and moment along the pile height for varying abutment height under temperature (i) rise and (ii) fall loading

5.2.4 Effect of Pile Type and Pile Reinforcement

Figures 5.12 and 5.13 show the lateral deflection and the bending moment of the abutment wall and connecting concrete pile as a function of pile depth for different percentage of pile reinforcement. The effect of pile size and pile longitudinal reinforcement is studied by using 1.0 m and 1.2 m dia pile with 1.0%, 1.5% and 2.0% reinforcement under both temperature rise and fall load conditions taking M-35 concrete and Fe-500 Steel. The increase in the longitudinal reinforcement of the piles resulted in the increase in yield displacement capacity of pile. The formation of plastic hinge in the pile depends on both axial and flexural capacity of the pile. Increasing the longitudinal reinforcement from 1.0 % to 1.5 % and 2.0% in 1.2m dia pile resulted in 70% to 130% increase in the yield displacement capacity of the pile. Varying the pile diameter from 1.0 m to 1.2 m has insignificant effect on the pile yield displacement for pile reinforcement upto 1.5% and for 2.0% reinforcement nearly 12% increase in the pile yield displacement capacity is observed.

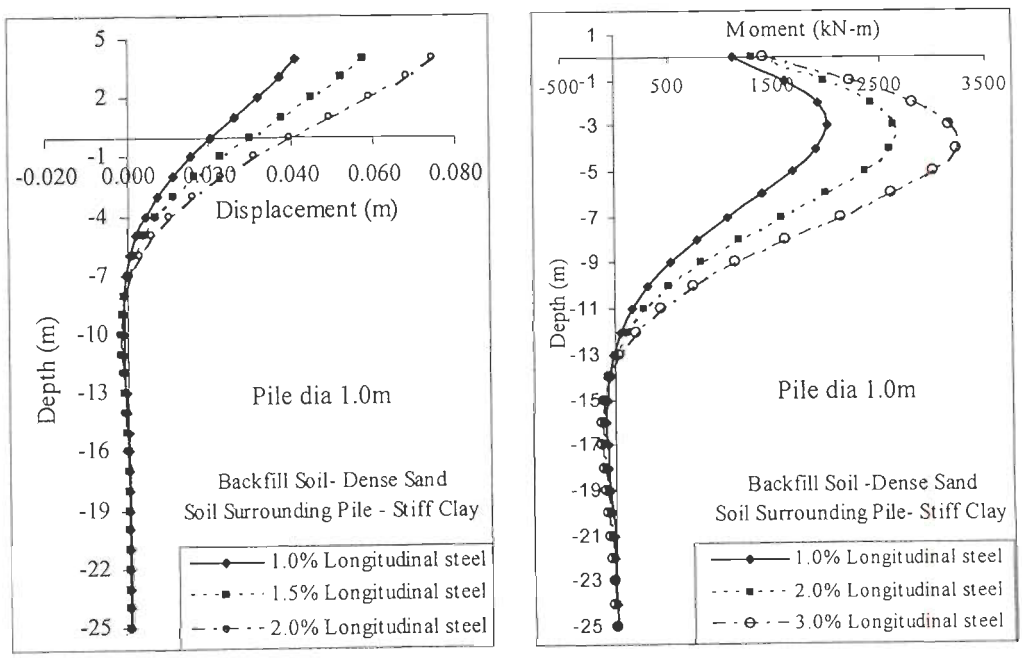

(a) (b)

Fig. 5.12: Variation of displacement and moment along the pile height with varying percentage of longitudinal reinforcement for temperature rise loading and DSB-STC condition

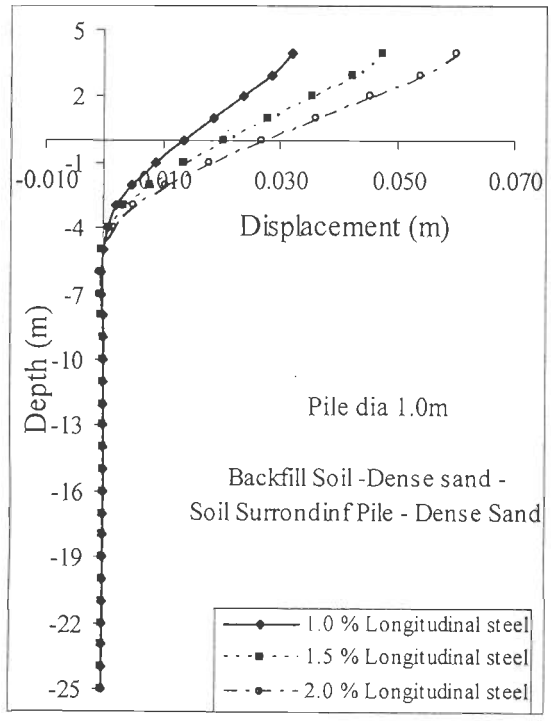

i (a)

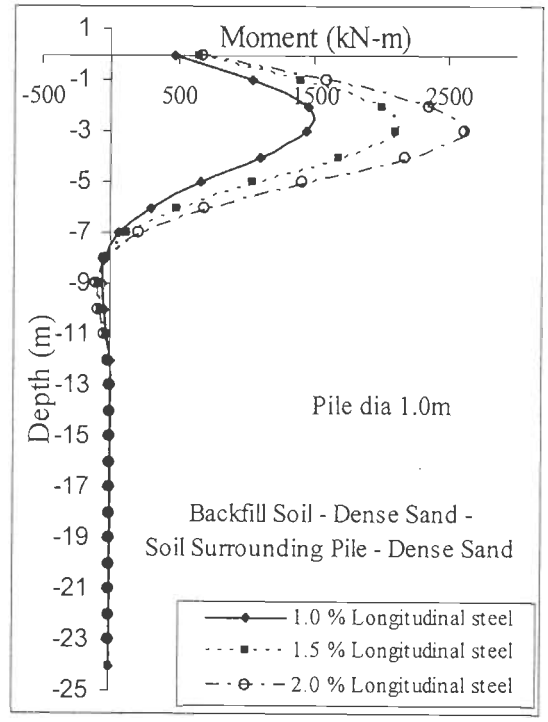

i(b)

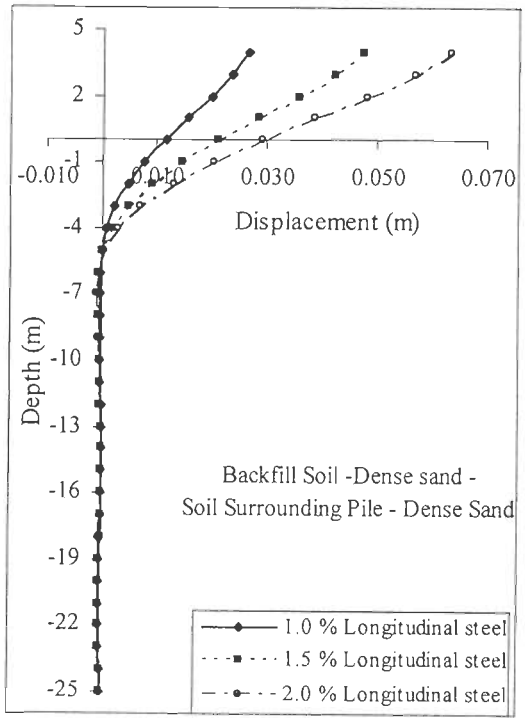

ii (a)

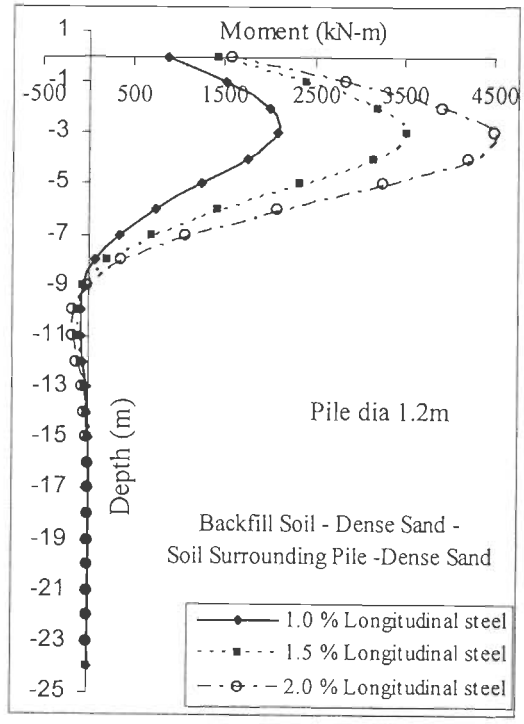

ii(b)

Fig. 5.13: Variation of displacement and moment along the pile height with varying percentage of longitudinal reinforcement in (i) 1.0m dia and (ii) 1.2m dia pile

5.3 VARIATION OF ABUTMENT FORCES

Stiffness of soil surrounding the pile is observed to have a remarkable effect on the bending moment of the abutment. Figures 5.14 and 5.15 show the variation of bending moment in the abutment as a function of abutment displacement to abutment height for varying density of sand and clay around the pile respectively. For 4 m height abutment and $\Delta / H = 0.01$, the maximum bending moment in the abutment increase from 2500 to 2900 kN-m and from 1500 to 1950 kN-m by varying soil surrounding pile from loose to dense sand and from soft to stiff clay, when subjected to temperature rise. It is observed that, the bending moment in the abutment increases with increase in the stiffness of soil surrounding the pile.

Abutments with higher heights are subjected to larger bending moments due to the higher passive pressure developed along the height of the abutment. From Fig. 5.16(i), it is observed that increase in abutment height from 3m to 5m results in 30% to 35% increase in the maximum bending moment of abutment for $\Delta / H = 0.01$ under temperature rise loading. Nearly, 45% variation is observed in abutment bending moment for 3m abutment height subjected to temperature rise and fall for $\Delta / H = 0.01$. Bending moments in the abutments are considerably less for temperature fall when compared to temperature rise case. This variation is due to the development of passive pressure behind the abutment during temperature rise.

Figures 5.17 and 5.18 show the variation of bending moment in the abutment as a function of abutment displacements for varying backfill soil. Changing the backfill soil from loose to dense sand and soft to stiff clay resulted in 10 to 14% increase in abutment moment for $\Delta / H = 0.01$ under temperature rise case. Variation of backfill soil is having very small effect on the abutment moment because, the forces in the abutments depends

on the loads transferred by piles and the backfill pressure. In stiffer soil-pile system the pile displacement will be comparatively less and the backfill pressure exerted on abutments will also be less. Change in backfill has negligible effect on abutment moment when subjected to temperature fall.

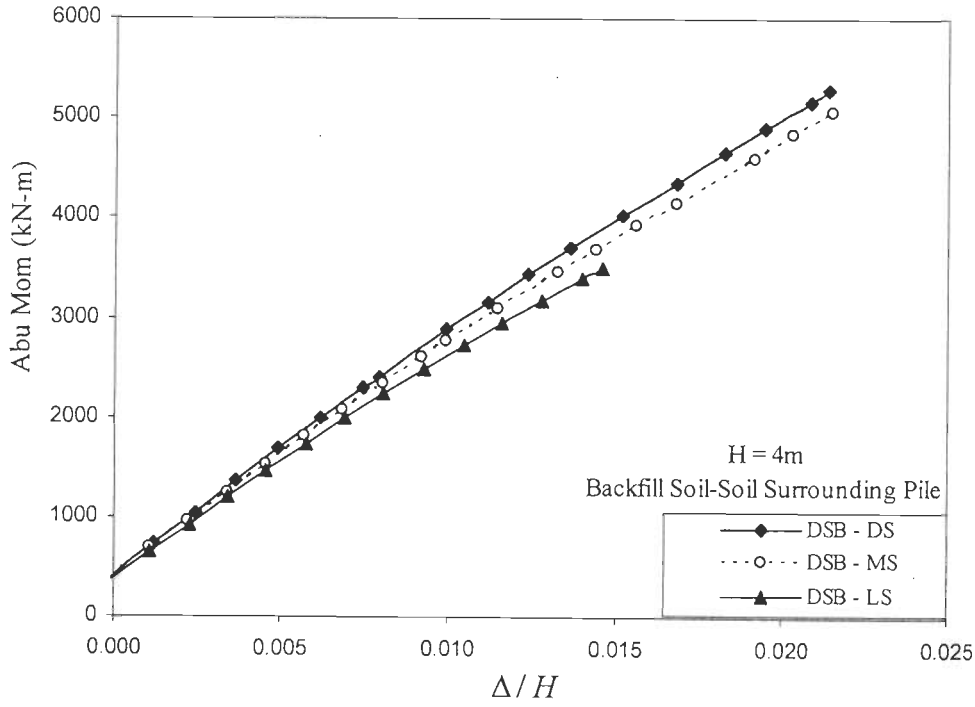

(i)

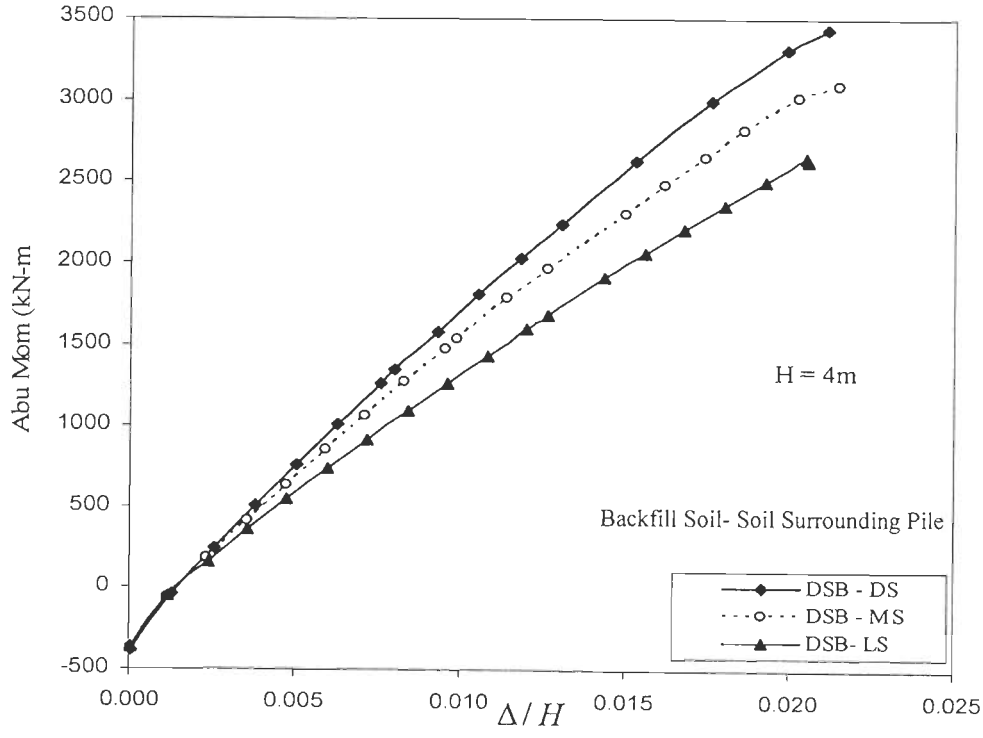

(ii)

Fig. 5.14: Variation of abutment moment Vs Δ / H for varying soil surrounding the pile (i) Temperature Rise (ii) Temperature Fall

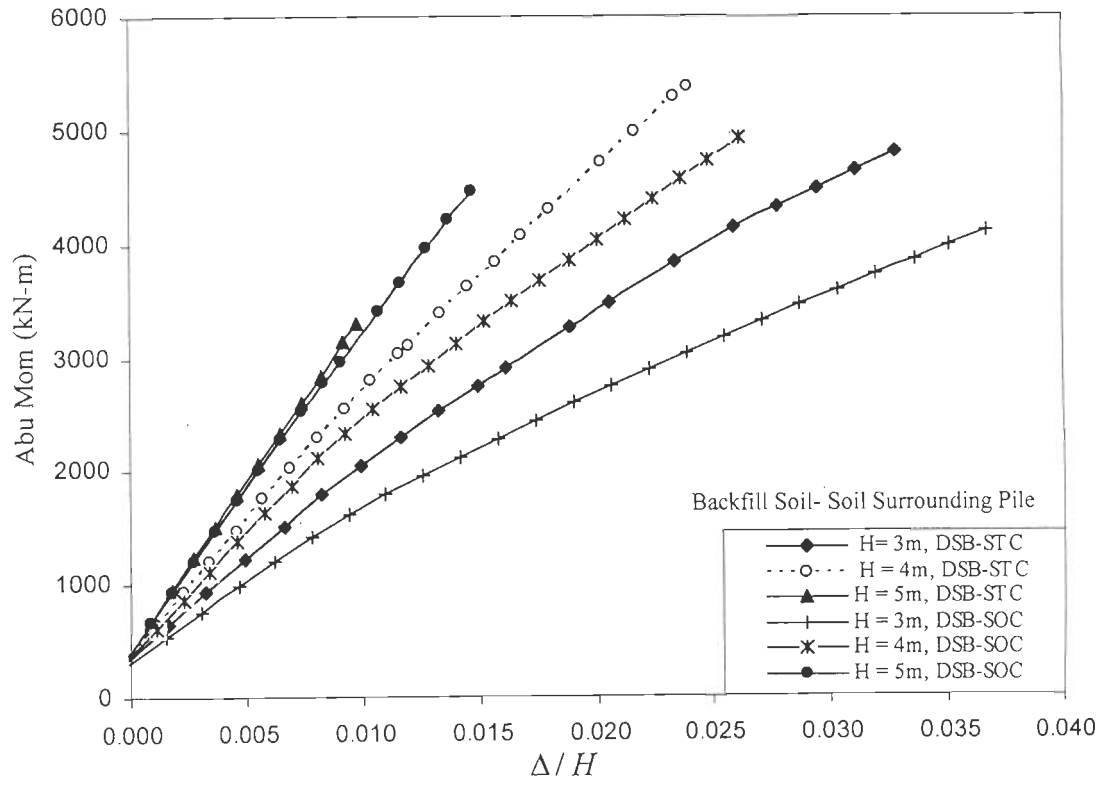

(i)

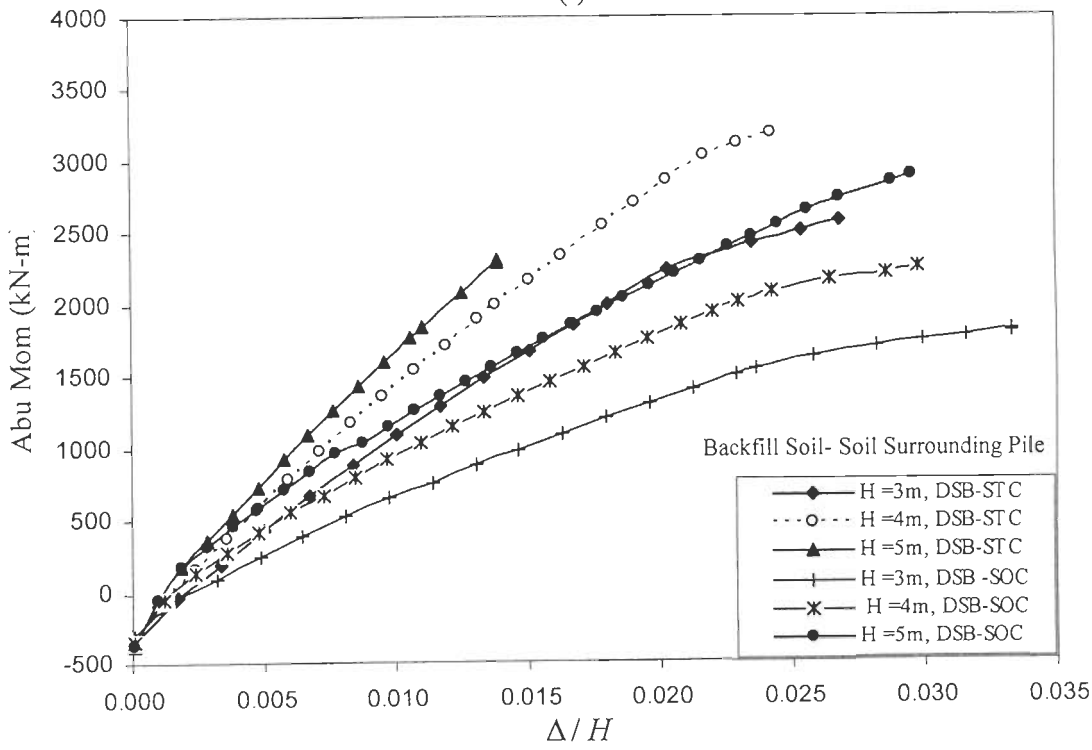

(ii)

Fig. 5.15: Variation of abutment moment Vs Δ / H for varying abutment height and soil surrounding the pile (i) Temperature Rise (ii) Temperature Fall

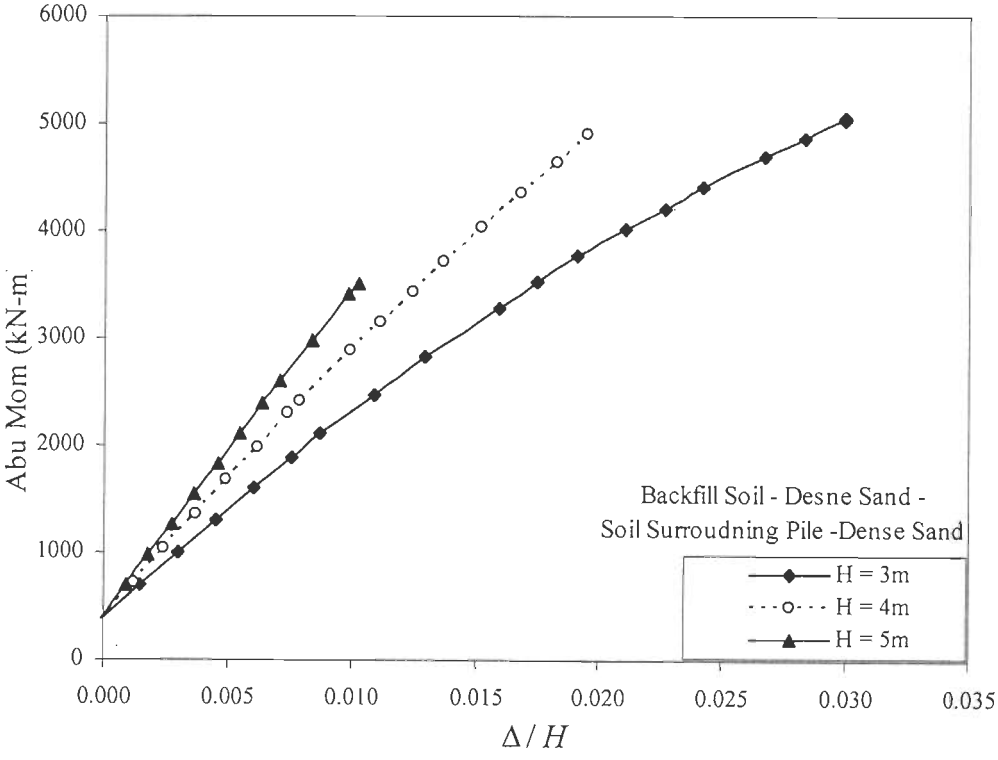

(i)

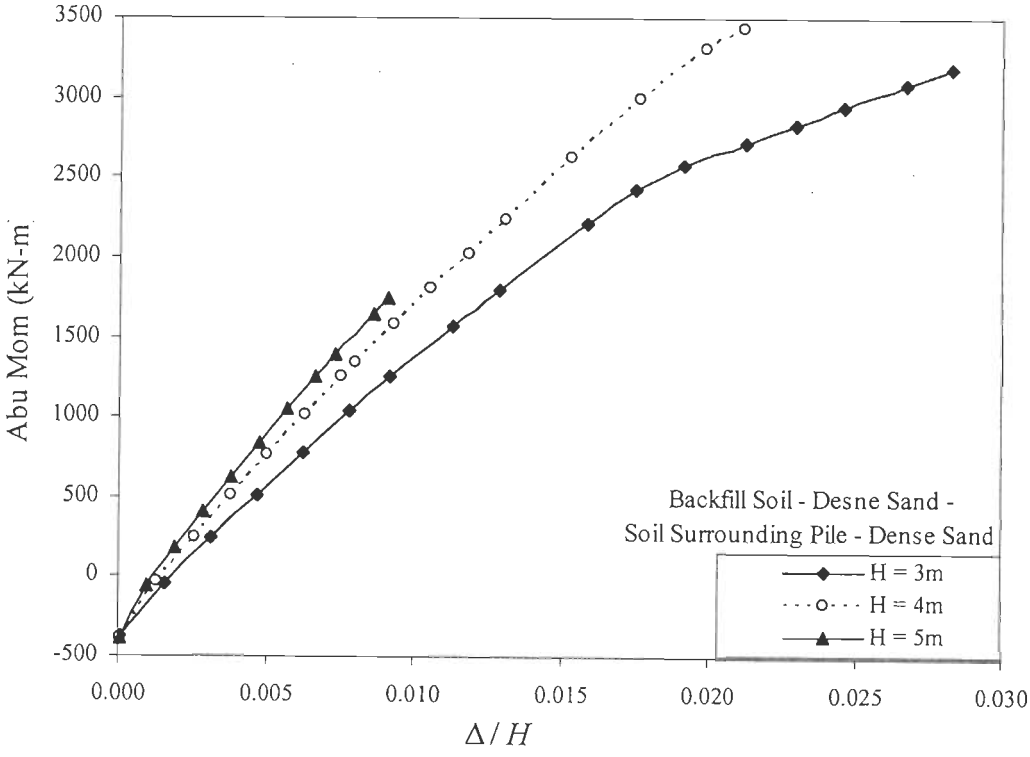

(ii)

Fig 5.16: Variation of abutment moment Vs Δ / H for varying abutment height
(i) Temperature Rise (ii) Temperature Fall

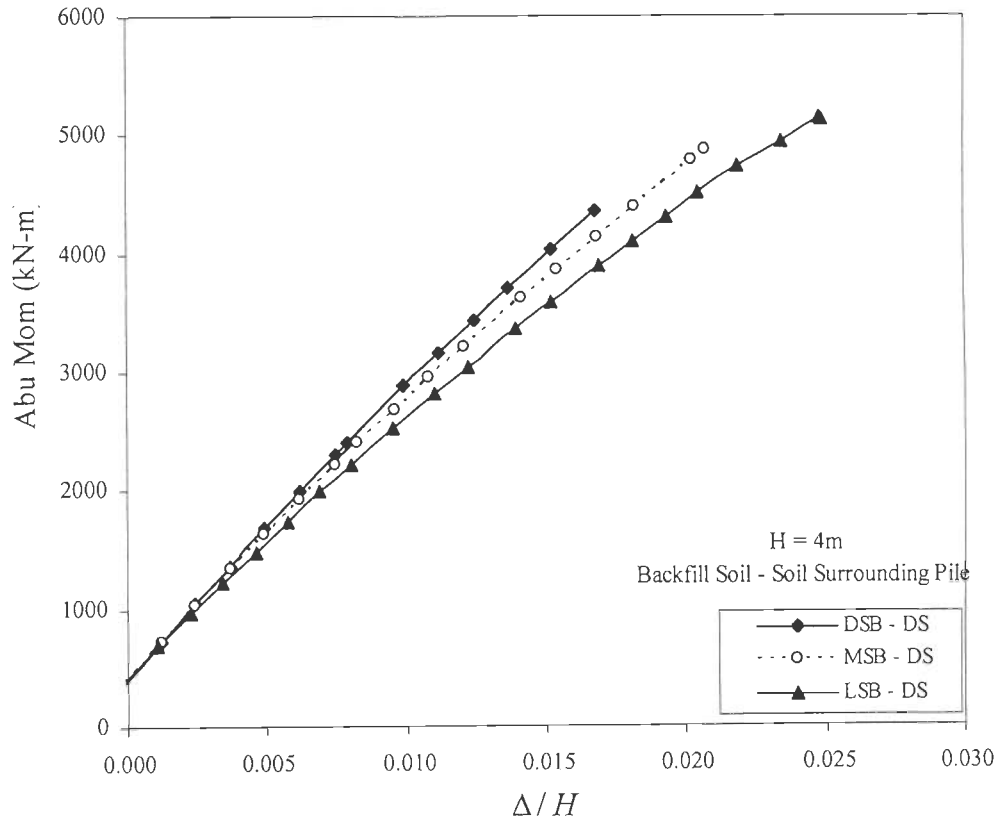

(i)

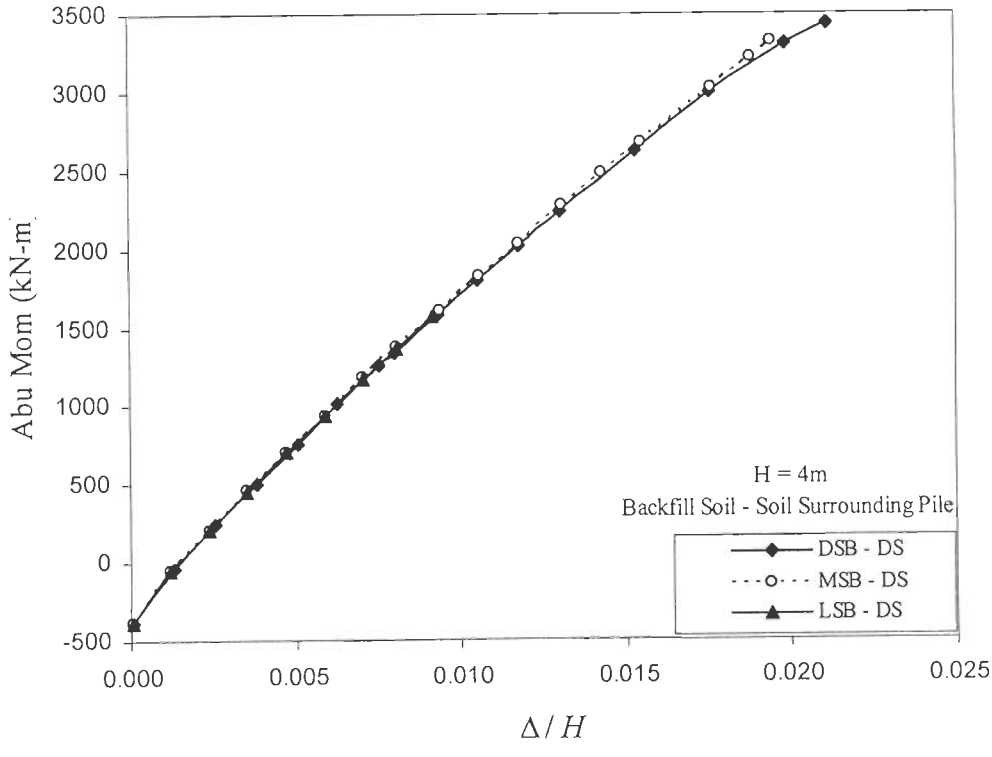

(ii)

Fig. 5.17: Variation of abutment moment Vs Δ / H for varying backfill soil with sand surrounding the pile (i) Temperature Rise (ii) Temperature Fall

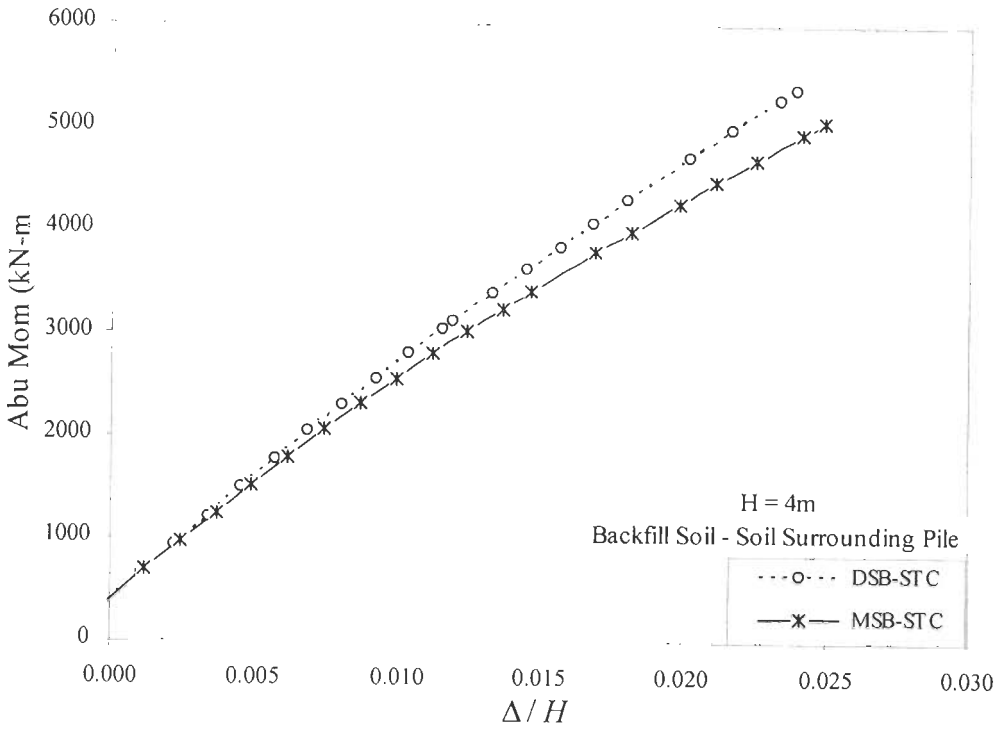

(i)

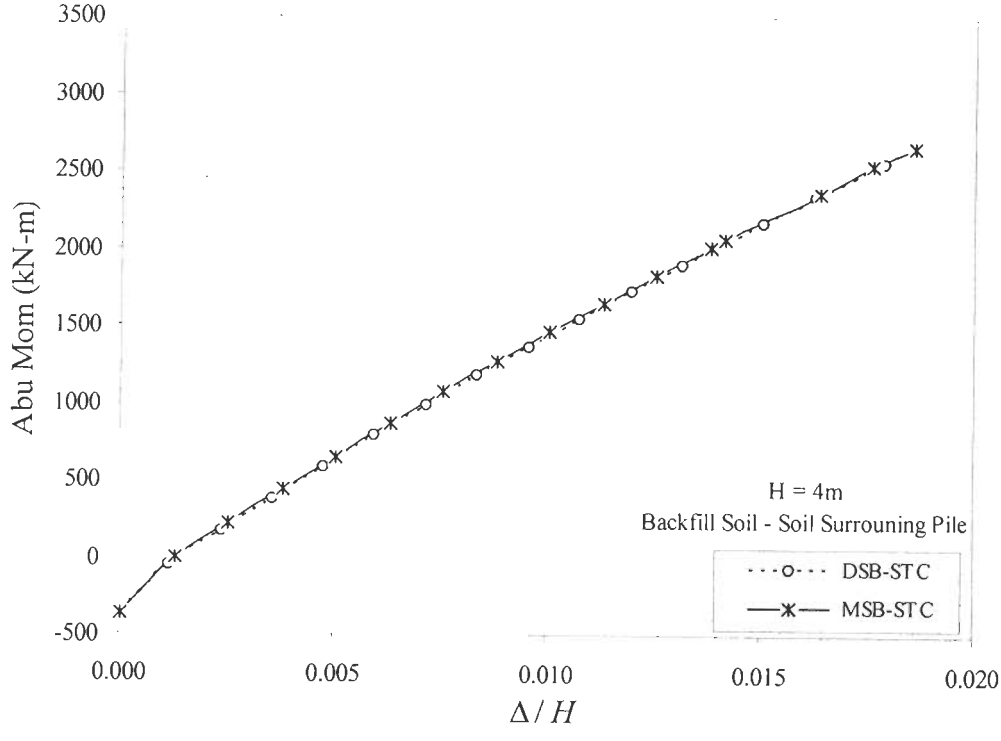

(ii)

Fig. 5.18: Variation of abutment moment Vs Δ / H for varying backfill soil with clay surrounding the pile (i) Temperature Rise (ii) Temperature Fall

5.4 LENGTH OF INTEGRAL ABUTMENT BRIDGE

The longitudinal expansion and contraction of an integral-abutment bridge that occurs at the neutral axis of the bridge can be determined by using

$$\Delta_t = \alpha \Delta T \, L/2 \qquad \ldots (5.6)$$

$$L = \frac{2\Delta_t}{\alpha \Delta T} \qquad \ldots (5.7)$$

The maximum length *'L'* of the integral abutment bridge is fixed based on the maximum yield displacement capacity Δ_{max} of the piles or formation of first plastic hinge. Considering the effect of soil surrounding the pile and abutment height, predrilled hole filled with loose sand and backfill soil the above equation can be modified as

$$\Delta_{max} = K_1 K_2 K_3 \alpha \Delta T \, L/2 \qquad \ldots (5.8)$$

$$\frac{2\Delta_{max}}{\alpha \Delta T \, H} = \frac{K_1 K_2 K_3 L}{H} \qquad \ldots (5.9)$$

where, $K_1, K_2 \& K_3$ are the coefficients depending upon soil surrounding pile and abutment height, predrilled hole filled with loose soil and backfill soil; H is the height of the abutment. Considering dense-dense and dense-stiff model subjected to temperature rise as an bench mark, the coefficients $K_1, K_2 \& K_3$ are normalized and represented in Figs. 5.19 to 5.22. The maximum length of integral abutment bridge can be calculated from Figs. 5.23 and 5.24.

K_1 is the coefficient depending upon the soil surrounding the pile and abutment height. From the nonlinear parametric study it is observed that increase in the abutment height results in the increase of the bridge yield displacement capacity under temperature fall

loading. In case of temperature rise with higher abutment heights, the yield displacement capacity of the pile reduces due to increase in the passive pressure behind the abutment and restricts the bridge length. Yield displacement capacity of pile was decreased by increasing the stiffness of the soil surrounding the pile. The ratio of maximum deck or abutment displacement depending upon the yield displacement capacity of pile for varying stiffness of soil surrounding the pile and different abutment height subjected to temperature rise and fall are shown in Figs. 5.19 and 5.20.

K_2 is the coefficient for predrilled hole, shown in Fig 5.21. In case of clay, predrilled hole is preferred only for stiff clay surrounding the pile. Piles in the predrilled hole filled with loose sand are found to be more flexible and significant amount of increase in the yield displacement capacity of piles was observed.

K_3 is the coefficient which depends on the backfill soil, shown in Fig 5.22. Change in the backfill soil from dense sand to medium sand and loose sand resulted in only 10% variation on the yield displacement capacity of 1.0 and 1.2m diameter piles in sand. Hence the backfill coefficient 'K_3' is taken as unity for piles in sand. Variation in the stiffness of intermediate piers had insignificant effect of the yield displacement capacity of piles under abutments.

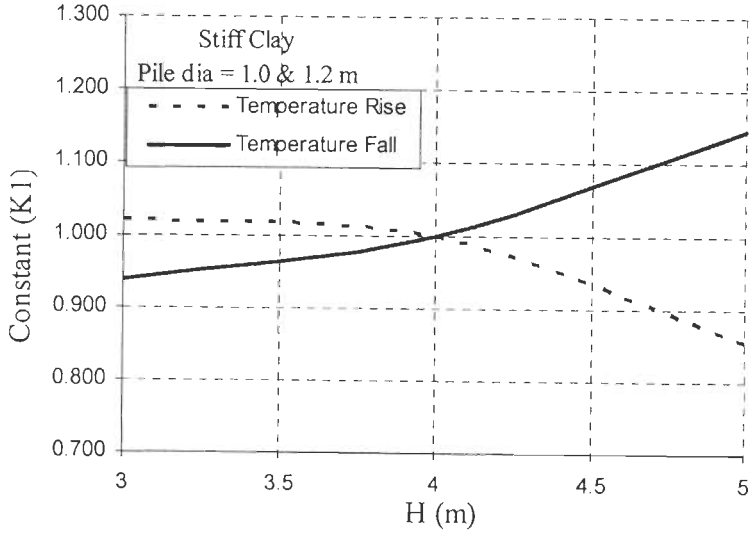

Fig. 5.19: Coefficient K_1 for varying abutment height and clay soil surrounding pile

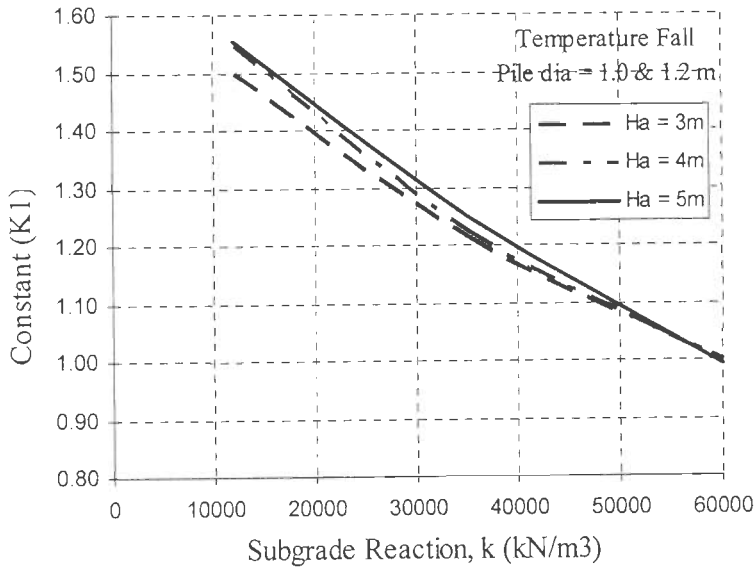

(i) Temperature Fall

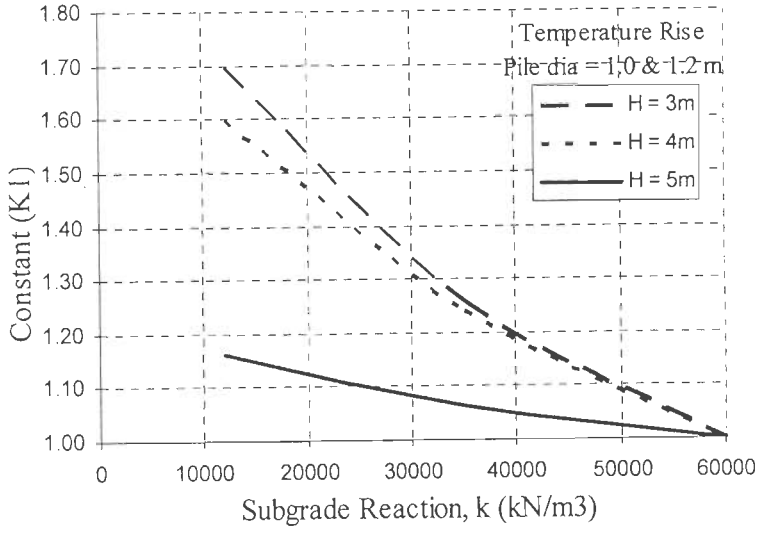

(ii) Temperature Rise

Fig. 5.20: Coefficient K_1 for varying abutment height and sand soil surrounding pile

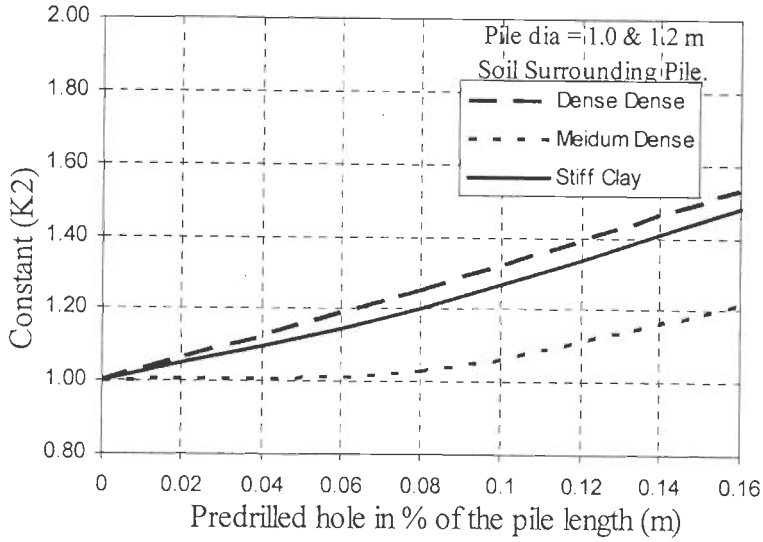

Fig. 5.21: Coefficient K_2 for varying length of predrilled hole

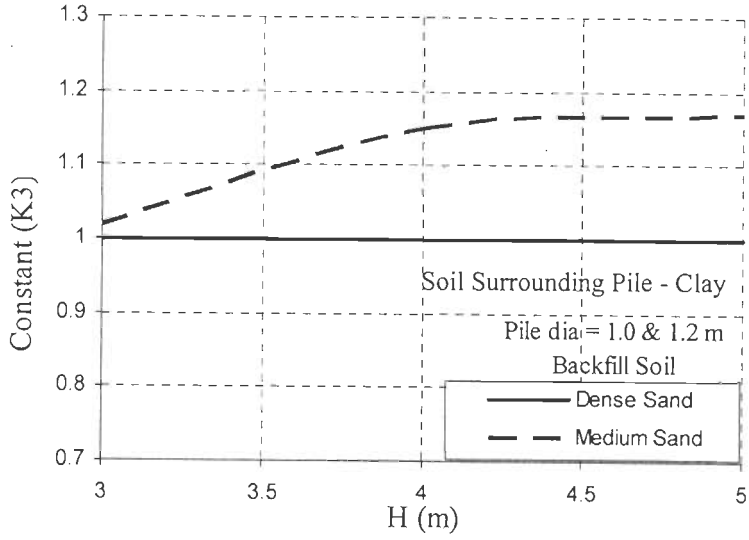

Fig. 5.22: Coefficient K_3 for varying backfill soil

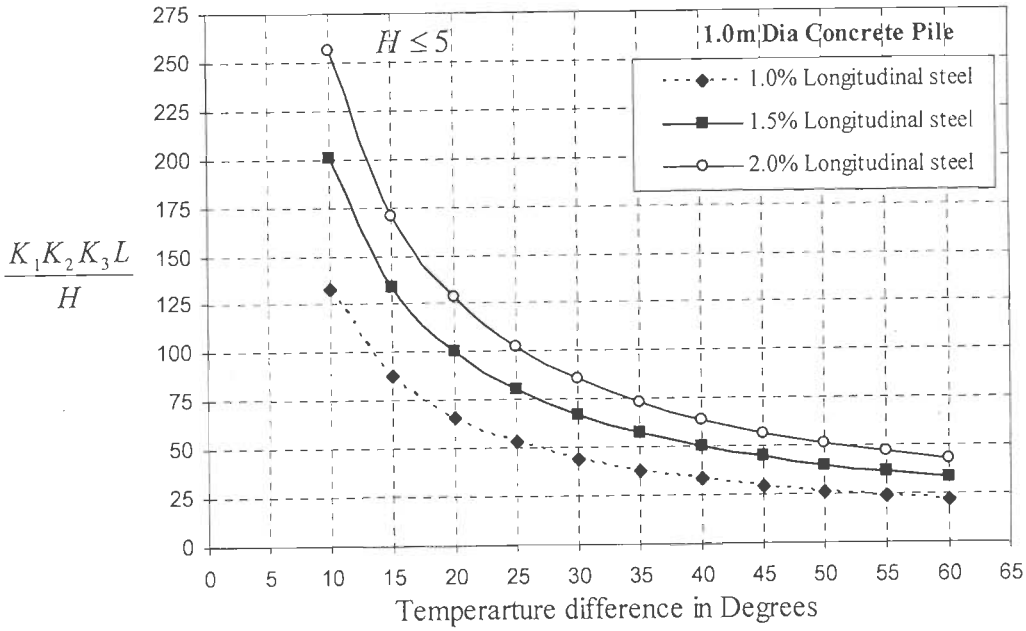

(a)

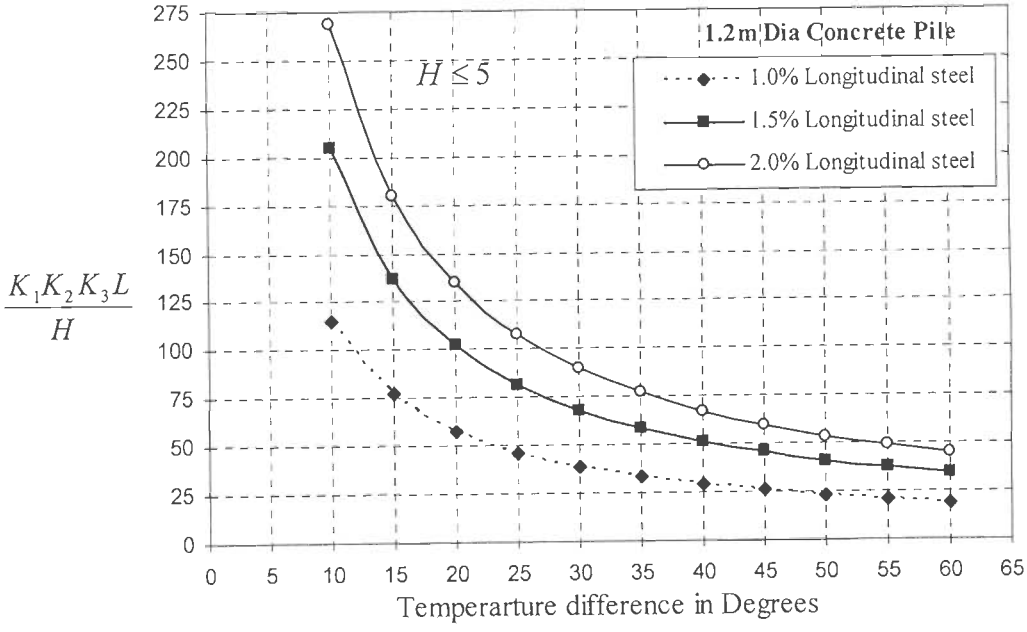

(b)

Fig. 5.23: Maximum length of integral abutment bridge on (a) 1.0m and (b) 1.2m diameter cast-in-situ concrete piles in sand (Concrete-M35)

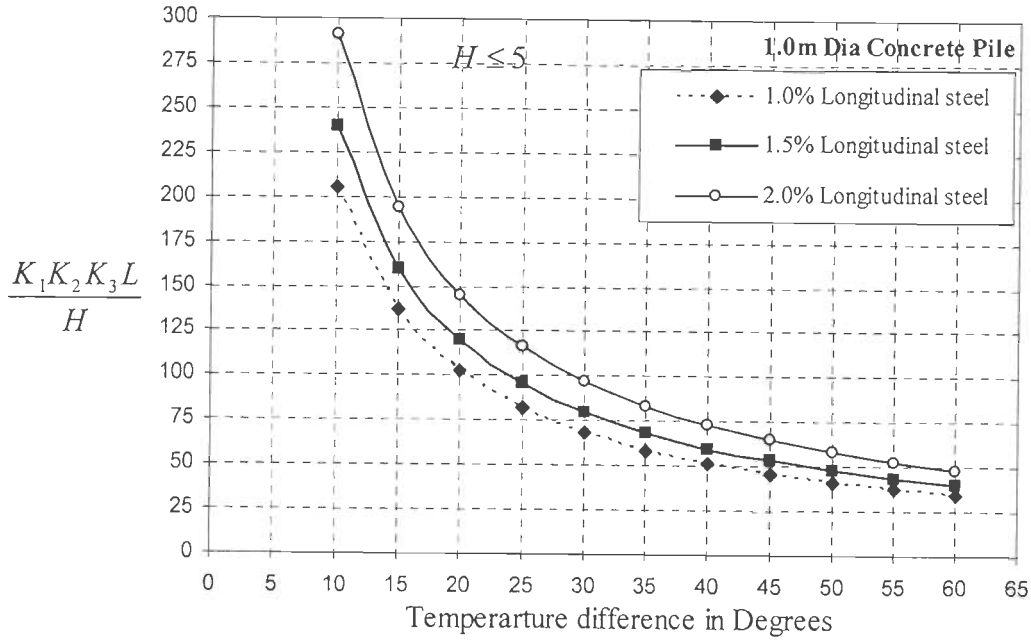

(a)

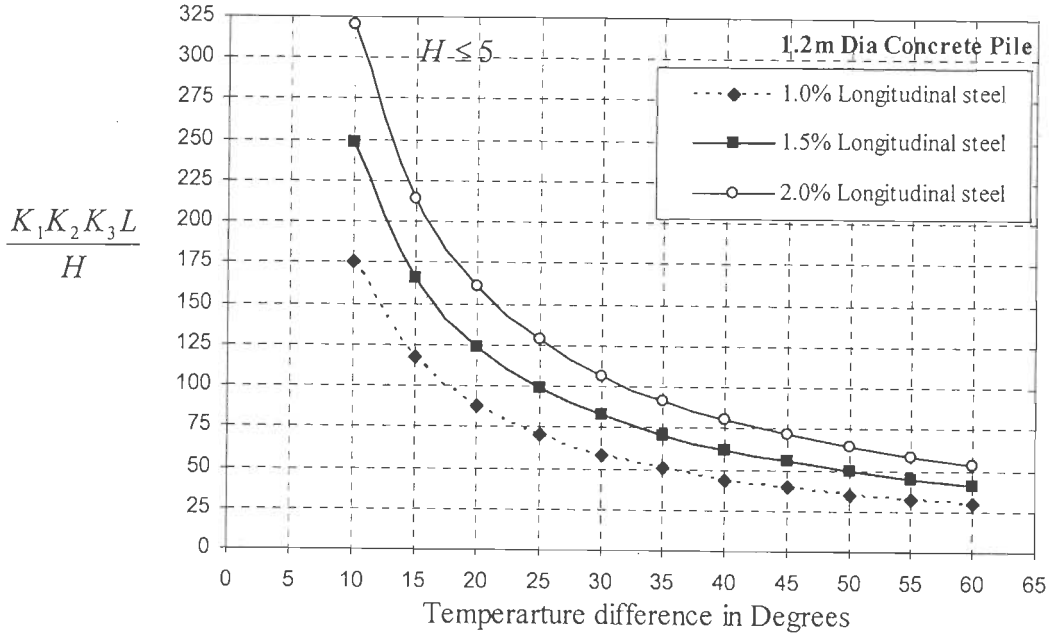

(b)

Fig. 5.24: Maximum length of integral abutment bridge on (a) 1.0m and (b) 1.2m diameter cast-in-situ concrete piles in clay (Concrete-M35),

5.5 CONCLUDING REMARKS

A parametric study is conducted on integral abutment bridges to investigate the effect of foundation soil and structural properties on its maximum length. The influence of abutment-backfill soil, soil surrounding the pile, predrilled hole, abutment and pier flexibility, pile type and pile longitudinal reinforcement on the length of integral abutment bridge is studied. The foundation consisting of 1.0m and 1.2 m diameter cast-in-situ pile having 1.0%, 1.5% and 2.0% longitudinal reinforcement is considered for the study. The height of the abutment is varied from 3m to 5m and flexibility of piers are considered by varying pier height from 5m to 9m. The soil conditions behind the abutment wall are varied as dense sand backfill, medium sand backfill and loose sand backfill and the soil surrounding pile are varied as dense sand backfill, medium sand, loose sand , stiff clay and soft clay. The effect of piles in the predrilled hole filled with loose sand is also taken into account. Non-linear pushover analysis is conducted on 3D model of an integral abutment bridge to find the maximum limits of bridge length that can be constructed under varying temperature conditions. The maximum length of the integral abutment bridge is worked out for temperature rise and fall based on the maximum yield displacement capacity of the piles. The following conclusion are derived from the study,

i. By varying the backfill soil from dense sand to loose sand and keeping the sand soil surrounding the pile unchanged for both the temperature rise and fall load conditions, the maximum variation in yield displacement and bending moment of the pile is found to be within 10%. Variation upto 15% has been observed in both the displacement and bending moment of the pile by changing the backfill soil from dense sand to medium sand and keeping the clay soil surrounding the pile unchanged. The stiffness of the soil does not affect the displacement 'capacity' of

the pile, but the resulting displacement of the pile; the (ductility) capacity is affected by the reinforcement of the pile.

ii. Increase in the soil stiffness from 12000 kN/m^3 to 60000 kN/m^3 results in the reduction of pile yield displacement capacity from 0.022 m to 0.013 m, nearly 50% reduction is observed. The stiffness of the subgrade soil surrounding the pile is observed to have a remarkable effect on the abutment top displacement and yield displacement capacity of the pile as also stated by Greiman, Kunin and Arsoy.

iii. The point of maximum bending moment in the piles placed in dense sand is found at a depth of 2D from the ground surface and for piles placed in loose sand it is found at a depth 4D from the ground surface. These results are comparable with the experimental results by Tuladhar *et al.* (2005) on full scale model, in which the plastic hinge in the pile was formed at the top 2D depth from ground level for fixed head piles subjected to monotonic loading condition and at 4D depth from ground level with decrease in soil stiffness.

iv. In case of piles placed in stiff clay formation of plastic hinge is observed at a depth of 3D from the ground level. For the piles placed in soft clay, plastic hinges were observed at two places one at the top of the pile and another at 7D below the ground level. Integral abutment bridges on soft clays are considered as incompatible, since the piles in the soft clay were subjected to higher bending moments and displacements throughout the length.

v. For the piles placed in dense sand, predrilled hole of 2.0m & 4.0m depth filled with loose sand at the top of the pile resulted in 28 to 71 % increase in the bridge length without allowing the piles to undergo hinge formation. The piles placed in medium sand, predrilled hole of 2.0m & 4.0m depth filled with loose sand at the

top of the pile resulted in 5 to 38 % increase in the bridge length without allowing the piles to undergo hinge formation.

vi. In case of dense sand backfill and stiff clayey soil surrounding the pile, abutment top displacement reduces from 0.016H to 0.008H by increasing the height of abutment from 3 m to 5m for temperature rise loading. Integral abutments with higher heights are subjected to larger bending moments due to the higher passive pressure developed along the height of the abutment. Bending moments in the abutments are considerably less for temperature fall when compared to temperature rise case. Temperature rise loading condition is critical for determining the displacement capacity of integral abutment bridges with greater abutment heights. Increase in the height of integral abutment resulted in the shifting of plastic hinge in the abutment piles from the depth 3D from ground level to the top of ground level.

vii. The relationship derived with respect to temperature rise and fall are useful for identifying the approximate length of integral abutment brdges built on cast-in-situ concrete piles of dia 1.0m and 1.2m, using the coefficients K_1, K_2 & K_3 which depends upon soil surrounding pile and abutment height, predrilled hole filled with loose soil and backfill soil. The shrinkage strain can be accounted along with temperature fall to find the bridge length. The minimum bridge length obtained from the combination of shrinkage and temperature fall or temperature rise alone should be considered for design.

viii. The maximum length of integral abutment bridges having 4.0 m abutment height with dense backfill constructed on 1.2 m dia pile with 1.5 % longitudinal reinforcement in dense subgrade can be restricted to 320m and 155 m, when

subjected to temperature variation of 20 and 30 degree respectively, taking load factor for thermal effects as 1.2 as per AASHTO.

CHAPTER 6

PERFORMANCE ASSESSMENT OF INTEGRAL BRIDGES FOR SEISMIC LOADING

6.1 INTRODUCTION

In high seismic regions, the seismic response demand of the integral bridges can be significantly more than the thermal response. Four distinct analytical procedures such as Linear Static, Linear Dynamic, Nonlinear Static (Pushover) and Nonlinear Dynamic procedure are available for the seismic analysis (FEMA-273, 1997). It is very important to know the force distribution in the integral bridge for its design. In case of integral abutment bridges the passive pressure behind the abutment increases with increase in abutment displacement and the stiffness of soil surrounding the pile decreases with increase in pile displacement. It is difficult to account these variations in both linear static and linear dynamic procedure. Nonlinear static or Nonlinear dynamic procedures are the solution to obtain the actual behavior of structure to find out the force distribution by taking into account the non-linear behavior of soil as well as the nonlinear behavior of structure. These procedures also have the ability to show the performance level under varying loading conditions.

In this Chapter, Nonlinear Dynamic Analysis or Nonlinear Time History Analysis (NDA) is carried out to study the force and displacement distribution in the bridge by taking five spectrum compatible time histories. The performance point which represents the target displacement and base shear of the structure is computed by Nonlinear Static Analysis (NSA) also called as Pushover Analysis as per ATC-40 and FEMA 273, FEMA 356 and FEMA 440 standards. A simplified method other than Capacity Spectrum Method (CSM) and Displacement Coefficient Method (DCM) is proposed to calculate target displacement. To have a displacement similar or close to the actual displacement due to

earthquake, it is important to use a force distribution equivalent to the expected distribution of the inertia forces. Different formats of force distributions such as Modal, Uniform and Spectral are implemented in this study to represent the actual earthquake behavior. Spectral approach is used to consider the higher modes which as a great contributes on the response of bridges (Kappos, 2001 & 2006).CSM, DCM and proposed simplified method is used to find target displacement and base shear of the structure. In the proposed simplified method, the capacity curve and design curve are retained without converting them into spectral ordinates. The results of the NDA and NSA are compared to validate the results and to find out suitable distribution in NSA to estimate maximum integral bridge length.

The seismic responses of integral bridges are greatly affected by soil-structure interaction (Youssef and Hassiotis 2000 and Kumar *et al.* 2006). Soil-structure interaction can be classified into kinematic and inertial interaction. The inertial interaction is due to soil deformation caused by inertial induced forces. Neglecting kinematic interaction the inertial soil-structure interaction is modeled by using nonlinear *p-y* springs along the piles and non-linear backfill springs along the length of abutment. The overall structure responds non-linearly to the typical seismic load. The inelastic model of the pier, pile and soil provides hysteretic energy dissipation. The implementation of various foundation dampings such as radiation damping and material damping in the design is difficult. In most of the bridge projects in California (Polam *et al.* 1998), ten percent foundation damping has been adopted. Five percent of material damping is assumed for concrete and ten percent for soil as per IS: 1893-2002 in the present study. Hysteretic material damping is more reliable and can be implemented with non-linear material models.

6.2 NON LINEAR DYNAMIC OR TIME HISTORY ANAYSIS (NDA)

Nonlinear dynamic analysis is the most reliable and realistic and considers the whole mass of the structure in the analysis. This method is realistic, sophisticated, time consuming and

also highly sensitive to small changes in assumption with regards to either the character of the ground motion used in the analysis or the stiffness of the elements. Time histories recorded in past earthquakes which have caused severe damage to the bridges and having frequency contents close to the bridge fundamental frequency are considered in the present study. Motions are made compatible to IS-1893:2002 response spectra for medium soil using the algorithm developed by Kumar (Kumar, 2004). The algorithm is iterative and first iteration has the assumption that Fourier magnitude spectrum of the desired time history is same as target velocity response spectrum. Signal is synthesized in frequency domain taking magnitude value from target spectra and phase from given input history. Notch filtering is done at frequency where target spectra is having abrupt change. All computations in this algorithm like band pass filtering, notch filtering, response spectrum etc. are performed in frequency domain in an optimal manner. Use of notch filter, as well as efficient management of frequency domain operations substantially reduces number of iterations required for convergence.

In the present study, one component of ground motion is applied in both the principal directions independently. The analysis has been carried out one at a time in each direction to get the maximum response separately. Figures 6.1 and 6.2 show the time history compatible records and their response spectra for 5% damping level.

Table 6.1: Summary of ground motions considered

	Earthquake (Recorded Station)	Magnitude	PGA (g)	PGV (mm/sec)	PGD (mm)
TH_1	EL Centro, USA (Imperial Valley Irrigation)	7.10	0.349	37.80	09.34
TH_2	Kobe (KAK090), Japan (Kakogawa)	6.90	0.345	27.60	09.60
TH_3	Kobe(KAK000), Japan (Kakogawa)	6.90	0.251	18.70	05.83
TH_4	Chi Chi, Taiwan (CHY006)	7.60	0.364	55.40	25.59
TH_5	Northridge, USA (Arleta)	6.70	0.344	40.60	15.04

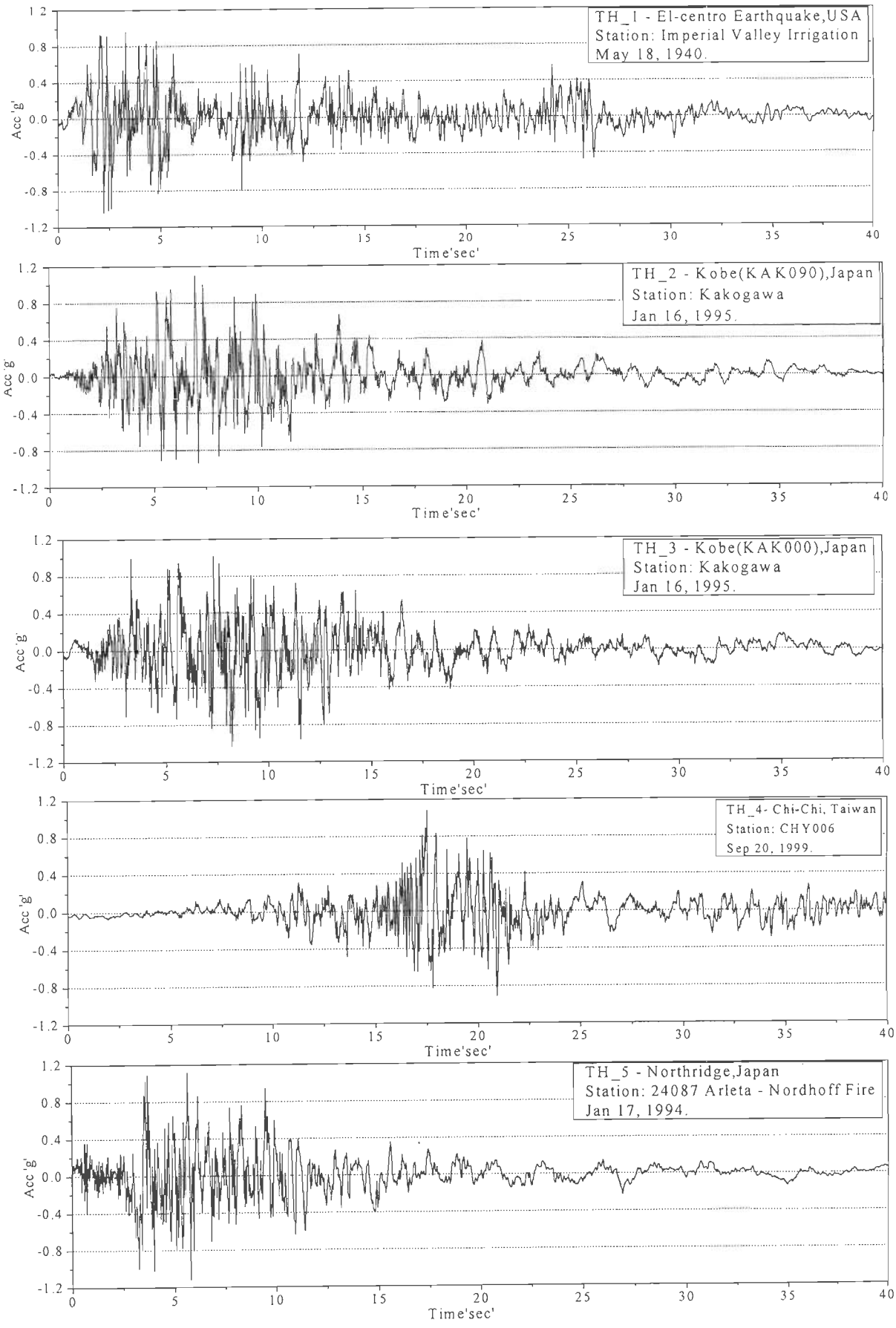

Fig. 6.1: Spectrum compatible ground motions using recorded time histories

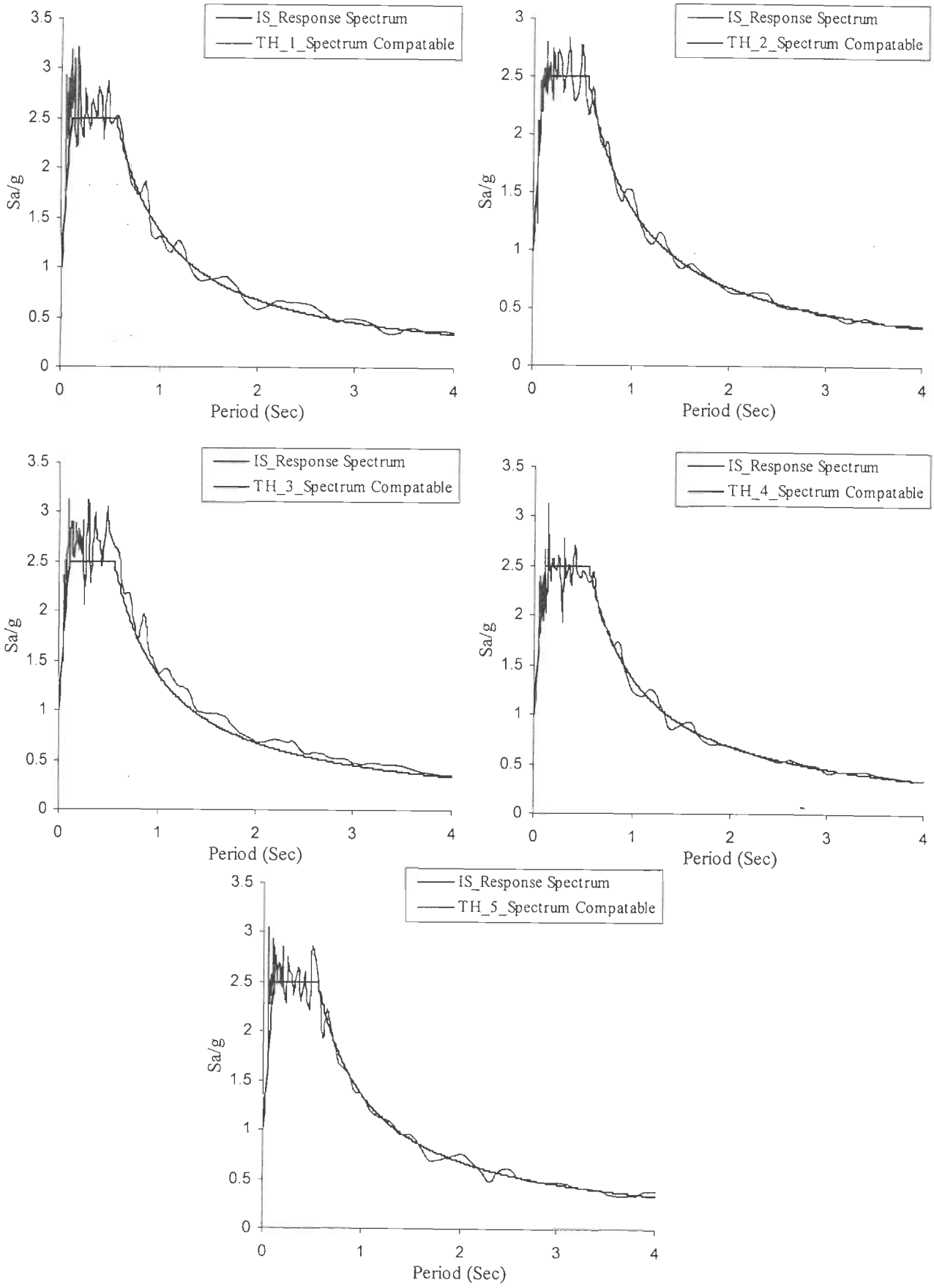

Fig. 6.2: Response spectra for compatible time histories (Kumar, 2004)

6.3 NONLINEAR STATIC OR PUSHOVER ANALYSIS (NSA)

Capacity curves are obtained for three load distributions such as Uniform distribution, Modal distribution and Spectral distribution that are recommended by FEMA-273, FEMA-356 and ATC-40. From the capacity curve, the performance point or target displacement is estimated by using CSM and DCM. Three categories of structural types such as A, B and C are defined by ATC-40 depending upon the hysteresis behavior of structures in CSM. 'A' represent reasonably full hysteresis loop, 'B' represent moderate reduction in hysteresis area and 'C' represent poor hysteric behavior. To have compatible inelastic behavior bridge models for both NDA and NSA, the structural type "A" and "B" are taken for the study. The alternative simplified method (SM) based on the concept of CSM has been proposed to find target displacement. Simplified method is as explained below,

6.3.1 Proposed Simplified Method (SM) for Evaluating Target Displacement

In this proposed simplified method the target displacement can be obtained by retaining the capacity curve and design curve without converting them into spectral ordinates. This simplified method is based on the concept of CSM. The technique is very much similar to that of equal displacement approximation or DCM. For structures having short period the target displacement obtained by equal displacement method may significantly vary from the results obtained using CSM. DCM fails to associate the behavior of structural types as specified in ATC-40. The SM overcomes both the above drawbacks and the result is close to CSM and DCM. The SM procedure can be used to evaluate the performance of components and elements.

The bilinear representation of the capacity spectrum is shown in Fig. 6.3. The damping that occurs in the inelastic range of structural behavior is a combination of viscous

damping that is structural and hysteretic dampings. The equivalent viscous damping β_{eff} associated with hysteretic damping β_0 can be represented by **(Naeim & Kelly)**

$$\beta_{eff} = \beta_0 + 0.05 \quad \ldots (6.1)$$

$$\beta_0 = \frac{1}{4\pi}\frac{E_D}{E_S} \quad \ldots (6.2)$$

E_D is the energy dissipated by damping or area enclosed in a single hysteresis loop of capacity curve, shown in Fig. 6.3

Note: ATC considers the damping in capacity spectral coordinates for energy dissipation

$$E_D = 4(V_y D_i - D_y V_i) \quad \ldots (6.3)$$

E_S is the maximum strain energy = Area of triangle OD_iB in Fig. 6.3

$$E_{So} = \frac{V_i D_i}{2} \quad \ldots (6.4)$$

$$\beta_0 = \frac{1}{4\pi}\frac{8(V_y D_i - D_y V_i)}{V_i D_i} = 0.637\left(\left(\frac{V_y}{V_i}\right) - \left(\frac{D_y}{D_i}\right)\right) \quad \ldots (6.5)$$

For structures which are not typically ductile, the Eq. 6.5 over estimates the equivalent viscous damping. Imperfect hysteresis loop are taken care by multiplying the effective viscous damping using a damping modification factor, k (ATC-40). The Eq. 6.1 becomes

$$\beta_{eff} = k\beta_0 + 0.05 \quad \ldots (6.6)$$

k depends on the structural type behavior. The different values of k for structural type A, B and C are shown in Table 6.2, which are derived based on the spectrum reduction factors.

Table 6.2: Values for damping modification factor, k given in ATC-40 (1996)

Structural Behavior type	β_0 (Percent)	k
Type A	≤16.25	1.0
	>16.25	$1.13-\frac{0.51(V_y D_i - D_y V_i)}{V_i D_i}$
Type B	≤25	0.67
	>25	$0.845-\frac{0.446(V_y D_i - D_y V_i)}{V_i D_i}$
Type C	Any Value	0.33

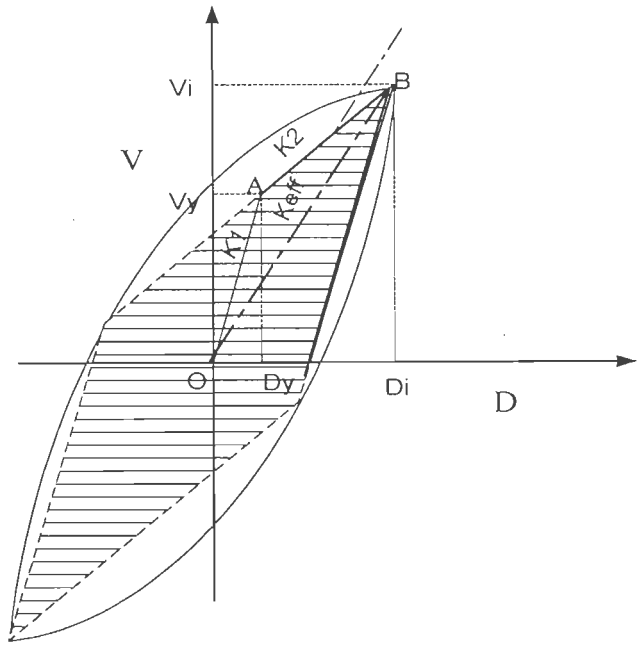

Fig.6.3: Hysteresis behavior of structure from capacity curve

The design spectrum in CSM is reduced using spectral reduction factor which is a function of effective damping associated with capacity curve of the structure. Spectral reduction SR_A and SR_V as per ATC-40 are given by

$$SR_A = \frac{1}{B_S} = \frac{3.21 - 0.68\ln(\beta_{eff})}{2.12} \quad \ldots (6.7)$$

$$SR_V = \frac{1}{B_L} = \frac{2.31 - 0.41\ln(\beta_{eff})}{1.65} \quad \ldots (6.8)$$

The ranges of SR_A and SR_V are limited by ATC-40, the values are shown in Table 6.3.

Table 6.3: Minimum allowable SR_A and SR_V values given in ATC-40 (1996)

Structural Behavior Type	SR_A	SR_V
Type A	0.33	0.5
Type B	0.44	0.56
Type C	0.56	0.67

Figures 6.4 and 6.5 show the plots of spectral reduction factors, obtained by substituting the value of k from Table 6.2 & β_0 from Eqn.6.5 into Eqn. 6.6 and Eqn.6.6 into Eqns. 6.7- 6.8.

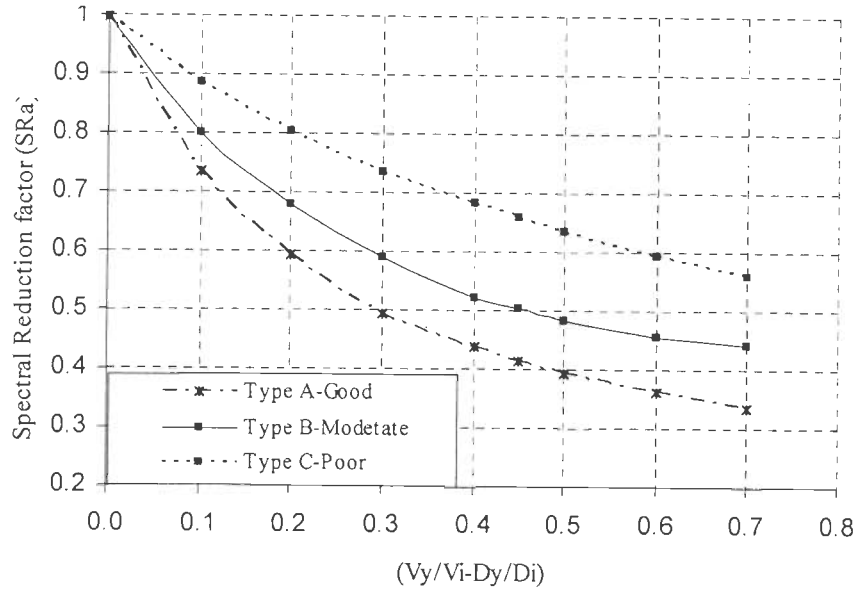

Fig.6.4: Reduction factor for $T_i \leq T_0$ sec

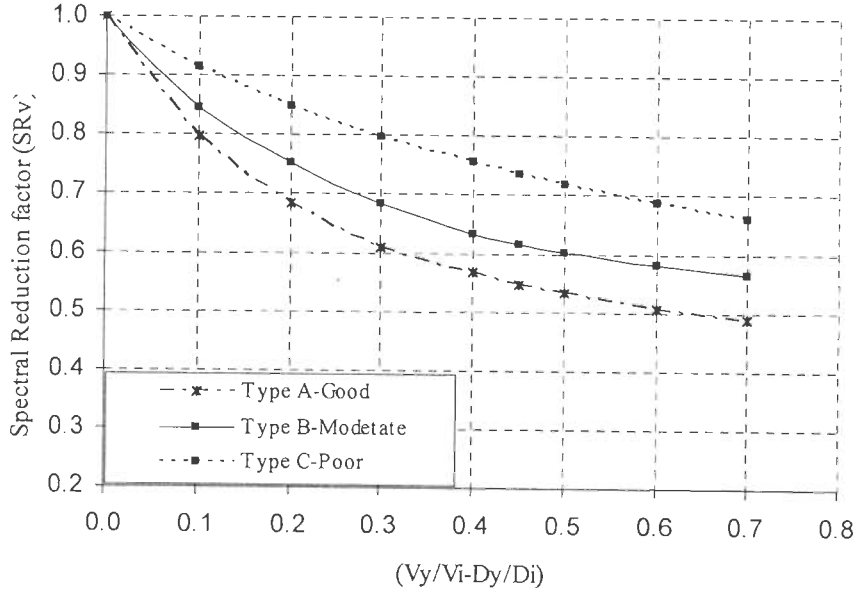

Fig.6.5: Reduction factor for $T_i > T_0$ sec

where, T_0 is the characteristic period associated with the transition from the constant acceleration to constant velocity segment of the spectrum.

In capacity spectrum method the design spectrum is reduced by using spectral reduction factors. Instead of applying reduction factors to the design spectrum, a trial is made to apply incremental displacement factor like DCM, to find target displacement directly using capacity curve. Following assumptions are made to derive the displacement factors.

i) Displacement incremental factor is assumed as inverse of spectral reduction factor.

ii) Taking reciprocal of spectral reduction factor leads to higher displacement incremental factor for structural type A and lesser for type C, but the target displacement will be lesser for structural type A and more for structural type C, so the curves are interchanged for structure type A and C. Figures 6.6 and 6.7 show the plots of incremental factors D_a and D_v.

$$B_S = D_a = \frac{2.12}{3.21 - 0.68\ln(\beta_{eff})} \quad \ldots (6.9)$$

$$B_L = D_v = \frac{1.65}{2.31 - 0.41\ln(\beta_{eff})} \quad \ldots (6.10)$$

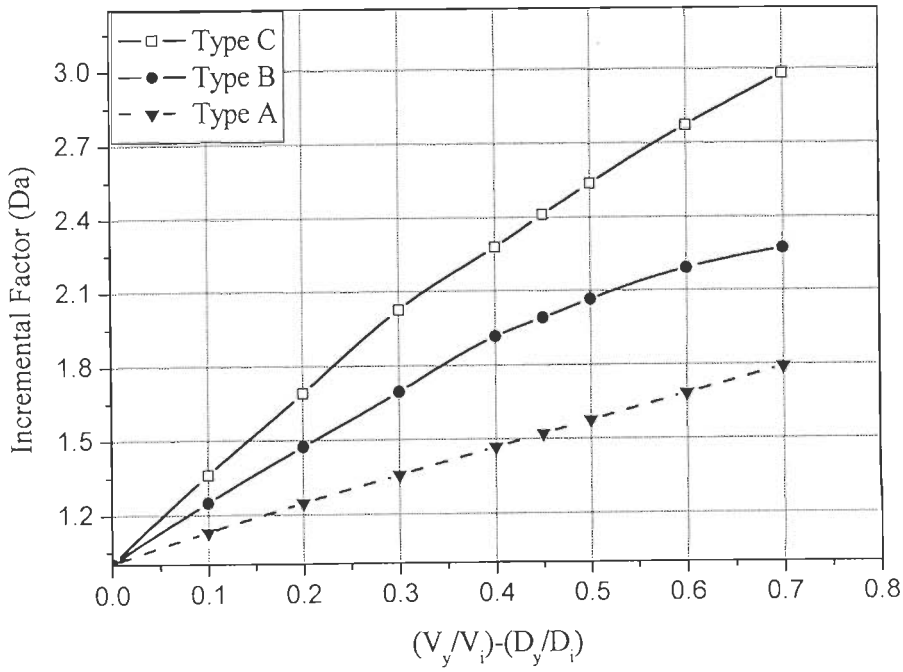

Fig.6.6: Incremental factor for $T_i \leq T_0$ sec

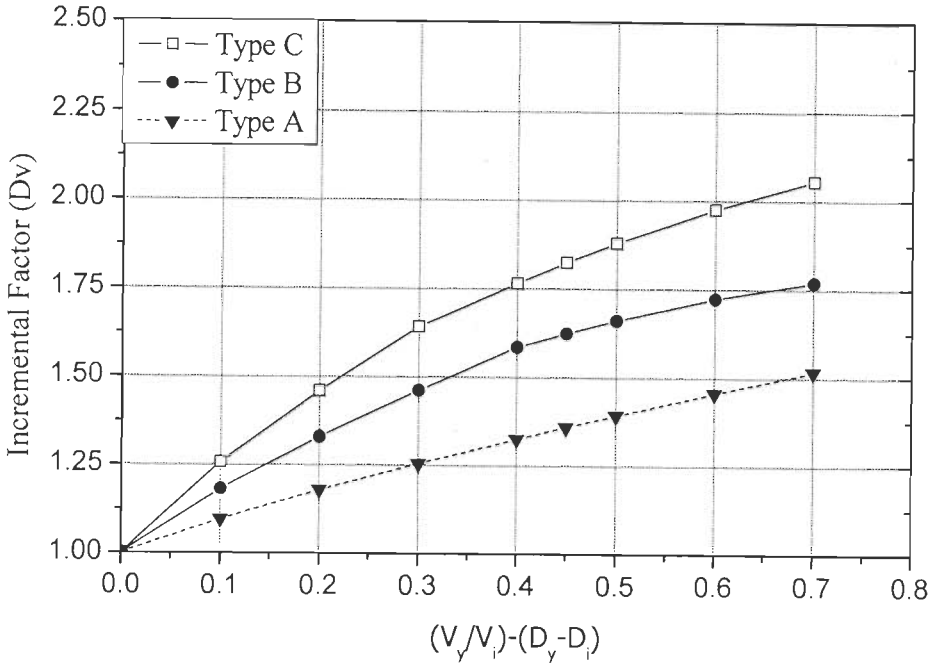

Fig.6.7: Incremental factor for $T_i > T_0$ sec

6.3.1.1 Stepwise Procedure for the Proposed Simplified Method (SM).

1) Calculate equivalent spectral displacement of the structure by using

$$S_{RD} = \frac{T_i^2 S_a}{4\pi^2} \qquad \ldots (6.11)$$

where, T_i is the elastic fundamental period in the direction under consideration and it will be the time period of mode shape considered for Modal distribution and S_a is the spectral acceleration at T_i.

2) The roof or control node displacement corresponding to equivalent spectral displacement can be obtained by

$$D_i = PF(S_{RD}) \qquad \ldots (6.12)$$

where, PF is the mode participation factor, taken as unity for all structures, assuming that actual displacement is equal to equivalent spectral displacement.

3) Get the value of V_i for corresponding D_i from capacity curve and find the value of $\left(V_y/V_i - D_y/D_i\right)$

$$\beta_{eff} = (0.637 * k * \left(V_y/V_i - D_y/D_i\right) + 0.05), \qquad k = 1 \qquad \ldots (6.13)$$

$$\left(V_y/V_i - D_y/D_i\right) \leq \beta_{eff} \quad \ldots (6.14)$$

For calculating target displacement, the incremental factor D_a and D_v corresponding to $\left(V_y/V_i - D_y/D_i\right)$ is obtained from Figs. 6.6 and 6.7.

4) Target displacement is obtained either by

$$\delta = \begin{cases} D_i D_a & for \quad T_i \leq T_0 \\ D_i D_v & for \quad T_i > T_0 \end{cases} \quad \ldots (6.15)$$

6.3.1.2 Validation of the Proposed Simplified Method

Example: The example illustrated in ATC-40 (1996), Chapter-8 is considered for the verification of the proposed simplified method. The elastic time period of the structure in first mode is 0.88 sec and corresponding spectral acceleration for soil type B and D are 0.45g and 0.73g respectively. A participation factor 'PF' at roof of the structure is 1.21 and modal participation factor α is 0.828. Incremental load is applied to the structure in proportion to the first mode. From the capacity curve represented in ATC-40, Fig 6.7.1 (Fig. 8-45 in ATC-40), the base shear and displacement at first point of yielding are 2200 kN and 2.51 inches. The base shear and displacement at ultimate limit of the structure are 3000 kN and 10.9 inches. Capacity Curve, Design Spectrum and Acceleration-Displacement Response Spectrum of the structure are shown in Fig 6.7.2 (Fig. 8-46 in ATC-40). The results obtained by simplified analytical method is compared with CSM and DCM, results are tabulated in Table 6.4.

Simplified Method: Case 1: Soil type B

1) Equivalent spectral displacement of the structure is obtained by using

$$S_{RD} = \frac{T_i^2 S_a}{4\pi^2} = 3.4\ in$$

2) The roof or control node displacement corresponding to equivalent spectral displacement gives

$$D_i = PF(S_{RD}) = 3.4\ in$$

3) For $D_i = 3.4$ in, from the capacity curve given in ATC-40, Fig. 8-72, $V_i = 2500$ kN

$$(V_y/V_i - D_y/D_i) = 0.142$$

$\beta_{eff} = 0.140$ (using Eqn. 6.13)

$(V_y/V_i - D_y/D_i) > \beta_{eff}$;

Taking, $(V_y/V_i - D_y/D_i) = 0.14$; $D_v = 1.32$ (Structural type C, using Fig.6.7)

4) Target displacement is obtained by using Eqn. 6.15

$\delta = 4.49\ in$

Case 2: Soil type D

1) Equivalent spectral displacement of the structure is obtained by using

$$S_{RD} = \frac{T_i^2 S_a}{4\pi^2} = 5.5\ in$$

2) The roof or control node displacement corresponding to equivalent spectral displacement gives

$$D_i = PF(S_{RD}) = 5.5\ in$$

3) For $D_i = 5.5$ in, from the capacity curve given in ATC-40, Fig. 8-72, $V_i = 2850$ kN

$$(V_y/V_i - D_y/D_i) = 0.32$$

$\beta_{eff} = 0.252$ (using Eqn. 6.13)

$(V_y/V_i - D_y/D_i) > \beta_{eff}$

Taking, $(V_y/V_i - D_y/D_i) = 0.252$; $D_v = 1.54$ (Structural type C, using Fig.6.7)

4) Target displacement is obtained by using Eqn. 6.15

$\delta = 8.37\ in$

From Table 6.4, it can be concluded that the SM gives the target displacement which are

comparable with CSM and DCM. SM is much simpler than CSM and can be used for the quick estimation of target displacement.

Table 6.4: Comparison of results obtained from SM, CSM and DCM

	Soil Type	SM	CSM	DCM
Actual	B	4.490	4.500	5.100
Displacement (in)	D	8.370	8.400	8.300
Base	B	2900	2900	N.A
Shear(kN)	D	2900	2900	N.A

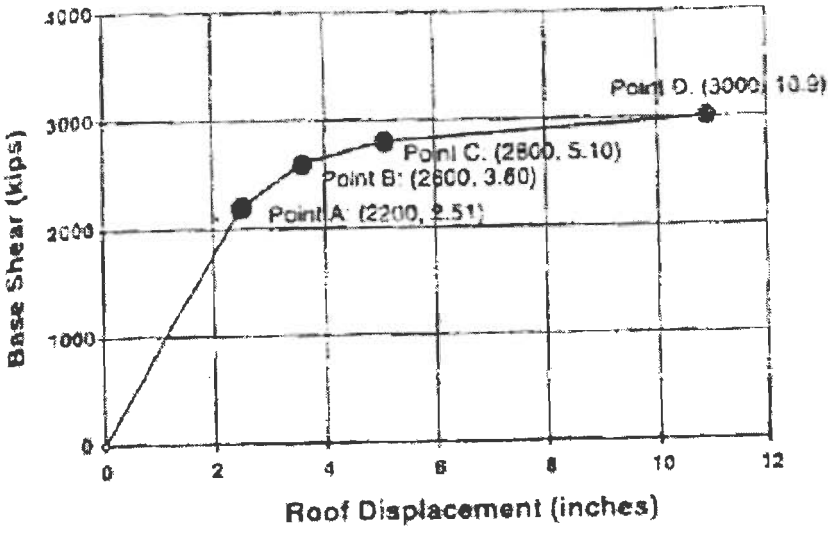

Fig 6.7.1: Capacity Curve ((Fig. 8-45 in ATC-40)

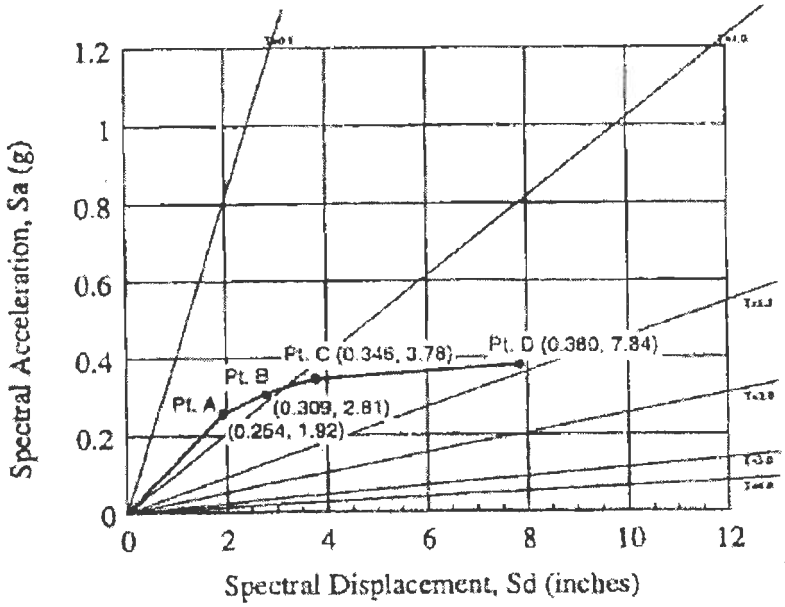

Fig 6.7.2: Acceleration Displacement Response spectrum(Fig. 8-45 in ATC-40)

6.4 NUMERICAL EXAMPLE OF INTEGRAL ABUTMENT BRIDGE

A five span integral abutment bridge, explained in Chapter-4 is taken for analysis. Bridge is analysed for response spectrum compatible time histories taking two different soil conditions such as dense sand backfill and dense sand surrounding the pile (DSB-DS) and dense sand backfill and stiff clay surrounding the pile (DSB-STC). Pile of dia 1.0m with 1.0% longitudinal reinforcement and pier with 3 % reinforcement are considered for study. Structural analysis program SAP v10.1.3 is used for analysis. The dead load of the entire structure is found to be 47850 kN, in which nearly 50% is contributed by foundation. To calculate the natural time period and spectral displacement the moments of inertia of cracked sections is used. 50% of live load is considered for seismic analysis along transverse direction. Considering the bridge to be in Zone-V of seismic zoning map of India, the peak ground acceleration of 0.36 g and response spectrum corresponding to 5% damping for the medium soil site is taken to generate Spectrum compatible time histories. The rock out crop motion is applied to the base of the model. Soil spring is considered as frequency independent. Hysteretic behavior and energy dissipation of soil is taken into consideration. Changes for the formation of gap beyond the abutment backfill and in between soil-pile interaction are neglected. For pushover analysis, any node at the top of the deck can be used as a control node in longitudinal direction. For the present study, the node at the top of the abutment is used as the control node. The C.G of the superstructure is used as a control node to monitor displacement in transverse direction.

6.4.1 Free Vibration Analysis

The natural vibration modes of the bridges are evaluated considering the soil and structural stiffness. In modal analysis, equivalent linear soil stiffness is required for approximate calculation of natural time period of the structure. It is recommended to slightly

overestimate the soil stiffness than underestimating it. During earthquake, one abutment backfill will be in compression while other abutment backfill will be in tension. Therefore the backfill of abutment which will be in tension will not contribute to stiffness, but the pile and the abutment wall will contribute to the stiffness. To account this effect half-half abutment stiffness approach is considered. As per this approach half of the backfill soil stiffness is used at each abutment assuming that full passive pressure is developed during earthquake. Table 6.5 lists the natural periods of vibration and percentage of mass participation in longitudinal and transverse directions for DSB-DS and DSB-STC.

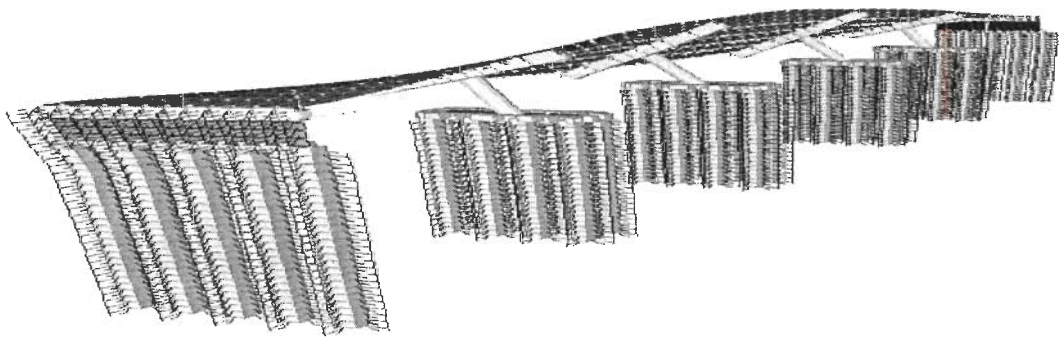

(a) Mode – 1 in transverse direction (T_n = 0.687 sec.)

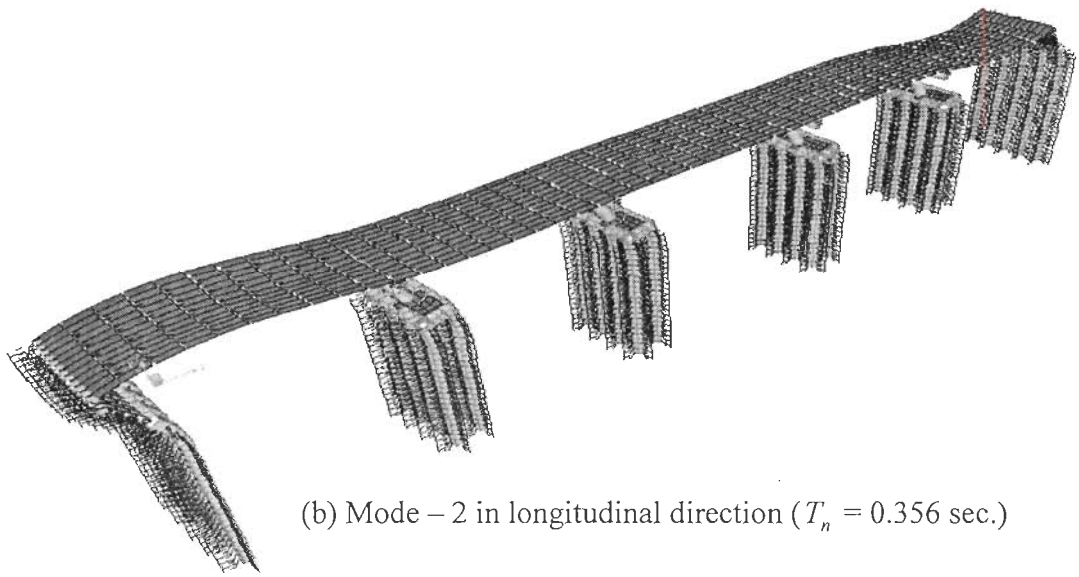

(b) Mode – 2 in longitudinal direction (T_n = 0.356 sec.)

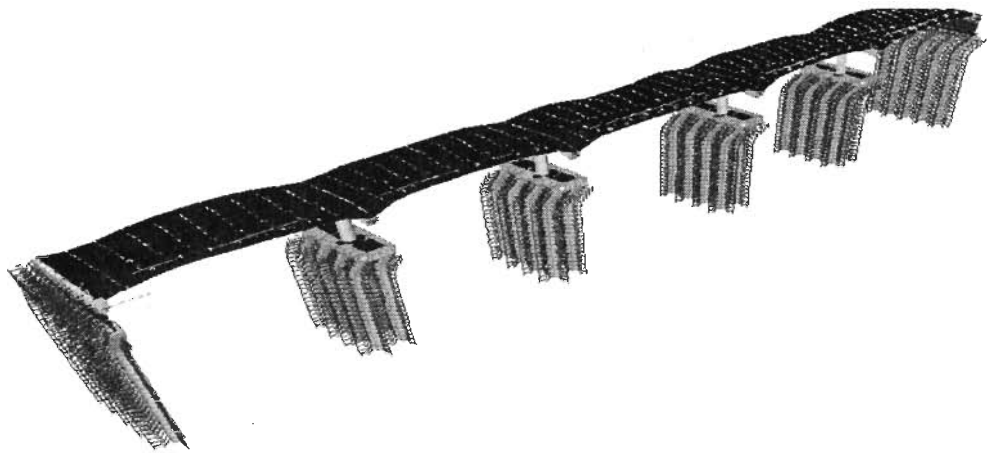

(b) Mode – 24 in transverse direction (T_n = 0.016 sec.)

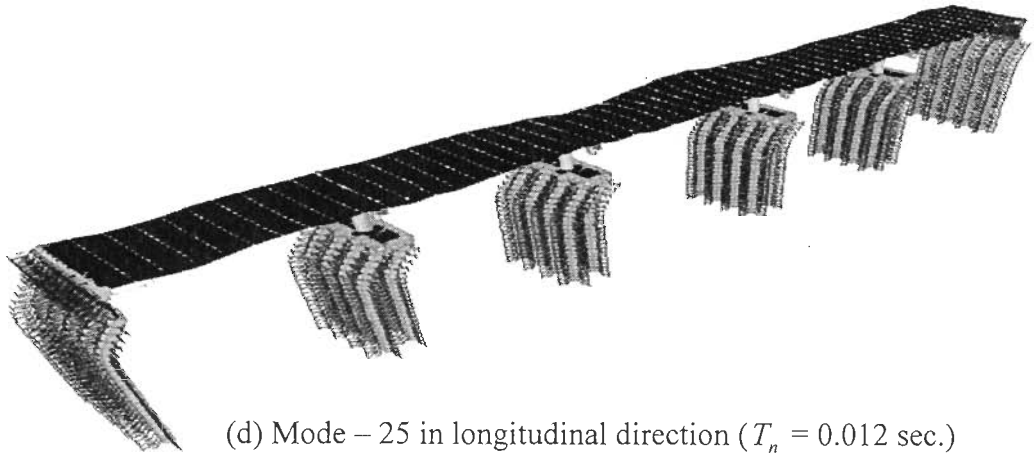

(d) Mode – 25 in longitudinal direction (T_n = 0.012 sec.)

Fig. 6.8: Deformed mode shape of integral abutment bridge

A total of 25 Ritz modes were considered to achieve a 90% and above mass participation in the global X, Y and Z directions. Majority of the mass were contributed by predominantly six distinct modes in all the three directions. The fundamental mode for both DSB-DS and DSB-STC models are corresponding to transverse mode with a period of 0.687 sec and 0.586 sec respectively. The second mode is the longitudinal mode with a time period of 0.356 sec and 0.324 sec for DSB-DS and DSB-STC models respectively. Transverse and longitudinal mode shapes of DSB-DS model are shown in Figs 6.8 (a) and (b), respectively.

Table 6.5 (a): Summary of natural time period (T_n) and mass contribution (Considering Foundation mass)

Modes	DSB-DS			DSB-STC		
	T_n (Sec)	Mass_X (%)	Mass_Y (%)	T_n (Sec)	Mass_X (%)	Mass_Y (%)
1	0.687	0.000	0.220	0.586	0.000	0.227
2	0.356	0.440	0.000	0.324	0.441	0.000
3	0.322	0.000	0.000	0.307	0.000	0.000
4	0.280	0.000	0.072	0.254	0.000	0.039
5	0.242	0.000	0.000	0.241	0.000	0.000
6	0.241	0.000	0.037	0.211	0.000	0.029
7	0.239	0.000	0.000	0.209	0.000	0.000
8	0.205	0.000	0.079	0.201	0.000	0.096
9	0.198	0.090	0.000	0.189	0.007	0.000
10	0.191	0.007	0.000	0.184	0.000	0.000
11	0.187	0.000	0.017	0.180	0.000	0.032
12	0.183	0.000	0.002	0.174	0.005	0.000
13	0.175	0.013	0.000	0.174	0.000	0.004
14	0.172	0.000	0.001	0.135	0.010	0.000
15	0.122	0.000	0.090	0.119	0.000	0.000
16	0.116	0.001	0.001	0.114	0.000	0.011
17	0.108	0.000	0.011	0.110	0.000	0.003
18	0.099	0.001	0.012	0.092	0.000	0.013
19	0.088	0.093	0.000	0.079	0.090	0.003
20	0.083	0.000	0.087	0.078	0.004	0.063
21	0.069	0.000	0.061	0.066	0.000	0.090
22	0.056	0.027	0.000	0.052	0.026	0.000
23	0.048	0.020	0.000	0.043	0.026	0.000
24	0.016	0.000	0.244	0.020	0.002	0.341
25	0.012	0.244	0.000	0.020	0.288	0.002
Sum		0.935	0.937		0.900	0.957

In the total mass of the structure, nearly 50% of mass was contributed by foundation (Piles and Pile cap). By comparing the table 6.5 (a) & 6.5(b), it was observed in the 25th and 24th mode in both longitudinal and transverse directions the foundation mass contributed nearly 24.0% of the total mass. The large contribution of mass at these higher modes are due to the contribution of foundation mass (piles and pile cap), which are having high rigidity due to soil-pile interaction.

Table 6.5(b): Summary of natural time period (T_n) and mass contribution (Foundation mass is neglected)

Modes	DSB-DS			DSB-STC		
	T_n (Sec)	Mass_X (%)	Mass_Y (%)	T_n (Sec)	Mass_X (%)	Mass_Y (%)
1	0.510	0.000	0.269	0.584	0.000	0.335
2	0.279	0.604	0.000	0.316	0.648	0.000
3	0.239	0.000	0.000	0.303	0.000	0.000
4	0.201	0.000	0.116	0.253	0.000	0.055
5	0.177	0.000	0.000	0.240	0.000	0.001
6	0.176	0.000	0.000	0.209	0.000	0.068
7	0.172	0.000	0.041	0.207	0.000	0.000
8	0.160	0.000	0.166	0.194	0.000	0.099
9	0.140	0.005	0.000	0.187	0.012	0.000
10	0.139	0.002	0.000	0.184	0.000	0.000
11	0.132	0.000	0.004	0.178	0.000	0.065
12	0.128	0.000	0.001	0.169	0.000	0.007
13	0.126	0.002	0.000	0.169	0.008	0.000
14	0.123	0.000	0.000	0.119	0.000	0.000
15	0.094	0.000	0.000	0.112	0.000	0.022
16	0.083	0.000	0.019	0.109	0.000	0.000
17	0.080	0.176	0.000	0.098	0.000	0.012
18	0.076	0.000	0.200	0.077	0.010	0.000
19	0.071	0.014	0.000	0.072	0.000	0.120
20	0.056	0.000	0.041	0.071	0.122	0.000
21	0.049	0.013	0.000	0.055	0.000	0.050
22	0.042	0.000	0.018	0.051	0.008	0.000
23	0.034	0.012	0.000	0.036	0.010	0.000
24	0.020	0.000	0.096	0.023	0.000	0.098
25	0.011	0.036	0.000	0.013	0.027	0.000
Sum		0.864	0.971		0.844	0.931

6.5 EVALUATION OF EARTHQUAKE RESPONSE

6.5.1 Model-1: Dense Sand Backfill-Dense Sand Surrounding Pile (DSB-DS)

Figures 6.9 and 6.10 show the base shear time history and displacement time history at the control node for the five ground motions in both longitudinal and transverse directions. Tables 6.6-6.7 summarize the maximum force and deformation obtained by nonlinear time history analysis in longitudinal and transverse directions respectively. The average of forces and deformations obtained for five time histories by NDA are compared with results obtained by NSA.

Table 6.6: Summary of forces in the longitudinal direction obtained by NDA

Ground Motion	Disp. (mm)	Base Shear (kN)	Rotation (rad)				
			Bottom of the				Abutment Pile (top)
			Pier 1	Pier 2	Pier 3	Pier 4	
TH_1	18.10	16704	0.0012	0.0013	0.0012	0.0013	0.0025
TH_2	18.65	13044	0.0010	0.0010	0.0011	0.0010	0.0017
TH_3	18.33	15842	0.0012	0.0010	0.0010	0.0011	0.0024
TH_4	16.92	14540	0.0010	0.0010	0.0010	0.0010	0.0021
TH_5	23.06	17098	0.0012	0.0012	0.0012	0.0012	0.0027
Average	19.02	15445	0.0011	0.0011	0.0011	0.0011	0.0023

Table 6.7: Summary of forces in the transverse direction obtained by NDA

Ground Motion	Disp. (mm)	Base Shear (kN)	Rotation (rad.)				
			Bottom of the				Abutment Pile (top)
			Pier 1	Pier 2	Pier 3	Pier 4	
TH_1	55.59	15330	0.0008	0.0009	0.0009	0.0008	0.0013
TH_2	52.87	15174	0.0007	0.0008	0.0008	0.0007	0.0012
TH_3	60.97	14775	0.0006	0.0007	0.0007	0.0006	0.0012
TH_4	52.97	14453	0.0006	0.0006	0.0006	0.0006	0.0013
TH_5	52.70	14166	0.0008	0.0009	0.0009	0.0008	0.0012
Average	55.02	14780	0.0007	0.0008	0.0008	0.0007	0.0012

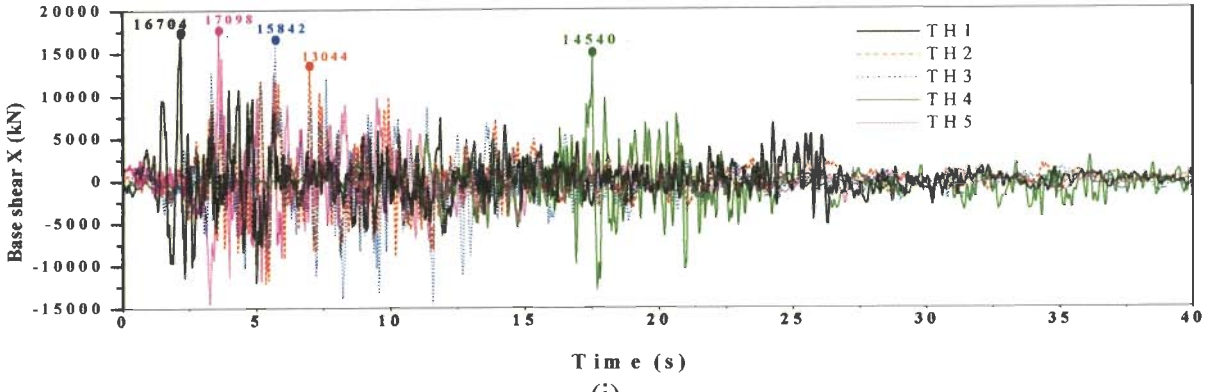

(i)

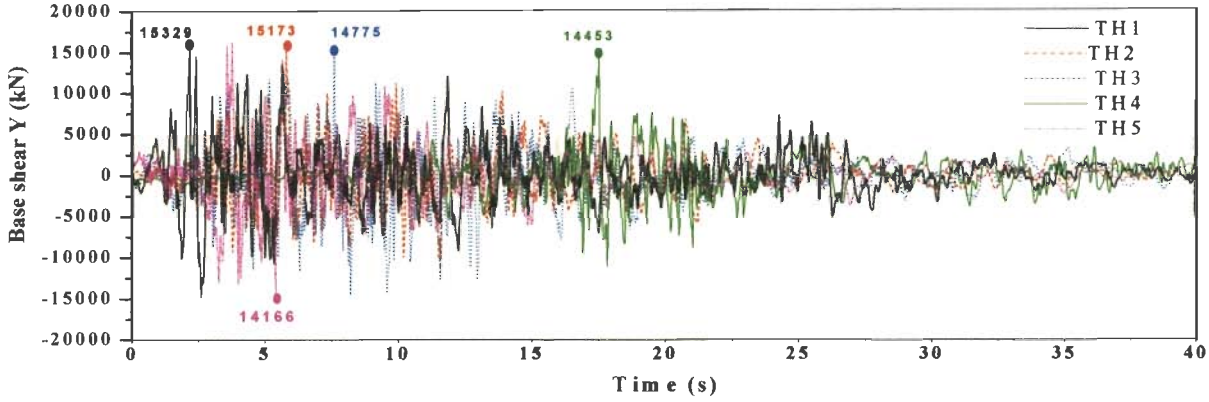

(ii)

Fig. 6.9: Base shear time histories (i) Longitudinal direction (ii) Transverse

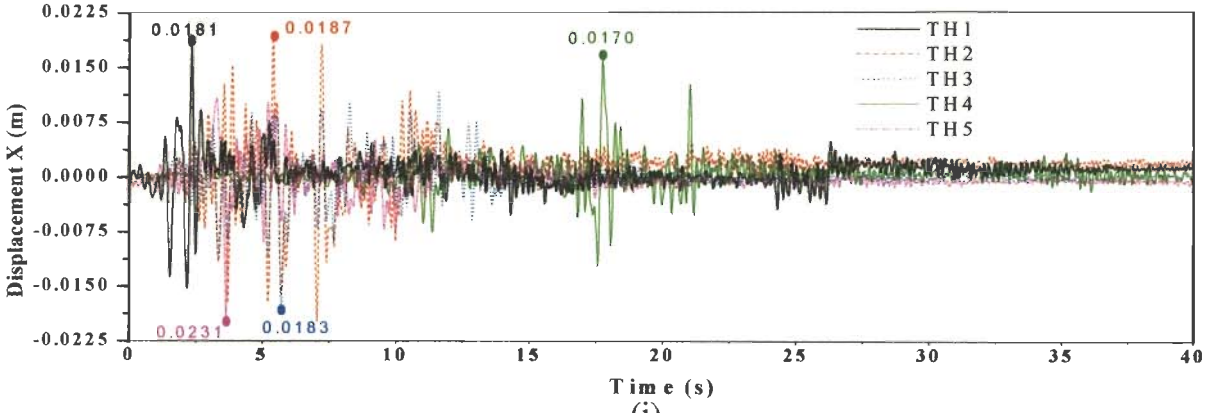

(i)

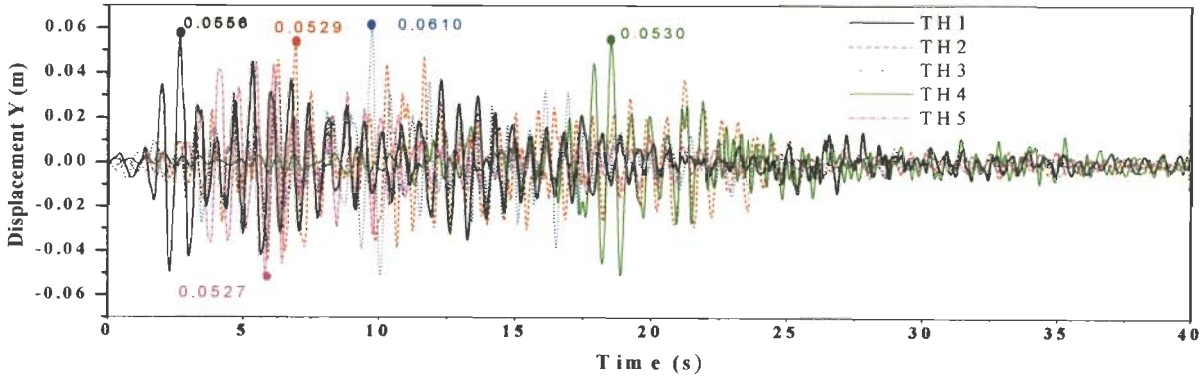

(ii)

Fig. 6.10: Displacement time histories (i) Longitudinal direction (ii) Transverse direction

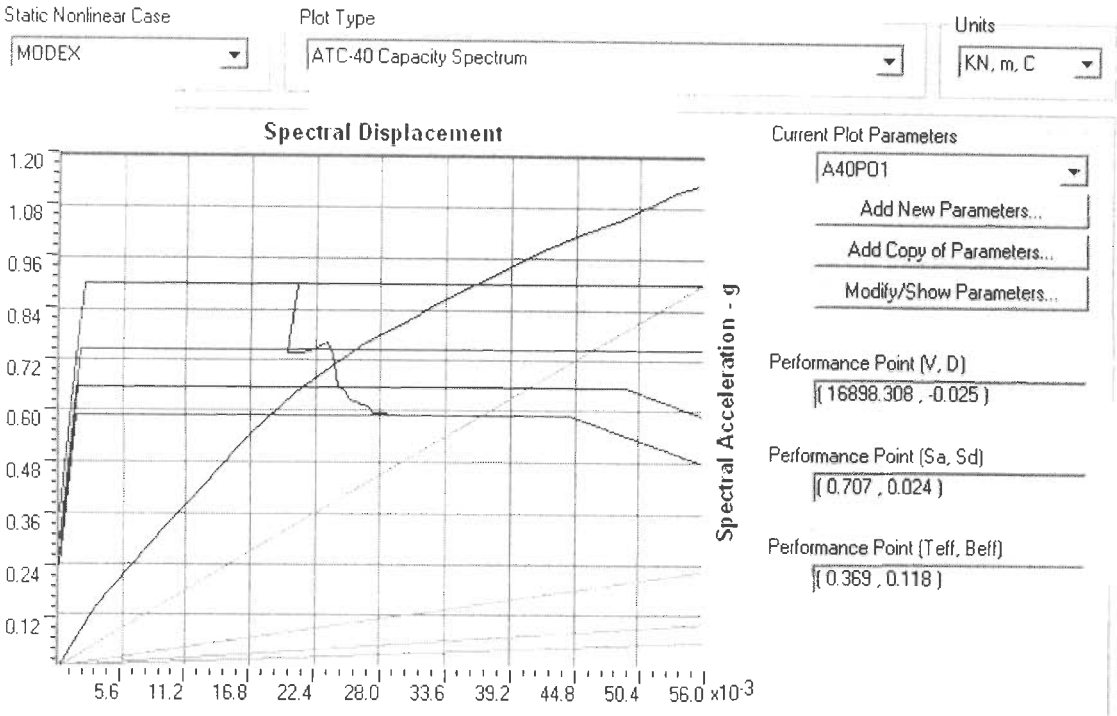

(i)

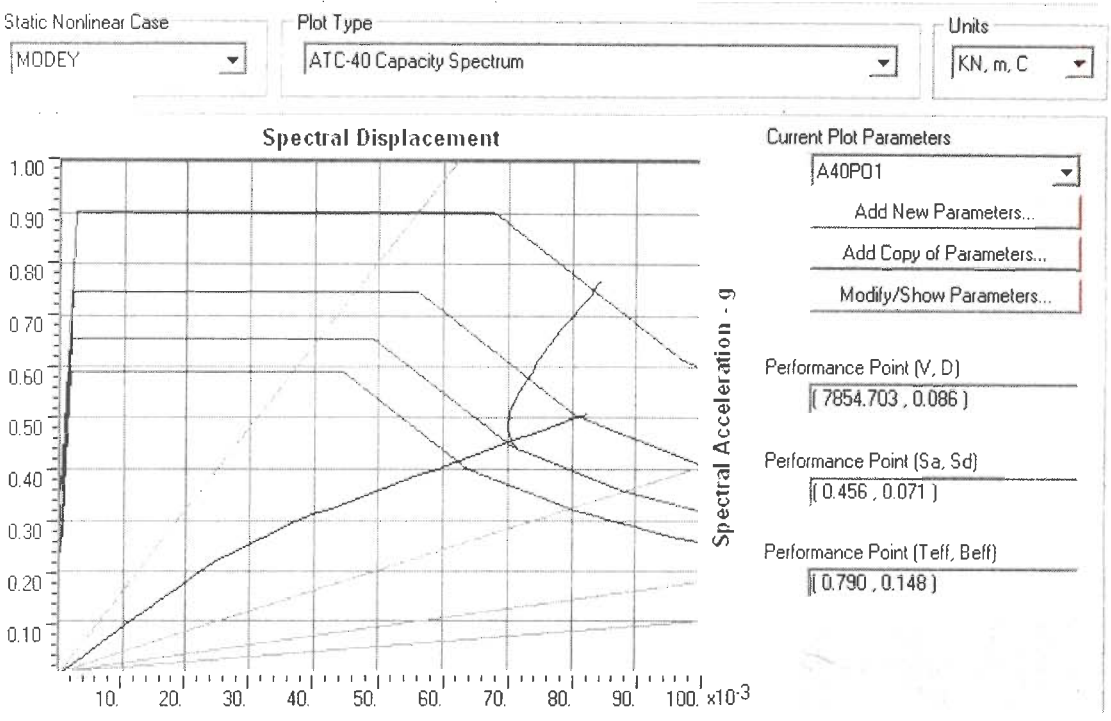

(ii)

Fig. 6.11: Acceleration Displacement Response Spectra (ADRS) for Modal distribution in (i) Longitudinal and (ii) Transverse directions.

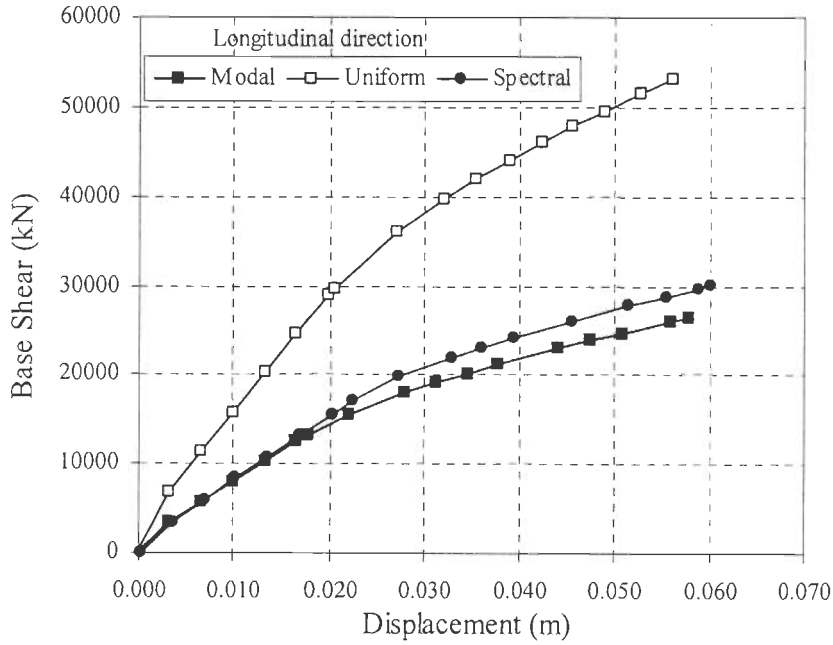

Fig. 6.12: Capacity curves for longitudinal static pushover

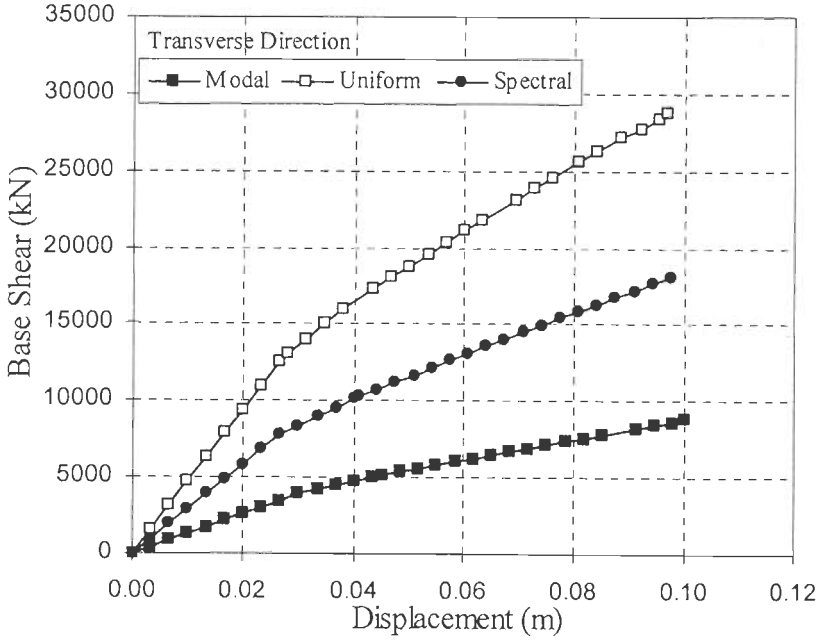

Fig. 6.13: Capacity curves for transverse static pushover

Acceleration Displacement Response Spectra (ADRS) for Modal distribution in longitudinal and transverse directions is shown in Fig. 6.11. Figures 6.12 and 6.13 show the relationship between the base shear and the displacement at the control node in longitudinal and transverse directions for Modal, Uniform and Spectral distribution respectively. The spectral distribution is based on the first 25 modal forces combined using CQC method. The load distribution plays an important role in the pushover analysis since the modal mass contribution is just 45% and 22% in fundamental mode in

longitudinal and transverse directions respectively. Pushover curve in longitudinal direction is shown in Fig. 6.12, the initial slope of Spectral distribution follows the Modal distribution upto yield limit and from there the difference in the capacity curve is observed. This change in Spectral distribution is due to the foundation contribution which is not reflected in the fundamental mode. In the transverse direction, pushover curves shown in Fig 6.13, Spectral distribution seems to be an average of Modal and Uniform distributions.

Table 6.8 gives the comparison of forces and deformations between NDA and NSA in the longitudinal direction for 0.36g PGA. In longitudinal direction, the stiffness offered by the foundation is higher in the longitudinal direction, hence even though the mass participation ratio in modal is lesser compare to spectral distribution, displacements obtained by modal and spectral distributions are nearly same, The displacement obtained by uniform distribution is underestimated as the resistance offered by the soil-pile interaction and backfill abutment soil is much higher and restricts the displacement in the pile. The base shears obtained by modal, spectral and uniform distributions are comparable than the NDA values. However, the base shears obtained by all three distributions are close to each other

$$Diff(\%) = \frac{R_P - R_{NT}}{R_p} \quad \ldots (6.16)$$

where, R_p and R_{NT} are the response obtained from NSA and NDA.

Table 6.8: Comparison of results of NSA with NDA in the longitudinal direction

Analysis Methods	Distribution	Structure Behavior	Disp	Base Shear	Rotation (rad)				
					Piers				End Pile
					Pier 1	Pier 2	Pier 3	Pier 4	
			Mm	kN					
NDA			19.012	15445.84	0.00108	0.00110	0.00110	0.00108	0.00226
CSM	Modal	A	31.50	9.44	26.37	25.68	25.00	31.02	28.43
		B	36.76	14.04	27.30	29.33	25.91	35.66	37.29
SM		A	20.98	3.59	25.44	23.86	23.19	30.09	24.00
		B	26.24	4.88	25.44	25.68	24.09	31.95	26.22
DCM			52.54	30.33	40.31	41.17	40.40	49.60	88.22
CSM	Uniform	A	-42.14	20.86	-15.44	-18.03	-18.48	-7.08	-3.45
		B	-36.88	20.86	-15.44	-18.03	-18.48	-7.08	-3.45
SM		A	-36.88	21.33	-15.44	-18.03	-18.48	-7.08	-3.45
		B	-36.88	20.86	-15.44	-18.03	-18.48	-7.08	-3.45
DCM			-36.88	21.33	5.00	0.18	-0.36	7.79	17.80
CSM	Spectral	A	26.24	17.49	2.21	0.18	4.17	13.36	30.20
		B	31.50	22.27	12.43	10.20	14.13	19.87	37.73
SM		A	26.24	17.49	6.86	5.65	11.41	19.87	41.72
		B	31.50	22.27	12.43	10.20	14.13	19.87	37.73
DCM			15.72	5.53	6.86	5.65	11.41	19.87	41.72

Table 6.9: Comparison of results of NSA with NDA in the transverse direction

Analysis Methods	Distribution	Structure Behavior	Disp	Base Shear	Rotation (rad)				
					Piers				End Pile
					Pier 1	Pier 2	Pier 3	Pier 4	
			mm	kN					
NDA			55.02	14779.698	0.00072	0.00081	0.00081	0.00072	0.00124
CSM	Modal	A	56.31	-46.72	-2.46	-8.28	-8.28	-3.85	11.29
		B	69.03	-43.31	0.33	-0.84	-0.84	0.33	34.68
SM		A	67.21	-43.50	0.33	-0.84	-0.84	1.72	27.42
		B	81.75	-41.00	931.16	1.64	1.64	3.12	46.77
DCM			41.77	-52.64	-6.64	-12.00	-12.00	-15.00	-3.23
CSM	Uniform	A	-38.20	3.09	-16.39	-16.96	-16.96	-16.39	-54.03
		B	-38.20	3.09	-16.39	-16.96	-16.96	-16.39	-54.03
SM		A	-38.20	3.09	-16.39	-16.96	-16.96	-16.39	-54.03
		B	-34.57	5.21	-15.00	-14.48	-14.48	-15.00	-50.81
DCM			-30.93	11.64	-8.03	-10.76	-10.76	-8.03	-43.55
CSM	Spectral	A	-1.85	-17.52	-2.46	-5.80	-5.80	-2.46	-42.74
		B	7.23	-12.71	0.33	-0.84	-0.84	0.33	-39.52
SM		A	-5.49	-18.81	-3.85	-8.28	-8.28	-3.85	-43.55
		B	3.60	-14.75	0.33	-2.08	-2.08	0.33	-41.94
DCM			-1.85	-17.52	-2.46	-5.80	-5.80	-2.46	-42.74

Table 6.10: Summary of forces in the longitudinal direction obtained by NDA

Ground Motion	Disp. (mm)	Base Shear (kN)	Rotation (rad.)				
			Bottom of the				Abutment Pile (top)
			Pier 1	Pier 2	Pier 3	Pier 4	
TH_1	16.35	20067	0.0013	0.0015	0.0015	0.0013	0.0021
TH_2	17.01	15940	0.0009	0.0011	0.0011	0.0009	0.0013
TH_3	15.90	18690	0.0011	0.0013	0.0013	0.0011	0.0020
TH_4	16.92	17547	0.0010	0.0013	0.0013	0.0010	0.0017
TH_5	18.70	22921	0.0015	0.0019	0.0019	0.0015	0.0024
Average	17.00	19033	0.0012	0.0014	0.0014	0.0012	0.0019

Table 6.11: Summary of forces in the transverse direction obtained by NDA

Ground Motion	Disp. (mm)	Base Shear (kN)	Rotation (rad)				
			Bottom of the				Abutment Pile (top)
			Pier 1	Pier 2	Pier 3	Pier 4	
TH_1	58.14	16561	0.002	0.0024	0.0024	0.002	0.0022
TH_2	48.37	16924	0.0023	0.0029	0.0029	0.0023	0.0021
TH_3	51.7	16582	0.0019	0.0023	0.0023	0.0019	0.002
TH_4	51.31	14794	0.002	0.0024	0.0024	0.002	0.0022
TH_5	45.01	14288	0.0017	0.0021	0.0021	0.0017	0.0019
Average	50.91	15830	0.002	0.0024	0.0024	0.002	0.0021

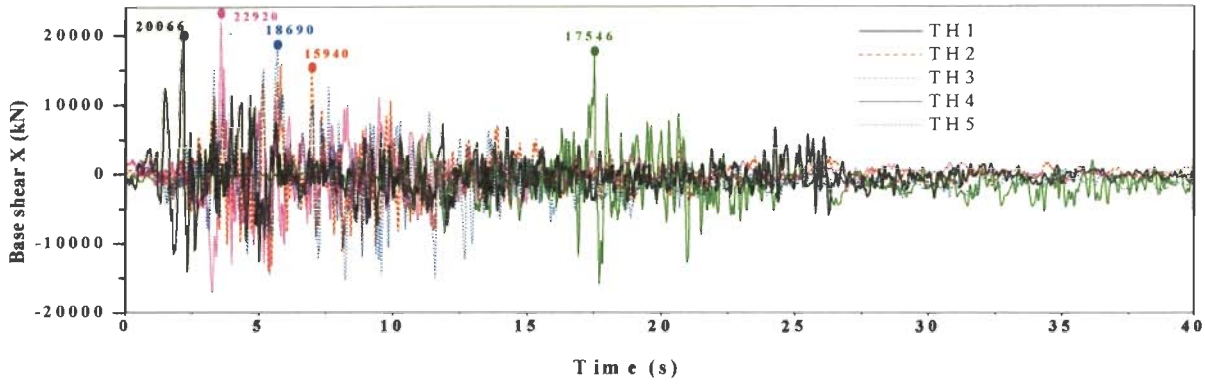

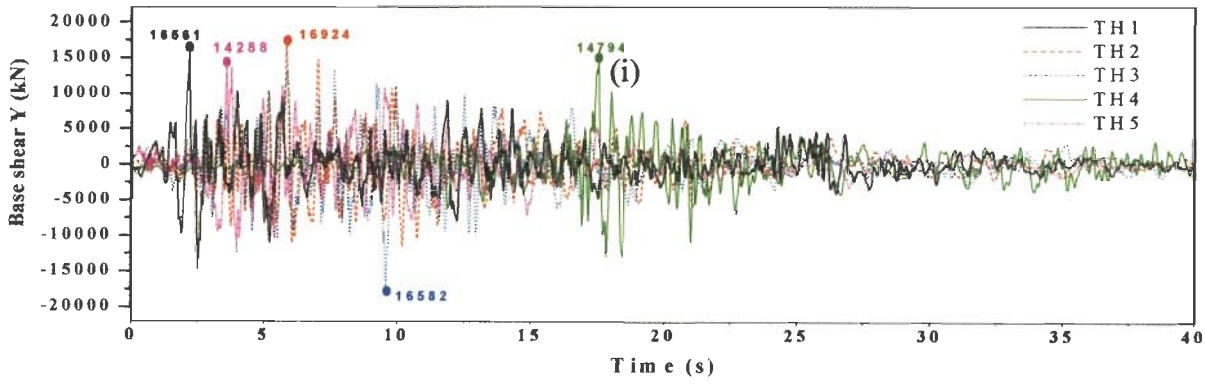

(ii)

Fig 6.14: Base shear time histories (i) Longitudinal direction (ii) Transverse direction

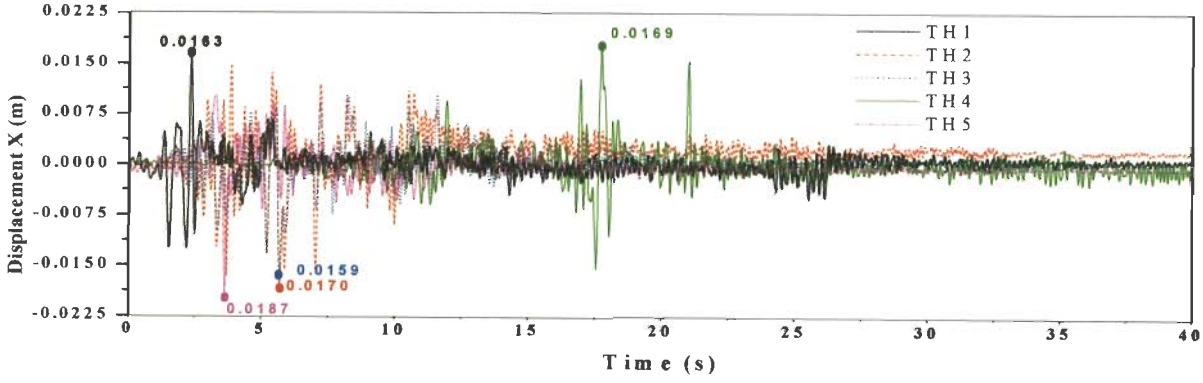

(i)

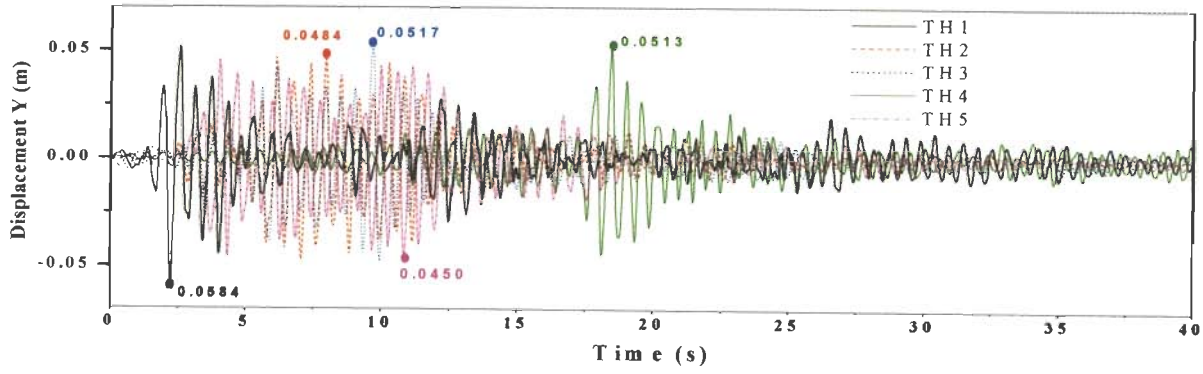

(ii)

Fig 6.15: Displacement time histories (i) Longitudinal direction (ii) Transverse direction

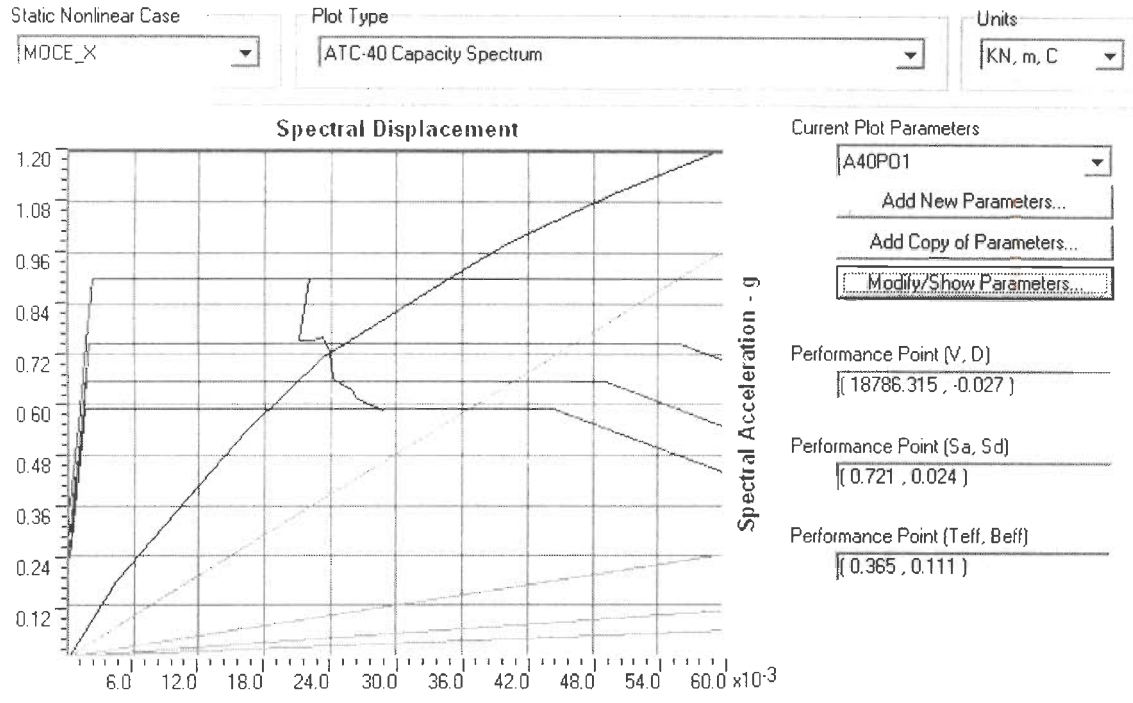

(i)

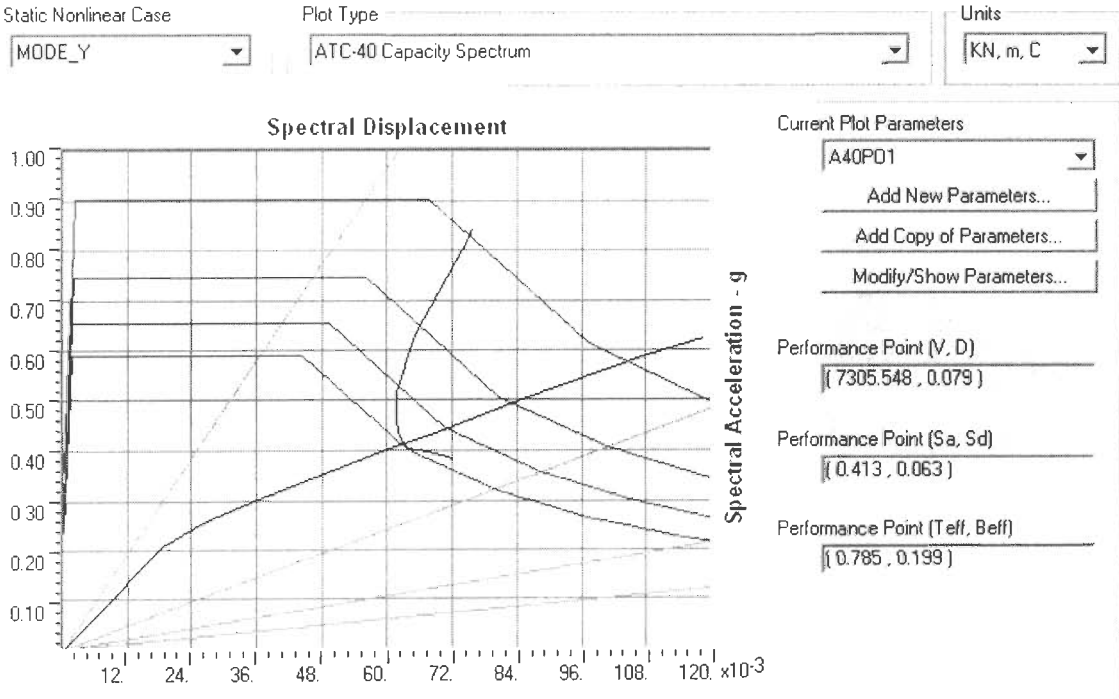

(ii)

Fig. 6.16: Acceleration Displacement Response Spectra (ADRS) for Modal distribution in (i) Longitudinal and (ii) Transverse directions.

Table 6.9 gives the comparison of forces and deformations between NDA and NSA in the transverse direction for 0.36g PGA. In transverse direction, Modal distribution overestimated the displacements because the stiffness of foundation in transfer direction is contributed by higher modes which is neglected in fundamental transverse mode. Uniform distribution underestimates the displacement because the soil stiffness throughout the pile depth and abutment height contributes uniformly which restricts the superstructure displacement at the top. Spectral distributions accounts for more than 90% mass contribution and also it accounts for the foundation stiffness accounting from pile and abutment which is proportional to modal shapes, hence the displacements obtained by spectral distributions are close to NDA values. The base shears obtained by spectral and uniform distributions are comparable with the NDA values. However, the base shears obtained by modal distributions is underestimated.

6.5.2 Model-2: Dense Sand Backfill –Stiff Clay Surrounding Pile (DSB-STC)

Figures 6.14 and 6.15 show the base shear timehistory and displacement time history at the control node for the five ground motions in both longitudinal and transverse directions. The average of forces and deformations obtained for five time histories by NDA is compared with the results obtained by NSA. Tables 6.10-6.11 summarize the maximum force and deformation obtained by NDA in longitudinal and transverse direction respectively for 0.36g PGA. Acceleration Displacement Response Spectra (ADRS) for Modal distribution in longitudinal and transverse directions is shown in Fig. 6.16. Figures 6.17 and 6.18 show the relationship between the base shear and the displacement at the control node in longitudinal and transverse directions for Modal, Uniform and Spectral distribution respectively. The load distribution plays an important role in pushover analysis since the modal mass contribution in the fundamental mode is nearly 44% and 23% in longitudinal and transverse directions respectively. Pushover curve in longitudinal

direction shown in Fig 6.17, the initial slope of Spectral distribution nearly follows the average of Modal and Uniform distributions. The Spectral distribution considers the mass contribution of the foundation which is not reflected in the fundamental mode. In transverse direction, pushover curve as shown in Fig 6.18, Spectral distribution seems to be an average of Modal and Uniform distributions.

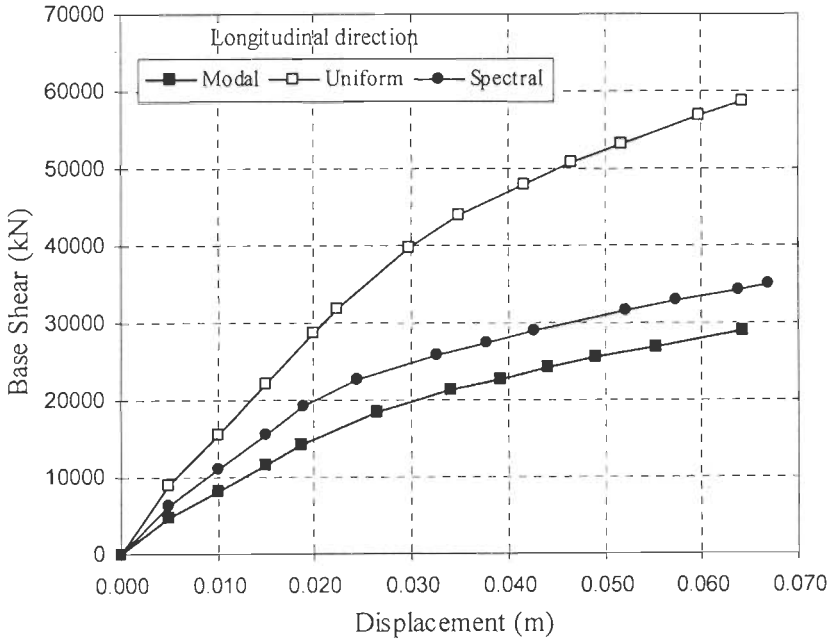

Fig 6.17: Capacity curves for longitudinal static pushover

Table 6.12 gives the comparison of forces and deformations between NDA and NSA in the longitudinal direction for 0.36g PGA. In longitudinal direction, the displacements obtained by spectral and uniform distributions are nearly same and slightly more than NDA values. The displacement obtained by modal distribution is overestimated as the resistance offered by the soil-pile interaction is very low because clay looses its strength after yielding. The base shears obtained by modal, spectral and uniform distributions are comparable with the NDA values and the variation is within 12%.

Table 6.13 gives the comparison of forces and deformations between NDA and NSA in the transverse direction for 0.36g PGA. In transverse direction, Modal distribution overestimated the displacements because the stiffness of foundation in transfer direction is

contributed by higher modes which is neglected in fundamental transverse mode. Uniform distribution underestimates the displacement because the soil stiffness throughout the pile depth and abutment height contributes uniformly which restricts the superstructure displacement at the top. Spectral distributions accounts for more than 90% mass contribution and also it accounts for the foundation stiffness accounting from pile and abutment which is proportional to modal shapes, hence the displacements obtained by spectral distributions are close to NDA values. The base shears obtained by spectral and uniform distributions are comparable with the NDA values. However, the base shears obtained by modal distributions is underestimated.

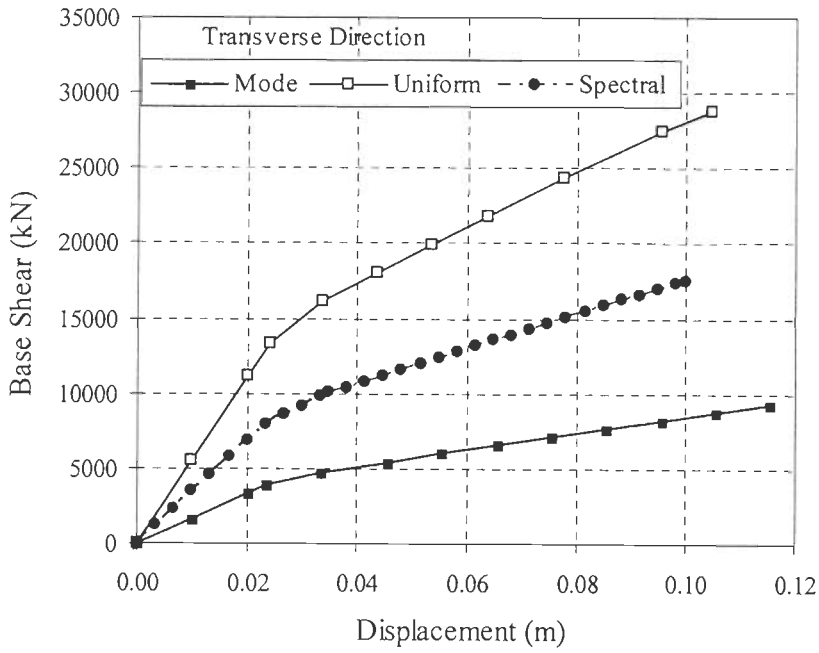

Fig 6.18: Capacity curves for transverse static pushover

Table 6.12: Comparison of results of NSA with NDA in the longitudinal direction

Analysis Methods	Distribution	Structure Behavior	Disp	Base Shear	Rotation (rad)				
					Piers				End Pile
					Pier 1	Pier 2	Pier 3	Pier 4	
			Mm	kN					
NDA			17.00	19033	0.0012	0.0014	0.0014	0.0012	0.0020
CSM	Modal	A	58.82	-1.30	52.83	25.35	21.13	63.25	60.00
		B	70.59	1.98	60.65	37.32	34.51	71.93	85.00
SM		A	52.94	-2.64	52.83	25.35	21.13	63.25	60.00
		B	64.71	0.43	58.04	35.92	33.10	68.46	72.50
DCM			52.94	-2.64	52.83	25.35	21.13	63.25	60.00
CSM	Uniform	A	-23.53	0.88	-12.30	-23.94	-28.87	-2.74	-5.50
		B	-23.53	0.88	-12.30	-23.94	-28.87	-2.74	-5.50
SM		A	-23.53	0.88	-12.30	-23.94	-28.87	-2.74	-5.50
		B	-17.65	11.10	-10.04	0.00	-4.23	-9.00	-5.00
DCM			-17.65	11.10	-10.04	0.00	-4.23	-9.00	-5.00
CSM	Spectral	A	17.65	2.82	-2.74	-7.75	-10.56	7.68	-2.00
		B	23.53	6.79	9.41	-16.90	-10.56	11.15	11.50
SM		A	23.53	6.79	9.41	-16.90	-10.56	11.15	11.50
		B	35.29	12.79	13.75	-13.38	-2.11	18.96	19.00
DCM			29.41	8.86	12.02	-14.79	-7.75	14.62	15.50

Table 6.13: Comparison of Results of NSA with NDA in the transverse direction

Analysis Methods	Distribution	Structure Behavior	Disp	Base Shear	Rotation (rad)				
					Piers				End Pile
					Pier 1	Pier 2	Pier 3	Pier 4	
			mm	kN					
NDA			50.09	15830	0.0020	0.0024	0.0024	0.0020	0.0021
CSM	Modal	A	57.72	-53.57	12.56	36.78	36.78	12.00	16.67
		B	75.68	-50.40	45.73	81.82	81.82	45.00	31.43
SM		A	65.70	-51.99	8.04	32.64	32.64	7.50	33.33
		B	81.67	-49.38	55.78	65.29	92.15	55.00	52.38
DCM			59.71	-53.25	13.57	38.43	38.43	13.00	19.05
CSM	Uniform	A	-34.12	1.33	-46.23	-40.91	-40.91	-46.50	-52.38
		B	-30.13	3.92	-39.20	-47.11	-47.11	-40.00	-50.00
SM		A	-34.12	3.61	-46.23	-40.91	-40.91	-46.50	-50.48
		B	-28.13	13.58	-32.66	-26.03	-26.03	-33.00	-47.62
DCM			-28.13	13.58	-32.66	-26.03	-26.03	-33.00	-47.62
CSM	Spectral	A	5.81	-23.30	-10.55	9.50	9.50	-11.00	-3.81
		B	19.78	-17.78	-6.53	28.10	28.10	-7.00	16.67
SM		A	-0.18	-25.14	-15.58	7.44	7.44	-16.00	-4.76
		B	5.81	-23.30	-10.55	9.50	9.50	-11.00	-3.81
DCM			1.82	-24.33	-23.62	-6.20	-6.20	-24.00	-9.52

Following observations are made by comparing the results obtained from NSA with NDA,

i) In the longitudinal direction, the base shear obtained by NSA using three load distributions such as Modal, Uniform and Spectral are comparable with NDA values for both DSB_DS and DSB-STC soil models. The target displacement estimated by NSA using Spectral are slightly overestimated than NDA values for both DSB-DS and DSB-STC soil condition, but displacement estimated by Uniform distribution are underestimated when compared to NDA values for both DSB-DS and DSB-STC soil conditions. Modal distribution overestimates the target displacement in both DSB-DS and DSB-STC soil conditions. The comparison of results shows that all the three methods used by NSA to get displacements are not close to NDA values but the values of Spectral distribution are close to NDA values among the three distributions and since the displacement values are under conservative side, it can be used to estimate the target displacement.

ii) In transverse direction, for both DSB_DS and DSB-STC soil models the base shear by modal distribution are underestimated when compared to NDA values because the mass participation ratio in Modal is lesser and it does not consider the foundation and abutment mass and stiffness participation for base shear calculation. In both Uniform and Spectral distribution the more than 90% of mass participation and the stiffness of soil-pile and abutment-backfill are considered and hence the base shear obtained by Uniform and Spectral distribution is comparable with NDA values. The target displacement estimated by NSA using Spectral and Uniform distributions are comparable with NDA values for both DSB-DS and DSB-STC soil condition, but Modal distribution underestimates the target displacement in both DSB-DS and DSB-STC soil conditions because of lesser mass participation factor.

iii) In both longitudinal and transverse directions, the rotational values obtained by spectral distributions are compatible with NDA values. Whereas the rotational values

obtained by modal distributions are overestimated and the values obtained by Uniform distributions are underestimated compared to NDA values.

In integral bridges, Spectral distribution gives more accurate results compared to Modal and Uniform distribution. The base shear and displacement obtained by NSA can give the results close to NDA values but it needs complex model analysis and good understanding of soil-pile and abutment-backfill behavior. It is always better to use minimum of two different load distributions to obtain conservative structural response in case of integral bridges.

6.6 INTEGRAL ABUTMENT BRIDGE LENGTH IN SEISMIC REGIONS

Figures 6.19 and 6.20 show the comparison of the lateral deflection of the abutment wall in compression and connecting concrete pile for Temperature, Modal and Spectral distributions for DSB-DS and DSB-STC soil conditions respectively. It is observed that the Modal and Temperature distributions follow the same trend of deflection in both DSB-DS and DSB-STC soil conditions. It can be seen from Figs. 6.19 (i) and 6.19(ii), by increasing the displacement limit of the bridge, the difference between Modal and Temperature distributions reduce. In DSB-DS soil condition the deflection trend obtained by Spectral distribution, shown in Fig. 6.19 is quite similar to the temperature and modal distribution but it differs in DSB-STC soil conditions, shown in Fig 6.20.

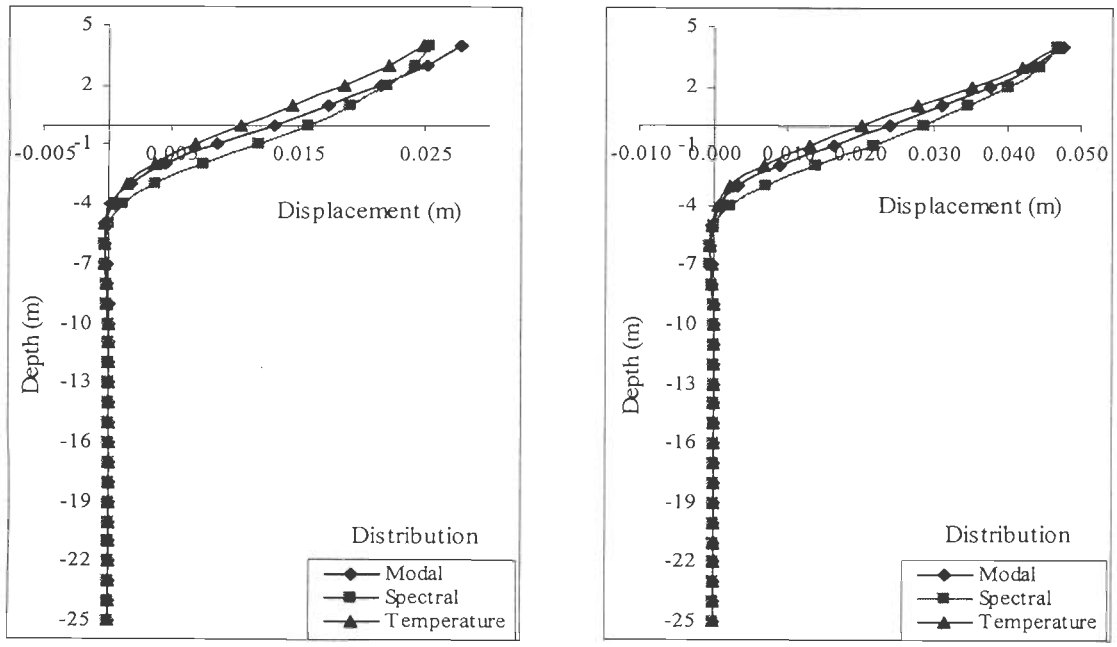

Fig. 6.19: Variation of displacement pattern along the abutment and pile height for temperature and seismic load distribution in DSB-DS soil condition

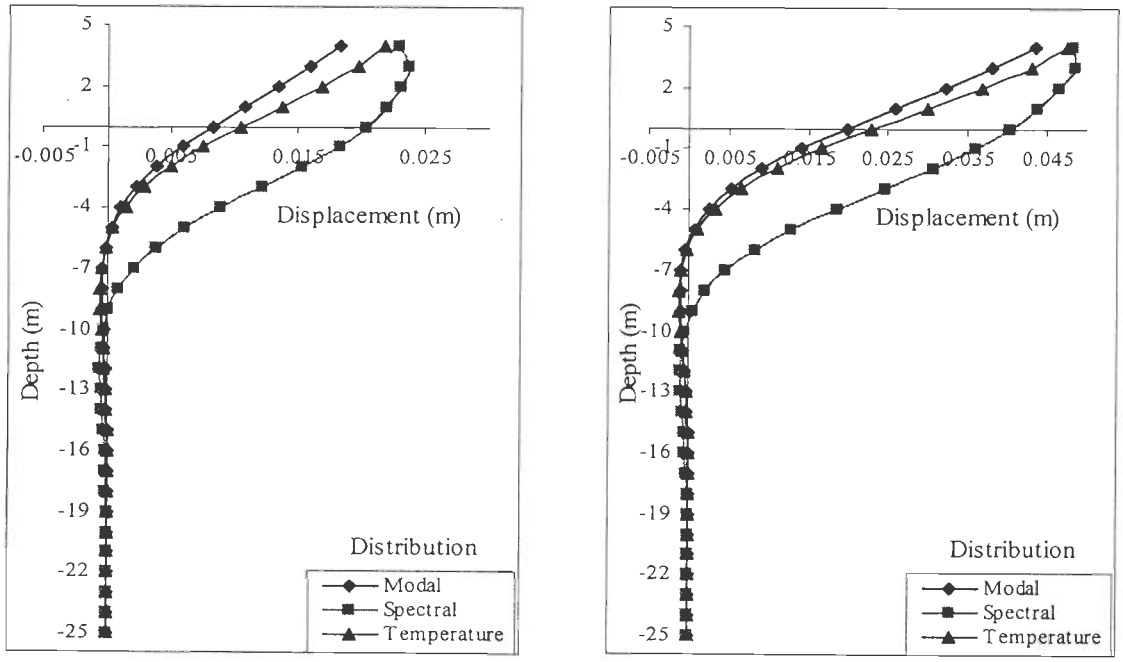

Fig. 6.20: Variation of displacement pattern along the abutment and pile height for temperature and seismic load distributions in DSS-STC soil condition

The comparison of results between the NDA and NSA has shown that Modal distribution slightly overestimate the target displacement when compared to Spectral distribution but it can be considered to find the target displacement, since it is on conservative side. Considering the structure to behave elastically during the design basis earthquake,

longitudinal seismic displacement at the control node or at top of the abutment (Δ_{LS}) using modal distribution can be calculated by

$$\Delta_{LS} = \frac{T_i^2 S_a}{4\pi^2} \quad \ldots (6.17)$$

The total maximum longitudinal deck displacement of integral abutment bridge subjected to temperature and seismic can be represented as

$$\Delta_{max} = \Delta_{LS} + \Delta_t \quad \ldots (6.18)$$

$$\Delta_t = \frac{K_1 K_2 K_3 L \alpha T_{ave}}{2} \quad \text{(Eqn. 5.10)} \quad \ldots (6.19)$$

The maximum total displacement can be represented in terms of temperature as

$$\Delta T_{max} = \frac{\Delta_{max}}{\alpha L} \quad \ldots (6.20)$$

$$\Delta_{LS} = \Delta_{max} - \Delta_t$$

$$\Delta_{max} = \frac{K_1 K_2 K_3 L \alpha T_{max}}{2} \quad \ldots (6.21)$$

where, Δ_t is total longitudinal displacement due to temperature; ΔT_{ave} is the average bridge temperature (^{0}C); α is the coefficient of thermal expansion (mm/mm/^{0}C); $K_1, K_2 \& K_3$ are the coefficients depending upon soil surrounding pile and abutment height, predrilled hole filled with loose soil and backfill soil as defined in Chapter-5; T_i is the elastic fundamental period of the bridge for Modal distribution in the longitudinal direction and S_a is the spectral acceleration for design basis earthquake at T_i.

Δ_{max} is limited to the yield displacement capacity of cast-in-situ piles obtained from nonlinear static analysis for temperature loading. Assuming the response reduction factor of 2.5 for the integral abutment bridges and taking IS response spectrum with spectral acceleration for design basis earthquake as 50% of 0.24g and 0.36g PGA, which

corresponds to Zone IV and Zone V of seismic zoning map of India and taking average bridge temperature 35 degree, the length of the integral abutment bridge in different soils can be worked out by trial and error method using the curves shown if Figs. 6.21 to 6.24.

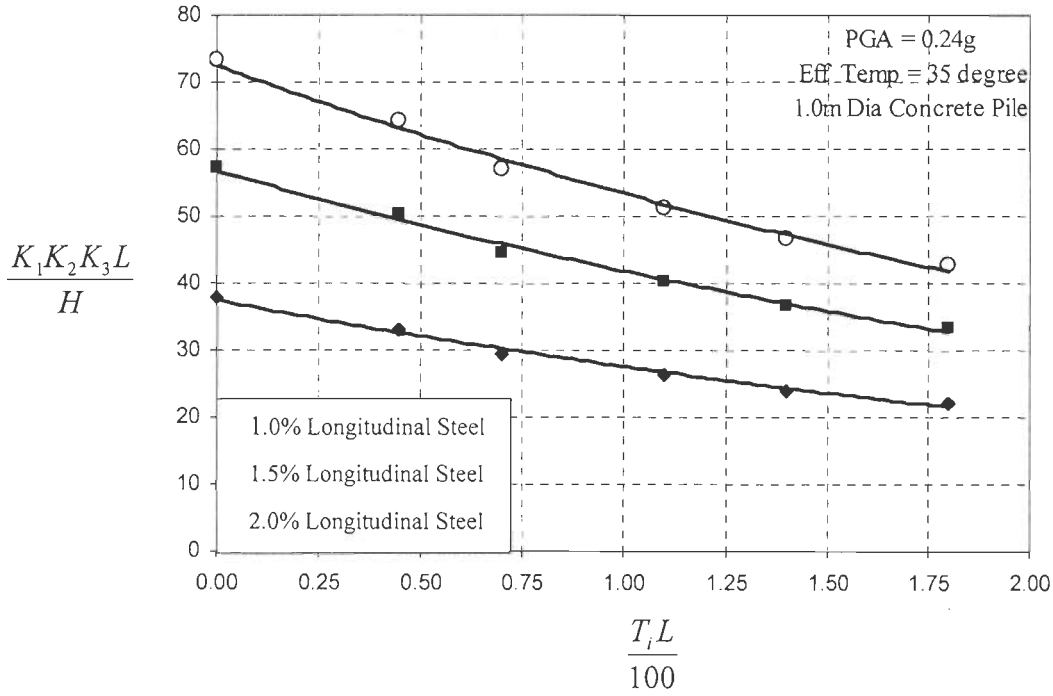

Fig. 6.21: Maximum length of integral abutment bridge on 1.0 dia cast-in-situ concrete piles in sand (M35 Concrete) subjected to 0.24g PGA

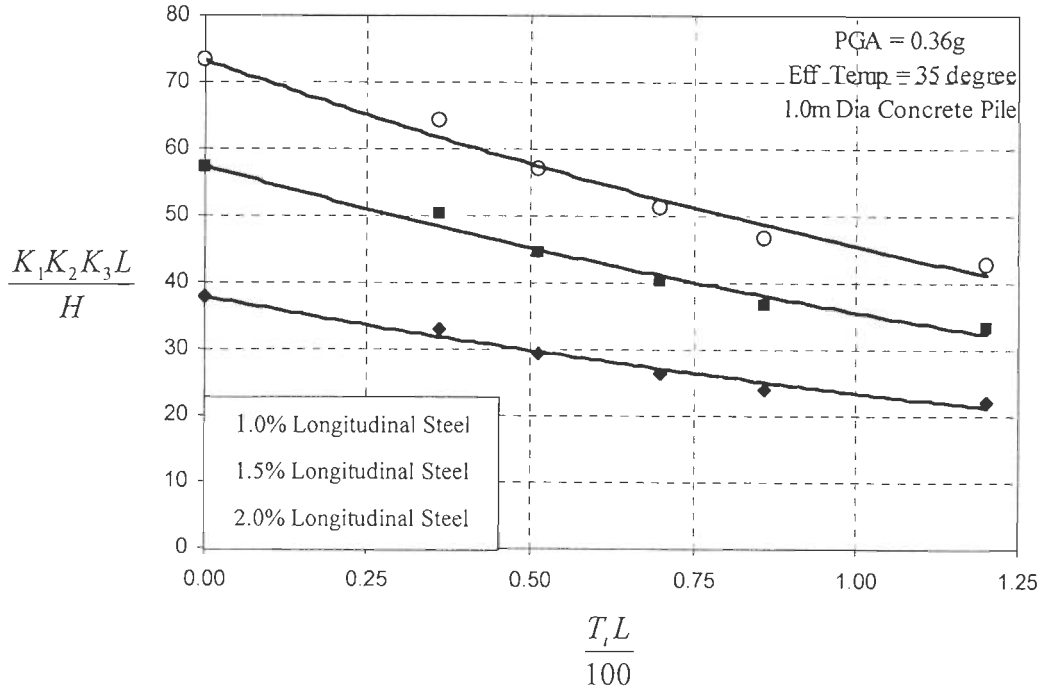

Fig. 6.22: Maximum length of integral abutment bridge on 1.0 m dia cast-in-situ concrete piles in sand (M35 Concrete) subjected to 0.36g PGA

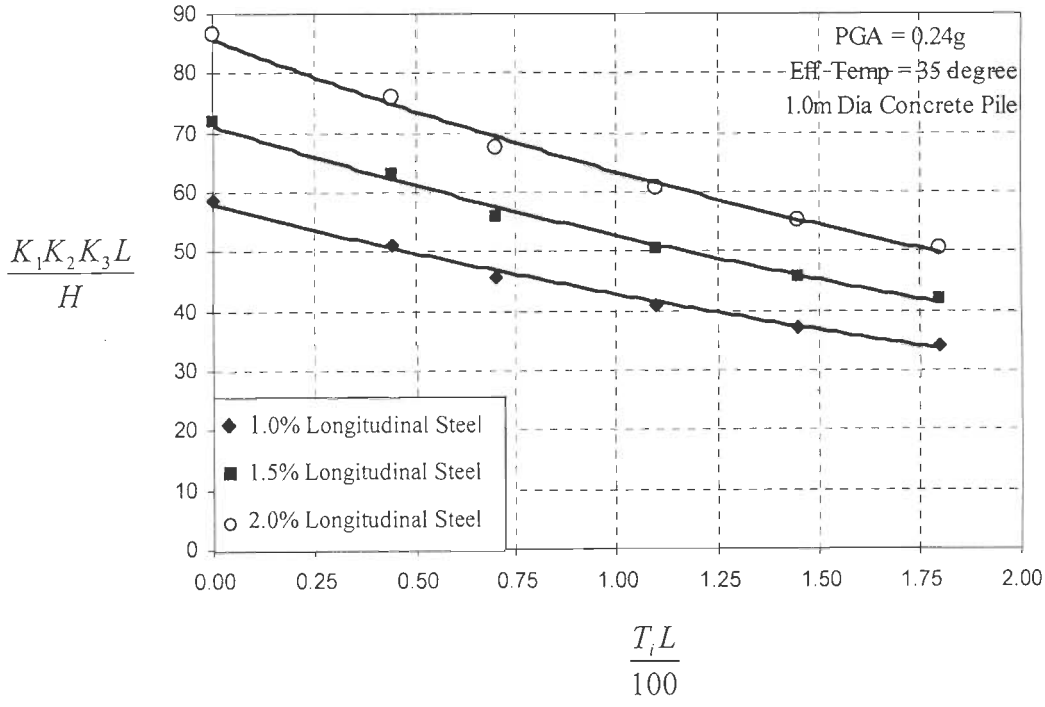

Fig. 6.23: Maximum length of integral abutment bridge on 1.0 m dia cast-in-situ concrete piles in clay (M35 Concrete) subjected to 0.24g PGA

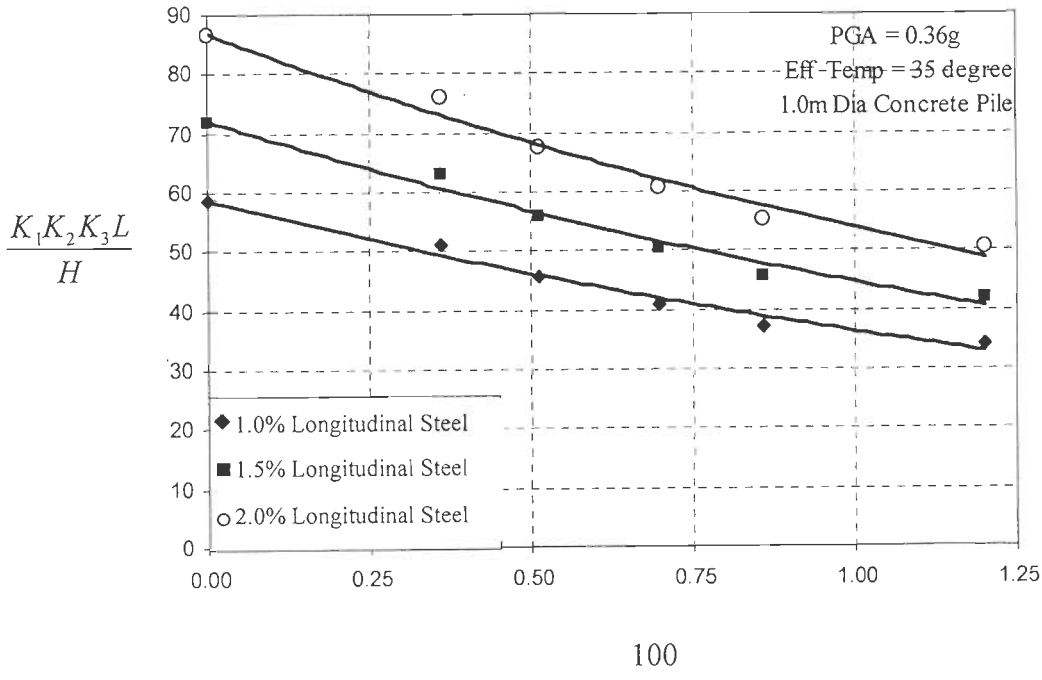

Fig. 6.24: Maximum length of integral abutment bridge on 1.0 m dia cast-in-situ concrete piles in clay (M35 Concrete) subjected to 0.36g PGA

Numerical Example:

Consider the bridge site having a peak ground acceleration of 0.24g, bridge temperature difference = 35 degree and the soil subgrade k = 30000kN/m^3. The integral bridge length required is 100m with abutment height 4.0m.

Assuming, the natural time period of the bridge in the longitudinal direction $\approx$0.6 sec, using Fig 6.21, considering 1.0m dia pile with 1.0% longitudinal reinforcement in pile

Trial: 1

$$\frac{K_1 K_2 K_3 L}{H} = 31 \text{ for} \frac{T_i L}{100} = \frac{0.6*100}{100} = 0.6,$$

From Fig 5.20; for k = 30000 kN/m^3 and abutment height =4m, K_1 = 1.30

(For both temperature rise and temperature fall – the least of temperature rise or fall value of K_1 has to be considered)

From Fig 5.21; K_2 = 1.0 (Without predrilled)

From Fig 5.22; K_3 = 1.0 (Dense Sand backfill)

$$\frac{K_1 K_2 K_3 L}{H} = \frac{1.30*1.0*1.0*L}{4} = 31$$

L = 95.3 m,

The maximum length of the integral bridge which can be achieved using 1.0 m dia pile with 1.0% longitudinal reinforcement is 95.3 m with abutment height 4.0m, it is less than the required length (100m). To achieve the required length, it is necessary to reconsider the pile either with higher diameter or with higher reinforcement. Consider 1.5 % longitudinal reinforcement in pile

Trial: 2

$$\frac{K_1 K_2 K_3 L}{H} = 44 \quad \text{(Fig 6.21)}$$

$$\frac{K_1 K_2 K_3 L}{H} = \frac{1.30*1.0*1.0*L}{4} = 44$$

L = 135.0 m,

This preliminary calculations shows that the integral bridge of length 135m with abutment height 4.0m can be constructed at the site to withstand 0.24g and 35° effective bridge temperature in dense soil (30000kN/m^3) using 1.0m dia cast-in-situ pile with 1.5% longitudinal reinforcement.

6.7 DECK-EXTENSION AND SEMI- INTEGRAL ABUTMENT BRIDGES

Deck-extension integral bridge and semi- integral abutment bridge are adopted by most designers to avoid the complex soil-structure interaction mechanism in abutment backfill analysis. The main advantages in these bridges are the number of bearings and movable deck joints in a structure can be minimized. The movable expansion deck joints in these bridges should be able to accommodate the movement of bicycles, motorcycles and pedestrians without much impair in the riding characteristics. The maximum allowable joints spacing restricts the length of deck-extension integral bridge and semi- integral abutment bridge. AASHTO restricts the maximum joint width due to secondary effects to 25mm in ordinary conditions without appropriate criteria. By adopting the proper modular bridge joint system between the two deck extension integral bridges, joint width can be increased. In this case the length of these integral bridges can be worked out in the similar manner as worked out in this thesis for integral abutment bridges depending upon the yield displacement capacity of end piles. The length should be restricted depending upon either yield displacement capacity of the end piles or maximum allowable joint spacing which ever is minimum.

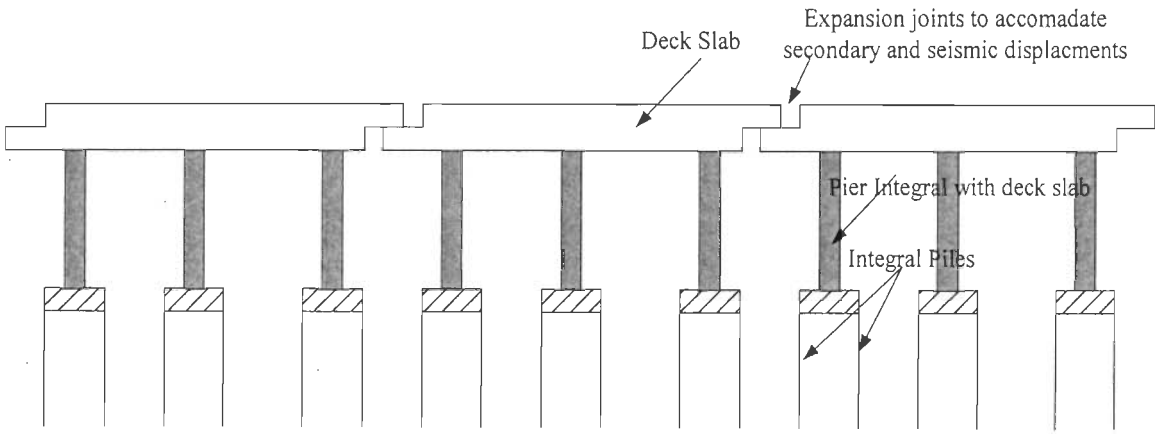

Fig: Deck extension integral bridges adopted in most urban cities

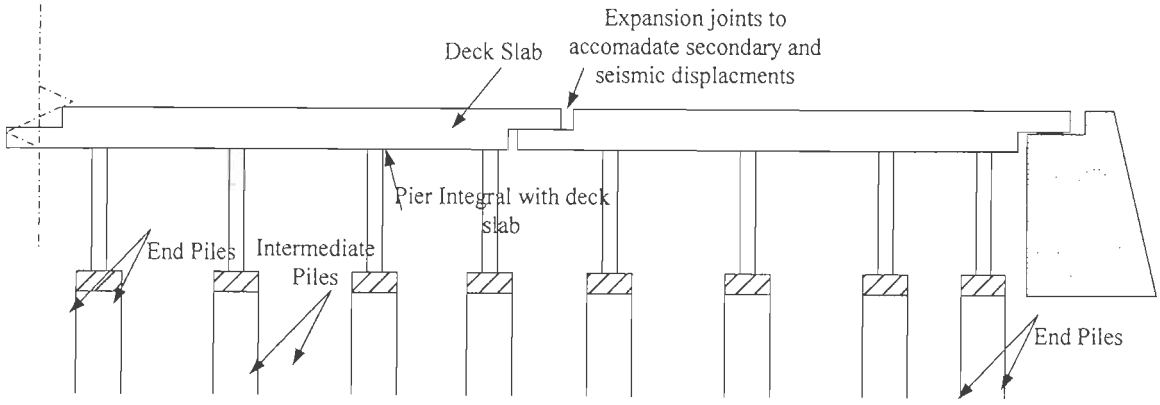

Fig 6.25 : Deck extension integral bridges adopted in urban cities

6.8 CONCLUDING REMARKS

Seismic behavior of integral abutment bridges is studied by nonlinear time history analysis taking the material nonlinearity of soil and structure. Applicability of pushover analysis on integral abutment bridges is investigated using three distributions such as Modal, Uniform and Spectral. Capacity Spectrum method and Displacement Coefficient method are used to find target displacement and base shear. A simplified method is proposed to find out target displacement by retaining the capacity curve and design demand curve without converting them into spectral ordinates. This proposed simplified method is based on the concept of Capacity Spectrum method with some assumptions. Bridge with two different soil conditions such as DSB-DS and DSB-STC are presented as case studies. The results

obtained from nonlinear time history analysis are compared with the results of pushover analysis to validate the results and to use suitable pushover analysis to estimate maximum bridge length. The following observations are made from the analysis,

i. In integral abutment bridges, the maximum mass contribution is distributed in higher modes in both longitudinal and transverse direction.

ii. The Proposed Simplified Method gives target displacement close to the values of CSM and DCM. The target displacement estimated by three different methods such as CSM, DCM and SM for all the load distributions are within the 10% variation. Hence the proposed Simplified Method can be used for approximate estimation of target displacement with suitable damping factor for bridges. The Simplified Method is applicable for both longer and shorter time period structures and it can be applicable even for buildings with different structural types.

iii. In the longitudinal direction, the base shear obtained by NSA using three load distributions such as Modal, Uniform and Spectral are comparable with NDA values for both DSB_DS and DSB-STC soil models. The target displacement estimated by NSA using Spectral distribution are comparable with NDA values for both DSB-DS and DSB-STC soil condition, Modal distribution overestimates the target displacement in both DSB-DS and DSB-STC soil conditions. But displacement estimated by Uniform distribution is underestimated when compared to NDA values for both DSB-DS and DSB-STC soil conditions. Though modal distribution overestimates the displacement it is on conservative side and hence Spectral and Modal distribution can be used to study longitudinal response of integral bridges.

iv. In transverse direction, for both DSB_DS and DSB-STC soil models the base shear and the displacement obtained by modal distribution are underestimated when

compared to NDA values because the mass participation ratio in Modal is lesser and it does not consider the foundation and abutment mass and stiffness participation for base shear calculation. In both Uniform and Spectral distribution the more than 90% of mass participation and the stiffness of soil-pile and abutment-backfill are considered and hence the base shear and displacement obtained by Uniform and Spectral distribution are comparable with NDA values. In transverse direction, both Spectral and Uniform distribution can be used to study response of integral bridges.

v. The comparison of the lateral deflection of the abutment wall in compression and connecting concrete pile for Temperature, Modal and Spectral distribution revealed that the displacement pattern of Modal distribution follows the displacement pattern of Temperature distribution.

vi. Modal distribution which has been proved to give conservative value of longitudinal seismic displacement of integral bridge is used to limit the length of integral bridge.

vii. The relationship between the time period of the bridge, temperature difference and length of integral abutment bridges are presented in the form of curves, which helps to estimate the length of integral abutment bridges by few trials, for the preliminary studies in high temperature variation and high seismic zones.

CHAPTER-7

CONCLUSIONS

Integral bridges have shown lot more promise over conventional bridges with bearings. These bridges are safe, aesthetically pleasing, cheaper, faster in construction, requires less maintenance and show better seismic performance. A comprehensive literature review has been undertaken to study its behavior. The behavior of integral abutment bridges is studied by taking the material nonlinearity of soil and structure subjected to temperature and seismic loadings. Based on the basis of maximum yield capacity of the piles the possible maximum length of the integral abutment bridge is fixed. Parametric study is conducted by using nonlinear static analysis for both temperature rise and fall conditions. Sensitive nonlinear time history and pushover analyses on integral abutment bridges are investigated to provide analysis guidelines to restrict its length. Simplified Method of CSM is proposed to find the target displacement by retaining the capacity curve and design curve without converting them into spectral ordinates. This Simplified Method is based on the conceptual basis of capacity spectrum method with few assumptions. The target displacement obtained by pushover analysis or seismic load is combined with temperature displacement to find the maximum length of integral abutment bridges built on cast-in-situ concrete piles in high temperature variation and high seismic zones. Some of the important conclusions that are drawn from the present study are as follows,

i. Predrilled hole filled with soft soil is having a great effect on yield capacity of the pile and abutment displacement. Results show that, predrilled hole filled with loose sand allows the pile to be more flexible and results in the increase of overall bridge length.

ii. Formation of plastic hinges in the integral abutment piles is observed at a depth of 2D from the ground surface for piles placed in dense sand and at a depth of 4D from the ground surface for piles placed in loose sand. These results are comparable with the experimental results on full scale model, in which the plastic hinge in the pile was formed at the top 2D depth from ground level for fixed head piles subjected to monotonic loading condition and at 4D depth from ground level with decrease in soil stiffness.

iii. Integral abutments with higher heights are subjected to larger bending moments due to the higher passive pressure developed along the height of the abutment. Bending moments in the abutments are considerably less for temperature fall as compared to temperature rise case. Temperature rise loading condition is critical for determining the yield displacement capacity of integral abutment bridges with greater abutment heights. Increase in the height of integral abutment resulted in shifting of plastic hinge from a depth of 3D to the ground surface.

iv. The variation in the intermediate pier flexibility has a negligible effect on the yield displacement capacity of the abutment pile.

v. A relationship is derived with respect to average seasonal temperature variations for identifying the approximate maximum length of integral abutment bridges built on cast-in-situ concrete piles for diameter 1.0m and 1.2m in different soil conditions.

vi. From the free vibration analysis, it is found that maximum mass contribution in integral abutment bridges is also from higher modes in both longitudinal and transverse directions.

vii. The proposed Simplified Method of CSM gives the target displacement close to the values of Capacity Spectrum Method and Displacement Coefficient Method.

viii. In pushover analysis, the lateral loads applied based on spectral distribution alone is sufficient to obtain the dynamic response of integral abutment bridges in longitudinal direction. Modal distribution slightly overestimates the target displacement as compared to Spectral distribution.

ix. For the pushover analysis in transverse direction, minimum two lateral load distribution such as Spectral and Uniform distributions are needed to obtain conservative structural response of integral abutment bridges. Spectral distribution gives a conservative estimation of displacement and rotations but underestimates the base shear, while Uniform distribution underestimates the displacement but gives good estimation of base shear and bending moments.

x. A relationship between the time period of the bridge, seasonal temperature difference, height of abutment and length of bridge in different soil conditions is proposed for the initial estimation of maximum length of integral abutment bridge in a specified high temperature and high seismic regions. From the proposed relationship, the maximum length of integral abutment bridge can be worked out by using few trials. This approach to handle both temperature and seismic loadings together may open up new research ground in bridge engineering.

xi. Integral bridges with lower abutment heights built on the concrete piles located in predrilled hole filled with loose sand are recommended to achieve the maximum length without attracting high forces on abutments.

7.1 SCOPE FOR FUTURE RESEARCH

i. Instrumentation of existing bridges will be helpful to validate the curves proposed to find maximum length of integral bridges which are based on the yield capacity of cast-in-situ piles.

ii. Behavior of integral bridges for temperature and seismic loadings under the friction piles or the combination of friction and end bearing piles is needed to be studied. Also study on curved and skewed integral abutment bridges with different configuration are needed to be studied.

iii. Study on the behavior of integral abutment bridges for seismic loading along with liquefaction of soil is needed to be concentrated.

REFERENCES

1. AASHTO LRFD (2004). "*Standard specifications for highway bridges*", American Association of State Highway and Transportation Officials Inc., Washington, DC.

2. AlAyed, H., (2002). "Seismic analysis of bridges using displacement – based approach", *Net Document,* Dept. of Civil and Environmental Engineering, University of Maryland.

3. American Petroleum Institute (API RP 2A-WSD: 1993). "*Recommended practice for planning, designing and constructing fixed offshore platforms-working stress design*", 1993, Washington, 20th ED., D. C.

4. American Petroleum Institute (API RP2A-WSD: 2000). "*Recommended practice for planning, designing and construction fixed offshore platforms-working stress design*", 2000, Washington, D. C.

5. Applied Technology Council (ATC-32:1996). "*Improved seismic design criteria for California bridges." ATC-32,* Redwood City, CA, 1996.

6. Applied Technology Council (ATC-40: 1996). "*Seismic evaluation and retrofit of concrete buildings." ATC-40,* Volumes 1 and 2, Redwood City, CA, 1996.

7. Applied Technology Council (FEMA-440: 2005) "I*mprovement of nonlinear static seismic analysis procedures*", FEMA-440, ATC, California, USA

8. Arockiasamy, M., Narongrit Butrieng, and Sivakumar, M., (2004). "State-of-the-art of integral abutment bridges: design and practice." *J. of Bridge Engg., ASCE,* Vol. 9, No. 5, September 1, 2004.

9. Arsoy, S., Duncan, J. M., and Barker, R. M. (2002). "Lateral load behavior of piles supporting integral bridges", Transportation Research Record 1808, TRB, National Research Council, Washington, D.C., 162-167.

10. Arsoy, S., (2000). "Experimental and analytical investigations of piles and abutment of integral bridges." *PhD Thesis*, Virginia Polytechnic Institute and State University, Blacksburg, Virginia.

11. Arsoy, S., Richard M. B., and Duncan, J. M., (1999). "The behavior of integral abutment bridges." *Appendix A, Final Report submitted to VTRC,* University of Virginia.

12. Bekir S., and Chung C. Fu., (1999). "Use of integral piers to enhance aesthetic appeal of grade separation structures." *Net document,* University of Maryland, Maryland

13. Bhowmick, A., (2005). "Design and detailing of integral bridges: suggested guidelines", *Indian Concrete Journal*, Vol. 79, September 2005, India.

14. Bonczar, C., Brena, S., Civijan, S., DeJong, J., and Crovo, D., (2005). "Integral abutment pile behavior and design – field data and fem studies." FHWA Conference on *IAJB-2005*, Baltimore, Maryland, 2005.

15. Boominathan, A., and Ayothiraman, R., (2005). "Dynamic behaviour of laterally loaded model piles in clay," *Geotechnical Engineering J.,* Vol. 158, GE4, pp. 207 – 215.

16. Boominathan, A., Elango, J., and Ayothiraman, R., (2001). "Lateral dynamic testing of full scale single piles," Proceedings of the Eighth East Asia-pacific Conference on Structural Engineering & Construction, EASEC-8, Singapore, Paper No: 1526.

17. Broms, B. B., (1964). " Lateral resistance of piles in cohesionless soils" *Soil Mechanics and Foundation Division proceedings of American Society of Civil Engineering journal*, May 1964

18. Brown, D. A., Reese, L. C., and O'Neill, M.W., (1985). "Cyclic lateral loading of a large scale pile group." J. of Geotechnical Engg., Vol. 113, No. 11, PP. 1326-1343, November.

19. BS 5400, (1990). "Steel, concrete and composite bridges." Part IV Code of practice for design of concrete bridges, *British Standard Institution.*

20. Burke. M.P (1994). "Semi-integral bridges: A concept whose time has come." *Continuous and Integral Bridges*, Edited by B.P Pritchard, London.

21. Caltrans (2004). Seismic design criteria, Version 1.3., *California Department of Transportation*, Sacramento , California

22. Canadian Foundation Engineering Manual (CFM 1992). Canadian Geotechnical Society, 3rd Ed., Toronto, Canada.

23. Chakrabarti (1993), Final Report, "Integral Bridges", by Edmund Hambly Ltd., Consulting Engineers London.

24. Chen, Ma-Chi., and Penzien, J., (1975). "Analytical investigations of seismic response of short, single or multiple–span highway bridges," *EERC 75-4, Earthquake Engineering Research Centre,* University of California, Berkely.

25. Chopra, A.K., and Goel, R.K., (2001)"A modal pushover analysis procedure to estimate seismic demands for buildings: theory and preliminary evaluation". Tech. Rep. 2001/3, Pacific Earthquake Engineering Research Centre, University of California, Berkeley, CA.

26. Clough, G.W., and Duncan, J.M., (1991). "Earth Pressure and Retaining Structures", Blackie Academic and Professional, Glasgow.

27. COM624P, "*Laterally Loaded Pile Analysis Program for the Microcomputer,*" Version 2.0, Manual.

28. Computers and Structures Inc. SAP 2000: *Three Dimensional Static and Dynamic Finite Element Analysis and Design of Structures.* Computers and Structures Inc.: Berkeley, CA, 1999.

29. Darley, P., and Alderman, G.H., (1995). "Measurements of thermal cyclic movements on two portal frame bridges on the M1," Transportation Research Laboratory Report 165, Transport Research Laboratory, England.

30. Dehne Youssef., and Sophia Hassiotis (2000). "Seismic analysis of integral abutment bridge", Final Report, Scotch Road I-95 Project.

31. Design Manual (1971) – "Soil Mechanics, Foundations and Earth Structures," NAVFAC DM-7, Dept. of the Navy, Naval Facilities Engineering Command, Alexandria, V A.

32. Dehne and Hassiotis (2000). "Seismic Analysis of Integral Abutment Bridge", Final Report, Scotch Road I-95 Project.

33. Dicleli, M., (2000). "A rational design approach for prestressed-concrete-girder integral bridges." *Engineering Structures* 22 (2000) 230–245.

34. Dicleli, M., (2000). "Integral abutment-backfill behavior on sand soil-pushover analysis approach." *J. of Bridge Engg., ASCE*, Vol. 10, No. 3, May 2001.

35. Dicleli, M., (2000). "Simplified model for computer-aided analysis of Integral bridges." *J. of Bridge Engg., ASCE*, Vol. 5, No. 3, August 2000.

36. Dicleli, M., (2001)." Computer-aided limit states analysis of bridge abutments." *Electronic J. of Structural Engg., (2001)* 74.

37. Dicleli, M., and M. A. Suhail (2003). "Maximum length of integral bridges supported on steel H-piles driven in sand." *Engineering Structures* 25 (2003) 1491–1504

38. Dicleli, M., and M. A. Suhail (2004). "Estimation of length limits for integral bridges built on clay." *J. of Bridge Engg., ASCE*, Vol. 9, No. 6, November 1, 2004.

39. Dicleli, M., and M. A. Suhail (2004). "Performance of abutment–backfill system under thermal variations in integral bridges built on clay." *Engineering Structures* 26 (2004) 949–962.

40. Dutta, A., (1999). "On energy based seismic analysis and design of highway bridges." *PhD dissertation.* Dept. of Civil Struct. and Envir. Engg., State University of New York at Buffalo, Buffalo.

41. Dutta, A., and J.B. Mander (2001). "Energy based methodology for ductile design of concrete columns." *J of Structural Engg, ASCE,* Vol. 127, Dec 2001.

42. England, G.L., Tsang, N.C.M., and Bush, D.L., (2000) "Integral Bridges" Thomas Telford Publishing, London.

43. Eurocode 8 – Design provisions for Earthquake resistant of structures , European prestandards ENV 1998, European Committee for Standardization, Brussels.

44. Faraji, S., (1997). "Behavior of integral abutment bridges in Massachusetts." *Research Report*, Highway Dept., University of Massachusetts, Transportation Center.

45. Faraji, S., John, M.T., Daniel, S. C., and Helmut E., (2001). "Nonlinear analysis of integral bridges: Finite-element model." *J. of Geotechnical and Geoenvironmental Engg.*, Vol. 127, No. 5, May, 2001

46. Federal Highway Administration, January 1980, " Integral, No-Joint Structures and Required Provisions for movement", FHWA Technical Advisory T 5140.13

47. FEMA 273 (1997). NHERP *guidelines for the Seismic rehabilitation of buildings*, Building Seismic Safety Council, ASCE, FEMA 273.

48. FEMA 356 (2000). "P*re-standard and commentary for the seismic rehabilitation of buildings"*, ASCE, FEMA 356. Washington, DC, November 2000.

49. Fenves.G.L and M. Ellery, (1998). "Behavior and failure analysis of a multiple-frame highway bridge in the 1994 Northridge earthquake" Research Report, University of California, Berkley

50. Forsch, R. J., (2005). "The in-service behavior of integral abutment bridges: abutment-pile response." *2005 FHWA Conference*, Baltimore, Maryland, U.S.A.

51. Goel, R. K., and Chopra, A. K., (1997). "Evaluation of bridge abutment capacity and stiffness during earthquakes." *Earthquake Spectra*, 13(1), 1-21.

52. Goel, R.K., (1997). "Earthquake characteristics of bridges with integral abutments." *J. of Structural Engg.*, Vol. 123, No. 11, Nov 1997

53. Greimann, L.F., Adendroth, R.E., Johnson, D.E., and Ebner, P.B., (1987). "Pile design and tests for integral abutment bridges," Final Report, Iowa DOT Project HR-273, Highway Division, Department of Transportation, Ames, Iowa.

54. Greimann, L.F., **Y**ang, P.S., Edmunds, S.K., and Wolde-Tinase, A.M. (1984). "Design of piles for integral abutment bridges", Final Report, Iowa Department of Transportation, ISU-ERI-Ames 84228.

55. Girton, D.D, Hawkinson T. R and Greimann, L. F (1989). "Validation of design recommendations for integral abutment piles," Final Report, Project HR-292, Iowa Department of Transportation, Ames, Iowa.

56. Girton, D.D, Hawkinson T. R and Greimann, L. F (1991). "Validation of design recommendations for integral abutment piles," *J. of Structural Engineering, ASCE,* 117 (7), 2117-2134.

57. Hassiotis, S. and Roman, E. (2005). "A survey of current issues on the use of integral abutment bridges." Journal of Bridge Structures, Vol 1, No. 2, June 2005, pp81-101

58. Hussain, I., and Bagnariol, D., (2000). "Performance of integral abutment bridges." *Final Report*, Ministry of Transportation Ontario Report BO-99-04.

59. Hussain, I., and Bagnariol, D., (1996). "Integral Abutment Bridges", Report. SO-96-01, Structural Office, Ministry of Transportation of Ontario, Canada.

60. Hutchinson, T.C., Boulanger., R.W, Chai,Y.H and Idriss. I.M., (2002) "Inelastic seismic response of extended pile shaft supported bridge structures" Pacific Earthquake Engineering Center, College of Engineering, University of California, Berkley.

61. IRC 78-2000 "Standard Specifications and Code of Practice for Road Bridges Section VII – Foundations and Substructure (Second Revision)" *The Indian Roads Congress*, New Delhi.

62. IRC: 6 (2000). "Standard specifications and code of practice for road bridges - Section: II Loads and Stresses (Fourth Revision)" *The Indian Roads Congress*, New Delhi.

63. IS – 1893 (Part 1) (2002), Criteria for earthquake resistant design of structures – Part 1: General provision and buildings, Bureau of Indian Standards.

64. IS – 456 (2000), Plain and reinforced concrete – Code of Practice, Bureau of Indian Standards.

65. IS: 1893 (1984) "Indian Standard : Criteria for earthquake resistant design of structures", Bureau of Indian Standards, New Delhi

66. IS: 2911 (1979) "Code of Practice for Design and Construction of Pile Foundations", Bureau of Indian Standards, New Delhi.

67. Jayaraman, R., Merz, P. B., and Mc Lellan. (2001). "Integral bridge concept applied to rehabilitate an Existing bridge and construct a dual-use bridge." *Our world in concrete and structures*, Singapore.

68. Jeremic, B., Kunnath, S.K. and Xiong, F. (2004). Influence of Soil-Foundation-Structure Interaction on Seismic Response of the I-880 Viaduct." *Engineering Structures.* 26: 391-402.

69. Kamel, M.R., Benak, J.V., Tadros, M.K., and Jamshidi, M. (1996). "Prestressed Concrete Piles in Jointless Bridges," *PCI Journal,* 41(20), 56-67.

70. Kappos, A.J. and Petranis, C. (2001) "Reliability of pushover analysis - based methods for seismic assessment of R/C buildings", *Earthq. Resistant Engng Structures III*, WIT Press, 407-416.

71. Kappos, A.J., Paraskeva, T. S and Sextos A. G., (2005) "Modal Pushover Analysis As A Means For The Seismic Assessment Of Bridge Structures" Proceedings of the 4th European Workshop on the Seismic Behaviour of Irregular and Complex Structures 26-27 August, Thessaloniki, Greece.Kaynia A., and Kausel, E., (1991), "Dynamics of piles and pile groups in layered soil media," *J. of Soil Dynamic and Earthquake Engg.*, Vol. 10, No. 8, Nov. 1991, pp 386-401.

72. Koh, S. K., and Stephen, R. I., (1991). " Mean stress effects on low-cycle fatigue for high strength steel", *Fatigue Fracture Engineering Material Structures* 1991, Vol. 14, 413-28.

73. Kumar, P. T. V., & Paul, D.K., (2007). "Force-deformation behavior of isolation bearings.", *J. of Bridge Engg., ASCE,* July -07.

74. Kumar, P. T. V., Paul D.K., Kumar, R., & Agarwal, P., (2006). "Seismic Analysis of Integral Abutment Bridges.", paper published in 13th Symposium on Earthquake Engineering, held at Indian Institute of Technology, Roorkee, December 18-20, 2006

75. Kumar, P. T. V., Paul D.K., Kumar, R., & Agarwal, P., (2006). "Seismic Response of Integral Bridges." In the proceedings of International Conference in Earthquake Engineering on 25th Feb. 2006 held at SASTRA, Tamilnadu.

76. Kumar, A. (2004) "Software for Generation of Spectrum Compatible Time History" 13th World Conference on Earthquake Engineering; Vancouver, B.C., Canada ; August 1-6, 2004; Paper no. 2096

77. Kunin, J., and Alampalli, S., (1999). "Integral abutment bridges: current practice in the United States and Canada." *Special Report 132.*, New York State Department of Transportation, July 1999.

78. Kunin, J., and Alampalli, S., (2000). "Integral abutment bridges: current practice in United States and Canada", *J. of Performance of Constructed Facilities:* 104-111

79. Lawver, A., French, C., and Shield, C.K., (2000). "Field performance of an integral abutment bridge," Paper presented at the Transportation Research Board 79th Annual Meeting, Washington, D.C.

80. Mander, J. B., Panthaki, F. D., Kasalanati, A.,(1994). "Low-cycle fatigue behavior of reinforcing steel," *J. Material Civil Engineering ASCE* 1994.

81. Mander, J. B., Priestley, M.I.N and Park, R. (1988). "Theoretical stess-strain model for confined concrete". Journal of Structural Engineering, ASCE, 114(8) 1804-1826.

82. MATLAB "The Language of Technical Computing," Version 7.5 program.

83. Matlock, H., (1970). "Correlations for design of laterally loaded piles in soft clay." Proceedings of the II Annual Offshore Technology Conference, Houston, Texas, (OTC 1204): 577-594.

84. Matlock, H., Ingram, W. B., Kelley, A. E. and Bogard, D., (1980). "Field tests of lateral load behavior of pile groups in Soft clay." Proceedings of the XII Annual Offshore Technology Conference, Houston, Texas, (OTC 3871): 163-174.

85. McVay, M., Casper, R., and Shang, Te-I., (1995). "Lateral response of three-row groups in loose to dense sands at 3d and 5d spacing," *J. of Geotechnical Engg.*, ASCE, Vol. 121, No.5.

86. Milutinovic, Z., Zoravkovic, S., Petrovski, J. and Thakkar, S. K., (1982). "Dynamic analysis of bridge system with restricted movements at supports." *Seventh Symposium on Earthquake Engineering*, University of Roorkee, Nov. 10-12, 1, 299-302.

87. Mistry, V. C., (2005). "Integral abutment and jointless bridges", FHWA Conference on *IAJB-2005*, Baltimore, Maryland, 2005.

88. Mitoulis., S .A ., Tegos., I. A., and Sextos., A (2006) "An Alternative Proposal For A "Movable" Abutment For Integral Bridges" Paper Number: 1377, First European Conference on Earthquake Engineering and Seismology (a joint event of the 13th ECEE & 30th General Assembly of the ESC) Geneva, Switzerland, 3-8 September 2006.

89. Naeim, F., and James, M. K., (2003) " Design of Seismic Isolated Structures : from theory to practice" James M. New York : John Wiley, 2003

90. NCHRP (1991), "*Manuals for the Design of Bridge Foundations*," Cooperative Highway Reseach Program Report 343, Dec

91. O'Neill, M. W., (1983). "Group action in offshore piles." *Proceedings of the specialty conference on Geotechnical Engineering in Offshore Practice,* ASCE.

92. Oesterle,. R.G., and Volz, J. S., (2005), "Effective temperature and longitudinal movement in integral abutment bridges", FHWA Conference on *IAJB-2005*, Maryland.

93. Oesterle, R.G., Tabatabai, H., Lawson, T.J., Refai, T.M., Voltz, J.S., and Scanlon, A. (1999). "Jointless and integral abutment bridges" Draft Summary Report, Construction Technology Laboratories, Skokie, Illinois.

94. Pandey, A., and Tandon, M., (2005). "Integral flyovers in Delhi", *Indian Concrete Journal,* Vol. 79, September 2005, India.

95. Paraskeva, T. S., Kappos, A. J., and Sextos A.G., (2006). "Extension of modal pushover analysis to seismic assessment of bridges." *J. of Earthquake Engg. Struct. Dyn. 2006*; 35:1269-1293

96. Patty, J., Frieder, S., and Unag, C., (2001). Seismic response of integral bridge connections, Final Report SSRP– 2001, Department of Structural Engineering, University of California, San Diego.

97. Patty, J., Frieder, S., and Uang, C., (2002), "Seismic response of integral bridge connections", Final Report SSRP– 2001, Department of Structural Engineering, University of California, San Diego.

98. Perera, R., Carnicero, A., Alarcon, E., and Gomez, S., (2000). A fatigue damage model for seismic response of RC structures, *J of Computers and Structures* 2000; 78: pg 293-302.

99. PoLam, I., Kapuskar, M., and Chaudhuri, D., (1998), "Modelling of pile footings and drilled shafts for seismic design," *Tech. Report MCEER-98-0018, Dec. 21.*

100. Poulos, H. G., (1971). "Analysis of laterally loaded piles: single piles." *ASCE J. Soil Mechanics and Foundation Division,* Vol. 97, No. SM5, pp. 130-138

101. Prestiley, M. J. N., Seible, F., Calvi G M (1996). Seismic design and retrofit of bridges, Wiley-Interscience, New York.

102. Prithchard, B.P., (1994). "Advantages of bridge deck continuity" *Continuous and Integral Bridges*, Edited by B.P Pritchard, London.

103. Jangid, R.S., and. Datta, T.K., (1993) "Spectral analysis of systems with non-classical damping using classical mode superposition technique", *Earthquake Engineering and Structural Dynamics*, USA, Vol. 22, pp. 723-735, 1993.

104. Reese, L.C., O'Neill, M.W., and Smith, R. E., (1970). "Generalised analysis of pile foundations." *J. of Soil Mechanics and Foundations Division, ASCE* 96(SM1): 235-250.

105. Reese, L.C., William, F, V., (2001). Single piles and pile groups under lateral loading. A A Balkema, Netherlands, 2001.

106. Reese, L.C., William, R. C., and Francis, D. K., (1974), "Analysis of laterally loaded piles in sand", Offshore Technology Conference- Paper No.: TC 2080, Texas

107. Rodolfo. F. Maruri and S. H. Petro (2005) "Integral abutment and jointless bridges (IAJB) 2004 survey summary" FHWA Conference on *IAJB-2005*, Maryland.

108. Roeder, C. W., (2003) "Proposed design method for thermal bridge movements" *J. of Bridge Engg, ASCE.* Jan/Feb-02.

109. Roman, E.K., Yasser, K., and Hassiotis, S., (1998). "Design details of integral bridges." *Bridges and Structures Design Manual., Third Edition.* New Jersey Department of Transportation.

110. Scottish Executive Development Department. (2003). *The design of integral bridges.*, BA 42/96 Amendment No. 1., Design Manual For Roads And Bridges.

111. Shinozuka, M., Feng, M.Q., Kim, H., and Kim, S. (2000). "Nonlinear static procedure for fragility curve development", *J. of Structural Engg., ASCE* 126 (12), 1287-1295.

112. Siros, K.A., (1995). "Three dimensional analysis of integral bridges", *Ph.D. Dissertation*, West Virginia University, Morgantown, West Virginia.

113. Soong, S. T., Chai, Y. H., Hale, T. H., (2005). Analytical model for ductility assessment of fixed-head concrete piles, *J of Structural Engineering, ASCE,* Vol. 131, No.7, July 1, 2005.

114. Sritharan, S., (2005). "Improved seismic design procedure for concrete bridge joints," *J. of Structural Engg., ASCE,* September 2005.

115. Sritharan, S., Werff, J. V., Abendroth, R. E., Wassef, W. G., and Greimann, L. F., (2005), "Seismic behavior of a concrete/ steel integral bridge pier system," *J. of Structural Engg., ASCE,* July 2005.

116. Tandon, M., (2000). "Computer-aided bridge design." *Indian concrete journal*, December 2000, 721-725.

117. Tandon, M., (2005). "Guest editorial comments-superior performance with integral bridge concept." *Indian Concrete Journal*, Vol-79, September 2005, India.

118. Terzaghi, K., (1966). "*Theoretical soil mechanics*". John Wiley, New York, Fourth printing, Sep1966.

119. Thippeswamy., Hemanth, K., and GangaRao, V. S., (1995). "Analysis of in-service jointless bridges", *Transportation Research Record 1476, TRB*, National Research council, Washington, D.C., 162-172.

120. Ting., J.M., and Faraji, S., (1998). "Streamlined analysis and design of abutment bridges." *Research Report*, Highway Dept., University of Massachusetts, Transportation Center

121. Tuladhar, R., Mutsuyoshi, H., Maki, T., and Daigo, K., (2005) "Lateral Loading test on Full Scaled Concrete Piles Embedded into the Ground" *Net Document*

122. Wassermann, E. P., and Walker, J. H., (1996). " *Integral abutments for steel bridges*", Highway Structures Design Handbook, VII, Chapter 5, American Iron and Steel Institute, Washington , D.C

123. Wolde-Tinsae, A. M., and Klinger, J. E., (1987). "Integral abutment bride design and construction", *J. of Performance of Constructed Facilities, ASCE*, 2(2), 111-124.

124. Yannotti, P., Alampallli, S., and Harry, L. W., (2005). "New York state department of transportation's experience with integral abutment bridges" FHWA Conference on *IAJB-2005*, Baltimore, Maryland.

125. Yasser, A. K., (2004) "Numerical and experimental analysis of integral abutment bridges" Ph.D Dissertation Report, Stevens Institute of Technology, Hoboken, NJ 07030.

126. Yasser, A. K., and Hassiotis, S., (2005). "Analysis of soil–pile interaction in integral abutment." *Computers and Geotechnics 32*, Jan 2005. 201-209.

127. Youssef, D., and Hassiotis, S., (2000). "Seismic analysis of integral abutment bridge." *Final report,* Scotch Road I-95 Project.